AD-779 773

# LOW NOISE PROPELLER TECHNOLOGY DEMONSTRATION

Edward D. Griffith, et al

Lockheed-California Company

Prepared for:

Air Force Aero Propulsion Laboratory

January 1974

DISTRIBUTED BY:

NTIS

National Technical Information Service
U. S. DEPARTMENT OF COMMERCE
5285 Port Royal Road, Springfield Va. 22151

NOTICE

When Government drawings, specifications, or other data are used for any purpose other than in connection with a definitely related Government procurement operation, the United States Government thereby incurs no responsibility nor any obligation whatsoever; and the fact that the government may have formulated, furnished, or in any way supplied the said drawings, specifications, or other data, is not to be regarded by implication or otherwise as in any manner licensing the holder or any other person or corporation, or conveying any rights or permission to manufacture, use, or sell any patented invention that may in any way be related thereto.

ACCESSION for
NTIS White Section
D C Buff Section
UNANNOUNCED
JUSTIFICATION
BY
DISTRIBUTION/AVAILABILITY CODES
Dist. AVAIL. and/or SPECIAL

Copies of this report should not be returned unless required by security considerations, contractual obligations, or notice on a specific document.

AIR FORCE/56780/6 May 1974 — 300

UNCLASSIFIED

Security Classification

AD-779 773

## DOCUMENT CONTROL DATA - R & D

(Security classification of title, body of abstract and indexing annotation must be entered when the overall report is classified)

1. ORIGINATING ACTIVITY (Corporate author)
Lockheed-California Company
A Division of Lockheed Aircraft Corporation
Burbank, California 91503

2a. REPORT SECURITY CLASSIFICATION
UNCLASSIFIED

2b. GROUP
N/A

3. REPORT TITLE
LOW NOISE PROPELLER TECHNOLOGY DEMONSTRATION

4. DESCRIPTIVE NOTES (Type of report and inclusive dates)
Final Technical Report (15 FEB 73 to JAN 74)

5. AUTHOR(S) (First name, middle initial, last name)
Edward D. Griffith
James D. Revell

6. REPORT DATE
January 1974

7a. TOTAL NO. OF PAGES
201

7b. NO. OF REFS
14

8a. CONTRACT OR GRANT NO.
F33615-73-C-2045

b. PROJECT NO.
3066

c. Task 12

d. Work Unit 12

9a. ORIGINATOR'S REPORT NUMBER(S)

9b. OTHER REPORT NO(S) (Any other numbers that may be assigned this report)
AFAPL-TR-73-115

10. DISTRIBUTION STATEMENT
Approved for public release; distribution unlimited.

11. SUPPLEMENTARY NOTES

12. SPONSORING MILITARY ACTIVITY
Air Force Aero Propulsion Laboratory
Turbine Engine Division
Wright-Patterson AFB OH 45433

13. ABSTRACT

Quiet aircraft used for covert aerial night reconnaissance employ low tip speed propellers to achieve a minimum acoustic noise signature. This study was initiated when certain unexpected and anomalous trends in the measured propeller noise of such aircraft were compared to predictions of noise made by the Air Force Propeller Noise Prediction Program. Large discrepancies in both trends and levels were noted between measured and predicted noise. Therefore, the goal of this study was the modification of an existing Air Force computer program such that accurate predictions of far field noise for low tip speed propellers can be made. Empirical data from previous quiet airplane experiments were used to develop modifications to both rotational and vortex noise prediction methods for propellers operating in the tip speed range from Mach 0.2 to 0.4. Tasks in this study involved a detailed analysis of data acquired on past programs, a review of propeller noise theory, development of empirical corrections for the Air Force computer program, and the construction of design charts for low tip speed propellers. The end result was a corrected Air Force computer program that accurately predicts the far field noise produced by low tip speed propellers and propeller design charts for application to future quiet aircraft designs employing such propellers.

Reproduced by
NATIONAL TECHNICAL
INFORMATION SERVICE
U S Department of Commerce
Springfield VA 22151

DD FORM 1 NOV 68 1473

UNCLASSIFIED

Security Classification

UNCLASSIFIED
Security Classification

| 14. KEY WORDS | LINK A ROLE | LINK A WT | LINK B ROLE | LINK B WT | LINK C ROLE | LINK C WT |
|---|---|---|---|---|---|---|
| Low Tip Speed Propeller Noise | | | | | | |
| Flyover Noise | | | | | | |
| Tone Noise | | | | | | |
| Harmonic Noise | | | | | | |
| Vortex Noise | | | | | | |
| Aural Detectability | | | | | | |
| Digital Computer Program | | | | | | |
| Rotational Noise | | | | | | |



UNCLASSIFIED
Security Classification

☆U.S. Government Printing Office: 1974 — 758-434/5.59

# LOW NOISE PROPELLER TECHNOLOGY

*EDWARD D. GRIFFITH*
*JAMES D. REVELL*

Approved for public release; distribution unlimited.

## FOREWORD

The research study reported herein was conducted by the Lockheed-California Company (CALAC), Burbank, California under Contract F33615-73-2045 for the Air Force Aero Propulsion Laboratory (AFAPL), Wright-Patterson Air Force Base, Ohio under Project 3066, Task 12, work unit 12. This study is part of a continuing program sponsored by AFAPL aimed at reducing aircraft propulsion system noise while minimizing performance and weight penalties. This contract effort was concerned particularly with assessing forward flight effects on propeller noise radiated from low tip speed propellers used on quiet covert observation aircraft.

Project Leader at CALAC was Mr. Edward D. Griffith who had also been responsible for the acquisition of the noise data in field experiments on past quiet aircraft programs. Most of these field experiments were conducted by the Airborne Systems Organization of the Lockheed Missiles and Space Company (LMSC) under sponsorship by Army Contract DAAJ01-69-C-0059. Acknowledgement is due in particular to Mr. David Paul III who had overall responsibility for these field tests with the YO-3A aircraft and who established and standardized many of the field test procedures. Detailed analysis of data was performed by the Lockheed Rye Canyon Acoustics Research Laboratory. Dr. James D. Revell at CALAC was responsible for the extensive theoretical review conducted during the study.

The Air Force provided estimates of propeller noise and aural detection ranges based upon parametric information supplied by CALAC. Mr. Jerry Martin (ASD/XRHD) and Mr. Walter Lichtenberg (ASD/XRHP) were responsible for these Air Force noise and range predictions. The study was conducted during the period from February 1973 through November 1973 under the direction of Air Force Project Engineers, Lt. Craig Lyon and Mr. Paul Shahady (AFAPL/TBC).

Acknowledgement is due Mr. Bruce Metzger and Mr. Don Hall of Hamilton-Standard and to Dr. Martin Lowson of Loughborough University for helpful consultation during the program. Dr. Glen E. Bowie of the Lockheed Rye Canyon Research Laboratory provided consultation on acoustic ground reflection and doppler phenomena.

Acoustic noise signature data for the Army YO-3A Observation Aircraft used in this study and formerly classified as Confidential, were declassified on February 3, 1973; therefore, there is no classified information in this succeeding report submitted by the authors in November 1973.

Publication of this report does not constitute Air Force approval of the report's finding or conclusions. It is published only for the exchange and stimulation of ideas.

ERNEST C. SIMPSON
Director
Turbine Engine Division
Air Force Aero Propulsion Laboratory

## ABSTRACT

Quiet aircraft used for covert aerial night reconnaissance employ low tip speed propellers to achieve a minimum acoustic noise signature. This study was initiated when certain unexpected and anomalous trends in the measured propeller noise of such aircraft were compared to predictions of noise made by the Air Force Propeller Noise Prediction Program. Large discrepancies in both trends and levels were noted between measured and predicted noise. Therefore, the goal of this study was the modification of an existing Air Force computer program such that accurate predictions of far field noise for low tip speed propellers can be made. Empirical data from previous quiet airplane experiments were used to develop modifications to both rotational and vortex noise prediction methods for propellers operating in the tip speed range from Mach 0.2 to 0.4. Tasks in this study involved a detailed analysis of data acquired on past programs, a review of propeller noise theory, development of empirical corrections for the Air Force computer program, and the construction of design charts for low tip speed propellers. The end result was a corrected Air Force computer program that accurately predicts the far field noise produced by low tip speed propellers and propeller design charts for application to future quiet aircraft designs employing such propellers.

TABLE OF CONTENTS


| | | Page |
|---|---|---|
| I | INTRODUCTION | 1 |
| | 1. LMSC Quiet Aircraft Program | 1 |
| | 2. Air Force Quiet Aircraft Research Studies | 4 |
| | 3. Present Study | 4 |
| | 4. Objectives | 7 |
| II | QUIET AIRCRAFT EXPERIMENTAL DATA | 8 |
| | 1. Flyover Experiments | 8 |
| | 2. Static Tests | 9 |
| | 3. Quality of Experimental Results | 10 |
| | a. Flyover Experimental Procedures | 10 |
| | b. Source of Observed Noise | 12 |
| | (1) Discrete Frequency Noise | 12 |
| | (2) Broadband Random Noise | 14 |
| | c. Corrections to Analyzed Data | 17 |
| | 4. Summary | 21 |
| III | AIR FORCE PROPELLER NOISE COMPUTER PROGRAM | 22 |
| IV | COMPARISON OF MEASURED AND PREDICTED NOISE | 23 |
| | 1. Rotational Noise | 23 |
| | 2. Vortex Noise | 25 |
| | 3. Summary | 32 |
| V | THEORETICAL REVIEW | 36 |
| | 1. Theoretical Review of Rotational Noise | 36 |
| | a. Blade Aerodynamic Effects | 36 |
| | b. Blade Non-Uniform Inflow Effects | 43 |
| | c. Chordwise Blade Loading Effects | 54 |
| | d. Blade Wake/Wing Interaction Effects | 57 |
| | e. Effects of Wing Separation and Airplane Angle of Attack on Rotational Noise | 57 |
| | f. Methods of Reducing Rotational Noise for a Fixed Aircraft Weight and Propeller Diameter | 58 |

| | | Page |
|---|---|---|
| | 2. Theoretical Review of Vortex Noise | 63 |
| | 3. Summary | 64 |
| VI | EMPIRICAL MODIFICATIONS FOR AIR FORCE COMPUTER PROGRAM | 68 |
| | 1. Propeller Rotational Noise | 68 |
| | 2. Propeller Vortex Noise | 69 |
| | 3. Summary | 74 |
| VII | DESIGN CHARTS FOR LOW TIP SPEED PROPELLERS | 77 |
| | 1. Use of Design Charts | 77 |
| | 2. Aural Detection Range | 78 |
| | a. Actual Field Operations | 86 |
| | b. Typical Calculations | 87 |
| | c. Simulated Field Tests | 87 |
| | 3. Example of Anomalous Propagation Effects | 87 |
| VIII | CONCLUSIONS | 92 |
| IX | RECOMMENDATIONS | 94 |
| | REFERENCES | 95 |
| | APPENDIX I - AIRCRAFT DESCRIPTION | 97 |
| | APPENDIX II - EXPERIMENTAL AND DATA ANALYSIS PROCEDURES | 103 |
| | APPENDIX III - CORRECTIONS TO ANALYZED DATA | 108 |
| | APPENDIX IV - THEORETICAL ANALYSIS | 122 |

LIST OF FIGURES


| Figure | | Page |
|---|---|---|
| 1 | YO-3A Army Observation Aircraft | 2 |
| 2 | Noise Reduction Features of Quiet Aircraft Design | 3 |
| 3 | Overall Sound Pressure Level and Brake Horsepower Vs. Air Speed | 5 |
| 4 | Narrow Band Plot of YO-3A Flyover Acoustic Noise Signature | 6 |
| 5 | Narrow Band Plot of Static Propeller Noise | 11 |
| 6 | Typical Acoustic Qualification Test Results | 13 |
| 7 | Propeller Rotational Noise Correction Chart for Ground Reflections | 19 |
| 8 | Smoothed Trends of Propeller Rotational Noise | 20 |
| 9 | Comparison of Measured and Predicted Rotational Noise (Standard 3 Blade Propeller) | 24 |
| 10 | Comparison of Measured and Predicted Rotational Noise (Acoustic 3 Blade Propeller) | 26 |
| 11 | Comparison of Measured and Predicted Rotational Noise (Standard 6 Blade Propeller) | 27 |
| 12 | Comparison of Measured and Predicted Directivity (Standard and Acoustic 3 Blade Propellers) | 28 |
| 13 | Measured Vortex Noise for Propellers With Tip Speeds Between Mach 0.2 and 0.4 | 29 |
| 14 | Comparison of Measured and Predicted Vortex Noise (Standard 3 Blade Propeller) | 30 |
| 15 | Comparison of Measured and Predicted Vortex Noise (Acoustic 3 Blade Propeller) | 31 |
| 16 | Comparison of Measured and Predicted Vortex Noixe Spectra (Standard 3 Blade Propeller) | 33 |
| 17 | Comparison of Measured and Predicted Vortex Noise Spectra (Acoustic 3 Blade Propeller) | 34 |
| 18 | Comparison of Measured and Predicted Vortex Noise Spectra (Standard 6 Blade Propeller) | 35 |
| 19 | Fundamental Axisymmetric Rotational Noise SPL vs. Horsepower at Various RPM | 38 |
| 20 | Propeller Thrust vs. Horsepower at Various Efficiencies at 125 Ft./Sec. Forward Speed | 39 |
| 21 | Propeller Horsepower vs. RPM for Various Induction Efficiency Assumptions and Comparisons with YO-3A Data | 40 |
| 22 | Comparison of Calculated Fundamental Rotational Noise SPL Values for Axisymmetric Noise With and Without Static Empirical Corrections vs. RPM; Comparison with YO-3A Data and USAF Calculation | 40 |
| 23 | Estimated Net Propeller Efficiency vs. RPM for Various Induction Efficiency Assumptions vs. RPM; Comparison With YO-3A Data and USAF Calculation | 41 |

| Figure | | Page |
|---|---|---|
| 24 | Propeller Efficiency vs. Effective Aspect Ratio of Propeller Blade | 42 |
| 25 | Fundamental Rotational Noise SPL vs. RPM at 220 Lb. Thrust; Comparison of Experimental Data vs. Non-Uniform Loading (NUL) Theory for YO-3A Standard Three Blade Propeller | 45 |
| 26 | Fourier Cosine Torque Loading Harmonic, $a_{\nu\varphi}$ | 46 |
| 27 | Fourier Sine Torque Loading Harmonic, $b_{\nu\varphi}$ vs. Loading Harmonic Number | 47 |
| 28 | Radial Variation of the First Fourier Sine Torque Loading Harmonic $b_{1\varphi}$ at various RPM and Propeller Efficiency Conditions | 48 |
| 29 | Correlation of First Torque Loading Harmonic vs. Blade Lift Coefficient | 49 |
| 30 | Reference Blade Lift Coefficient vs. RPM | 50 |
| 31 | Fundamental Rotational Noise Increment, $\Delta SPL_{NUL}$ Due To Non-Uniform Loading (NUL) vs. RPM at 220 Lb. Thrust For The Standard YO-3A 3 Blade Propeller | 51 |
| 32 | Fundamental Rotational Noise Increment Due to Non-Uniform Loading (NUL) vs. Radial Position for Loading Harmonic Evaluation at Various RPM | 52 |
| 33 | Fundamental Rotational Noise Increment Due to Non-Uniform Loading (NUL) vs. First Fourier Sine Torque Loading Harmonic, $b_{1\varphi}$ | 53 |
| 34 | Effect of Wing Separation Distance on the First Fourier Sine Propeller Torque Loading Harmonic at 480 RPM Evaluated at R/RT - .62 | 59 |
| 35 | Fundamental Rotational Noise Increment Due to Non-Uniform Loading (NUL) vs. Wing Separation Distance at 480 RPM | 60 |
| 36 | Effect of Propeller Shaft (Aircraft) Angle of Attack on the First Fourier Sine Torque Loading Harmonic, $b_{1\varphi}$, at 480 RPM Evaluated at R/RT = .75 | 61 |
| 37 | Fundamental Rotational Noise Increment Due to Non-Uniform Loading (NUL) vs. Propeller Shaft (Aircraft) Angle of Attack at 480 RPM | 62 |
| 38 | Comparisons of Measured Rotational Noise with Predictions of Original and Modified Air Force Computer Program (Standard 3 Blade Propeller) | 70 |
| 39 | Comparisons of Measured Rotational Noise with Predictions of Original and Modified Air Force Computer Program (Acoustic 3 Blade Propeller) | 71 |
| 40 | Comparisons of Measured Rotational Noise with Predictions of Original and Modified Air Force Computer Program (Standard 6 Blade Propeller) | 72 |
| 41 | Comparisons of Measured and Predicted Directivity with Recommended Directivity | 73 |

| Figure | | Page |
|---|---|---|
| 42 | Comparisons of Measured Vortex Noise with Predictions of Original and Modified Air Force Computer Program (Standard 3 Blade Propeller) | 75 |
| 43 | Comparisons of Measured Vortex Noise with Predictions of Original and Modified Air Force Computer Program (Acoustic 3 Blade Propeller) | 76 |
| 44 | Propeller Design Chart - Minimum Overall Sound Pressure Level (OASPL) and Aural Detection Range (ADR) | 79 |
| 45 | Propeller Design Chart - Diameter: 8 Feet | 80 |
| 46 | Propeller Design Chart - Diameter: 10 Feet | 81 |
| 47 | Propeller Design Chart - Diameter: 12 Feet | 82 |
| 48 | Propeller Design Chart - Thrust: 200 Pounds | 83 |
| 49 | Propeller Deisgn Chart - Thrust: 300 Pounds | 84 |
| 50 | Propeller Design Chart - Thrust: 400 Pounds | 85 |
| 51 | Typical Long Time History of High Altitude Flyover | 88 |
| 52 | Typical One-Third Octave Band Spectra for High Altitude Flyover | 89 |
| 53 | Anomalous Long Time History of High Altitude Flyover | 91 |
| I-1 | YO-3A Army Observation Aircraft | 98 |
| I-2 | Q/Star Research Aircraft | 99 |
| I-3 | Standard Three Blade Propeller | 100 |
| I-4 | Standard Six Blade Propeller | 101 |
| I-5 | Acoustic Three Blade Propeller | 102 |
| II-1 | Flyover Test Course Layout | 104 |
| II-2 | Altitude Measuring Station | 105 |
| II-3 | Static Test Course Layout | 106 |
| II-4 | Rye Canyon Research Laboratory Acoustic Data Analysis Instrumentation | 107 |
| III-1 | Point Source Model - Typical Flyover | 109 |
| III-2 | Plane Wave Model - Typical Flyover | 111 |
| III-3 | Destructive Ground Reflection Frequency As Function of Aircraft Position | 112 |
| III-4 | Ground Reflection Equations | 113 |
| III-5 | SPL Values vs. $R_g$ | 114 |
| III-6 | Interference and Reinforcement Observed in 1000 Feet Flyover | 115 |
| III-7 | Reflection Coefficient ($R_g$) vs. Frequency | 116 |
| III-8 | Data Correction Chart | 117 |
| III-9 | Doppler Shift Effects | 118 |
| III-10 | Doppler Shifted Frequencies as a Function of Aircraft Position | 120 |
| III-11 | Typical Flyover Time History Showing Effects of Doppler Shift | 121 |

| Figure | | Page |
|---|---|---|
| IV-1 | Blade Element Geometry | 124 |
| IV-2 | Laminar/Turbulent Boundary Layer Transition on a Propeller Blade | 125 |
| IV-3 | Angle of Attack Inflow Geometry | 130 |
| IV-4 | Wing Induced Inflow Disturbances | 131 |
| IV-5 | Blade Loading Distribution Around Disc | 133 |
| IV-6 | Propeller Axis/Wing Incidence Angle | 141 |
| IV-7 | Wake Impingement Planform Area | 142 |
| IV-8 | Blade Wake Velocity Defect Profile Approaching Wing | 142 |
| IV-9 | Blade Loading Time History Idealized | 143 |
| IV-10 | Realistic Chordwise Blade Loading Due to Angle of Attack | 144 |
| IV-11 | Effect of Induced Downwash on the Relative Velocity Vector | 147 |
| IV-12 | Frequency Spectra Employed in Vortex Noise Prediction (From Reference 7) | 155 |
| IV-13 | Cartesian Components of Field Point and Source Point Position Vectors | 160 |

## SYMBOLS

| | |
|---|---|
| $a$ | speed of sound in ambient air |
| $B$ | number of propeller blades |
| $b$ | blade chord |
| $b_{.7}$ | blade chord at 0.7 propeller radius |
| $C$ | coefficient |
| $C_F$ | force coefficient in vortex noise theory |
| $C_f$ | frequency coefficient in vortex noise theory |
| $C_L$ | lift coefficient |
| $C_P$ | power coefficient |
| $C_T$ | thrust coefficient |
| $D$ | diameter of propeller or cylinder |
| $d$ | differential operator |
| $d$ | distance between observer and propeller center |
| dB | decibels, for sound pressure level reference is 0.0002 dynes/cm$^2$ |
| $e$ | base of natural logarithms, 2.718... |
| $F$ | force |
| $f$ | cyclic frequency, $\omega/2\pi$, Hz |
| HP | propeller shaft horsepower |
| Hz | abbreviation for Hertz, cps |
| $h$ | blade thickness |
| $h_{.7}$ | blade thickness at 0.7 propeller radius |
| $i$ | $\sqrt{-1}$ |
| $J_n$ | Bessel function of first kind or order n and argument at $\Omega Yr/(aS_0)$ |
| $k$ | $mB\Omega/a$, wave number |

| | |
|---|---|
| $\log_{10}$ | common logarithm to base 10 |
| M | flight Mach number |
| m | order of rotational sound |
| OASPL | overall sound pressure level, dB re 0.0002 dynes/cm$^2$ |
| p | sound pressure |
| Q | propeller torque |
| R | Reynolds number |
| r | radius from propeller axis |
| $S_b$ | propeller blade area, $B\int_{hub}^{tip} b\,dr$ |
| SPL | sound pressure level, dB re 0.0002 dynes/cm$^2$ |
| $S_t$ | Strouhal number |
| $S_0$ | $\sqrt{X^2 + (1-M^2)\,Y^2}$ |
| T | propeller thrust |
| t | time |
| V | velocity |
| $V_t$ | tip velocity |
| $V_{.7}$ | rotation velocity at 0.7 propeller radius |
| X | distance to observer from propeller plane at time sound heard, positive if observer ahead of propeller |
| Y | distance to observer from propeller axis |
| $\alpha_b$ | blade angle of attack |
| $\alpha_{av}$ | advance angle |
| $\Theta$ | blade angle relative to propeller plane |
| $\Theta_{.75}$ | blade angle at 0.75 propeller radius |

| | |
|---|---|
| $\lambda$ | order of harmonic loading forces |
| $\pi$ | pi, 3.14159 |
| $\rho$ | mass density of air |
| $\varphi$ | circumferential angle about propeller axis, 0 in plane of observer |
| $\theta$ | azimuth angle between vector from propeller center to field point and propeller axis, 0 in forward axis, $90^{\circ}$ in propeller plane |
| $\Omega$ | propeller angular velocity, $n\pi/30$, radians/sec. |
| $\omega$ | circular frequency, radians/sec. |

## SECTION I

## INTRODUCTION

In 1966 the Honorable John Foster, Director of Defense Research and Engineering described in a Government/Industry briefing a problem concerning covert air surveillance needed in Southeast Asia (SEA). Even though the enemy in SEA lacked sophisticated aircraft detection devices (such as radar) the noise of existing observation aircraft provided advanced warning that minimized effectiveness of aerial night reconnaissance. The obvious solution to this problem was a quiet observation aircraft that would minimize the aural detection range.

Definition of this major problem area and recognition of the fact that the potential solution encompassed the design and development of quiet observation airplanes resulted in the launching of two important and parallel programs. The combined results from these programs eventually isolated the problem that is the subject of the present study. The Lockheed Missiles and Space Company (LMSC), using minimum radiated acoustic noise as the criterion, designed, built and flight tested a family of quiet aircraft. Concurrently, the Air Force sponsored a number of in-house and contract research studies on all aspects of reducing the far field radiated noise for this type of aircraft. One of these studies had, as the end result, a computer program for the prediction of the noise produced by low tip speed propellers. Differences between the computer-predicted propeller noise and that measured during the quiet aircraft flight tests form the basis for the present study.

### 1. LMSC QUIET AIRCRAFT PROGRAM

Under sponsorship of the Advanced Research Project Agency (ARPA), LMSC began development of propeller driven quiet aircraft in 1967 This program produced prototype aircraft that were successfully tested and later, in 1968, deployed in combat operations in SEA for the purpose of evaluating this type of aircraft. This successful deployment led to an advanced quiet observation aircraft, the YO-3A, that was produced in limited quantities under Army sponsorship. At the same time, LMSC designed and built the Q/STAR Research Quiet Aircraft. This experimental aircraft was used to test various noise reduction concepts.

In 1970-71 a number of YO-3A aircraft operated in service in SEA for a period of about twelve months. Figure 1 is a photograph of the Army YO-3A Observation Aircraft. This two place airplane, with a pilot and an observer and equipped with night viewing devices, had performance characteristics needed for effective low-level tactical night reconnaissance missions. The key performance factor was the low acoustic noise signature that resulted in minimum aural detection range and the capability of covert night operation. These low noise characteristics were achieved by a number of special design features illustrated in Figure 2. Of these, the major features were the clean aerodynamic lines that minimized aerodynamic noise, engine compartment

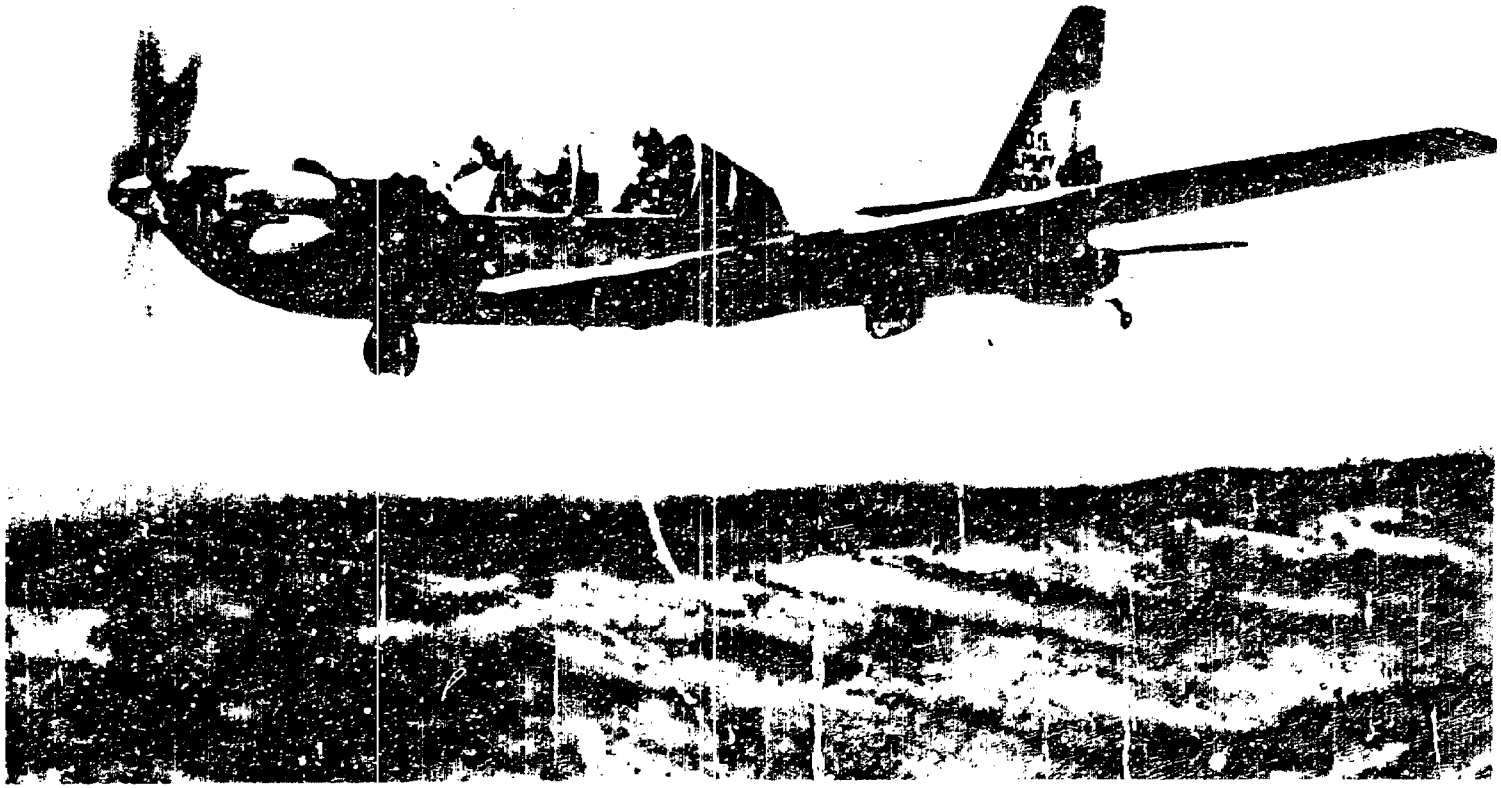

Figure 1. YO-3A Army Observation Aircraft

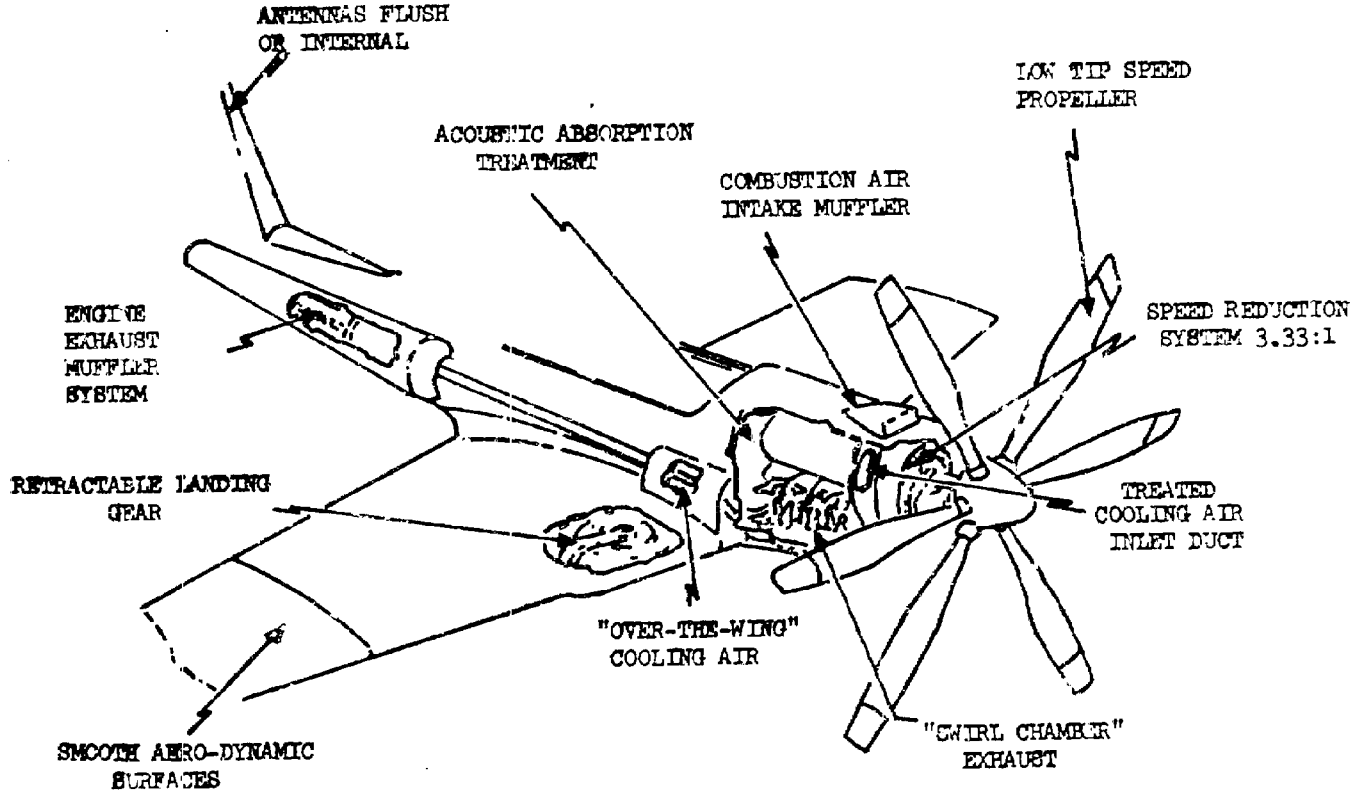


Figure 2 - Noise Reduction Features of Quiet Aircraft Design

soundproofing and exhaust muffling that reduced engine noise, and the use of low tip speed propellers that greatly reduced propeller noise. These quieting techniques have been discussed in the recently declassified reports on the YO-3A development program (references 1, 2, and 3).

Noise reduction features of the aircraft were designed to be most effective at the "quiet cruise" velocity where minimum power is required and minimum noise is produced. Figure 3 shows the correlation between required power and radiated noise. Detailed analysis of the YO-3A far field noise signature, measured during the quiet cruise operation, led to the conclusion that, after all the quieting features had been incorporated into the aircraft design, the propeller remained the predominant noise source. Evidence supporting this conclusion is presented later in this report. A typical narrow band plot of the YO-3A acoustic noise signature is shown in Figure 4.

In October 1970, flight tests on the YO-3A were conducted for qualifying a new propeller design. Since the far field noise signature is controlled by propeller noise, the opportunity was taken to acquire noise data from three different propellers. The empirical data from these fly-over tests comprise the most significant results obtained on the noise radiated by low tip speed propellers and were used exclusively throughout this study.

## 2. AIR FORCE QUIET AIRCRAFT RESEARCH STUDIES

Concurrent with the ARPA/Army sponsored quiet aircraft development programs that resulted in military hardware, the Air Force sponsored a number of comprehensive in-house and contract research studies that covered a wide range of aircraft noise generating and noise reduction factors. These studies covered: the measurement of the aerodynamic noise produced by gliders during flyover (reference 4); the aural detection of far field aircraft noise (reference 5); a summary of the overall technology of aircraft noise reduction (reference 6). While these studies contributed much useful technology for quiet aircraft design, the most significant programs, in light of the conclusion that the propeller is the predominant noise source for light-weight propeller driven quiet observation aircraft, were the studies on low tip speed propeller noise sponsored by the Air Force Aero Propulsion Laboratory (AFAPL). This work has been reported in references 7, 8 and 9. The result of these efforts was an Air Force computer program for predicting both the level and spectra of the noise of low tip speed propellers and the associated aural detection range. Unfortunately, only static propeller test data were available for the validation of this computer program during the period of the study.

## 3. PRESENT STUDY

Unexpected results were obtained in October 1970 tests. Anomalous trends in propeller noise were discovered in the flyover noise data that had not been observed in static testing of propellers nor were they predicted by conventional propeller noise theory. As a result it was suspected that the aforementioned computer program based on conventional theory and correlated with static test results, might not accurately predict low tip speed propeller noise in flight.

AIRCRAFT: Q/STAR ALTITUDE: 125 FEET

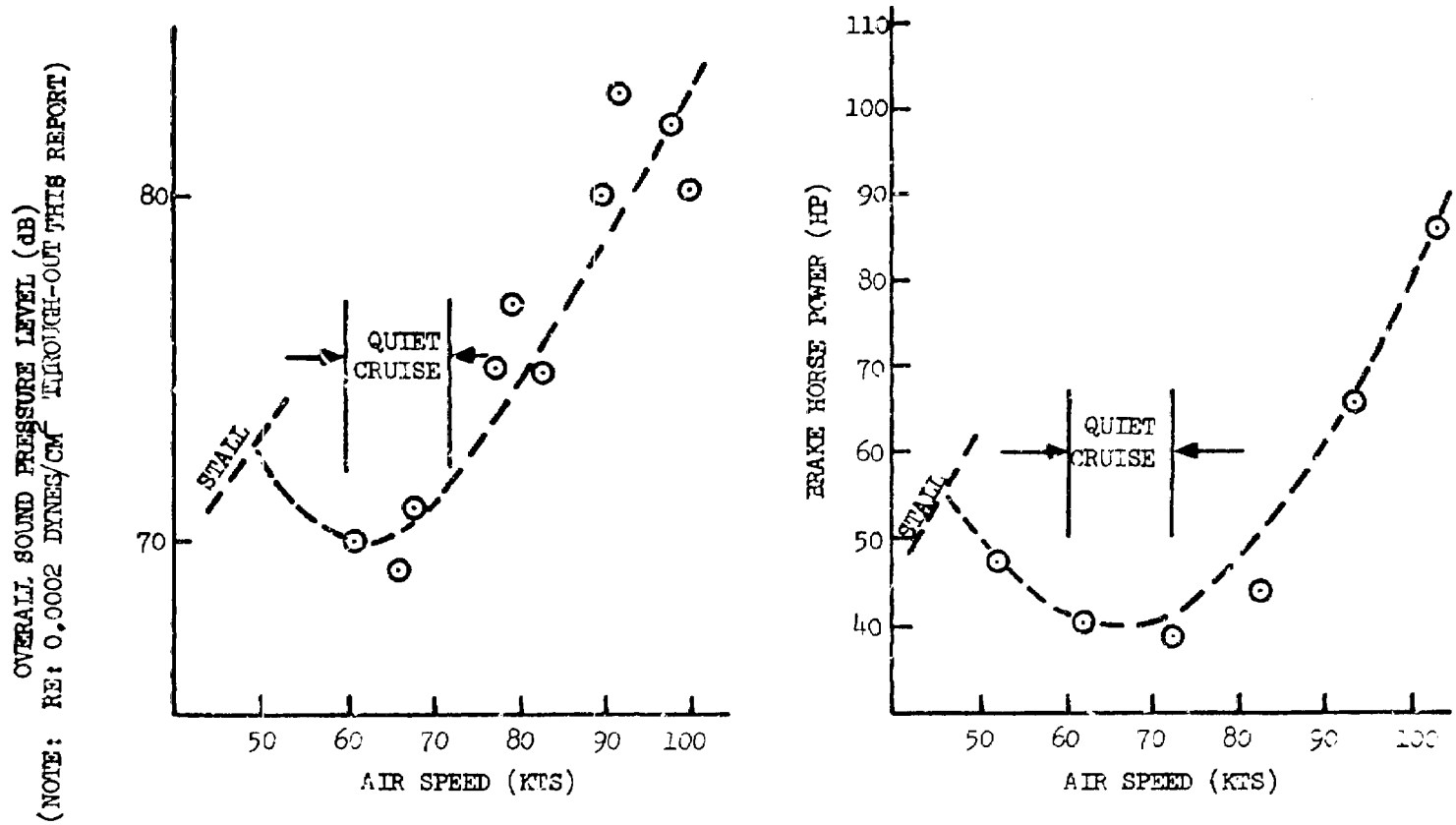


Figure 3 - Overall Sound Pressure Level and Brake Horsepower Vs. Air Speed

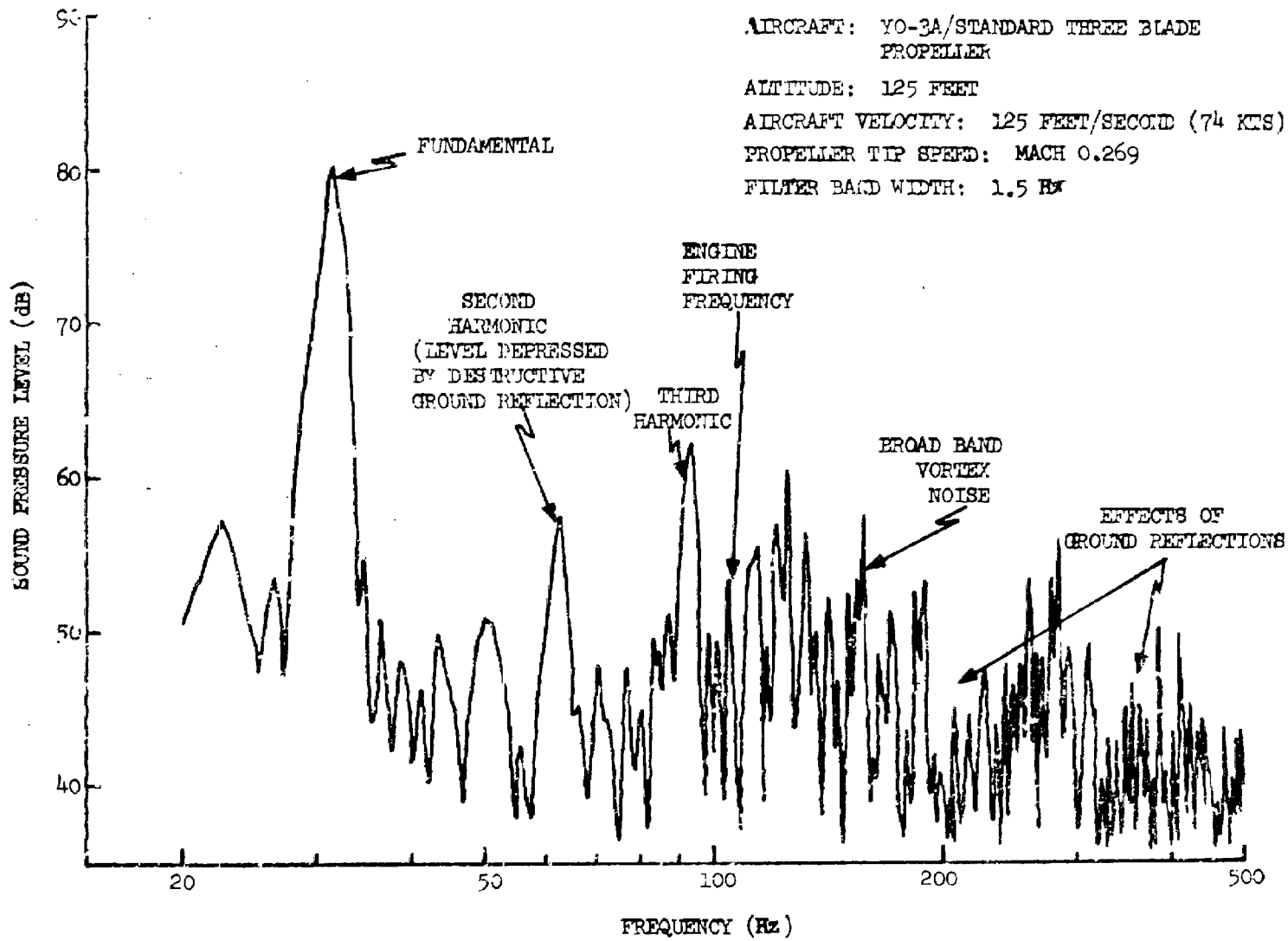


Figure 4 - Narrow Band Plot of YO-3A Flyover Acoustic Noise Signature

In early 1972 a comparison of measured and predicted noise was made and this proved to be the case. Serious discrepancies between measured and predicted levels and the associated trends were found for both the rotational and vortex noise components in the tip speed velocity range from approximately Mach 0.2 to 0.4.

The present study was structured to resolve the disagreement between measured and predicted results, and to modify the Air Force computer program so that accurate noise predictions from low tip speed propellers can be made.

## 4. OBJECTIVES

The objectives of this study were:

a. To analyze empirical data with sufficient detail for modifying the prediction methods,

b. To conduct a theoretical review of propeller noise generation and provide explanations for the anomalous trends observed in experimental results,

c. To modify the Air Force computer program in such a manner that accurate predictions of noise from low tip speed propellers can be made, and

d. To develop design charts for this type of propeller that will be useful in design of future quiet propeller driven aircraft.

The tasks leading to accomplishment of these objectives are discussed in the following sections.

## SECTION II

## QUIET AIRCRAFT EXPERIMENTAL DATA

A large quantity of experimental acoustic noise data were acquired during the various phases of the Quiet Aircraft Program. This program began with flight and ground tests of the prototype aircraft in 1967, extended through testing of experimental aircraft, and ended with field experiments of production aircraft in 1971. During this period of several years, experience with flying and testing this type of aircraft resulted in significant improvements in field test techniques and in the quality of field test results. New field test procedures were tried, evaluated and eventually standardized in order to produce consistent experimental data that could be used for detailed studies of the aircraft far field noise signature.

Near the end of the program, in 1970, flyover experiments were conducted with the YO-3A aircraft. In this same year static tests were also conducted using the Q/STAR experimental aircraft as the test stand. Three different propellers were used in both tests. Three and six blade propellers of standard propeller design were used along with a special three blade propeller that was designed from a low noise criterion. Descriptions of these aircraft and each of the propellers are presented in Appendix I. Experimental data from both flyover and static tests were considered in this study. However, only aircraft flyover test data were used to develop modifications for the Air Force computer program.

Specific experimental and data analysis procedures are discussed in Appendix II. The test data from these past field tests, recorded on magnetic tape, were subjected to a detailed analysis as part of this study. Once these data were analyzed, it was necessary to apply corrections for various factors including ground reflection and the doppler phenomena. These corrections are discussed in Appendix III.

Flyover and static tests are discussed below. Quality of experimental results and the evidence that the observed far field noise originated from the propeller are also discussed.

### 1. FLYOVER EXPERIMENTS

The original YO-3A aircraft was equipped with a fixed pitch six blade propeller of conventional or standard design. This standard six blade propeller performed well at the quiet cruise operating mode, but since propeller pitch could not be adjusted for different flight modes, both takeoff and climb performances were somewhat limited. To improve these performance characteristics, a propeller development program was conducted in 1970 that provided a variable pitch (or so called "constant speed") three blade propeller. Aside from this feature, the propeller was also of conventional or standard aerodynamic design.

For the purpose of qualifying the standard three blade propeller in a retrofit program for the aircraft deployed in SEA, a series of field experiments were conducted in October 1970. These experiments included measurement of the flyover noise from both the standard three and six blade propellers and an acoustic three blade propeller. The acoustic three blade propeller had been designed from noise rather than aerodynamic criteria, and it featured a rather thick airfoil section with a wide chord. This propeller also had a variable pitch capability.

Weather conditions during the flight tests, in October 1970, of the standard three blade, the standard six blade, and the acoustic three blade propellers were excellent with minimum wind and ambient background noise on most test days. These conditions, combined with the standardized flyover test procedures developed over several years of testing, provided unusually good quality propeller noise data. The two variable pitch propellers provided the first opportunity in the quiet aircraft program to vary propeller rpm while keeping other parameters (except torque) constant. Data from these experiments provide the best experimental results for the widest range of parametric variations that were acquired during the entire quiet aircraft program. Hereafter in this report these experiments will be referred to as the "October tests." These flyover results have been used exclusively in this study to develop the empirical modifications for the Air Force computer program for predicting noise of low tip speed propellers. Static test data were not used for the reasons discussed below.

## 2. STATIC TESTS

Prior to the flyover tests with the YO-3A, the three propellers were available for static testing, and in the summer of 1970 tests were conducted using the Q/STAR experimental aircraft as a static test stand. For these tests the wings were removed and the attitude of the fuselage adjusted so that the propeller disc plane was perpendicular to the ground. Description of the aircraft of each of the three propellers, and test and analysis procedures are presented in Appendix I and II along with flyover test information.

Although static tests were conducted for the standard three blade, the standard six blade, and the acoustic three blade for a variety of propeller rpm and pitch conditions comparable to the operating conditions for flyover tests, results from these static test stand experiments were disappointing. Static test noise results were difficult to interpret and showed little correlation with flyover noise results. One problem was that given propeller rpm conditions could be achieved on the static tests with much less power than required on flyover tests. Presumably this was related to non-realistic inflow conditions in static tests. This eliminated the possibility of correlation of far field noise levels using horsepower as the normalizing parameter.

However, a more basic problem is the inherent difference in the character of the noise observed in the two different types of testing. Narrow band spectral results from flyover tests show the traditional rotational noise harmonics decreasing in level so that only two or three harmonics can be

observed as discrete frequencies above the broadband random vortex noise levels. In narrow band plots of static tests of these low tip speed propellers the harmonic levels do not decrease nearly as quickly with harmonic number. Indeed, such plots show significant discrete frequency levels above the vortex noise levels to the ninth or tenth harmonic as illustrated in Figure 5. Thus, the basic character of the noise from the two types of tests is substantially different. The unusual character of far field noise from static tests of this type of low tip speed propeller was also observed in two research programs sponsored by AFAPL (references 7 and 9).

In view of the difficulties noted above, the static test data analyzed in this study were not considered when developing the empirical modifications for the Air Force computer program. However, the cause of the different noise characteristics generated by the same propeller in the flyover and static test modes of operation is considered worthy of additional investigation in future work.

## 3. QUALITY OF EXPERIMENTAL RESULTS

The quality of experimental results, on which validity of the empirical modifications developed in this study are dependent, is greatly influenced by three factors:

- the procedure for both the field tests and data analysis,
- the verification that the predominant source of the observed aircraft noise was the propeller, and
- the correction of the analyzed data for the effects of ground reflections and doppler frequency shifts.

These factors, their influence on the final quality of experimental results and the impact on empirical modifications developed for the Air Force computer program during this study are discussed below.

### a. Flyover Experimental Procedures

There are several conflicting requirements for conducting flyover tests with quiet airplanes if such tests are to provide valid measurements of the radiated far field low level noise signatures. The aircraft must fly at sufficient altitude to allow the measurement of far field noise; however, since the radiated noise from the quiet airplane is low, the aircraft altitude must be low enough to provide a recognizable noise level above the ambient background noise. This requirement can be partially alleviated by conducting experiments in remote locations away from the usual man-made noise sources and by testing in low natural background noise conditions. Minimum wind is also an essential test condition from the standpoint of both noise and flight operations. Flight safety is another factor which establishes a minimum fly-over altitude.

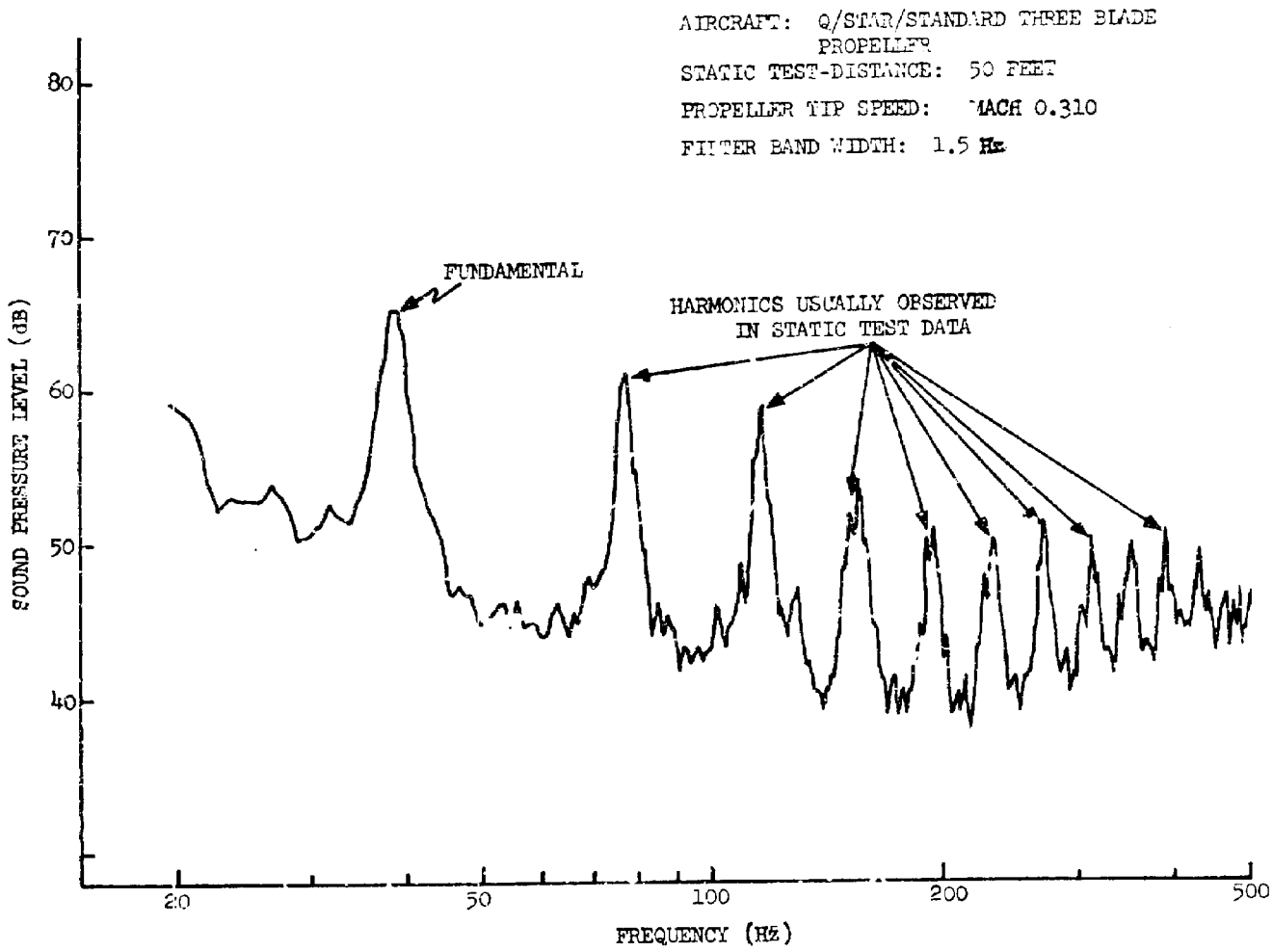


Figure 5 - Narrow Band Plot Of Static Propeller Noise

A standard flyover test was developed which satisfied these conflicting requirements; an altitude of 125 feet was used. This flyover altitude provided the required distance for far field measurement of propeller noise (i.e., about 15 propeller diameters). For wind conditions of less than 5 mph, background noise in remote locations was usually at least 10 dB below the peak aircraft noise level during the flyover for the frequency range of interest. Such tests were performed safely by experienced test pilots.

During these standardized flyover tests it was essential to control and measure a number of variables such as aircraft velocity, altitude, lateral position, propeller rpms, engine horsepower, etc. Consistent flyover procedures, described in Appendix II were used to accomplish the required control over the measurement parameters. Even so, it was found necessary for good results to average the data from several flyover runs. Individual flyover runs that are used in certain forms of data analysis (e.g. narrow band analysis) require normalization to the average levels. Under optimum test conditions, flyover test results were achieved that showed small statistical variations in noise levels. Figure 6 illustrates the statistical variability of octave band levels of peak noise in a series of 18 runs used for qualification purposes. Standard deviations of about one dB in octave band levels were achieved in these October tests. For the purpose of this study the mean value of at least three flyover runs was utilized in all cases to normalize individual data plots.

b. Source of Observed Noise

The subjective judgment of most observers listening to all quiet aircraft (from the QT-2 prototype through the YO-3A limited production aircraft) was that the propeller was the predominant noise source. Some test data from other studies of gliding aircraft supported this interpretation, and during the October 1970 tests of the YO-3A equipped with two propellers having variable pitch capability more positive evidence verifying this source was acquired. The sources of noise for the YO-3A acoustic noise signature are discussed below in terms of discrete frequency and broadband random noise.

(1) Discrete Frequency Noise

In narrow band plots of peak level flyover noise, discrete frequency tones can be observed in the spectra at low frequencies (i.e., below 250 Hz). When propeller rpm is varied, the frequencies of most of these tones can be correlated (when corrected for doppler shifts) with predicted emitted frequencies of propeller rotational noise harmonics. Frequencies of these harmonics are given by the equation

$$f_m = \frac{.30\ Bm\ (rpm)}{60}\ \text{Hz} \qquad (1)$$

where

f = frequency of rotational noise harmonic

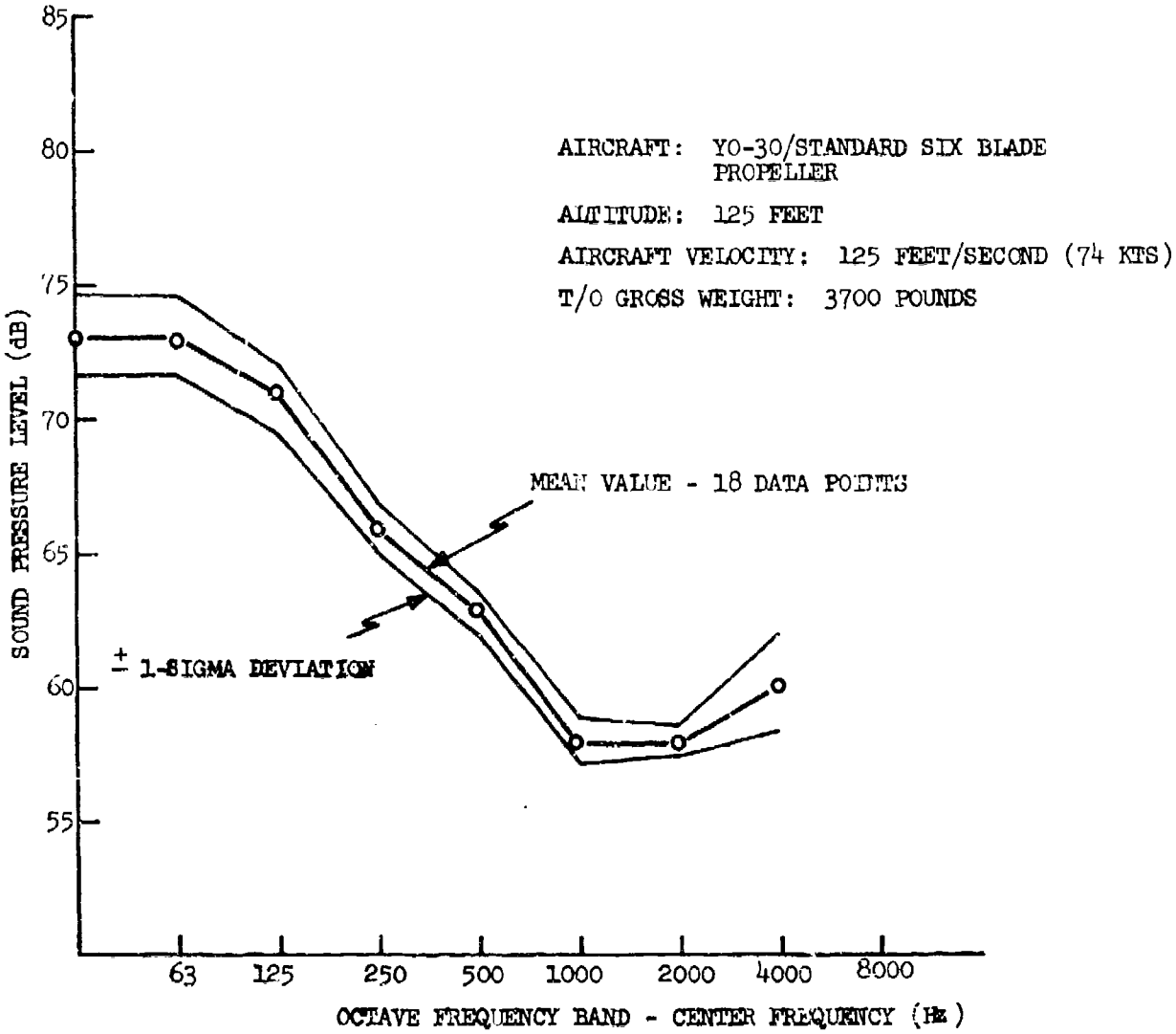


Figure 6 - Typical Acoustic Qualification Test Results

m = propeller rotational noise harmonic number

rpm = engine revolutions per minute

B = number of propeller blades

0.30 = speed reduction factor

For three blade propellers the first three harmonics can usually be observed above the level of broadband random noise while for the six blade propeller only the first two are present. The correlation of predicted and observed frequencies and the absence of other potential noise sources for these discrete frequency tones lead to the conclusion that propeller rotational noise is the source being measured.

Occasionally in the narrow band spectra a discrete frequency tone is observed that correlates with the predicted engine firing frequency. The frequency of this tone is given by the equation

$$f_F = \frac{(\text{rpm}) \times N}{120} \quad (\text{Hz}) \qquad (2)$$

where

$f_F$ = engine firing frequency

N = number of cylinders

It is believed that this pure tone noise originates at the engine exhaust and radiates from the tailpipe of the muffler system. A more efficient muffler design presumably would have eliminated this noise. For the purpose of this study these tones, when present, are removed from the spectral plots.

Prior to conducting acoustic field tests, many quiet aircraft delivered to the test site exhibited another type of discrete frequency noise that usually dominated the high frequency (i.e., above 250 Hz) spectra with levels of 5 to 15 dB above the levels of broadband noise. These tones were "whistles" generated by aerodynamic sources. Holes, cavities, and/or cracks in the airframe were usual sources. In the experimental flight tests these tones were eliminated in all acoustic test cases by taping over the noise sources to restore a clean aerodynamic configuration to the airframe. In military field operations of the aircraft these same corrective techniques were used to assure the proper acoustic noise signature. As a result, no discrete frequency (pure tone) noise, attributable to aerodynamic sources, was ever observed in the far field noise signatures of quiet airplanes.

(2) Broadband Random Noise

Verification of the source of the observed broadband random noise is more difficult because of the possibility that such noise may be generated by a variety of aerodynamic sources associated with the airframe. However,

there seems to be adequate evidence that this broadband noise was propeller vortex noise. This evidence is as follows:

(a) Levels of the broadband noise were shown in this study to change as functions of propeller tip speed when all other parameters (except torque) are held constant. This would not be true if airframe aerodynamic noise was a significant contributor to the broadband noise observed in experiment. (However, interaction of propeller wash with the airframe is a possibility.)

(b) Good correlation of peak one-third octave band levels for the broadband noise was found with rotational noise levels in this study over a range of tip speeds from approximately Mach 0.2 to 0.4. This correlation was incorporated into the recommended vortex noise modification. Such correlation could not be expected if the source of noise was the airframe moving through the air at constant velocity.

(c) In addition to this evidence, CALAC has measured and reported on the far field aerodynamic noise from gliding aircraft (reference 10). These data have been re-analyzed and extended to measured C-5A data under sponsorship of the Langley Research Center. The current improved equation for predicting the overall sound pressure level (OASPL) of airframe aerodynamic noise is:

$$OASPL = 60 \text{ LOG } V + 10 \text{ LOG } S - 20 \text{ LOG } h - 40 \text{ LOG } AR - 1.6 \text{ (dB)}$$

where,

V = Aircraft velocity (KTS)

S = Wing area ($ft^2$)

h = Aircraft altitude (ft)

AR = Aspect ratio

1.6= Empirical constant

Using appropriate values of these parameters for a typical YO-3A aircraft flyover, the result is:

$$OASPL = 54.2 \text{ (dB)}$$

This is well below the 68 dB in OASPL tabulated from measured one-third octave band results for the tip speed case that yields minimum levels for the broadband noise. If this prediction method is accurate (and it has been demonstrated to accurately predict aerodynamic noise for several gliding aircraft ranging in size and configuration from gliders to the C-5A), the broadband noise levels observed to be several dB higher must be propeller vortex noise.

Based on the considerable evidence cited above, the conclusions must be drawn that the levels of airframe aerodynamic noise are sufficiently below the levels of the observed broadband noise to obviate this as the source. Thus, the observed noise that correlated well with propeller rotational noise is, indeed, propeller vortex noise.

It is noteworthy that the observed broadband vortex noise peaks at a constant frequency instead of shifting upward as propeller tip speed increases (as expected from theory). This behavior is discussed below.

The theory that has been developed for aerodynamically generated noise relates peak frequency (f), velocity (V), and a physical dimension (h), by the so called "Strouhal" equation

$$f = \frac{S_t V}{h}$$

Where

$S_t$ = Strouhal Number

When velocity (in this case tip speed) increases, peak frequency increases. For simple aerodynamic forms such as rods and spheres, this simple equation works well; however, for more complex structures difficulties in applying this basic concept are usually encountered. For example, it is difficult to determine peak frequency trends in the results of glider flyovers reported by the Air Force in reference (6), and no increasing peak frequency trend can be found in the measured propeller vortex noise as propeller tip speed is increased on the YO-3A. Several factors should be noted:

Strong ground reflection reinforcements and cancellations occur in the midfrequency region where peak levels are expected. Higher rotational noise harmonics also exist in this region. Corrections applied to measured data for these phenomena may contain inaccuracies that obscure the actual peak frequencies.

One-third octave band plots are used to describe the broadband vortex noise spectra. Changes in peak frequency may be so small that such plots do not delineate trends.

Option 3 of the Air Force computer program contains a $X_{stall}$ term, which

represents the percentage of the propeller radius where separated flow conditions exist. For this option, this equation from reference (7) is used for predicting peak frequency.

$$f_{peak} = \frac{SV}{h\,(1 - kX_{stall})}$$

As the propeller tip speed increases, $X_{stall}$ decreases and a decreasing trend counter to the increasing velocity trend is introduced. Since this study involves low tip speed propellers where stall conditions probably exist, this equation provides a possible explanation for the lack of discernible peak frequency change in the measured data.

Consequently, the measured levels are considered valid vortex noise levels for this type of propeller. Minor errors in predicting peak frequency will not have major impact on predicted aural detection.

c. Corrections to Analyzed Data

The analyzed flyover noise data in the form of one-third octave band time history plots, tabulations and narrow band plots contain inherent inaccuracies due to certain test conditions. The microphones monitoring the aircraft noise were positioned five feet above the ground which provides a reflecting surface for noise radiated from overhead. Therefore, the effects of ground reflections of the aircraft noise in the form of either cancellation of reinforcement are included in the measured noise. Likewise, in all aircraft flyovers the moving noise source is monitored by the stationary microphone on the ground and doppler shifts in the frequencies of emitted noise are included in the measured noise. Methods used for applying corrections to analyzed data are discussed in Appendix III. The effect of these inaccuracies in measured data on the quality of corrected experimental results is discussed below.

The effects of ground reflection phenomena are present in all aircraft flyover data and can be identified in both narrow band and one-third octave band spectral plots. The narrow band analysis provides the best information on the discrete frequency rotational noise components while the one-third octave band analysis is considered a more appropriate measure for the broadband vortex noise. Thus, corrections for ground reflections following the methods described in Appendix III must be applied to both types of spectral plots. The manner in which the flyover tests were conducted produces some uncertainties with regard to these corrections. These uncertainties involve determination of overhead position and propeller rpm.

During the flyover tests no record of altitude position as a function of flyover time was maintained. The overhead position was estimated from peak flyover noise and the point of inflection in the doppler shift of certain discrete frequencies. If errors are made in determination of overhead position, significant shifts in related estimates of reinforcement and cancellation

frequencies due to the occurrence of ground reflections can produce significant inaccuracies in the applied corrections. Since the doppler shift in emitted frequencies is also related to aircraft position, uncertainties in estimating aircraft position can introduce errors in estimating the doppler effects.

Propeller rpm was controlled and monitored in the aircraft cockpit and a degree of variability was inherent in each test. The emitted frequencies of propeller rotational noise harmonics are directly related to rpm; therefore, errors in estimating rpm can produce errors in applied corrections. Thus, uncertainties in estimating aircraft position, doppler shift, and propeller rpm produces potential errors in knowing the actual frequencies of propeller rotational noise harmonics.

Figure 7 is a correction chart for removing the effects of ground reflections when the aircraft is in the overhead position. The range of frequencies for the first three harmonics of three blade propellers, where rpm variation was possible, is shown. For the six blade propeller the frequencies of the first two harmonics are also shown. The substantial corrections required at the cancellation frequencies yields some insight into the magnitudes of potential errors that can result from such corrections to narrow band plots.

The uncertainties described above may introduce errors of two or three Hz in determining the harmonic frequencies. Such errors will have minor impact on corrections in the level of the fundamental rotational noise harmonic frequency for the three blade propellers. The slope of the correction curve is rather gentle in the indicated range and errors less than one dB in level can be expected. However, this is not the case for the second harmonic. This rotational noise harmonic frequency exists in the region near the first destructive ground reflection where the slope is maximum. In this case a small error of two or three Hz in estimated frequency can result in an error of several dB in the corrected level. The potential error in correcting the third harmonic for the three blade propellers lies between these extremes. At lower frequencies the potential error is large, but is smaller at the higher frequencies in the indicated range of the potential error. For the six blade propeller the potential error in correcting the level of the rotational noise fundamental frequency is large while that of the second harmonic is small.

In producing corrected narrow band plots for determination of absolute and/or relative levels of propeller rotational noise harmonics in this study, data from at least three flyover runs were averaged. This procedure minimized the potential errors discussed above. However, it must be concluded that best experimental data quality exists for the fundamental rotational noise frequency of the three blade propeller where minimum correction is required. Fortunately, the corrections developed during this study for both higher harmonics of rotational noise and vortex noise are related to levels of the fundamental rotational noise frequency. In spite of the potential errors in correcting the rotational noise harmonic levels, the resulting trends for rotational noise based on narrow band plots are consistent and data are judged to be of sufficient quality to produce reliable results. An example of the noise trends based on corrected rotational noise levels is shown in Figure 8.

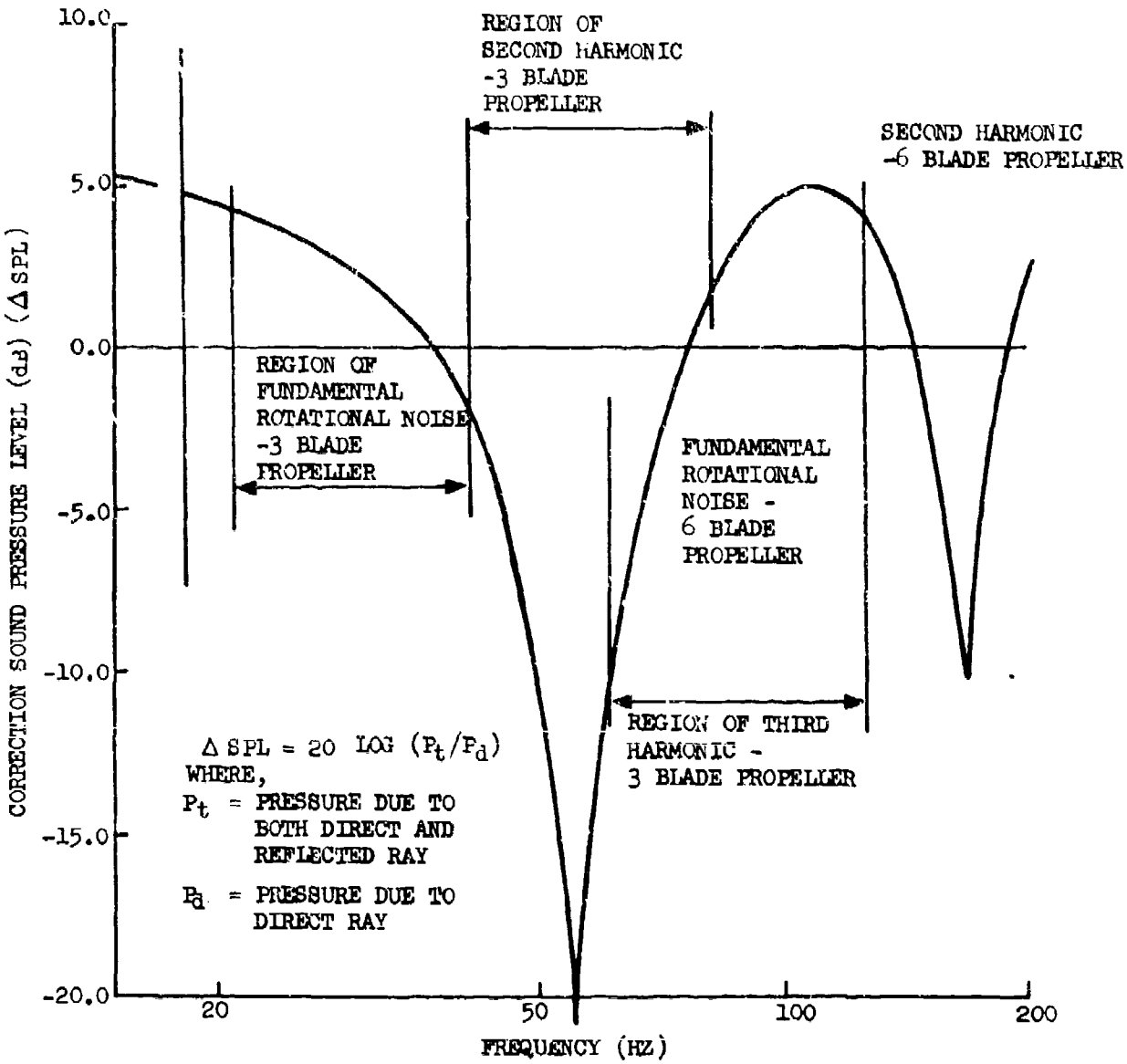


Figure 7 - Propeller Rotational Noise Correction Chart for Ground Reflections

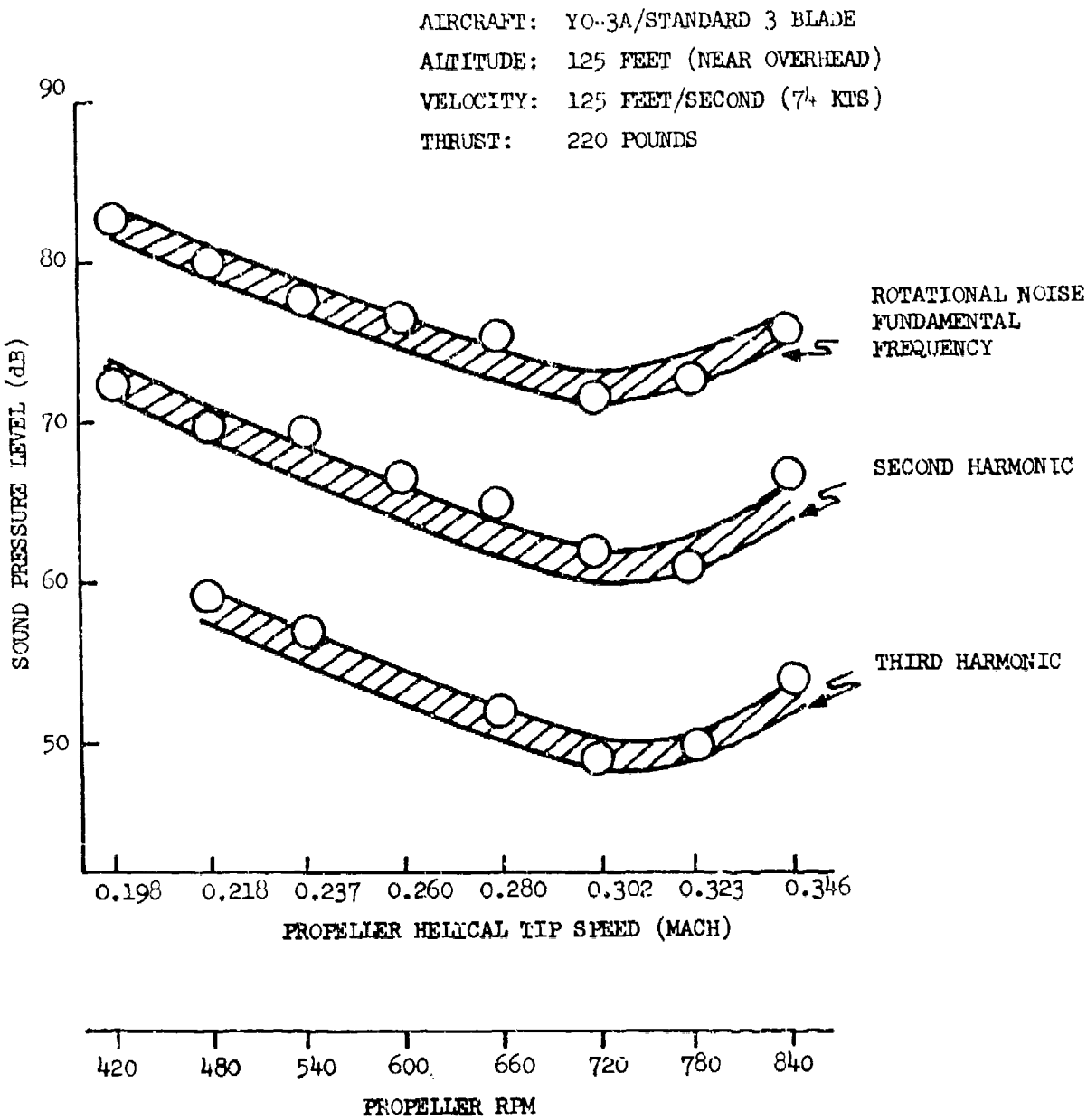


Figure 8 - Smoothed Trends of Propeller Rotational Noise

The uncertainties in aircraft position and propeller rpms are less of a problem in correcting one-third octave band plots for ground reflection and doppler shift phenomena due, primarily, to the wider bandwidth of the one-third octave filter compared to that of the narrow bandwidth analysis. Consequently, only minor errors in frequency are observed in these plots; however, broad dips in the continuous broadband spectra can be observed in the plots near the estimated destructive frequencies and presumably peak levels are influenced at constructive frequencies. Applied corrections smooth out the one-third octave band spectra but make identification of the exact frequency for peak levels uncertain. Thus, although the levels of measured broadband noise attributed to propeller vortex noise are considered of sufficient quality for the purpose of this study, they are not of sufficient quality to delineate trends in spectral shifts due to the conventional "Strouhal" shifts as propeller tip speed changes. This factor is considered of minor importance in the overall quality of the experimental data.

## 4. SUMMARY

The conclusion is that the quality of the corrected data from the fly-over experiments with the YO-3A aircraft is adequate for the development of empirical conditions to the Air Force computer program for prediction of propeller noise.

## SECTION III

## AIR FORCE PROPELLER NOISE COMPUTER PROGRAM

The Air Force Propeller Noise Computer Program was developed by Hamilton-Standard under contract to AFAPL and was reported in references 7 and 8 This program predicts near and far field propeller noise for low tip speed propellers, and, in addition, predicts aural detection range for assumed ambient background noise and atmospheric conditions. Of interest to the present study are the methods for predicting far field noise. These methods have been shown to be inaccurate by comparison of predicted propeller noise of quiet aircraft with measured field test data.

Specifically, the program predicts far field noise for both rotational and vortex components of low tip speed propellers. The rotational noise is divided into predictions of harmonic loading noise and thickness noise. These predictions are based on from parametric inputs such as propeller diameter, planform, number of blades, activity factor, thrust and aircraft velocity and altitude.

Parametric data from the October 1970 YO-3A tests were supplied to the Air Force by CALAC for tests with the standard 3 blade, acoustic 3 blade, and the standard 6 blade propellers. (These propellers are described in Appendix I. The Air Force produced predictions of propeller rotational noise and vortex noise for the overhead position at an altitude of 125 feet and for the fore and aft positions at ±45 degrees.

## SECTION IV

## COMPARISON OF MEASURED AND PREDICTED NOISE

The noise measured during the flyover tests with the variable pitch propellers proved to be most useful for making comparisons of measured and predicted noise. With these propellers, rpm (tip speed) was varied while holding thrust constant. Specifically, the parameters for these experiments were as follows:

Aircraft: YO-3A Observation Aircraft with standard 3 blade propeller

Aircraft Altitude: 125 Feet

Aircraft Velocity: 125 Feet/Second

Propeller RPM: 420 to 840

Propeller Helical Tip Speed: Mach 0.195 to 0.345

Thrust: 220 Pounds

The aircraft flying with the acoustic 3 blade propeller was tested over an rpm range from 660 to 780 while the fixed pitch standard 6 blade propeller was tested at 630 rpm which yielded the same 220 pounds of thrust. This series of tests provided noise data reflecting variation in propeller configuration, design and rpm (tip speed). Thus, measured and predicted results can be compared on the basis of absolute noise level, noise trends with tip speed, and, to some extent, propeller design parameters.

### 1. ROTATIONAL NOISE

Figure 9 is a comparison of the measured levels of the first three propeller rotational noise harmonics for the standard 3 blade propeller. In this figure sound is plotted against propeller tip speed. Propeller thrust, aircraft altitude and aircraft velocity are held constant. Measured levels and trends are shown to be in serious disagreement with predictions of the Air Force computer program.

The minimum levels of all three harmonics, for this propeller, occurs near a helical tip speed of approximately Mach 0.3. For higher or lower tip speeds the noise levels increase. Thus, a "bucket" is formed in the noise level vs. tip speed curve. Relative levels between harmonics remain approximately constant. To our knowledge, such bucket trends have not been previously obtained for this type of propeller noise. These trends were first observed in data from the October 1970 tests, and have been referred to as the "Quiet Airplane Paradox."

Predicted noise levels do not show this bucket trend but rather show constantly decreasing levels with decreasing propeller tip speed. Since the measured and predicted trends are different, a major modification of the Air Force computer program, based on a common parameter that predicts the minimum levels, is required.

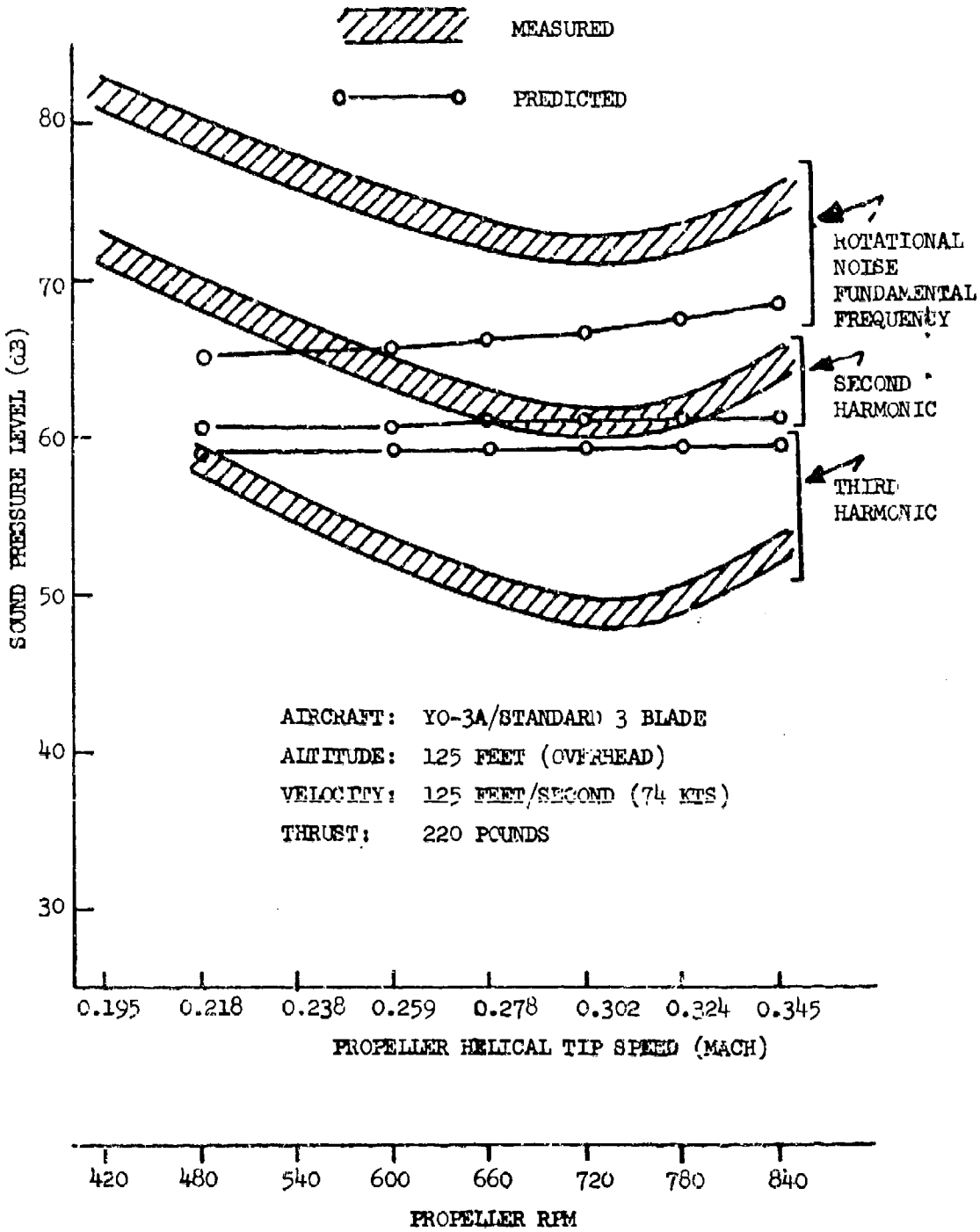


Figure 9 - Comparison of Measured and Predicted Rotational Noise (Standard 3 Blade Propeller)

Comparison of the measured and predicted rotational noise levels in Figure 9 shows that the predicted fundamental is several dB below the measured levels, the second harmonic is within a few dB and the third harmonid is several dB above the measured levels. Therefore, the modifications to the Air Force computer program must correct the absolute levels as well as the trends.

Figure 10 is a similar comparison of measured and predicted propeller rotational noise for the acoustic 3 blade propeller. The discrepancies shown are similar to those for the standard 3 blade propeller, but differ in magnitude. The modifications to the Air Force computer program must, therefore, account for these differences in magnitude as well as the bucket trend on the basis of differences in propeller configuration.

Figure 11 is a comparison plot for the single rpm and tip speed available for the fixed pitch standard 6 blade propeller. Discrepancies in levels for the fundamental rotational harmonic and for the second harmonic are similar to those noted for the standard 3 blade propeller at the given tip speed. The computer program modifications must also account for these differences in levels for this propeller.

Figure 12 is a comparison polar plot of the measured and predicted directivities of the fundamental rotational noise frequencies for both the standard 3 blade and acoustic 3 blade propellers. It can be concluded that the directivity factor in the Air Force computer program must be modified to provide more accurate results. The quality of measured data for the second and third rotational noise harmonics for the three blade propellers, and for any rotational noise harmonic for the six blade propeller was not adequate for comparison purposes.

2. VORTEX NOISE

The broadband noise observed in the acoustic signature of all propellers has a common spectral shape and bandwidth and is assumed, as discussed in the previous section, to be propeller vortex noise. These characteristics are illustrated in Figure 13. Spectral characteristics of corrected one-third octave band plots did not change appreciably with propeller tip speed. This plot shows the relative sound pressure level in dB as a function of one-third octave frequency band. These levels were averaged and normalized from band levels of corrected data over the entire tip speed range for the standard 3 blade propeller. Spectral data for the other two propellers show essentially the same characteristics. In all cases, the aircraft was in the overhead position.

Even though the shape of the observed vortex noise spectra does not change significantly over the range of propeller tip speeds investigated, spectral levels change in a manner similar to the levels of rotational noise. The levels of the 160 Hz one-third octave band, shown to represent the spectral peak levels in Figure 13, were adjusted for absolute level using the standard 3 blade propeller shown in Figure 14. A bucket shaped curve with the familiar trend observed for rotational noise results. This trend suggests that vortex noise level modification to the Air Force computer program may include a simple

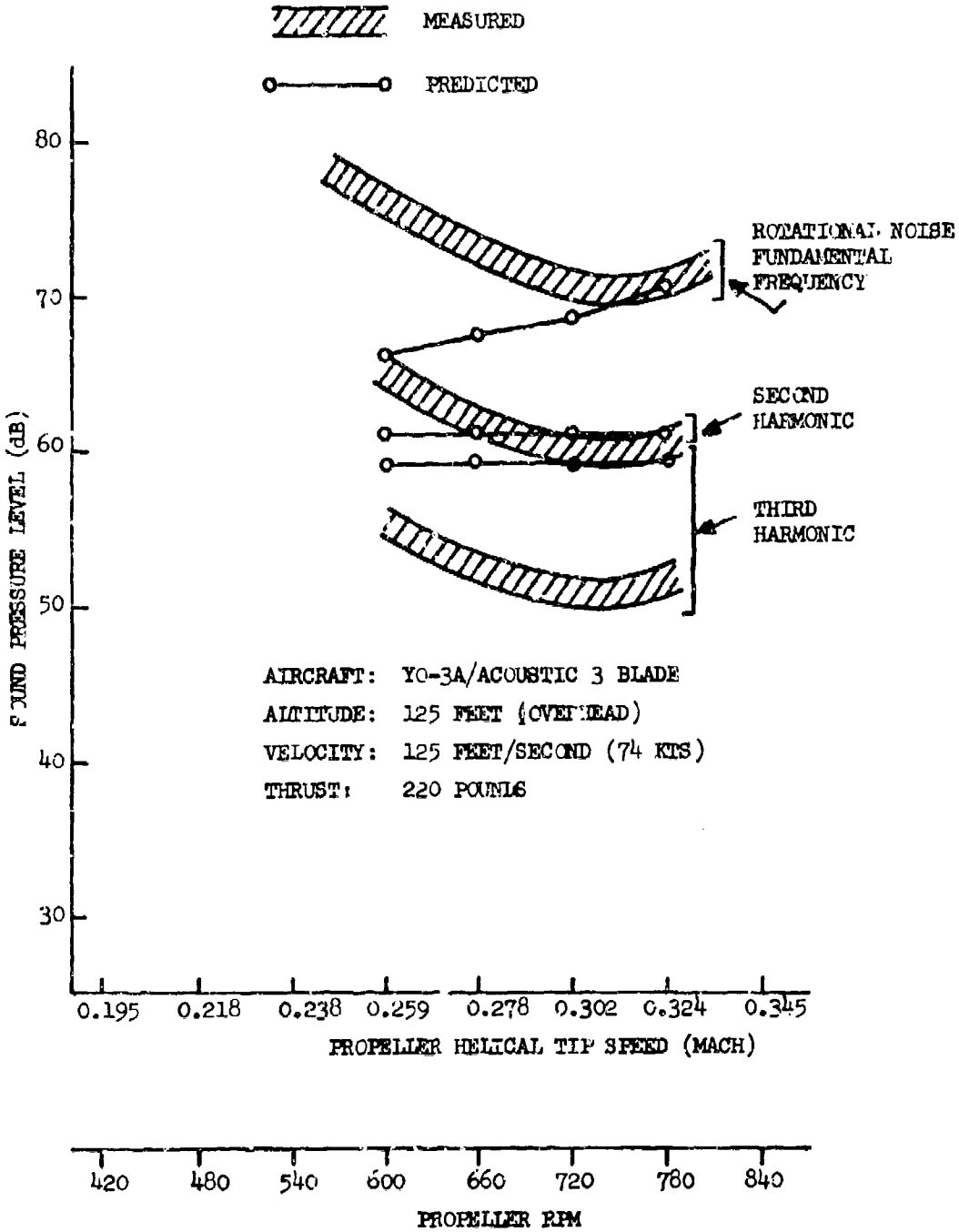


Figure 10 - Comparison of Measured and Predicted Rotational Noise (Acoustic 3 Blade Propeller)

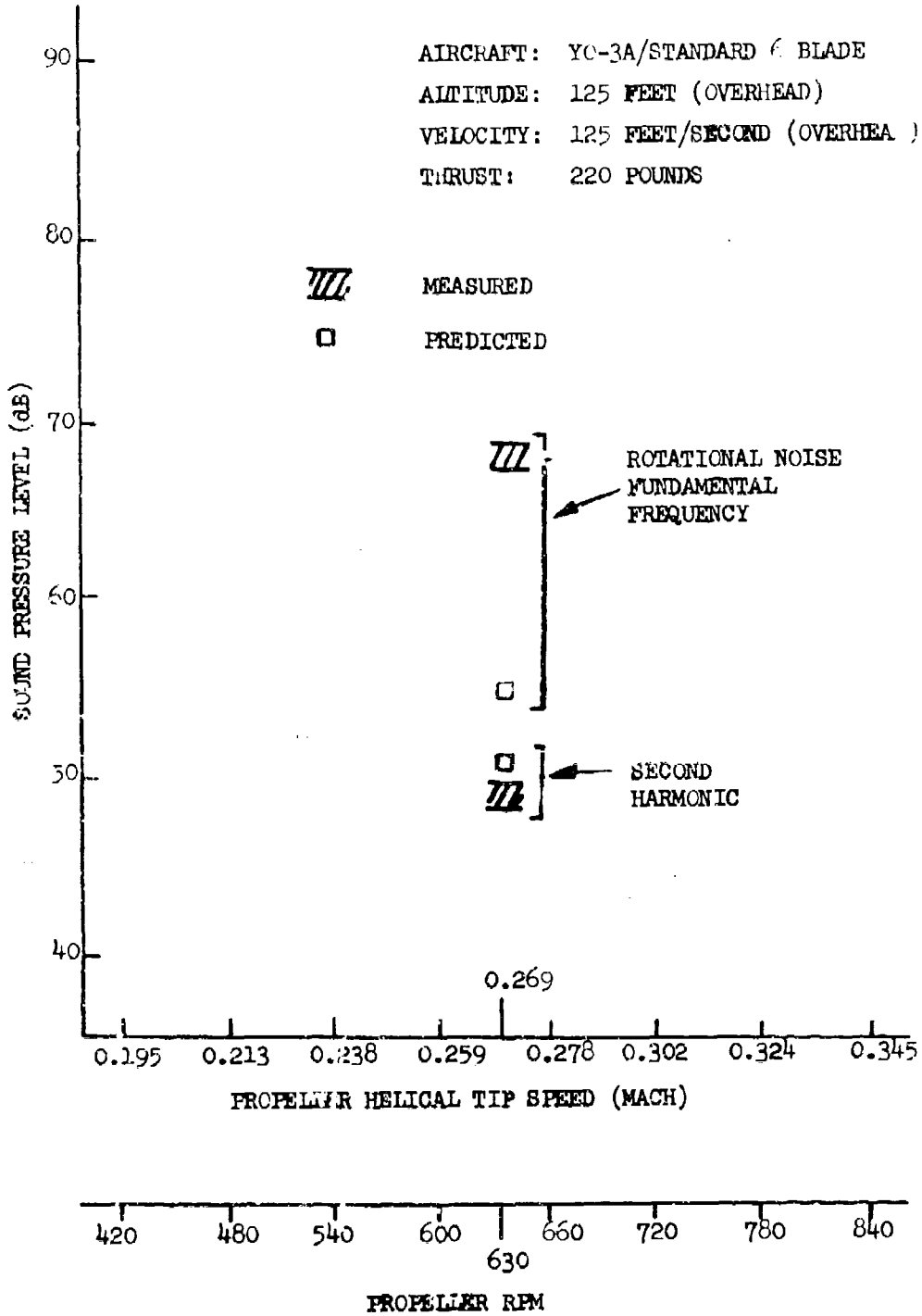


Figure 11 - Comparison of Measured and Predicted Rotational Noise (Standard 6 Blade Propeller)

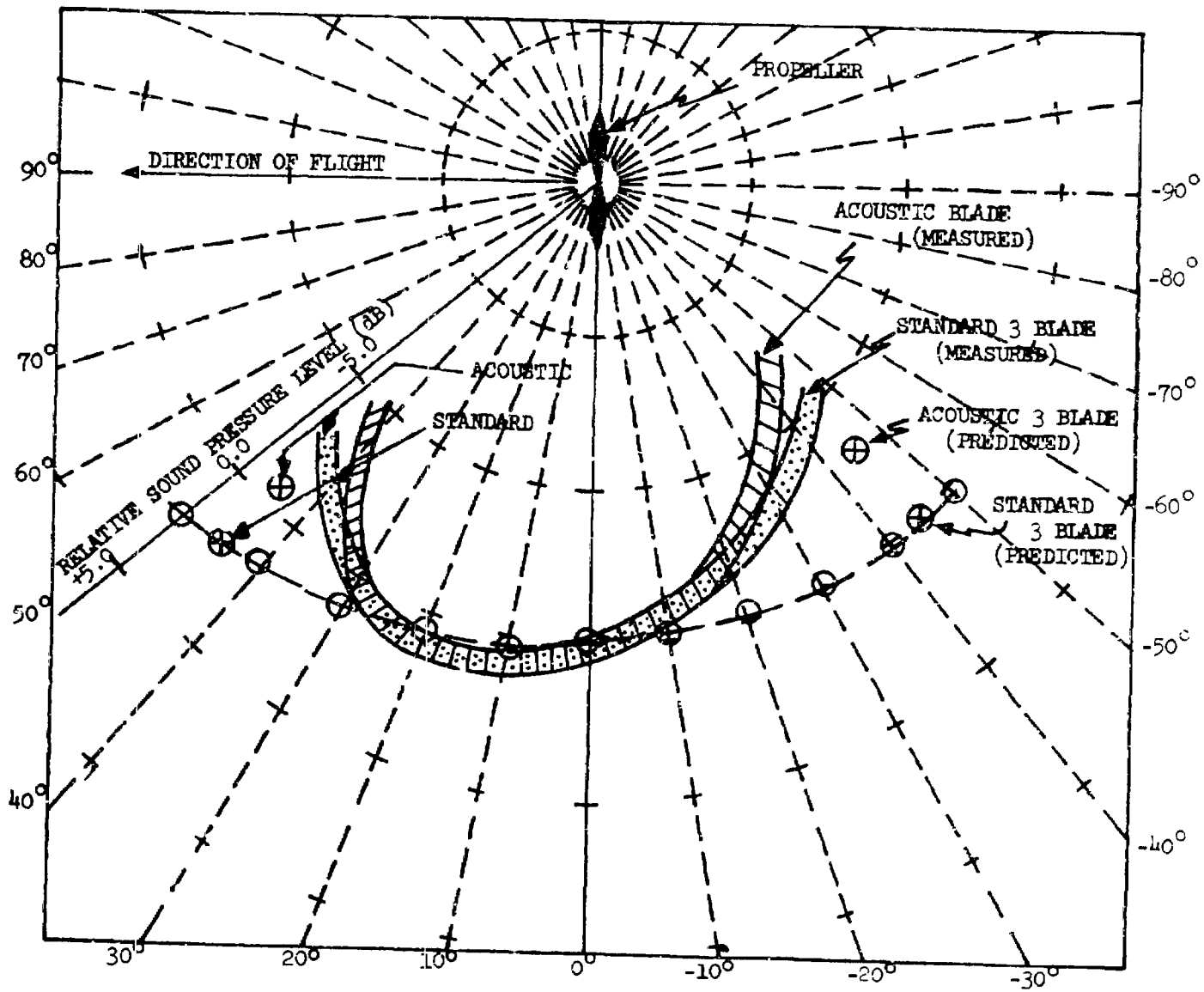


Figure 12 - Comparison of Measured and Predicted Directivity
(Standard and Acoustic 3 Blade Propellers)

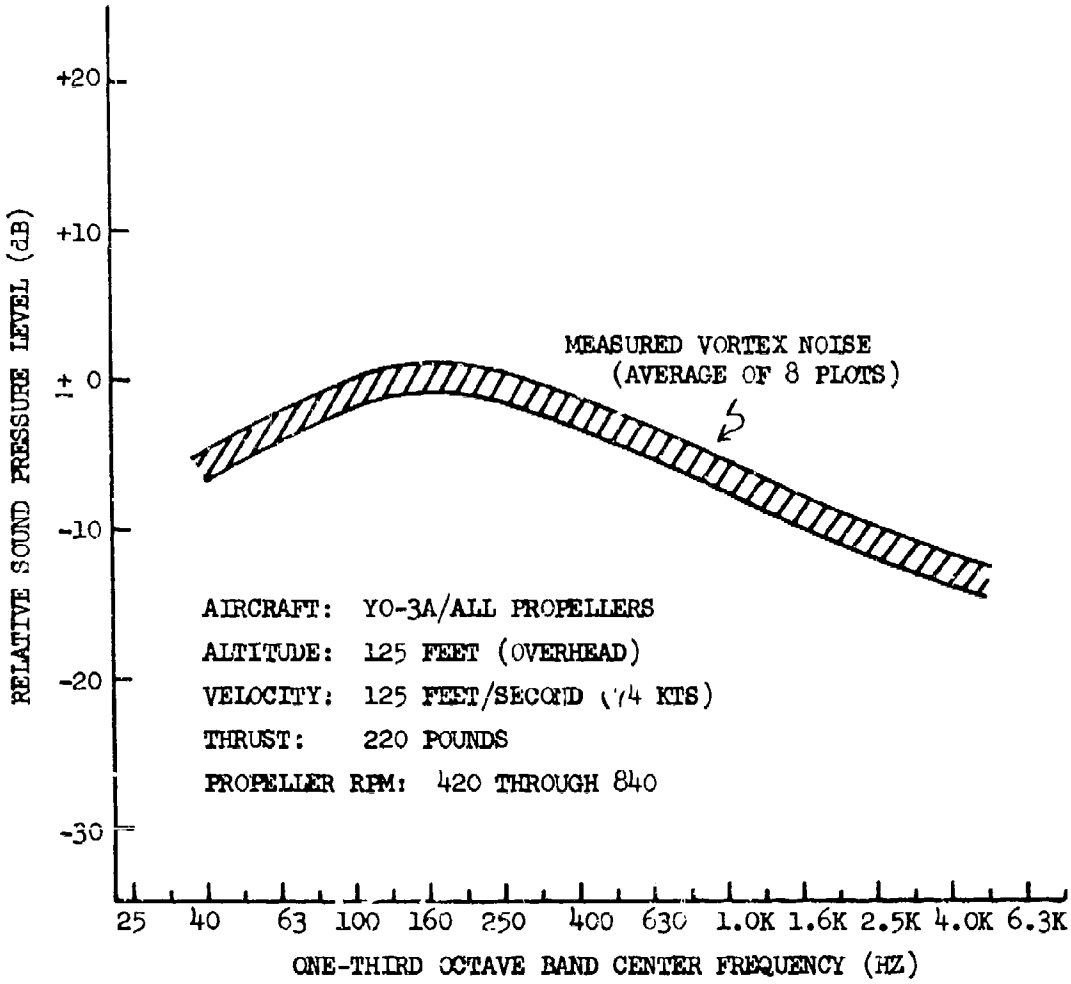


Figure 13 - Measured Vortex Noise for Propellers
With Tip Speeds Between Mach 0.2 and 0.4

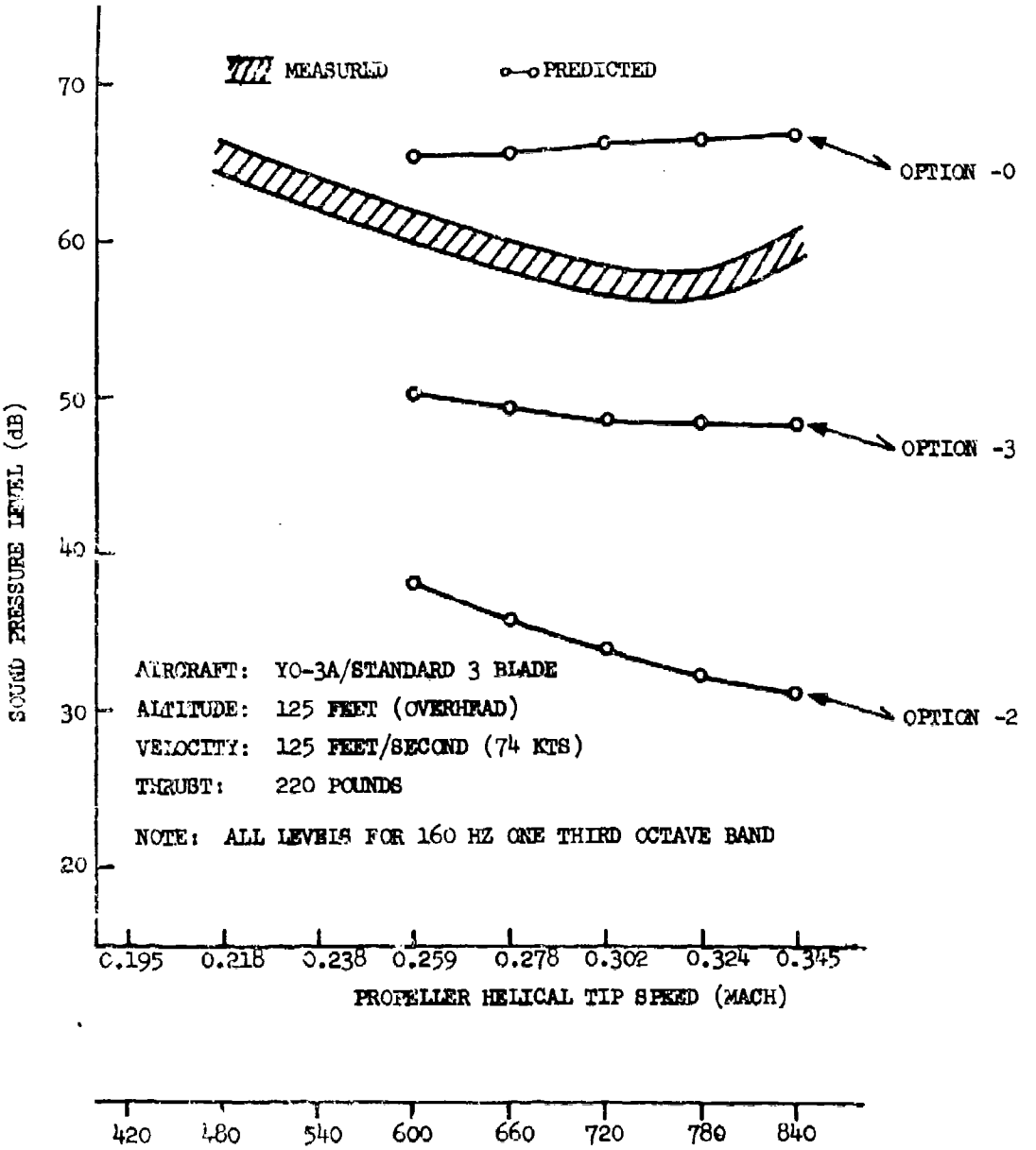


Figure 14 - Comparison of Measured and Predicted Vortex Noise (Standard 3 Blade Propeller)

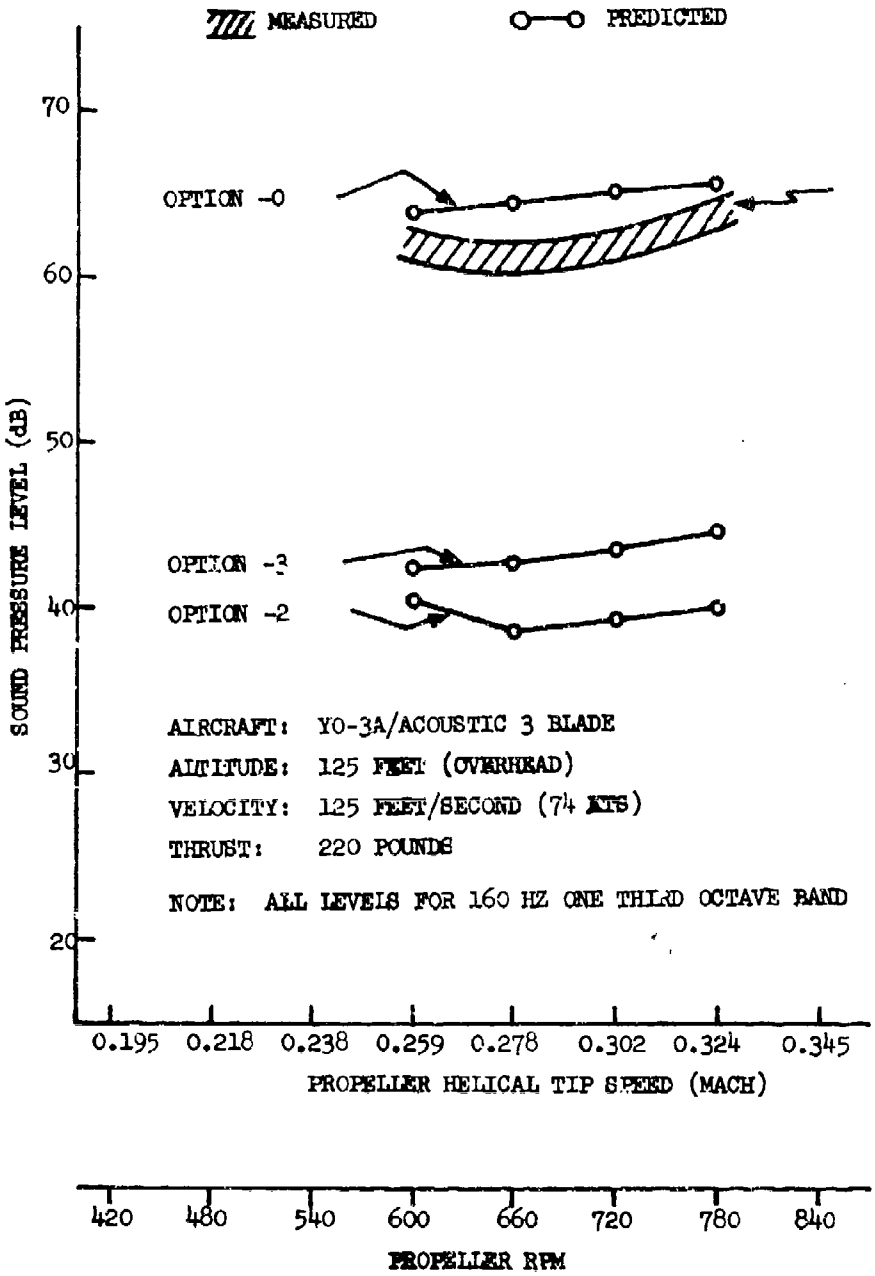


Figure 15 - Comparison of Measured and Predicted Vortex Noise (Acoustic 3 Blade Propeller)

relationship based on the rotational noise level. This figure also compares the measured vortex noise levels to predicted levels in this same band. Wide disagreement in measured and predicted levels is shown for all three vortex noise options. Data for the acoustic 3 blade propeller, Figure 15, shows similar results.

To show the wide disagreement in measured and predicted one-third octave band spectral characteristics, Figures 16, 17, and 18 are presented for the standard 3 blade, the acoustic 3 blade, and the standard 6 blade propellers, respectively. In addition to incorrect levels, the Air Force computer program does not accurately predict the peak frequency of the broadband vortex noise.

Figure 17 shows an unexpected and unexplained rising trend at the higher frequencies from approximately 1000 to 5000 Hz. The cause of this high frequency noise is not known but was observed in all flights of the acoustic 3 blade propeller installed on either the YO-3A or Q/STAR aircraft. This anomalous noise trend was not considered in development of empirical modifications for the Air Force computer program.

## 3. SUMMARY

Comparison plots of measured and predicted noise levels, spectra, and directivities revealed major discrepancies between these two forms of data. Resolution of these differences requires extensive modification of the Air Force computer program.

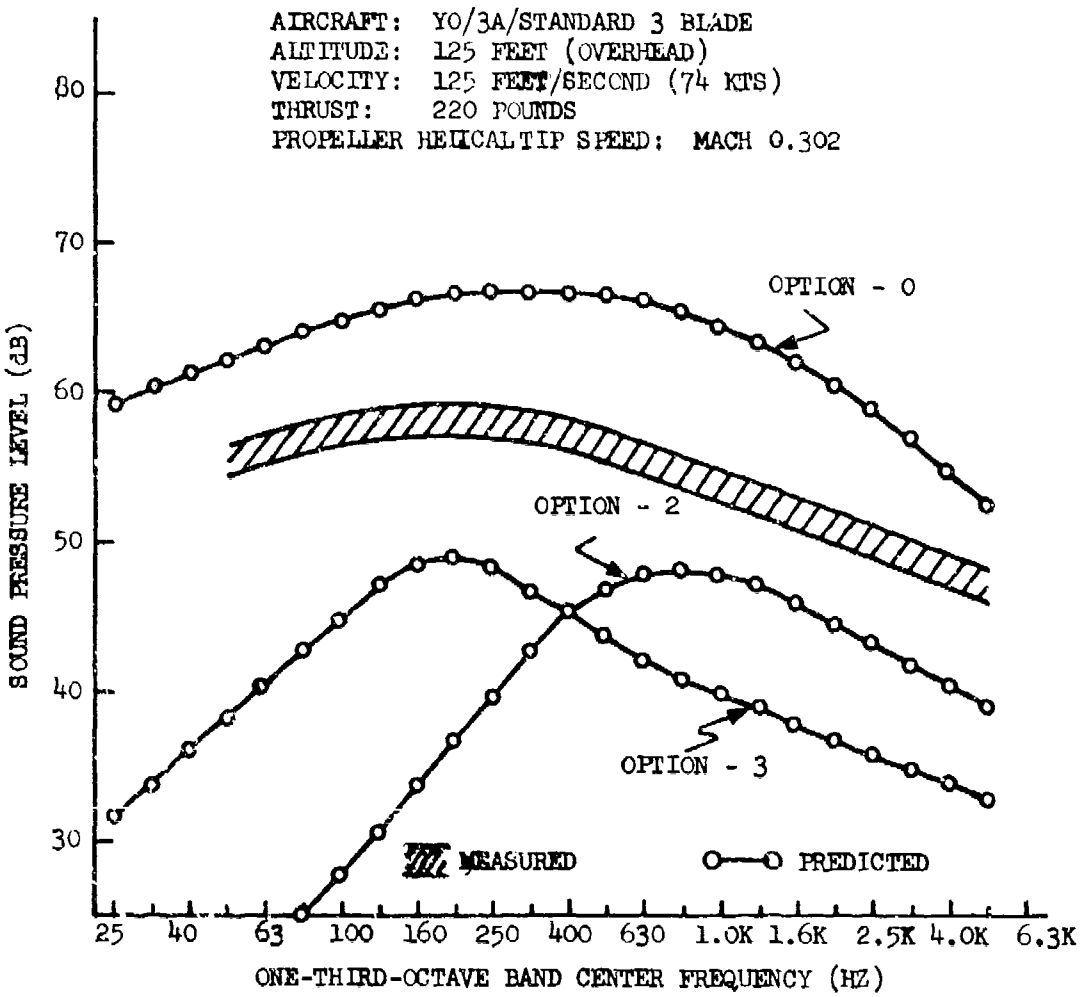


Figure 16 - Comparison of Measured and Predicted Vortex Noise Spectra (Standard 3 Blade Propeller)

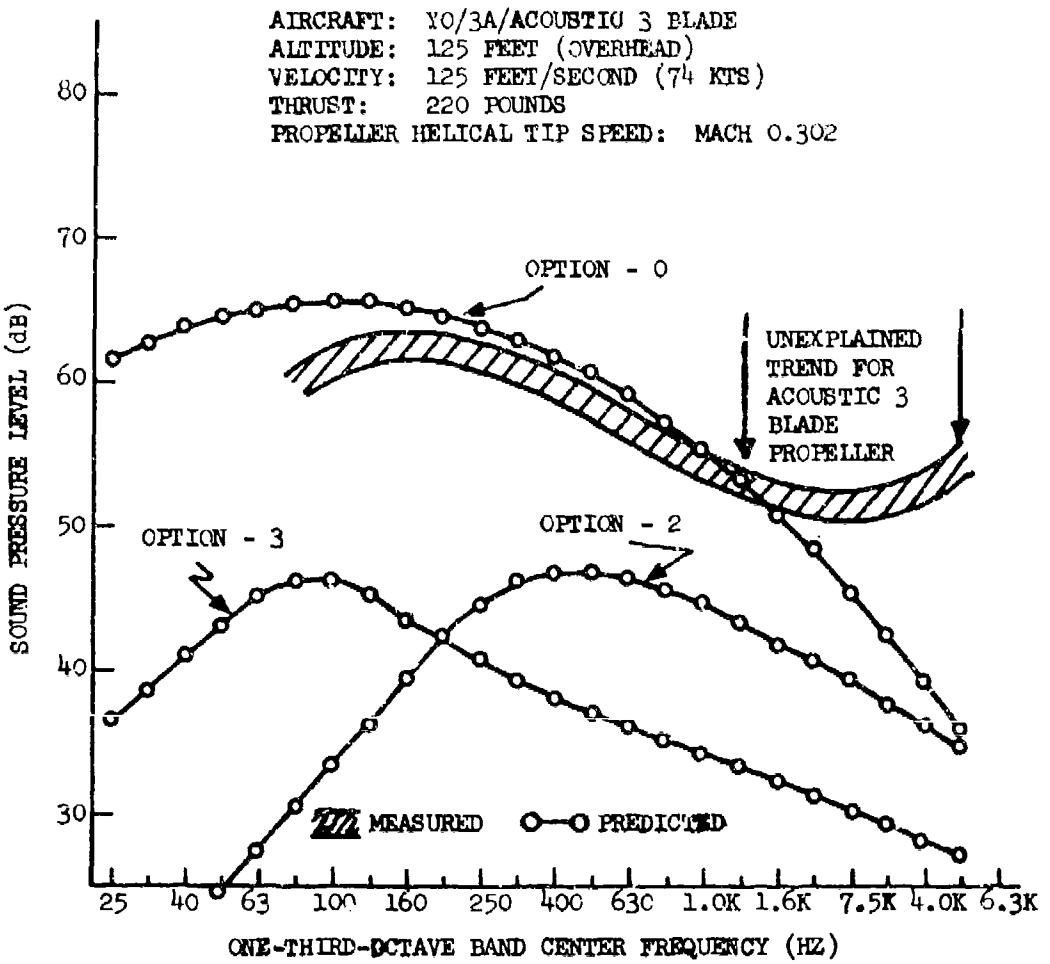


Figure 17 - Comparison of Measured and Predicted Vortex Noise Spectra (Acoustic 3 Blade Propeller)

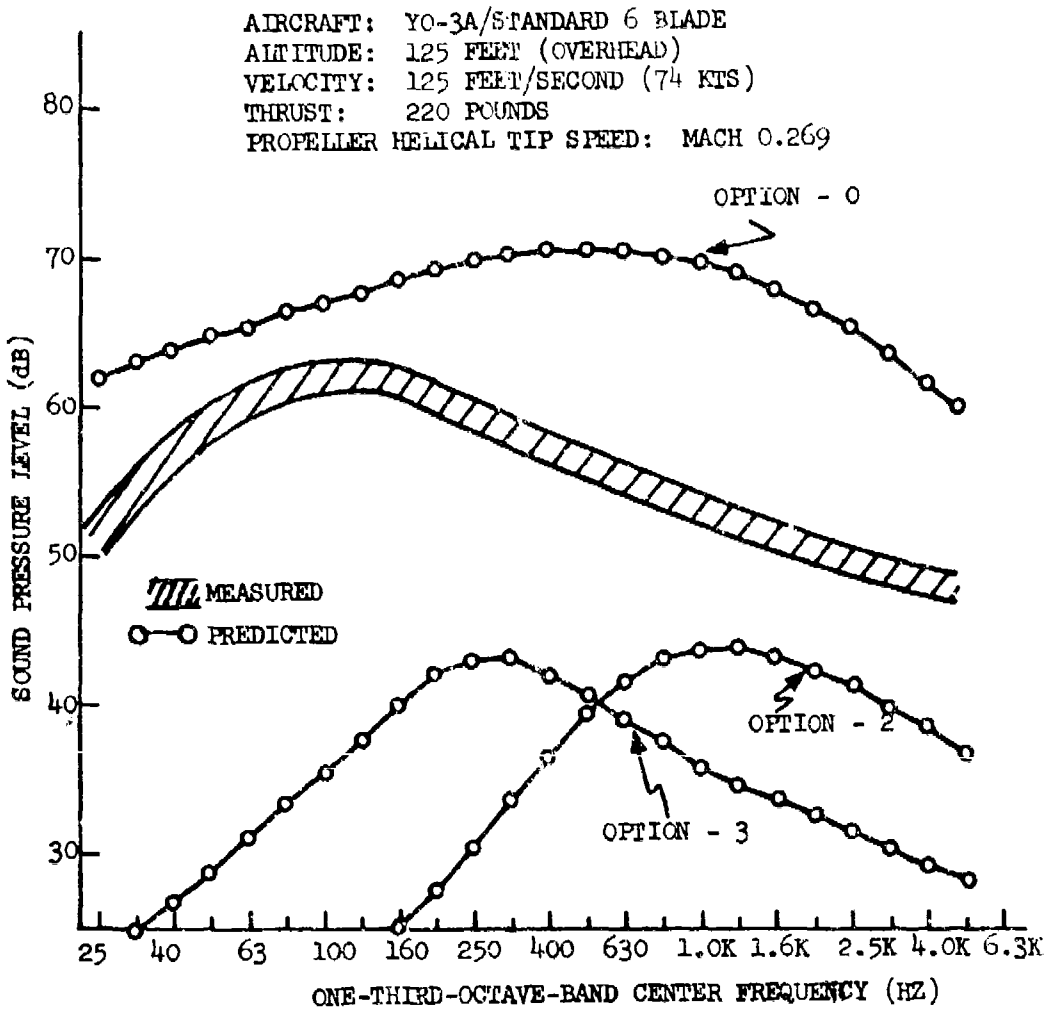


Figure 18 - Comparison of Measured and Predicted Vortex Noise Spectra (Standard 6 Blade Propeller)

## SECTION V

## THEORETICAL REVIEW

A major effort in this study was a thorough review of the underlying theory for the prediction of propeller noise. This review included investigation of discrepancies in measured and predicted data and an assessment of potential factors causing these discrepancies. A detailed summary of this effort is given in Appendix IV.

The theoretical review consists of two parts: (1) rotational noise analysis at low tip speeds and (2) vortex noise analysis. The major portion of this effort is directed toward the rotational noise for which the "bucket" in the SPL curve vs. rpm is regarded as more baffling than for the vortex noise case. Four effects were considered: (a) blade aerodynamics, (b) non-uniform inflow through the propeller, (c) chordwise blade loading, (d) propeller blade wake/wing interaction.

### 1. THEORETICAL REVIEW OF ROTATIONAL NOISE

#### a. Blade Aerodynamic Effects

It was suspected that the propeller blade aerodynamic model of Reference 8 may be inadequate to predict thrust and torque distributions at low tip speeds where the blade section lift coefficients must increase (inversely as rpm squared) to maintain a constant propeller thrust. Simultaneously, the Reynolds number based on blade chord and relative velocity is decreasing, which leads to increased drag and reduced lift for a given blade section angle of attack. To maintain the same blade lift, the blade angle of attack must be increased, resulting in further increases in the blade section drag. In an aerodynamic force system, the lift is perpendicular to the relative wind vector; therefore, the thrust and torque force per unit radius are related to the unit blade lift and drag according to blade element theory (Reference 11) as follows:

$$\frac{dT}{dr} = \frac{dL}{dr}\cos\alpha_{av} - \frac{dD}{dr}\sin\alpha_{av} \quad \text{(Thrust)} \tag{3}$$

$$\frac{dQ}{dr} = r\,\frac{dF_\varphi}{dr} = r\left(\frac{dD}{dr}\cos\alpha_{av} + \frac{dL}{dr}\sin\alpha_{av}\right) \quad \text{(Torque)} \tag{4}$$

where $\alpha_{av}$ is the blade advance angle defined by

$$\tan\alpha_{av} = \frac{V_\infty(1 + usb)}{\Omega r\,(1 - omsb)} \tag{5}$$

where $\Omega$ is the propeller rotational angular speed and r is the local propeller radius, $V_\infty$ the forward speed, and usb and omsb are slipstream corrections to linear and angular velocity. Appendix IV contains detailed discussions of slip

stream effects using two different approaches.

As $\Omega$ decreases, the advance angle increases for a given forward speed, causing a further reduction of thrust and an attendant increase in required torque force. Likewise, to maintain thrust at a large advance angle, the lift on the blade must be further increased by means of increased blade angle of attack. In view of a need to independently assess the above factors, a general aerodynamic blade loading mathematical model was developed, which is capable of matching any given propeller thrust with specified power or blade efficiency.

The results of the aerodynamic blade load study are shown in Figures 19 and 22 where it is found, for a given rpm, that predicted axisymmetric rotational SPL, when plotted vs. propeller horsepower is nearly a universal curve for all kinds of aerodynamic parameter variations (camber lift, blade angle of attack, friction drag level, etc.). Figure 21 shows the propeller power required vs. propeller efficiency at the required 220 lb. thrust. Figure 22 shows the variation of predicted axisymmetric SPL with rpm at 220 lb. thrust; the shaded band of the present CALAC axisymmetric theory reflects possible variations in propeller efficiency and, hence, variations in required horsepower at each rpm. The aerodynamic blade load mathematical model used in the present prediction method for axisymmetric acoustic radiation produces essentially the same rotational noise vs. rpm trend (Figure 22) as does the USAF Computer Program of Reference 7 . The difference in absolute levels is because Reference 7 employs an empirical correction to the axisymmetric theory which is based on static propeller noise test data. It is noted in Appendix IV that numerical integration differences cause negligible errors. Figure 19 shows the envelope of estimated YO-3A propeller efficiencies for three rpm values. A slight bucket tendency in the SPL vs. rpm curve (Figure 22) between 600 and 480 rpm might be inferred from the efficiency data of Figure 19 if it is assumed that the propeller efficiency at 480 rpm is near the lower range of possible values. The estimated propeller efficiency for the YO-3A from Reference 3 is somewhat in doubt at 480 rpm; however, it would appear to range between 40% and 50%. Figures 21 and 23 display the range of predictions, for the YO-3A standard 3 blade propeller, of horsepower and efficiency, as obtained from several sources: the YO-3A project data (Reference 3 ), the USAF Computer Program (Reference 7 ) and the first of present methods, wherein the induction efficiency $\eta_a$ was parametrically varied. The induction efficiency provides, for propeller theory, the counterpart of the induced drag associated with trailing vortices in the theory of wings of finite span, Reference 11. The induction efficiency is further discussed in Appendix IV. The suitability of the choice of induction efficiencies in the present theory is justified by its usefulness as a parameter in matching the LMSC YO-3A horsepower and efficiency data of Reference 3 , as can be seen in Figures 21 and 23.

It is noted in Figure 23 that the USAF/Hamilton Standard (Reference 8) propeller efficiencies are much higher than the values obtained from the YO-3A flight test report (Reference 3 ). Because the induction efficiency is related to the trailing vortex system, an approximate lifting line theory calculation

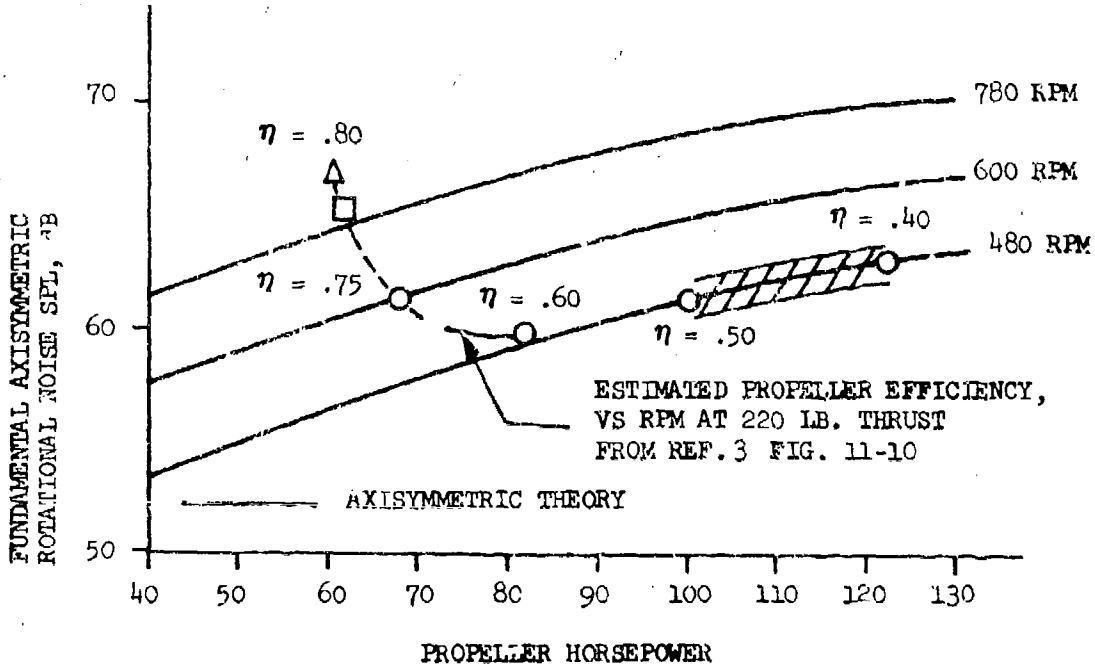


Figure 19. Fundamental Axisymmetric Rotational Noise SPL vs. Horsepower at Various RPM

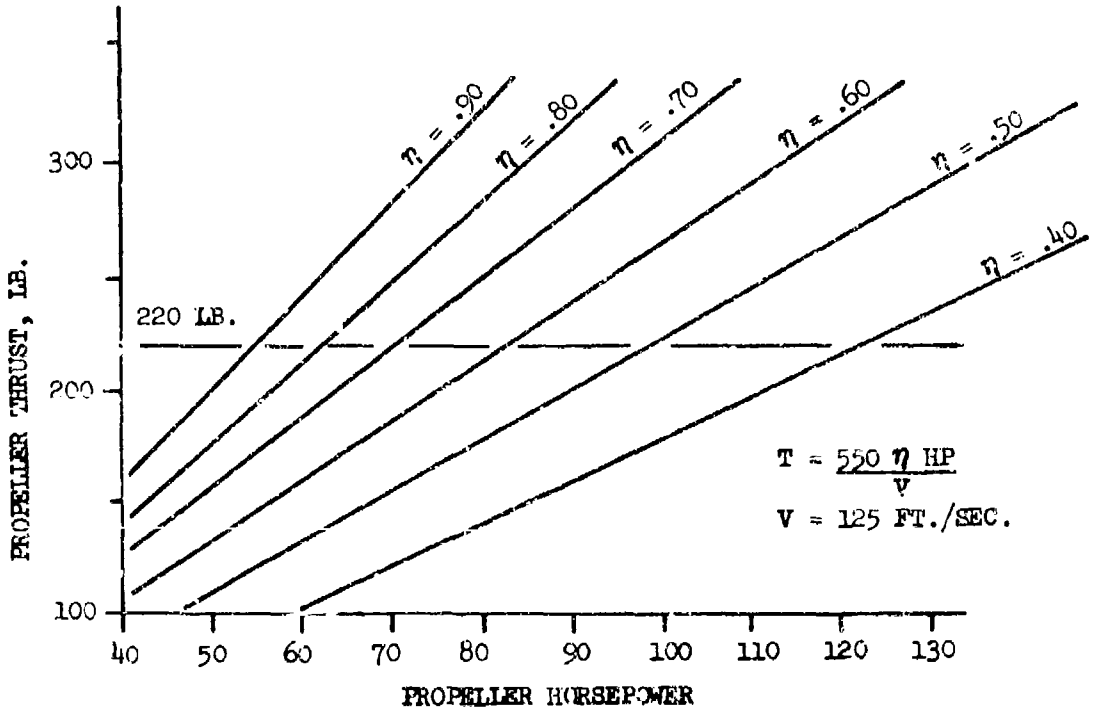


Figure 20. Propeller Thrust vs. Horsepower at Various Efficiencies at 125 Ft./Sec. Forward Speed

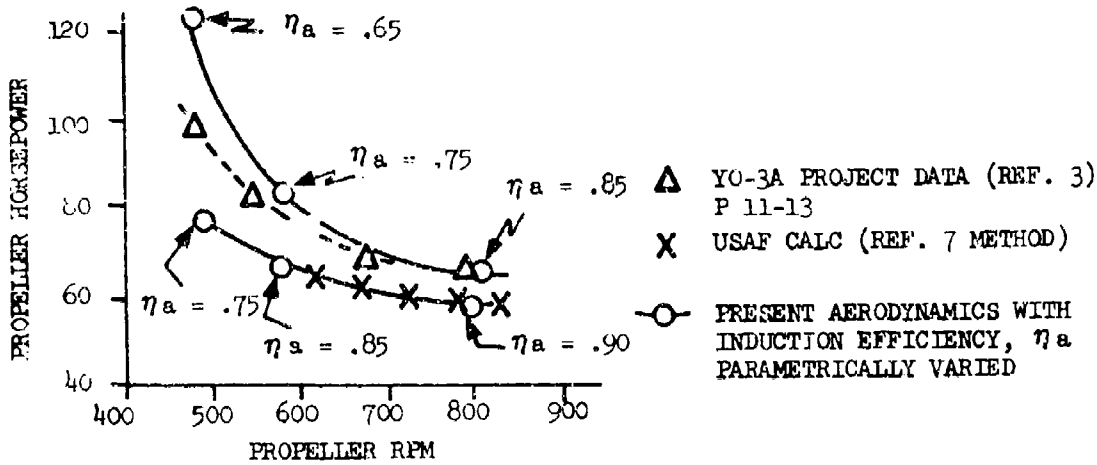


Figure 21. Propeller Horsepower vs. RPM for Various Induction Efficiency Assumptions and Comparisons with YO-3A Data

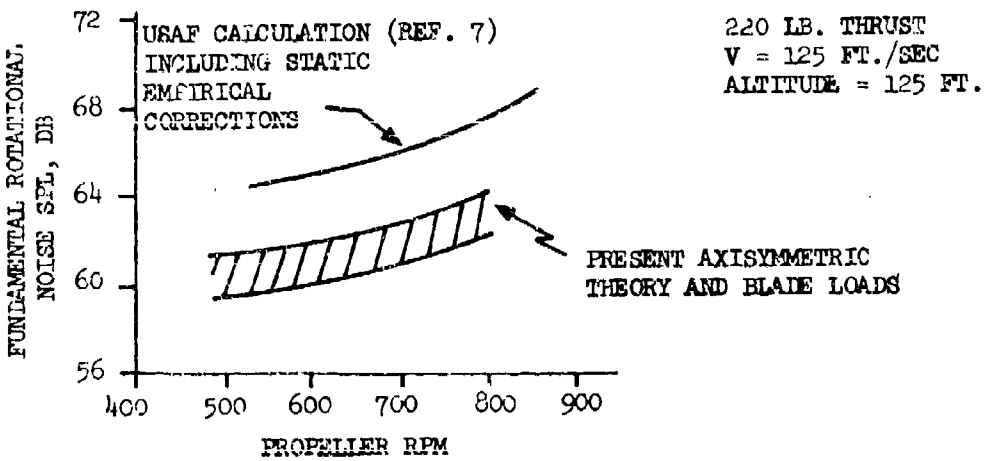


Figure 22. Comparison of Calculated Fundamental Rotational Noise SPL Values for Axisymmetric Noise With and Without Static Empirical Corrections vs. RPM; Comparison with YO-3A Data and USAF Calculation

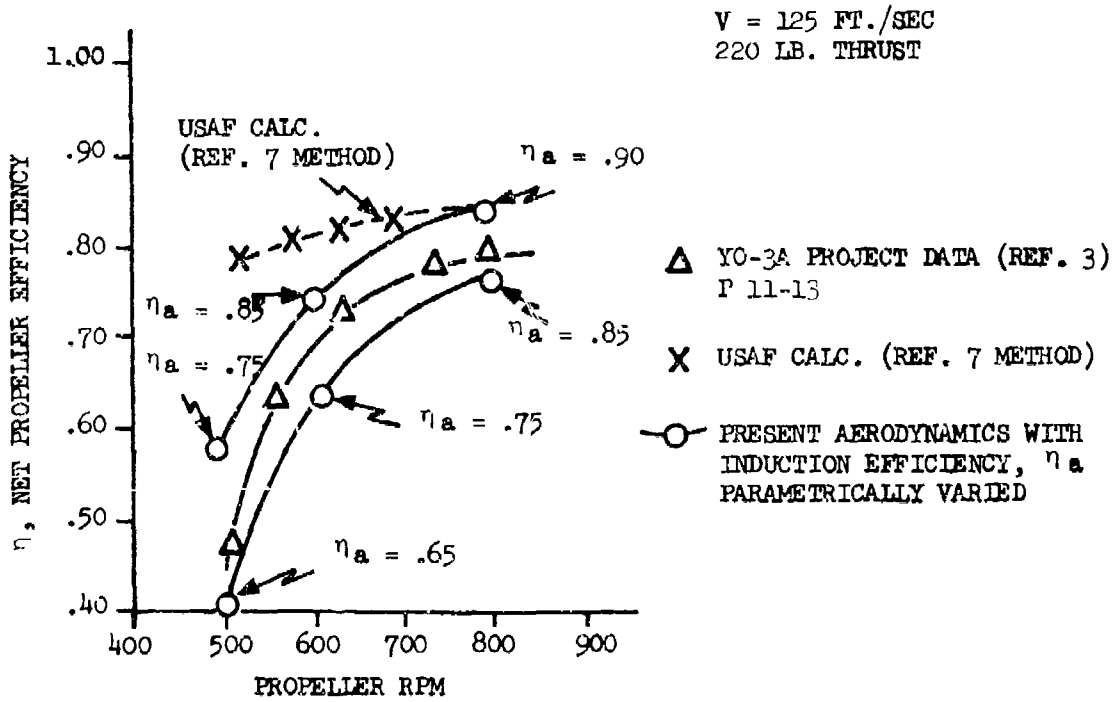


Figure 23. Estimated Net Propeller Efficiency vs. RPM for Various Induction Efficiency Assumptions vs. RPM; Comparison With YO-3A Data and USAF Calculation

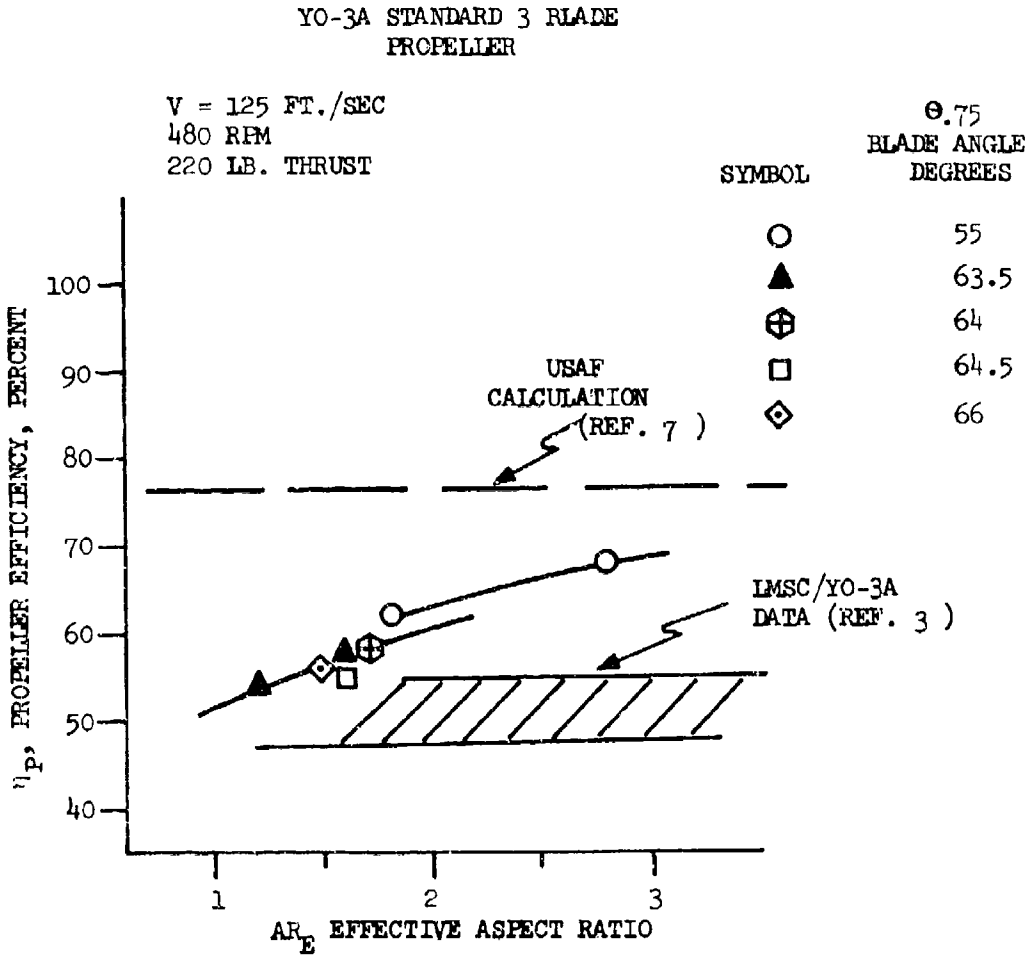


Figure 24. Propeller Efficiency vs. Effective Aspect Ratio of Propeller Blade

(Reference 12) was performed, as a second method to provide an independent check. This second method uses an effective propeller blade aspect ratio concept (see Appendix IV). The geometric aspect ratio is 3 which is, therefore, an upper limit . The resulting propeller efficiency at 480 rpm is plotted vs. effective aspect ratio in Figure 24. The effective aspect ratio is determined by an iterative downwash matching procedure described in Appendix IV. It is found that the propeller blade effective aspect ratio is 1.7 yielding a propeller efficiency of 58% (Table I).

TABLE I

| Source | Thrust | Efficiency | HP | Fundamental Rotational SPL, dB |
|---|---|---|---|---|
| USAF (Ref. 7 ) | 220 | 76% | 66 | 57* |
| YO-3A/LMSC (Ref. 3 ) | | 50% | 100 | 62 |
| Present Lifting Line Theory | | | | |
| $AR_e$ = 1.7 | | 58% | 86 | 60 |
| 3.0 | | 69% | 73 | 58 |

*Not including empirical corrections for static test results

It is seen that the present rotational SPL results are 3 dB higher than the USAF results on a basis of HP (this comparison excludes the empirical corrections in the USAF/Hamilton Standard method which are included in the USAF/Hamilton Standard data of Figure 22). It is noted from Table I above that since $AR_e$ must be less than 3, the propeller efficiency could not exceed 69%. It is noted that the present lifting line results are much closer to the propeller efficiency data obtained from the YO-3A flight test performance report, and, despite some uncertainty about lifting line theory for such low aspect ratios, it is seen that even by assuming a 100% span loading efficiency ($AR_e$ = 3) one predicts much lower efficiency (69%) than is calculated in the USAF computer program.

While the 3 dB difference in axisymmetric SPL is only a small part of the empirical discrepancy, it will be seen later that the deterioration of propeller blade efficiency has a much more significant role through the enhancement of the circumferential non-uniformity of the blade loading.

b. Blade Non-Uniform Inflow Effects

The effects of non-uniform inflow which produce circumferentially non-uniform loads are analysed in detail in Appendix IV. The basic causes are (1) the velocity field induced by the wing lift circulatory flow producing both upwash and backwash velocity components, and (2) the propeller disc angle of attack upwash component. These upwash and backwash velocities, when expressed

in cylindrical coordinates in the propeller disc plane, provide circumferential and axial flow components which vary around the circumference of the propeller disc. The circumferential changes of inflow velocities produce changes in thrust and torque forces, via changes the dynamic pressure (based on relative blade velocity) and via changes in the blade angle of attack. These circumferential changes in thrust and torque are then expressed as a complex Fourier series which allows use of existing theory (Morse and Ingard Reference 13) for non-uniform loading (NUL) effects.

The basic results of the inflow non-uniformity effects are given in Figure 25. These are considered the most important results of the theoretical study. The solid curve labeled "present axisymmetric theory" also includes an improved chordwise blade loading solidity factor to be discussed below. The top solid curve shows that the effect of inflow non-uniformities on loading produce a 8 to 14 dB increase of absolute levels, compared to axisymmetric theory and 5 to 6 dB of the "bucket" noise level differential. The comparison between experimental data and the top dashed curve shows good agreement. This indicates that the propeller blade wake/wing interaction effect which, in combination with the inflow non-uniformities, very nearly accounts for the entire "bucket" in the SPL vs. rpm curve at constant thrust speed and at 125 ft. altitude. At low rpm, the inflow non-uniformity (e.g. "loading harmonics") increases relative to high rpm values, which explains most of the measured 7 dB increase above the bottom of the "bucket." As discussed in Appendix IV (Section 2b(3)(a)) non-axisymmetric radiation efficiency increases greatly over axisymmetric radiation efficiency which is characterized by circumferential destructive interference. This leads mathematically to higher order Bessel functions which are small in magnitude at low tip Mach numbers.

Analysis of the loading harmonic data (see Figure 26 and 27) which was used in generating Figure 25 shows that the first loading harmonic (the coefficient of $\sin \varphi_1$) is by far the dominant term. Furthermore as shown in Figures 28 through 30 the loading harmonics increase with decreasing rpm in a manner which correlates as a function of the blade lift coefficient. This correlation provides a rational basis for using the blade lift coefficient as a parameter for correlating the empirical corrections to the USAF computer program.

Figure 31 shows the increment in SPL due only to non-uniform load (NUL) effects. This was obtained by taking fully into account the radial variation of the loading harmonics. Figure 32 shows the results of an alternative approximate calculation of NUL effects, obtained by calculating the first two loading harmonics (LH) at only a single radial position, $(r/r_t)_{LH}$. It is found that a value of $(r/r_t)_{LH}$ of about .55 would nearly duplicate results which account for the radial variation of the LH. Figure 33 shows a correlation of the $\Delta$SPL due to non-uniform loading as a function of the first torque loading harmonic, $b_{1\varphi}$. Also shown is a simple analytical approximation valued for small values of wave number times radius. The result is

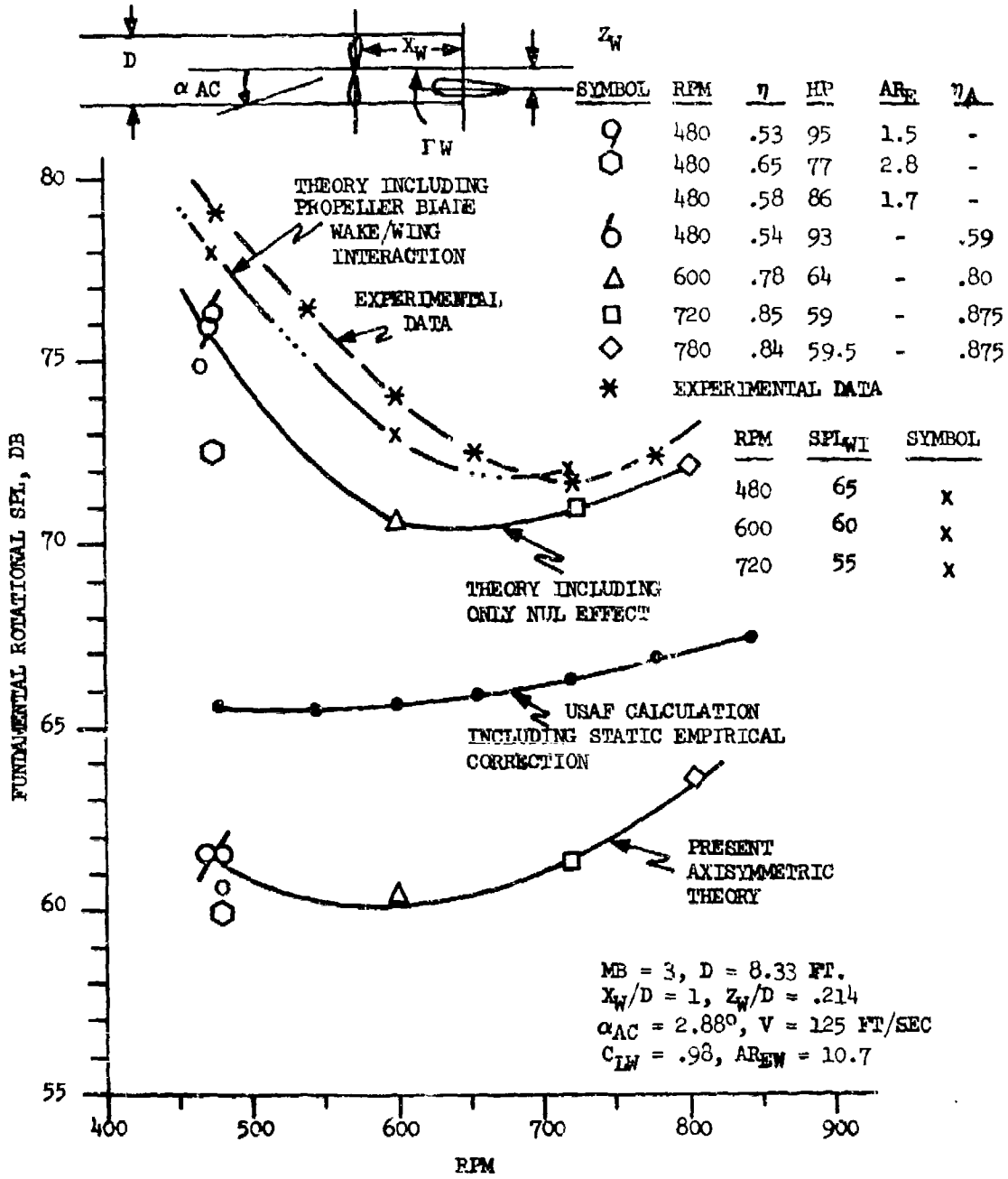


**Figure 25.** Fundamental Rotational Noise SPL vs. RPM at 220 Lb. Thrust; Comparison of Experimental Data vs. Non-Uniform Loading (NUL) Theory for YO-3A Standard Three Blade Propeller

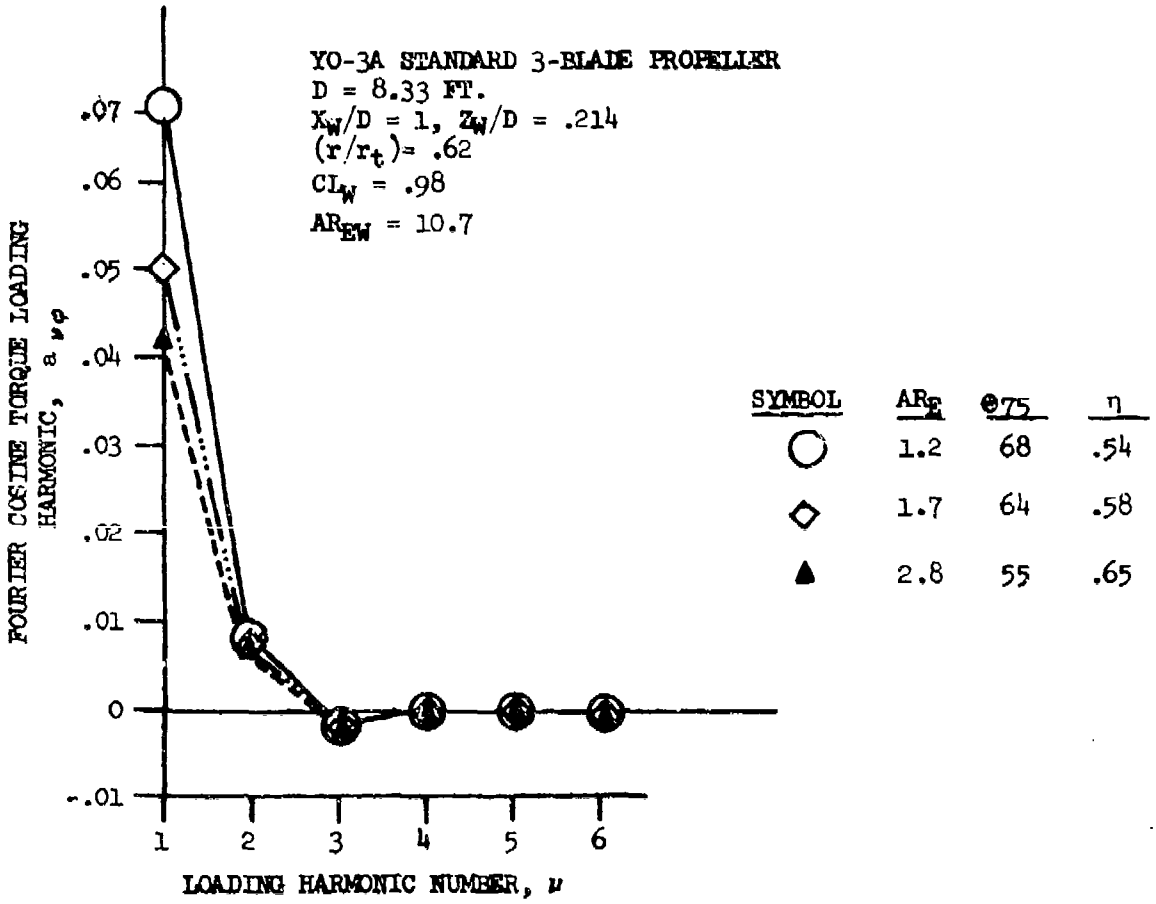


Figure 26. Fourier Cosine Torque Loading Harmonic, $a_{\nu\varphi}$ vs. Loading Harmonic Number, $\nu$

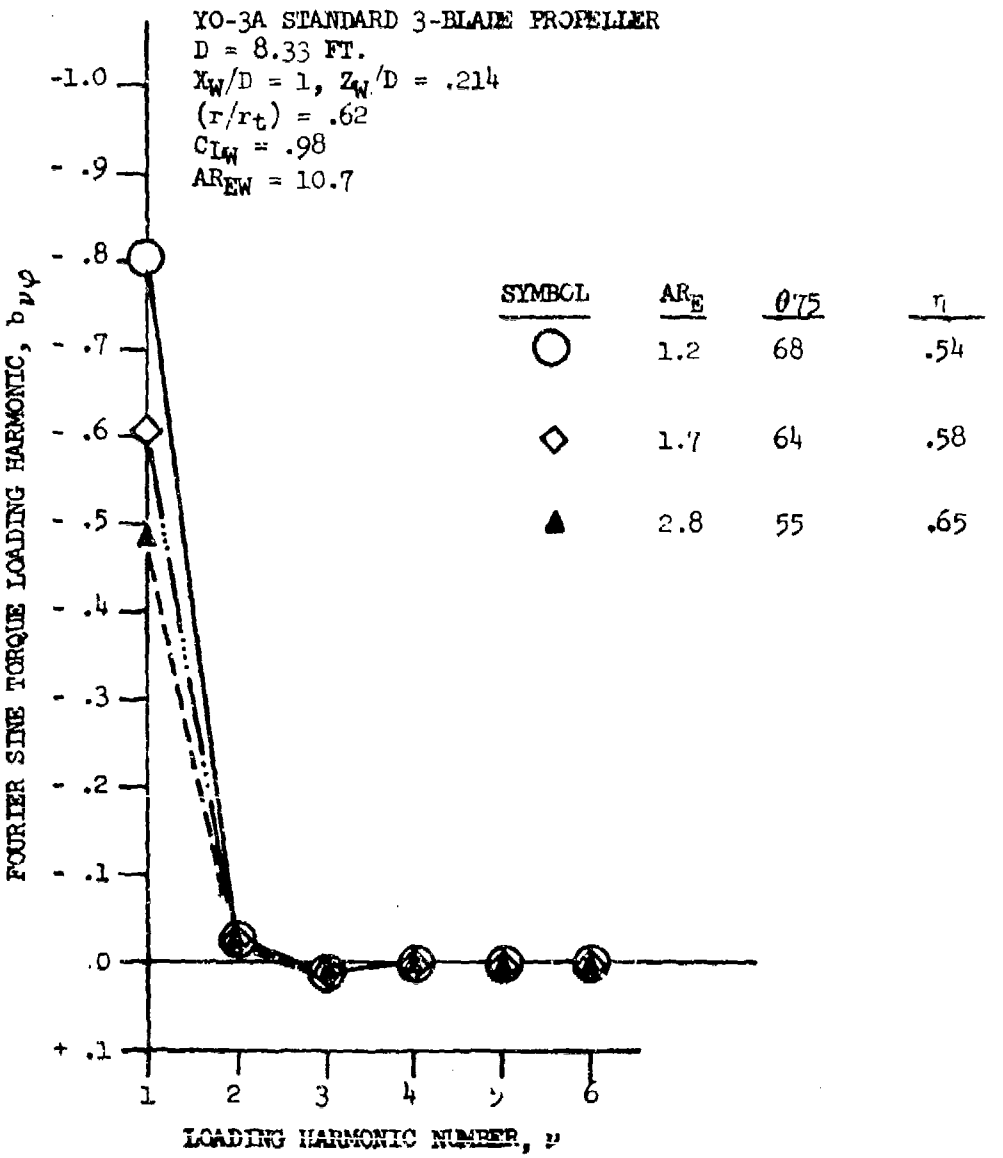


Figure 27. Fourier Sine Torque Loading Harmonic, $b_{\nu\varphi}$ vs. Loading Harmonic Number

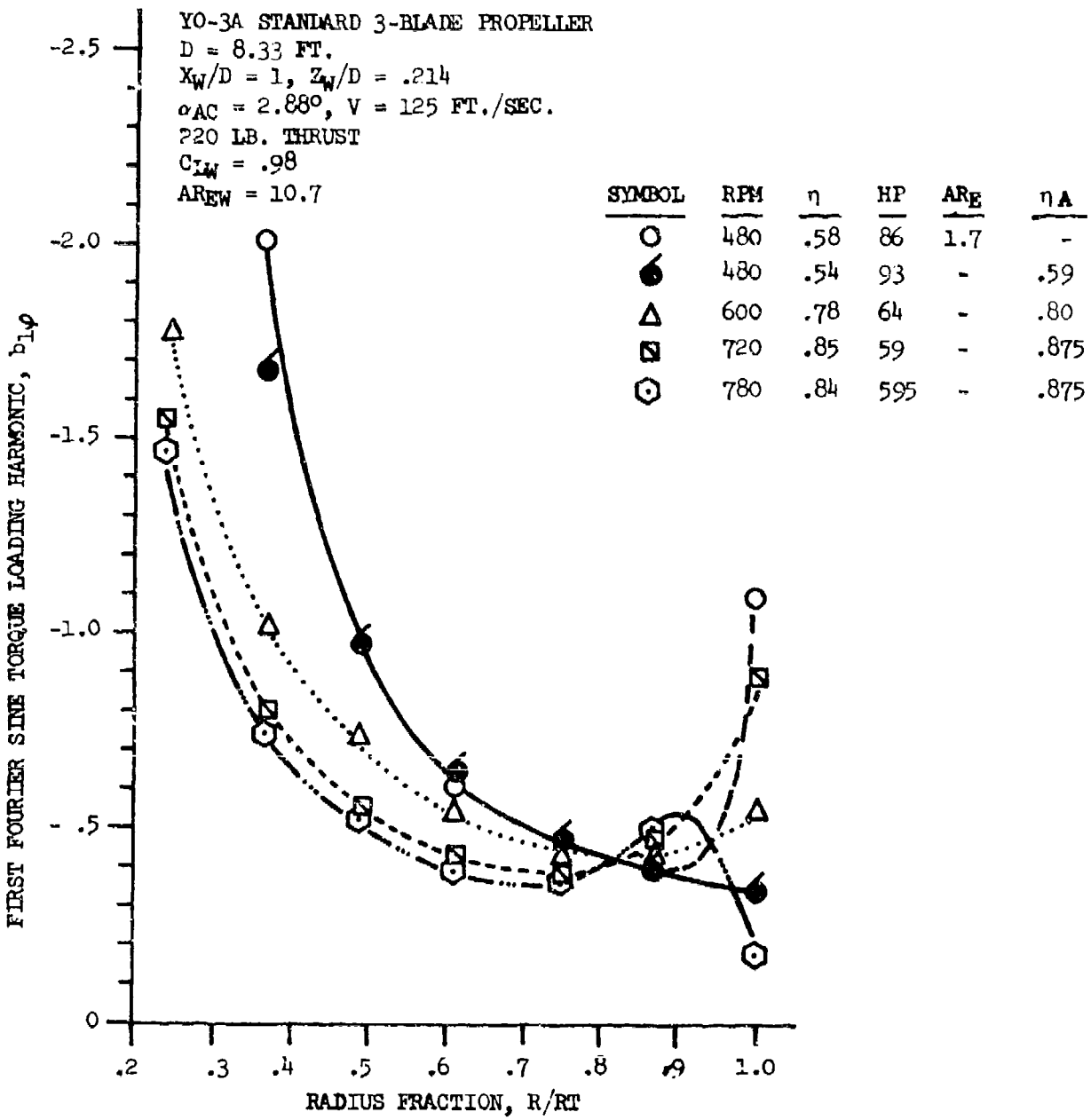


Figure 28. Radial Variation of the First Fourier Sine Torque Loading Harmonic $b_{1\varphi}$ at various RPM and Propeller Efficiency Conditions

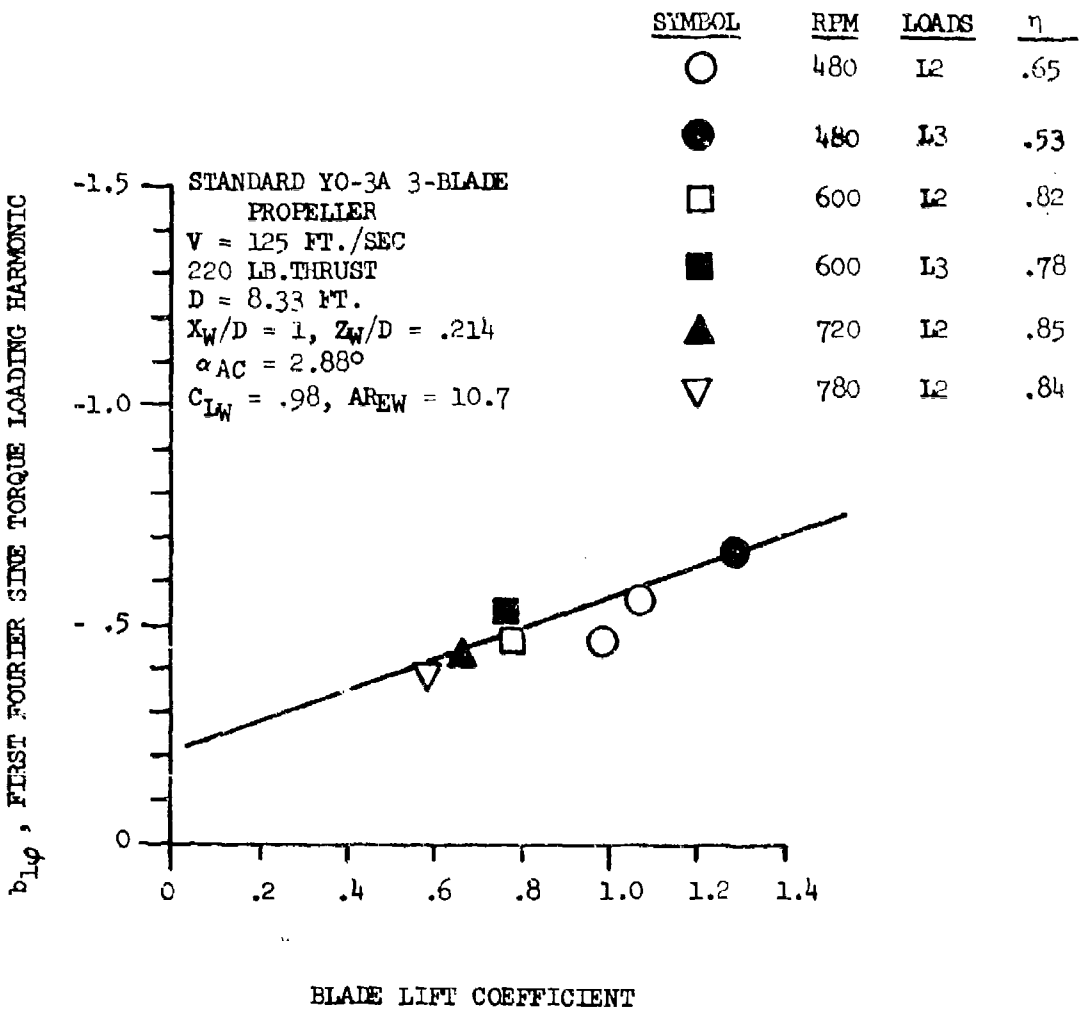


Figure 29. Correlation of First Torque Loading Harmonic vs. Blade Lift Coefficient

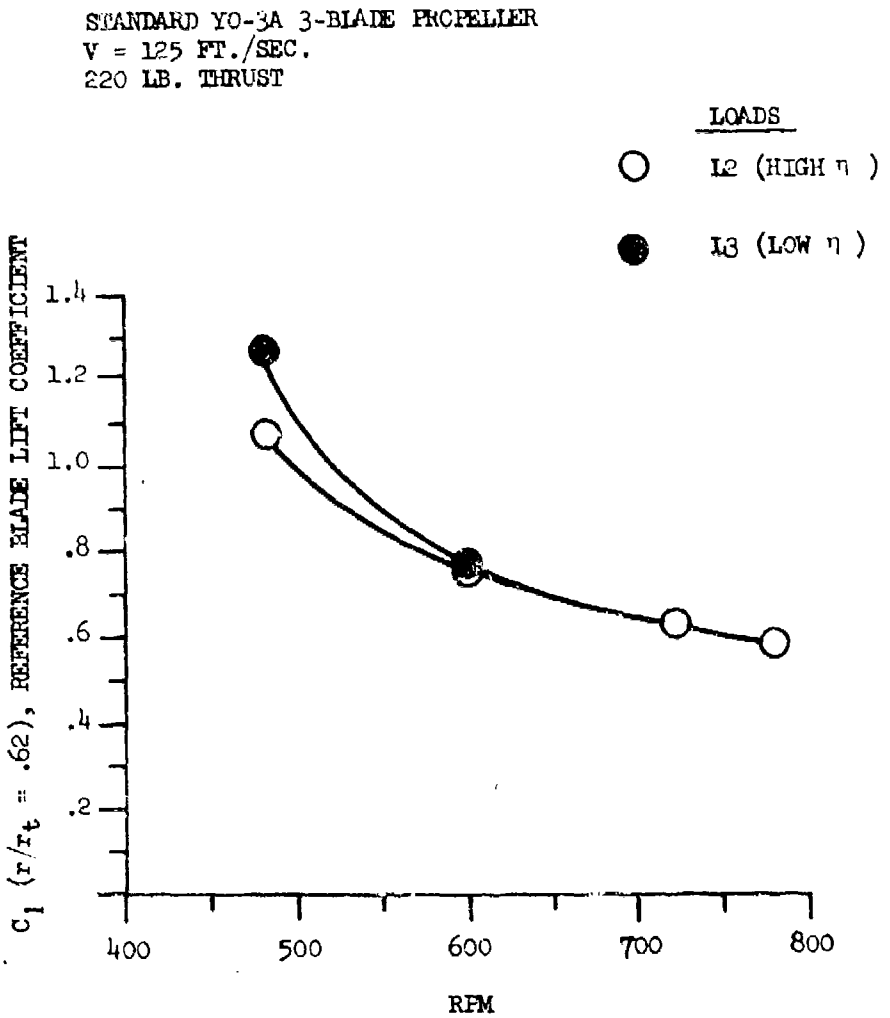


Figure 30. Reference Blade Lift Coefficient vs. RPM

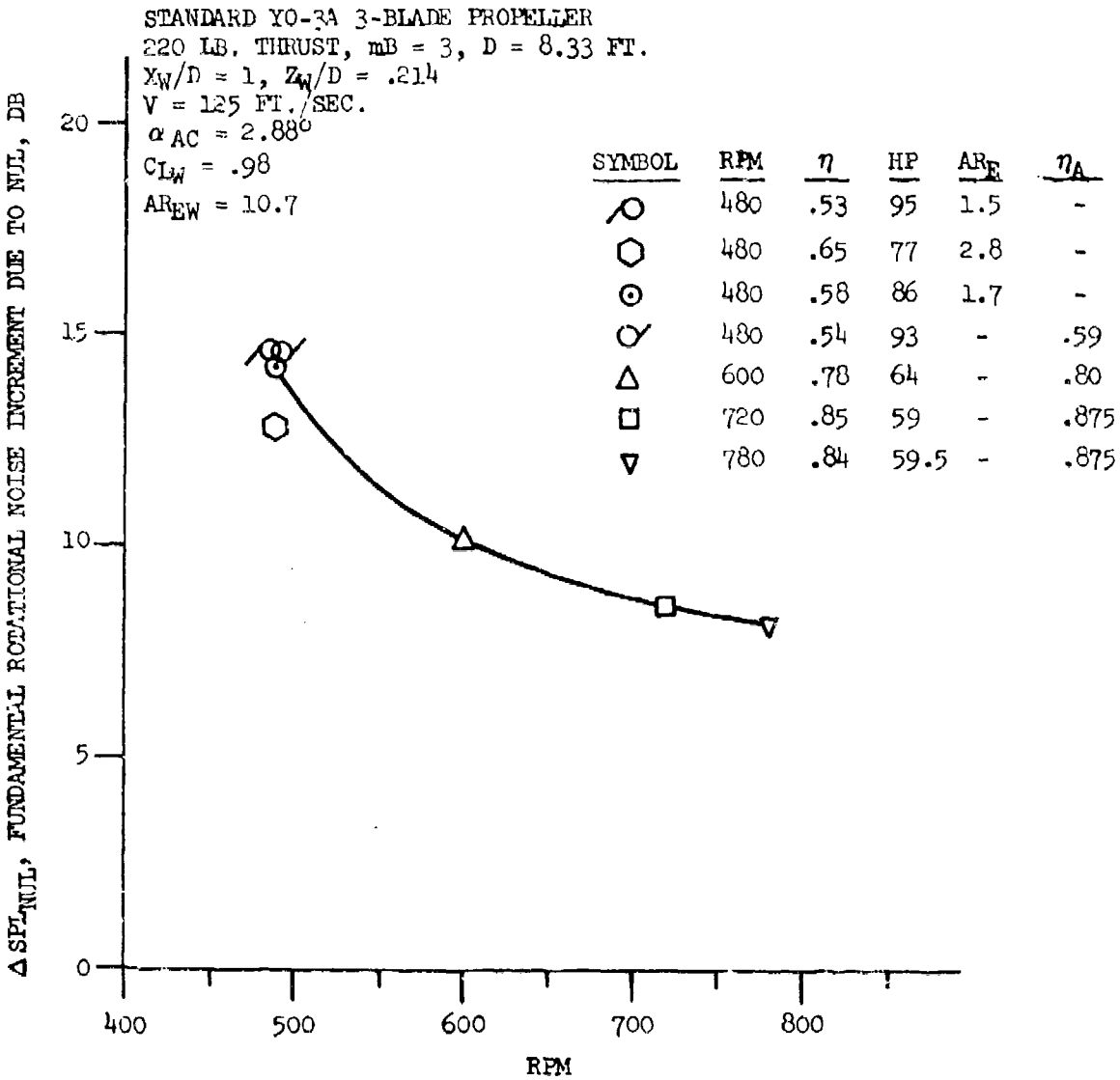


Figure 31 Fundamental Rotational Noise Increment, $\Delta SPL_{NUL}$ Due To Non-Uniform Loading (NUL) vs. RPM at 220 Lb. Thrust For The Standard YO-3A 3 Blade Propeller

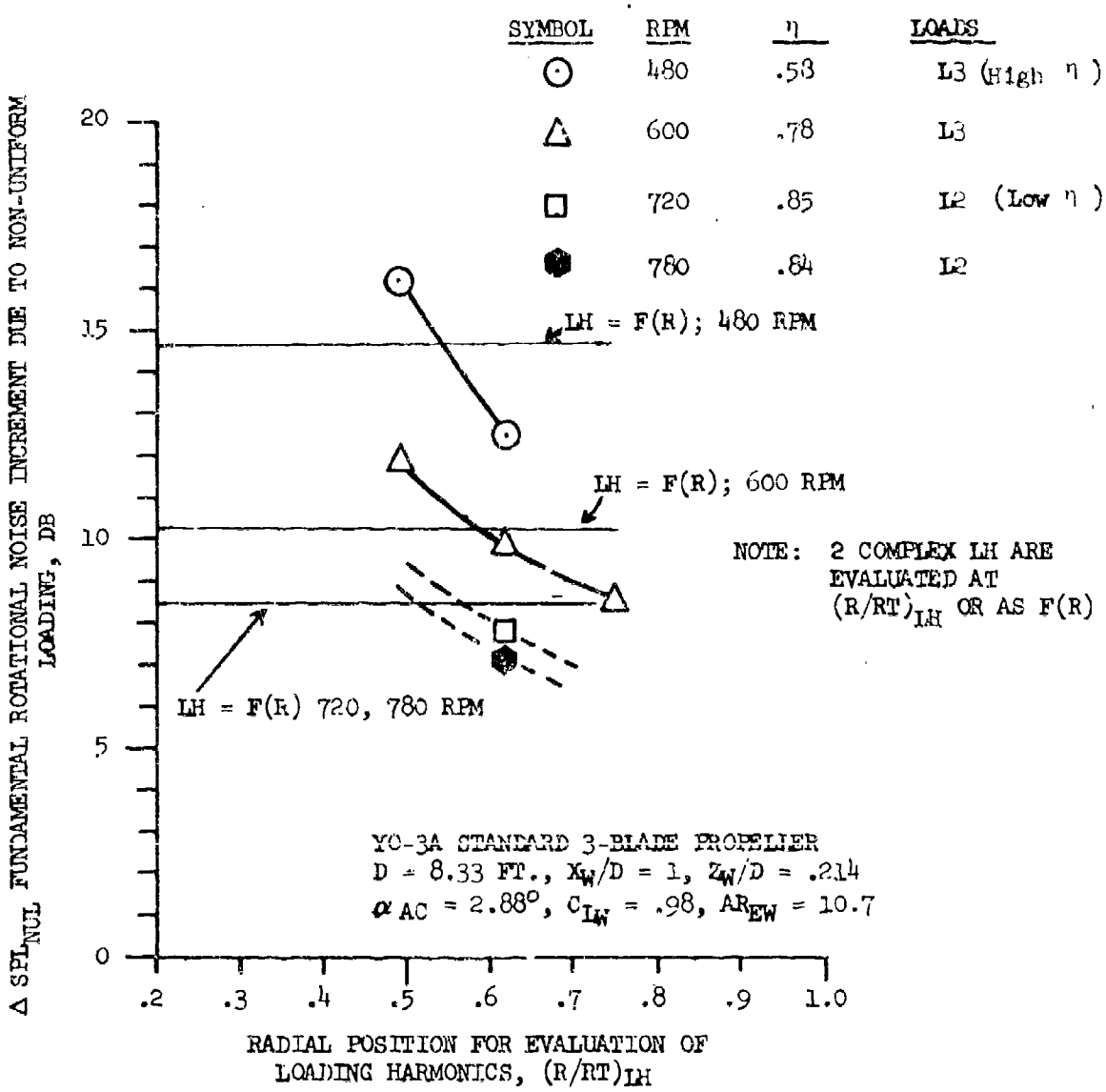


Figure 32. Fundamental Rotational Noise Increment Due to Non-Uniform Loading (NUL) vs. Radial Position for Loading Harmonic Evaluation at Various RPM

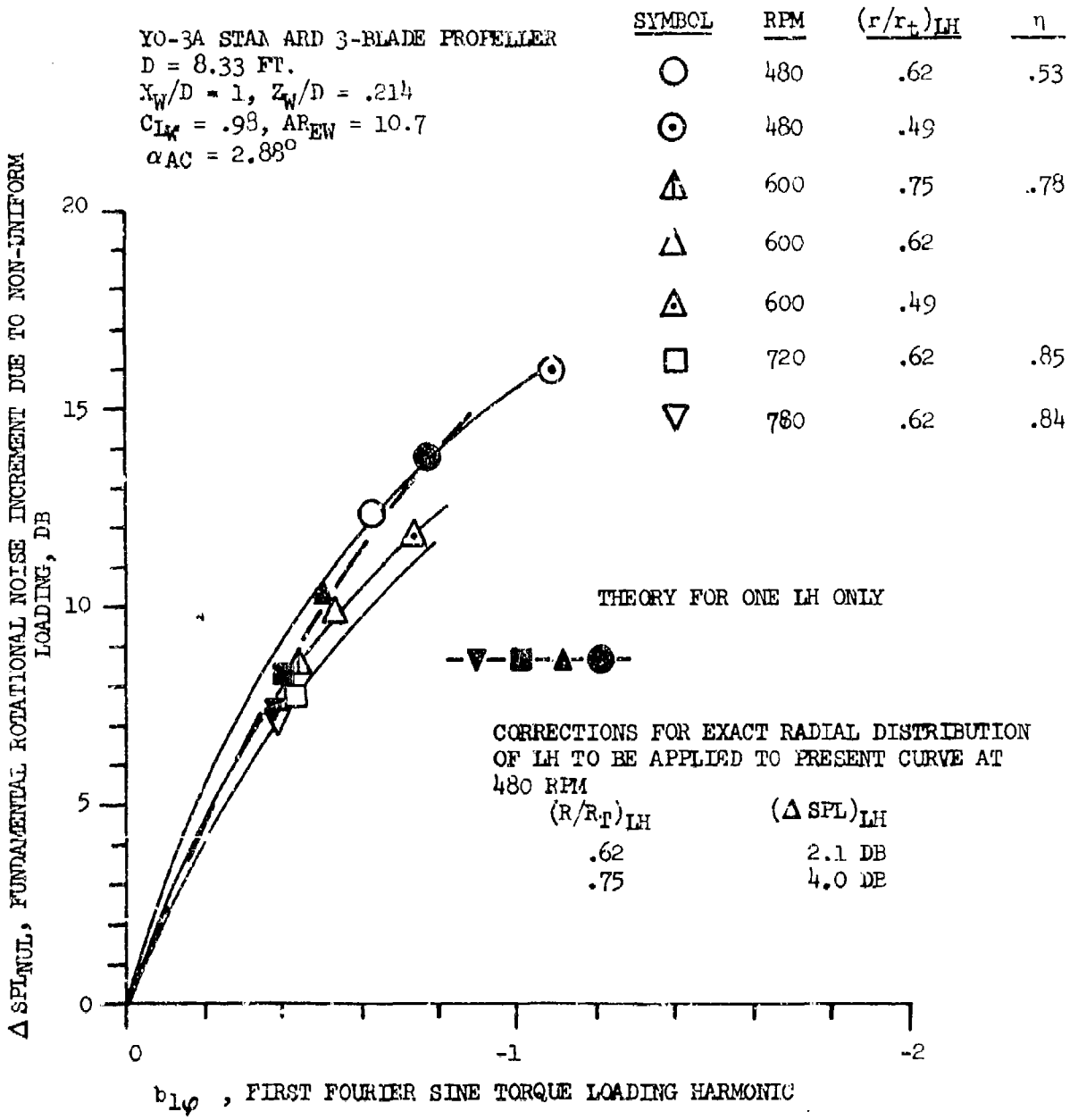


Figure 33. Fundamental Rotational Noise Increment Due to Non-Uniform Loading (NUL) vs. First Fourier Sine Torque Loading Harmonic, $b_{1\varphi}$

$$\Delta SPL_{NUL} = 20 \log_{10} \left( \frac{1 + \left| b_{1\varphi} \right| \left( \frac{mB - 1}{mB} \right)}{\left( \frac{\Omega r Y}{a S_o} \right)} \right); \; kr << 1 \tag{6}$$

$$kr = \left( \frac{mB \Omega r}{a} \right) \frac{Y}{S_o} \; ; \; S_o = \sqrt{X^2 + (1 - M)^2} \tag{7}$$

where, Y is the altitude, X is the observer distance ahead of the propeller disc plane, $\Omega$ is the shaft rotation frequency (radians/sec.) a is the speed of sound, and k is the wave number.

The above approximations will be found very useful for considering effects such as changing the ratio of wing separation distance to propeller diameter, or changing the propeller shaft angle of attack. For such parametric studies one needs only to calculate $(b_{1\varphi})$ at $(r/r_t) = .55$ and determine the $\Delta$ SPL due to non-uniform loading from Figure 33 or Equation 6 above.

c. Chordwise Blade Loading Effects

In Appendix IV a new solidity factor for blade loading is derived which differs from the standard assumption of uniform chordwise loading leading to the solidity factor (Equation IV-54)

$$SF_o = \frac{r}{b \cos \Theta_b} \sin \left( \frac{mBb \cos \Theta_b}{2r} \right) \tag{8}$$

This term is the leading factor in the axisymmetric radiation equation (Equation 5 of Reference 7 and Equation IV-15 of Appendix IV herein).

The new solidity term pertains to the chordwise loading appropriate to the angle of attack component or additional lift from airfoil theory. Figure IV-10 of Appendix IV shows the angle of attack chordwise loading which is expressible as (See Appendix IV Section 2b(3)(c), Equation IV-55)

$$\frac{dc_l}{d\bar{x}} = 2 \sin \alpha_b \sqrt{\frac{1 - x}{1 + x}} \left( \frac{c_{l\alpha}}{2\pi} \right) \tag{9}$$

where $(-1 \leq x \leq 1)$ defines the dimensionless chordwise position on the blade, referred to the semichord, with origin at midchord. Near the leading edge, $x = -1$, the loading increases inversely as the square root of leading edge distance. This is a consequence of well-known thin airfoil theory assumptions, and the load variation has been found to be accurate experimentally except within a distance from the leading edge of about one leading edge radius. As described in Appendix IV, when this loading is Fourier analyzed employing certain Bessel function identities, one obtains a new (complex) solidity factor (see Equation IV-59, IV-60)

$$SF = SF_r + iSF_i \tag{10}$$

where

$$SF_r = \frac{1}{\tilde{c}_{\varphi o}} \left\{ SF_o \left( c_d \cos\alpha_{av} + c_{lo} \sin\alpha_{av} \right) + \frac{mB}{2} \left( 2\pi \sin\alpha_b \sin\alpha_{av} \right) J_0 (Z) \right\}$$

$$SF_i = \frac{1}{\tilde{c}_{\varphi o}} \left\{ \frac{mB}{2} \frac{cl_\alpha}{2\pi} \left( -2\pi \sin\alpha_o \sin\alpha_{av} \right) J_1 (Z) \right\} \tag{11}$$

$J_0$ (Z) and $J_1$ (Z) are Bessel functions of the first kind of orders zero and one, respectively, whose argument is

$$Z = (mBb \cos\theta_b / 2r) \tag{12}$$

Here, b $\cos\theta_b$ is the blade chord projection on the propeller disc plane; r, the local propeller radius; m, the harmonic number; and B, the number of blades. The tangential force coefficient in the blade (Equation I-34)

$$\tilde{c}_{\varphi o} = \frac{(dF\varphi/dr)}{(\frac{1}{2}\rho V r^2)b} = \left\{ c_d \cos\alpha_{av} + c_l \sin\alpha_{av} \right\} \tag{13}$$

$c_{lo}$ is the camber lift coefficient and $c_l$ is the total section lift coefficient. One can see that if the angle of attack goes to zero that

$$\begin{aligned} c_l &= c_{lo} \\ SF_r &= SF_o \quad ; \quad \alpha_b \to 0 \\ SF_i &= 0 \end{aligned} \tag{14}$$

For small values of Z (low solidity)

$$\begin{aligned} J_0 (Z) &\cong 1 \\ J_1 (Z) &\cong Z/2 \end{aligned} \tag{15}$$

The new solidity factor produces only a minor increase in noise within the practical operating regime for the YO-3A. In Appendix IV, it is estimated not to exceed 1.5 dB; however, in the major noise radiating region of the propeller disc ($r/r_t > .5$), the local blade angles of attack do not exceed 7 degrees. Therefore, the effect is probably less than 1 dB in most cases.

A Minor Theoretical Correction to the Axisymmetric Theory

The blade aerodynamic parametric study was based on the following axisymmetric radiation formula (Equation 18, page 744 of Reference 13; See also Equation IV-15 of Appendix IV

$$p_m = e^{-imB\,\Omega\,t + i\Phi_m} \frac{\rho\Omega^2 D^4}{4\pi\, {}^3S_o} \int_{hub}^{tip} \left[SF_o\right] \left\{ \frac{(M+X/S_o)}{(1-M^2)^4} \left( \frac{-\Omega}{a} \frac{dC_T}{dr} \right) + \frac{D}{2\pi\, r^2} \frac{dC_p}{dr} \right\} \left[ {}^{r}{}_{rad} \right] dr \quad (16)$$

$$\Phi_m = \frac{mB\Omega\, S_o}{a} \left( 1 + \frac{MX}{S_o} \right) + mB \left( \phi + \frac{\pi}{2} \right) \quad (17)$$

In Reference 7 , the radiation factor is stated to be (see Equation IV-15, Appendix IV, Section 1b(2) (a), and Equation 7 of Reference 7)

$$\eta_{rad} = \left\{ J_{mB}\left(arg_{mB}\right) - \frac{i\,(1-M^2)\,Yr}{2S_o^{\,2}} \left[ J_{mB-1}\left(arg_{mB}\right) - J_{mB+1}\left(arg_{mB}\right) \right] \right\} \quad (18)$$

An independent derivation of this factor shows that it should be (Equation IV-21)

$$\tilde{\eta}_{rad} = \left\{ J_{mB}\left(arg_{mB}\right) + \frac{i(1-M^2)Yr}{2S_o^{\,2}} \left[ J_{mB-1}\left(arg_{mB}\right) - J_{mB+1}\left(arg_{mB}\right) \right] \right\} \quad (19)$$

$$arg_{mB} = \left( \frac{mB\,\Omega\, r}{a} \right) Y/S_o \quad (20)$$

The second and third terms are minor corrections for source position along the propeller radius and in general $Yr/S_o^{\,2} << 1$ where Y is the altitude. The new theoretical correction is to change the sign of the 90 degree phase shifted term (i factor). The quantative difference is negligible; however, this is mentioned, since it was discovered as part of the overall quest for significant errors.

In the present calculations, involving complex numbers, the radial integrations for real and imaginary parts were conducted separately and then the vector magnitudes of the integrated far field pressures were calculated. According to present thinking, the axisymmetric theory for far field noise should read

$$p_m = e^{-imB\Omega t + i\Phi_m} \frac{\rho\Omega^2 D^4}{4\pi^3 S_o} \int_{hub}^{tip} \left[ SF_r + iSF_i \right] \left\{ \frac{(M+X/S_o)}{(1-M^2)^4} \left( \frac{\Omega}{a} \frac{dC_T}{dr} \right) + \frac{D}{2\pi r^2} \frac{dC_p}{dr} \right\} \left[ \tilde{\eta}_r + i\,\tilde{\eta}_i \right] dr \tag{21}$$

where $(\tilde{\eta}_r, \tilde{\eta}_i)$ are the real and imaginary parts of $\tilde{\eta}$ above (Equation 20) We remark that $p_m$ as calculated above defines peak amplitude and exceeds the RMS value by the factor $\sqrt{2}$.

d. Blade Wake/Wing Interaction Effects

The effects of blade wake/wing interaction are shown in the top dashed curve of Figure 25. The explanation is detailed in Section 1b(3)(b) of Appendix IV. Briefly, the propeller blade/wake velocity defect appears to the wing like a gust of short wave length, setting up a fluctuating force on each side of the wing occurring at the blade passage frequency, with a weaker unsteady force fluctuation over the entire wing at twice the blade passage frequency. The radiating area is large, roughly equal to the wing root chord times the prop diameter, and is estimated to be nearly in phase with the direct propeller rotational noise, since the wing interaction occurs at almost exactly one revolution after blade passage. Also the wing radiation efficiency is taken to be that of a point dipole. At low wave number, dipole efficiency increases with wave number squared, while for an axisymmetric 3 bladed propeller, radiation efficiency is proportional to wave number to the sixth power for the fundamental frequency, thus being a very inefficient radiator at low wave numbers. This weak efficiency is the result of destructive acoustic interference between blades when the circumferential integration of the propeller disc is carried out, leading mathematically to the Bessel functions which describe axisymmetric propeller noise radiation.

e. Effects of Wing Separation and Airplane Angle of Attack on Rotational Noise

The earlier discussion of the non-uniform loading effects for the YO-3A pertains to a configuration where the wing separation distance is

$$Xw/D = 1, \; Zw/D = .214$$

where Xw, and Zw are respectively the streamwise and vertical separation distances between the center of the propeller disc plane and the quarter chord point of the mean aerodynamic chord of the wing where the wing lift is known to act (Reference 12 ). The aircraft propeller axis angle of attack is estimated to be 2.88° for the following wing loading parameters given in Table II (see also Appendix IV, page 136)

TABLE II

YO-3A Aerodynamic Parameters

| | True Values | Reference Values |
|---|---|---|
| Aircraft Weight | 3750 lb. | |
| Wing Area | 204 $ft^2$ | 180 $ft^2$ |
| Forward Speed | 125 ft/sec | |
| Dynamic Pressure | 18.6 psf | |
| Wing Lift Coefficient, $C_{L_W}$ | .985 | 1.12 |
| $C_{L_W}$ $(\alpha_w = 0)$ | .375 | .33 |
| Wing Incidence | $2.5^\circ$ | |
| Wing Angle of Attack | $5.38^\circ$ | |
| Propeller Angle of Attack | $2.88^\circ$ | |
| Wing Span | 57 feet | |
| Effective Wing Span | 40 feet (e = .7) | |

Later in this report, propeller design charts will be presented wherein the propeller diameter is changed. The design charts include the empirical corrections for the YO-3A which implies a constant ratio of wing separation distance to propeller diameter, and maintenance of the same propeller shaft angle of attack. It is therefore of interest to examine the effect of changing these wing separation and angle of attack factors.

Figures 35 to 37 present, as examples, the desired information at 480 rpm. Figures 34 and 36 display the variation of the first torque loading harmonic, $b_{1\varphi}$, as functions, respectively of wing separation distance, and of propeller shaft (aircraft) angle of attack, $\alpha_{ac}$. Figures 35 and 37 show the corresponding rotational noise increments, $\Delta SPL_{NUL}$, due to non-uniform loading (NUL) effects. Figures 35 and 37 are derived from Figures 34 and 36 by means of the correlation of $\Delta SPL_{NUL}$ vs. $b_{1\varphi}$ shown earlier in Figure 33 and in Equation 6.

f. Methods of Reducing Rotational Noise for a Fixed Aircraft Weight and Propeller Diameter

From the previous discussion it can be seen that reducing non-uniform loading (NUL) effects on the rotational noise at low rpm depends primarily on two basic effects:

(1) Reducing the upwash and backwash at the propeller disc plane due to the wing lift circulatory flow fields

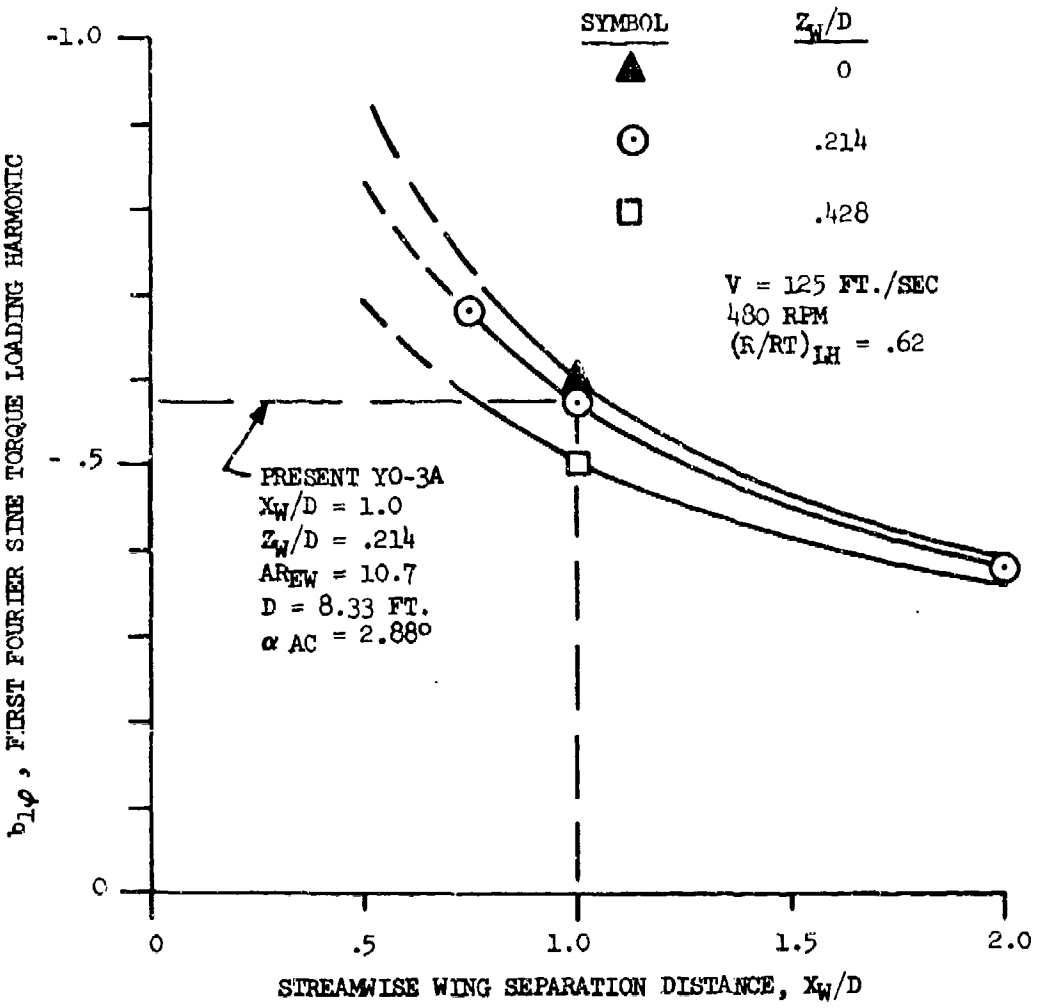


Figure 34. Effect of Wing Separation Distance on the First Fourier Sine Propeller Torque Loading Harmonic at 480 RPM Evaluated at R/RT = .62

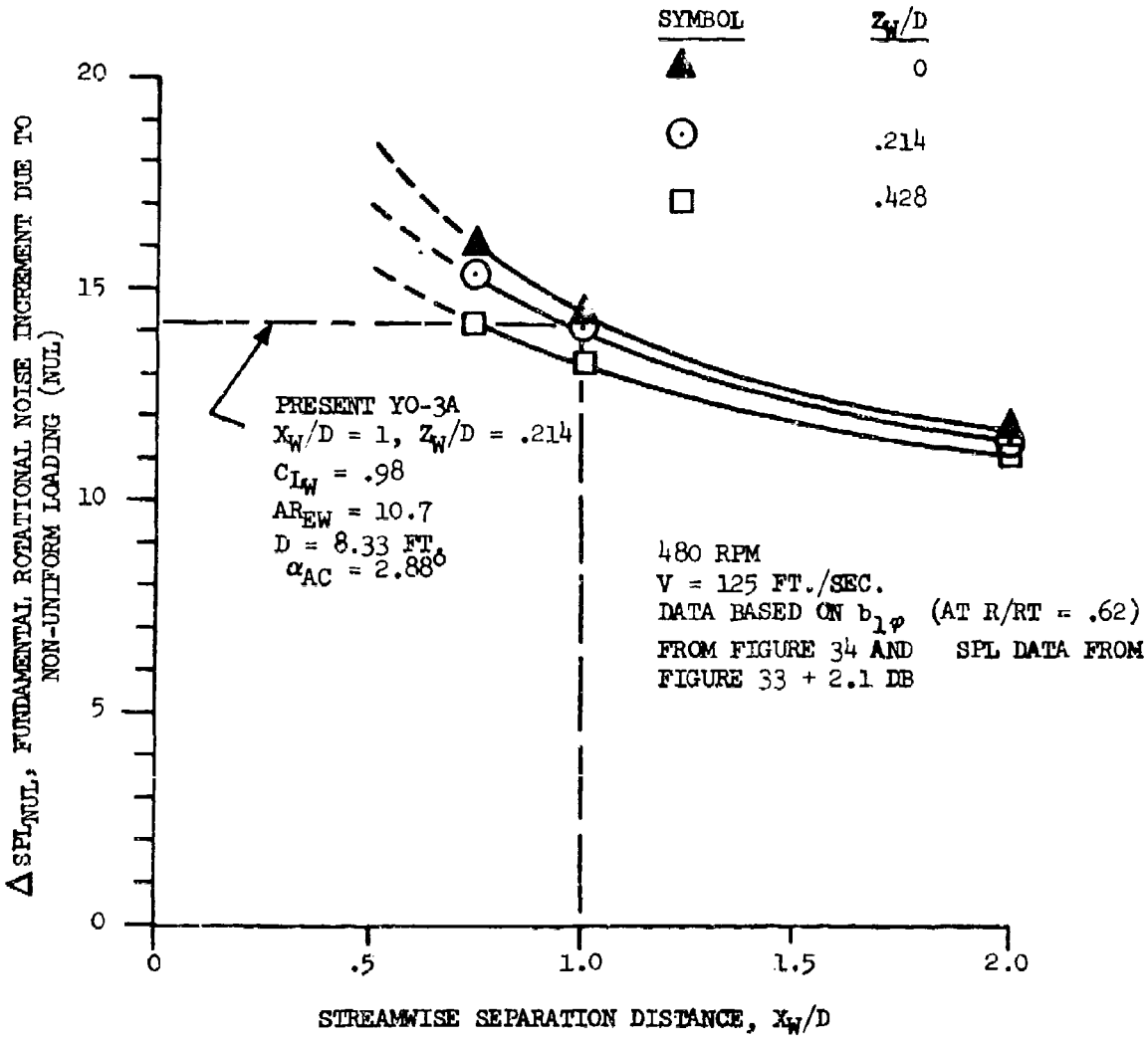


Figure 35. Fundamental Rotational Noise Increment Due to Non-Uniform Loading (NUL) vs. Wing Separation Distance at 480 RPM

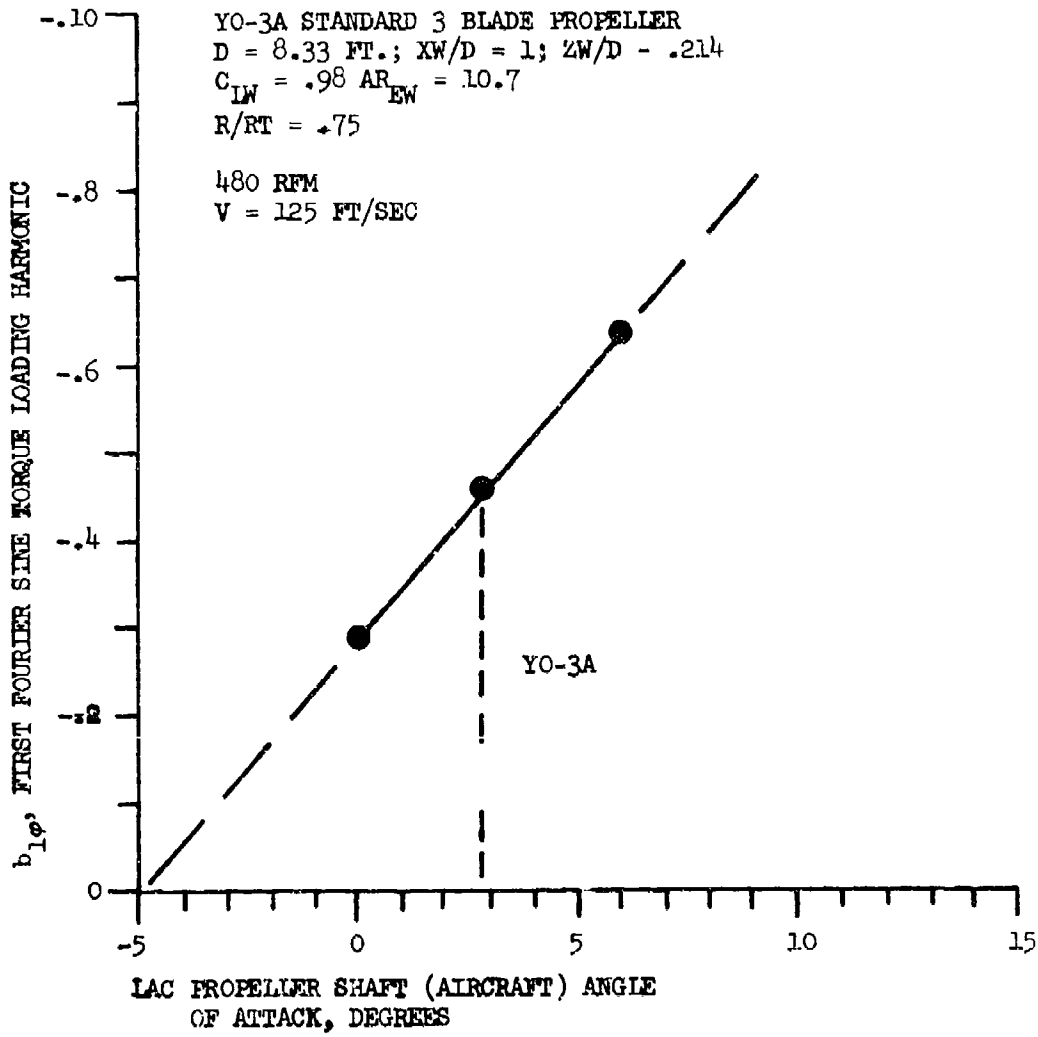


Figure 36 - Effect of Propeller Shaft (Aircraft) Angle of Attack on the First Fourier Sine Torque Loading Harmonic, $b_{1\varphi}$, at 480 RPM

Evaluated at R/RT = .75

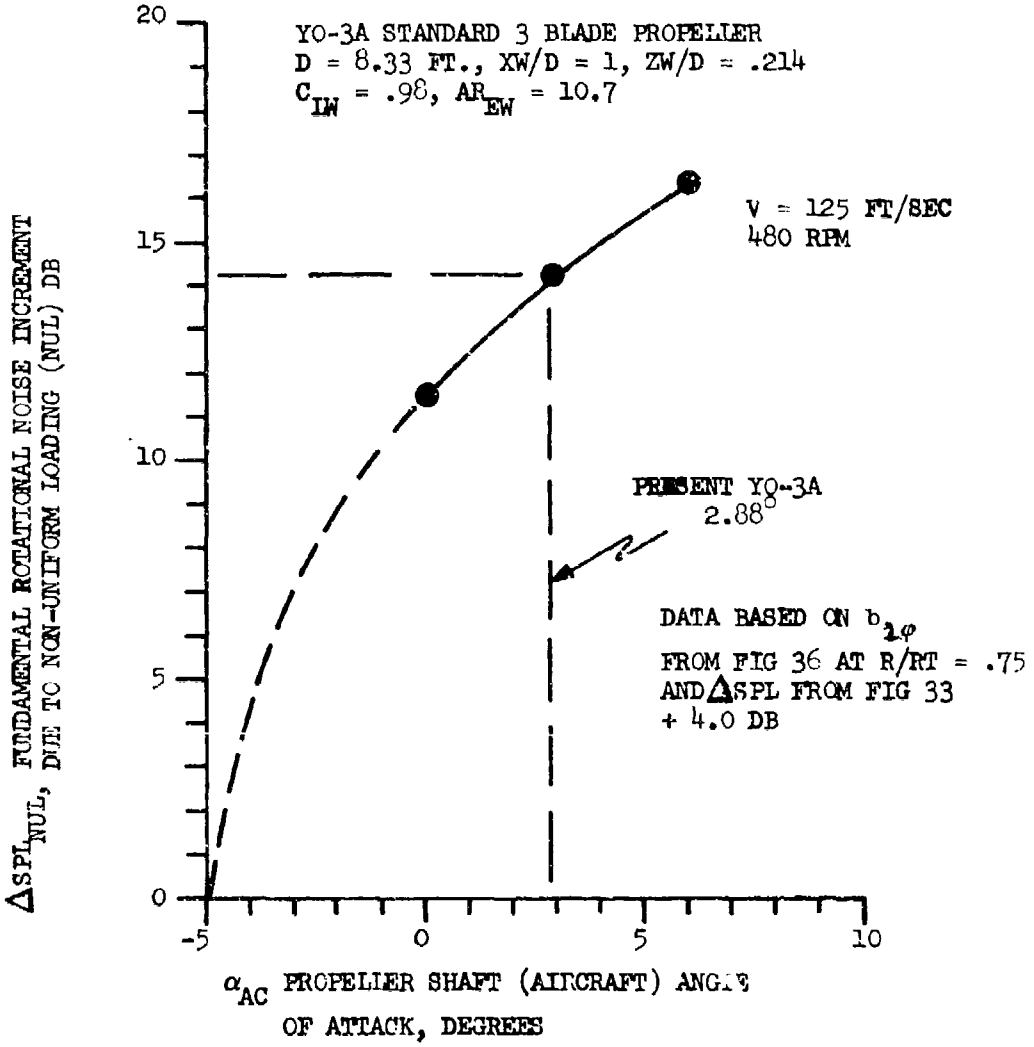


Figure 37 - Fundamental Rotational Noise Increment Due to Non-Uniform Loading (NUL) vs. Propeller Shaft (Aircraft) Angle of Attack at 480 RPM

(2) Reducing airplane angle of attack

The reduction of the NUL effects caused by the wing lift circulatory flow for a given aircraft weight and propeller diameter can be accomplished several ways:

- by increasing wing separation distance
- by increasing the effective wing span either through improved span loading efficiency or by physically increasing the wing span
- by increasing the forward speed at a given rpm. This also reduces the blade angle of attack required to develop a given thrust, slightly improving propeller efficiency

Aircraft weight balance and structural considerations limit the potential for increasing wing separation. Structural considerations generally limit the achievable aspect ratio on an airplane.

The reduction of aircraft angle of attack can be accomplished by several means,

- by increase of wing area to reduce wing lift coefficient
- by increase of wing incidence relative to the propeller shaft
- by use of trailing edge flaps
- by increase of forward speed

The wing area sizing and incidence setting are fundamental to the entire aerodynamic design; therefore, the possible changes are dependent on the total aircraft mission requirements. Trailing edge flaps are generally desirable from a standpoint of aircraft takeoff and landing performance, and consequently,it would appear easy to adjust the flap setting to give zero propeller axis angle of attack for a given wing incidence and forward speed.

The effectiveness of forward speed increases is limited by the airframe generated noise. Since the airframe generated noise follows a velocity to the sixth power times wing area law, a 26% forward speed increment would increase the airframe noise by 6 dB. Recent work by Healy (Reference 10 estimates that the OASPL for the YO-3A airframe noise is about 54 dB, therefore, a 6 dB increase in airframe noise might be permissible without masking the propeller vortex noise.

## 2. THEORETICAL REVIEW OF VORTEX NOISE

The vortex noise theoretical evaluation is detailed in Appendix IV, which provides a critique of the various options of the computer program of Reference 8 . Also Appendix IV provides a rationale for the empirical method

finally adopted to correct the vortex noise predictions of Reference 7 , namely a procedure to relate vortex noise levels to rotational noise. The rationale states that there exist random fluctuating tangential force dipoles (having their maximum directivity in the disc plane) and random fluctuating thrust dipoles (having their maximum directivity in the thrust direction).

It is further argued that the fluctuating tangential force dipole (which governs overhead noise) can be expressed in terms of fluctuating lift, $d\tilde{L}/dr$, fluctuating drag, $d\tilde{D}/dr$, and the advance angle $\alpha_{av}$ according to

$$\frac{d\tilde{F}_\varphi}{dr} = \left(\frac{d\tilde{D}}{dr} \cos \alpha_{av} + \frac{d\tilde{L}}{dr} \sin \alpha_{av}\right) \tag{22}$$

At low rpm, $\alpha_{av}$ is large and both the fluctuating lift and drag increase with blade lift coefficient, and contribute more to the torque dipole. Thus from both a directivity and an intensity standpoint the tangential force governing overhead vortex noise level would be expected to increase at low rpm.

It is postulated that the fluctuating tangential force is proportional to steady tangential force; hence, this implies a relationship to the fundamental rotational noise at overhead.

There is a further discussion of radiation efficiency in Appendix IV, where, because of the random phase of the fluctuating vortex dipole forces, one would not expect the destructive acoustic interference found in axisymmetric rotational noise; therefore, the acoustic radiation of the separate blades around the disc is likely to be additive on an energy basis and have the efficiency of a distribution of random point dipoles being proportional to wave number squared. This is in contrast to the inefficient (wave number to the sixth power) radiation efficiency of axisymmetric propeller rotational noise for the fundamental tone of a 3 bladed propeller.

In conclusion, the above theoretical discussion indicates that the principal causes of the discrepancy between theory and measured data, both for rotational noise and for vortex noise for the YO-3A are strongly dependent on the blade loading or lift coefficient. Accordingly, it seems reasonable to expect to find an empirical correction which is expressable as a function of the blade lift coefficient.

## 3. SUMMARY

The comprehensive theoretical study of propeller blade aerodynamic loads has been made to discover if errors in blade load predictions would explain the "bucket" in the curve of rotational noise vs. rpm. The results show that axisymmetric blade loading efficiency effects contribute to, but are not entirely responsible for the bucket phenomena. Independent Lockheed far field rotational noise calculations assuming axisymmetric blade loading show:

- Trends of fundamental rotational noise SPL vs. rpm which parallel the USAF computer program results at a constant propeller thrust.

- Rotational SPL vs. propeller horsepower tends to fall on a single curve at a given rpm, regardless of the blade aerodynamic parameter being varied. The Lockheed calculations were adjusted to match YO-3A project data for propeller performance. The blade aerodynamic parameters being varied include blade camber, lift coefficient, blade pitch angle, and zero lift drag level. This model is found to give an excellent representation of airfoil section characteristics, such as those of the NACA 63 series.

- A large discrepancy is noted between propeller efficiency data as predicted by the USAF computer program (Reference 8 ) when compared to YO-3A flight test performance data. An independent calculation was made in the present study using lifting line theory which predicts propeller efficiency values closer to the YO-3A performance data. These values are much lower than the USAF computer program values at low rpm conditions.

The failure to entirely explain the SPL vs. rpm "bucket" by means of axisymmetric blade loading effects led to a review of the acoustic radiation theory. This theoretical review revealed the following:

- A minor correction to axisymmetric theory was found for the source position term. This correction, however, has negligible effect on the predicted noise.

- The evaluation of non-uniform chordwise blade loading effects at high angles of attack leads to a new (complex) blade solidity factor, causing a slight increase in the predicted rotational SPL at low rpm (less than 1.5 dB) for axisymmetric blade loads.

The most likely explanation for the measured rotational noise level increase and "bucket" in the curve of SPL vs. rpm arises from two factors:

- Circumferentially non-uniform blade loads, caused by inflow variations into the propeller disc plane--these variations yield a 8 to 14 dB increase in rotational SPL level compared to the standard axisymmetric theory, and contribute about 5 dB towards the bucket effect.

- The interaction of the propeller blade wake with the wing generates fluctuating lift forces on the wing. This dipole source which produces significant far field radiation is assumed to be in phase with the basic propeller rotational noise. The strength of the wing interaction noise increases greatly at low rpm and high blade lift coefficients and radiates more efficiently than the propeller blades.

Two causes of the circumferential changes of propeller loading were analyzed:

- The propeller disc plane angle of attack effect (upwash effect)

- The induced upwash and backwash through the propeller disc plane caused by the wing lift circulatory flow.

The acoustical effects of circumferential non-uniformities in the blade loading were evaluated by means of deriving Fourier coefficients for the blade loading called loading harmonics (LH) and applying a modification of the theoretical expressions for far field noise given by Morse and Ingard. Physically, the effect of inflow non-uniformity of blade loading is to eliminate the destructive interference between the acoustic fields of individual blades which is characteristic of axisymmetric propeller noise theory. The decrease of destructive interference causes a large increase in radiation efficiency at low tip speeds for the non-uniform loading case.

The above mentioned wing interaction and propeller disc inflow non-uniformity effects are both airplane configuration effects; however, the YO-3A propeller installation is believed representative of a single engine propeller aircraft. Serious design limitations generally would prevent larger separation distances between the wing and the propeller, which would be one obvious approach to eliminating the above effects.

The theoretical studies of rotational noise indicate three possible paths to reducing propeller rotational noise:

- Increasing the separation distance between propeller and wing.

- Decreasing propeller shaft angle of attack at the desired forward speed for quiet operation.

- Decreasing the blade lift coefficients by means of:

  - Increasing the number of blades

  - Increasing the propeller diameter

The practicality of any of these measures must be carefully examined for each aircraft design, considering the total mission effectiveness.

A review of three vortex noise prediction options in the USAF computer program revealed minor theoretical inconsistencies, and shortcomings of empirical constants derived from static propeller tests. Also, it is shown that one may expect random fluctuating torque and random fluctuating thrust forces which are postulated as being proportional to the steady state thrust and torque forces. This hypothesis which leads to a rationale for empirically relating the vortex noise level to the rotational noise, is shown to be a successful means for estimating propeller vortex noise at overhead conditions.

The review of the theory of rotational and vortex noise indicates that the principal causes of discrepancy between theory and experiment are related

to the blade lift coefficient which is therefore suggested as a significant parameter for correlation of the empirical corrections to the USAF computer program.

## SECTION VI

## EMPIRICAL MODIFICATIONS FOR AIR FORCE COMPUTER PROGRAM

This section contains the empirical modifications for the Air Force computer program that were developed in this study from flyover data acquired in the October tests of the YO-3A flying with the three different propellers. These modifications included corrections for predicting these noise characteristics:

- Absolute and relative levels of rotational noise for fundamental, second and third harmonic frequencies,
- Directivity of the rotational noise,
- Absolute levels of vortex noise in the one-third octave band where the maximum level occurs,
- Spectral shape of the vortex noise,
- Prediction of the one-third octave band where the peak level occurs.

The quality of experimental data was not good enough to determine directivity of second and third rotational noise frequencies and, in the absence of valid data, it is suggested that directivity of fundamental rotational noise frequency be used to characterize directivity of the higher harmonic frequencies. Likewise, the directivity of the vortex noise, as determined by experimental data, is in question due to ground reflection effects near the peak levels. Therefore, it is recommended that the only changes in the computer generated directivity characteristics are those implicit in the empirical procedure for correction of vortex noise at the overhead position.

### 1. PROPELLER ROTATIONAL NOISE

It is recommended that the Air Force propeller rotational noise prediction program be modified in the following manner:

$$SPL_m = SPLT + 10\left|LOG\left(\frac{C_1 \times CHORD}{C_{1\,REF.} \times CHORD_{REF.}}\right)^a\right| + C$$

Where, SPLT = Predicted Sound Pressure Level (dB) of Loading Noise (only) for given rotational noise harmonic

$SPL_m$ = Corrected Sound Pressure Level (dB) of Rotational Noise Harmonic

m = Harmonic number

a = Empirical exponent = 3.0

C = Empirical constant

$C_{1\ REF.} \times CHORD_{REF.}$ = Product propeller lift coefficient times chord for the three-quarters propeller radius station. Reference values are taken near minimum values for measured data.

$C_{1\ REF.} \times CHORD_{REF.}$ = 0.433 (when chord is expressed in feet)

When,

$$m = 1,\ C = +4.0\ dB$$

$$m = 2,\ C = -1.0\ dB$$

$$m = 3,\ C = -10.0\ dB$$

Figures 38, 39, and 40 illustrate the use of this modification to the computer program for fitting measured and predicted data for the standard three blade, acoustic three blade, and standard six blade propellers. Figure 41 shows the recommended directivity for rotational noise. Measured data for the rotational noise fundamental frequency of the standard three blade and acoustic three blade propellers are shown for comparison. This directivity pattern should be substituted for the existing directivity pattern (i.e., does not modify existing directivity pattern).

2. PROPELLER VORTEX NOISE

It is recommended that the Air Force propeller vortex noise prediction program be modified in the following manner:

$$SPL_{vp} = SPL_{f} + 10\ LOG\left(\frac{C_{.75}}{C_{.75\ REF.}}\right) + C_{B}$$

$SPL_{vp}$ = Sound Pressure Level (dB) of Vortex Noise in Peak One-Third Octave Band

$SPL_{f}$ = Level of Fundamental Rotational Noise (i.e., M = 1) Frequency Predicted by Modified Air Force Computer Program

$C_{.75}$ = Chord of Propeller at 0.75 Radius

$C_{.75\ REF.}$ = Chord of Reference (i.e., Standard 3 Blade Propeller at 0.75 Radius) Propeller

= 1.0 foot

$C_{B}$ = Empirical Constant

B = Number of Propeller Blades

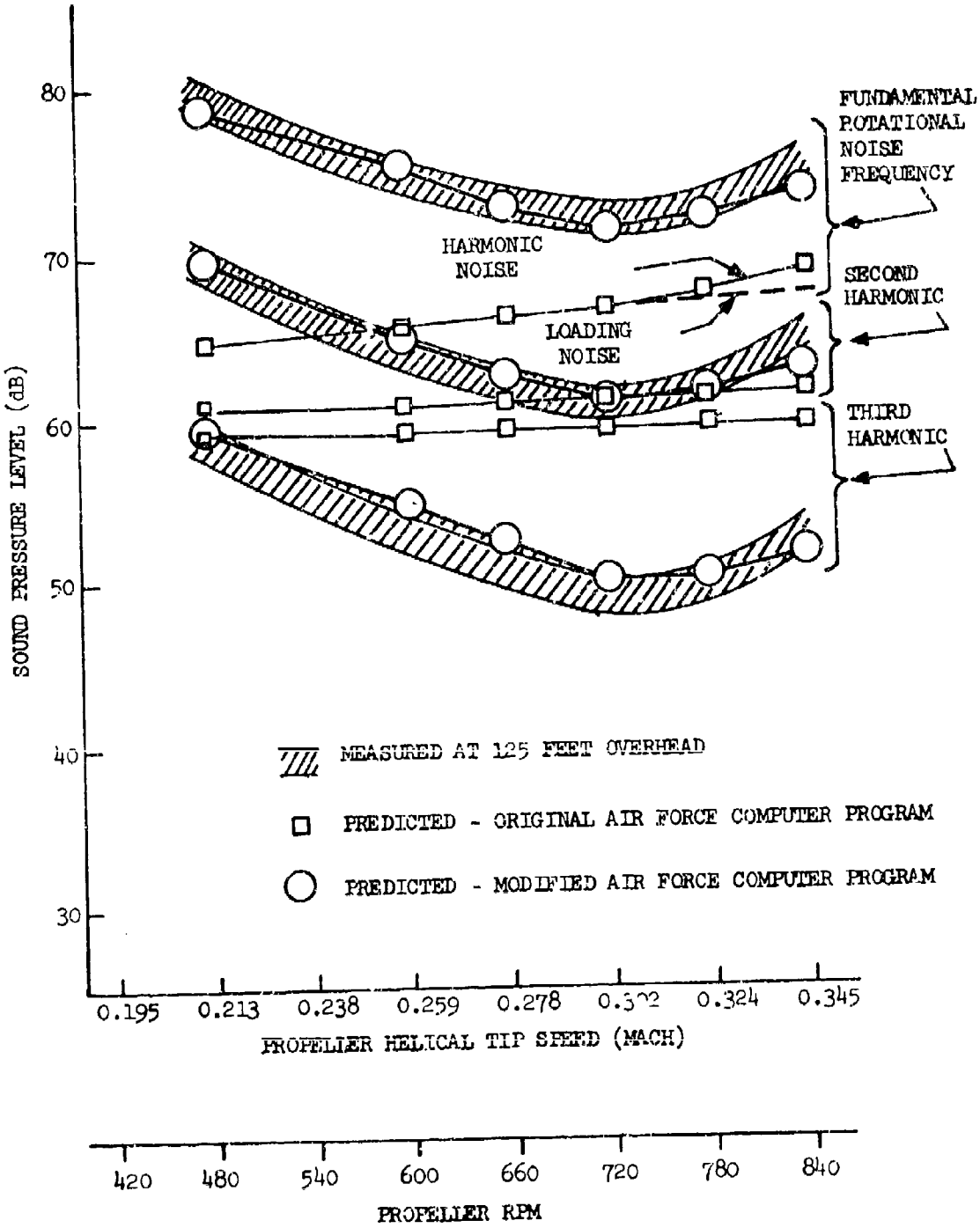


Figure 38. Comparisons of Measured Rotational Noise with Predictions of Original and Modified Air Force Computer Program (Standard 3 Blade Propeller)

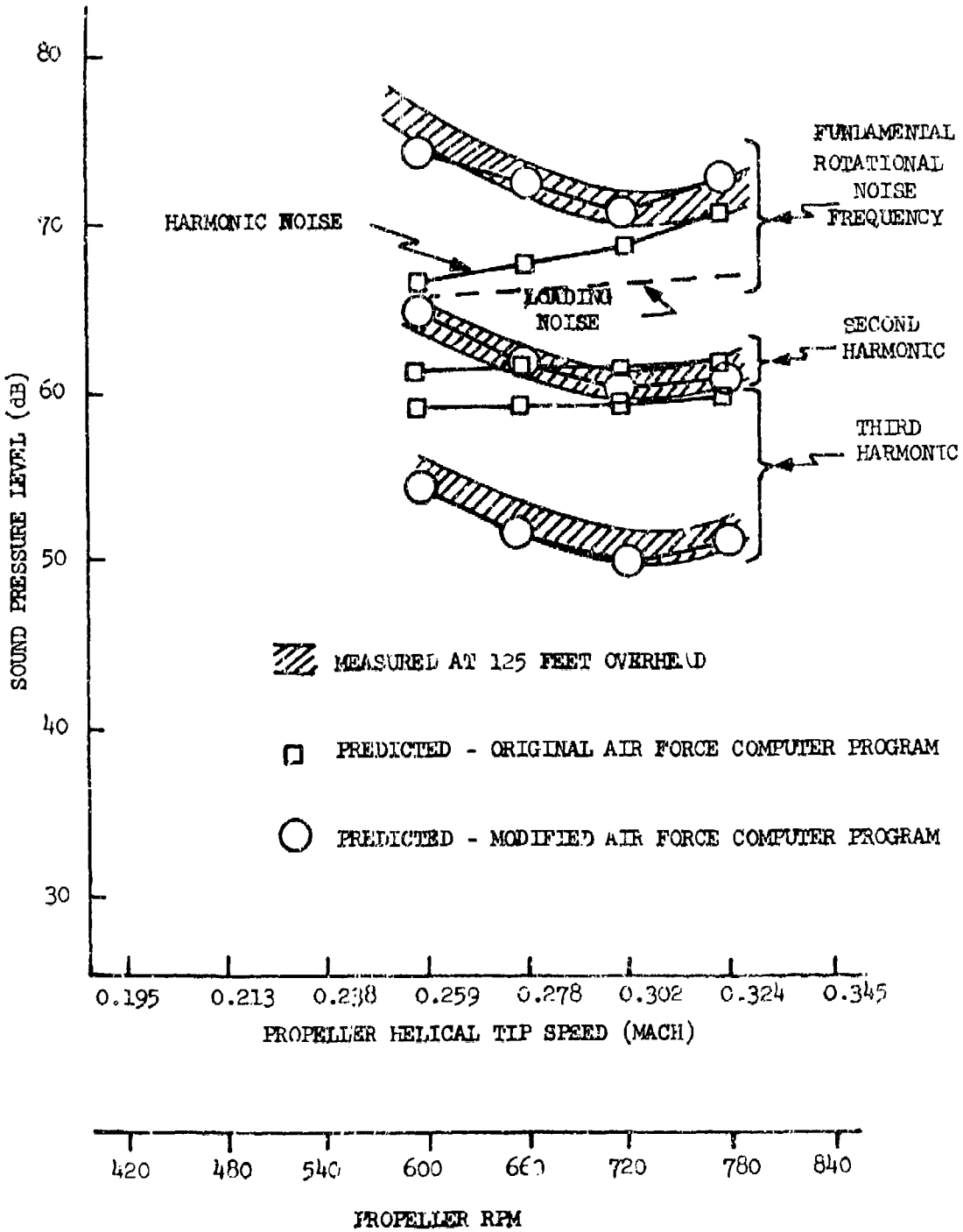


Figure 39. Comparisons of Measured Rotational Noise with Predictions of Original and Modified Air Force Computer Program (Acoustic 3 Blade Propeller)

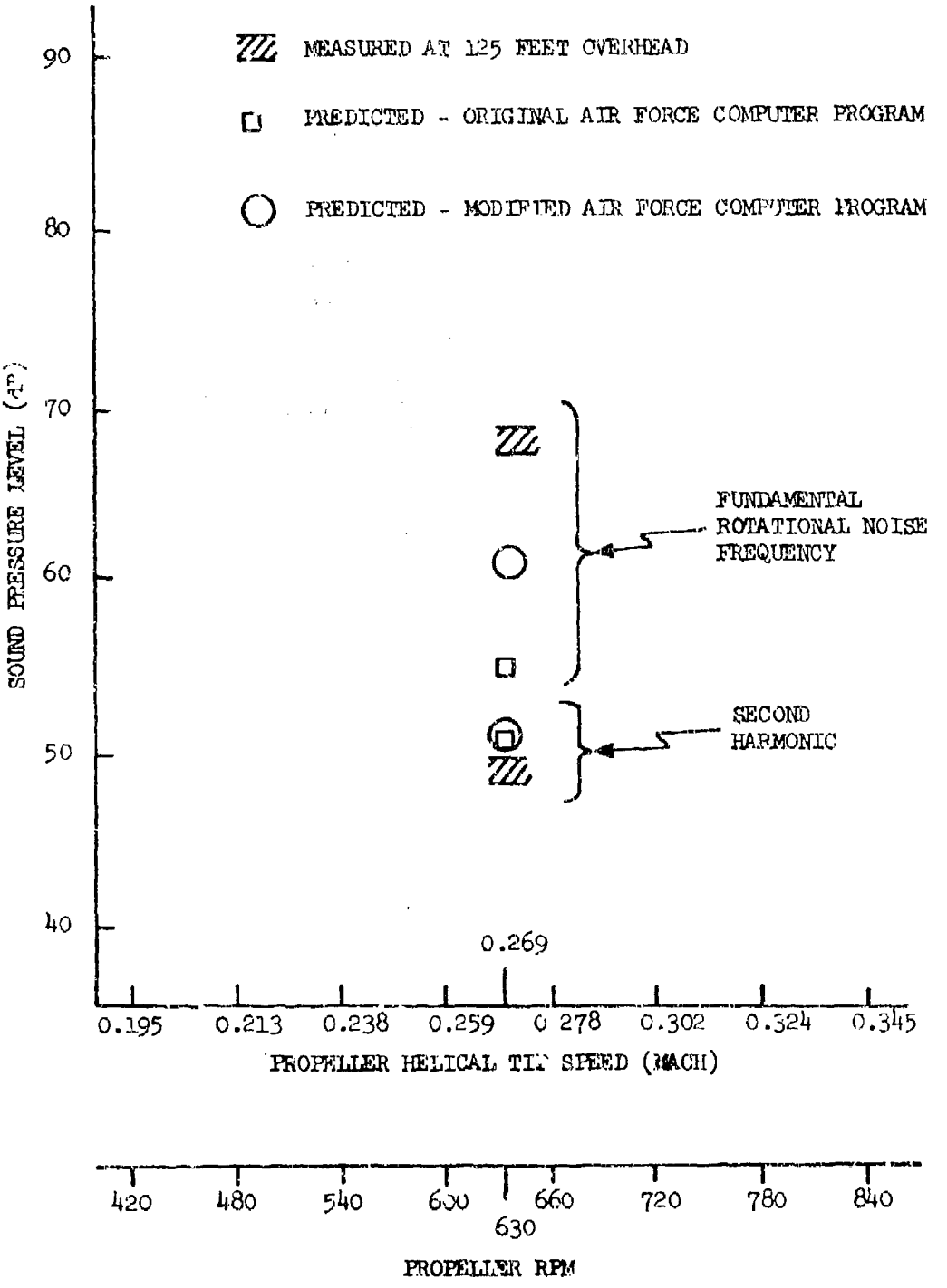


Figure 40. Comparisons of Measured Rotational Noise with Predictions of Original and Modified Air Force Computer Program (Standard 6 Blade Propeller)

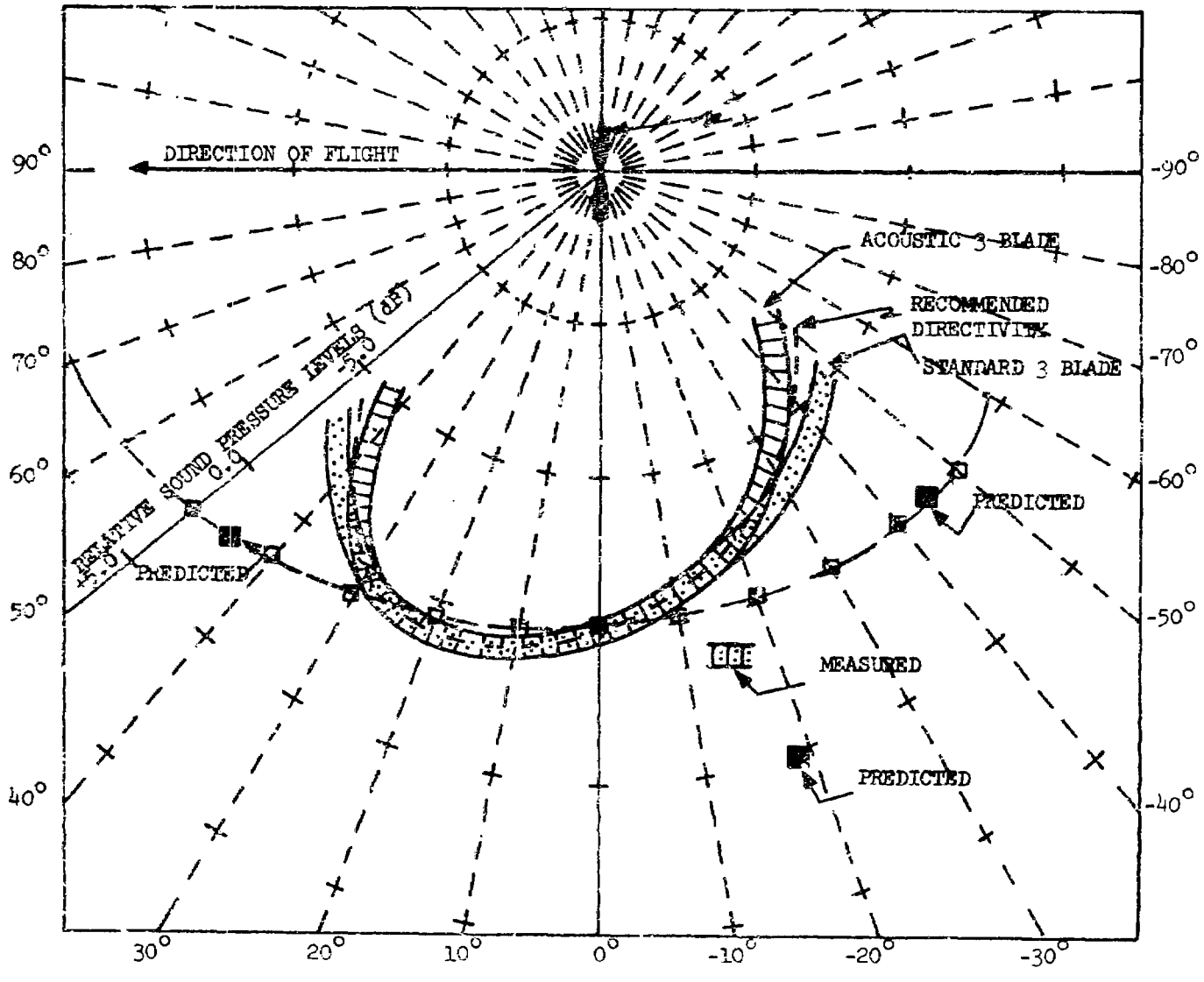


Figure 41 - Comparisons of Measured and Predicted Directivity with Recommended Directivity

$$C_2 = -16.0 \text{ dB}$$

$$C_3 = -13.7 \text{ dB}$$

$$C_4 = -10.5 \text{ dB}$$

$$C_5 = -8.0 \text{ dB}$$

$$C_6 = -5.3 \text{ dB}$$

Figures 42 and 43 illustrate the use of this modification to the computer program for fitting measured and predicted data for the standard three blade and acoustic three blade propellers, respectively.

## 3. SUMMARY

Figures 38 through 43 are comparison charts of measured and predicted noise using the original Air Force computer program and the modified program. The degree of change in predicted noise and the improved accuracy of the noise prediction can be observed in these charts. Figure 13 in the previous section shows the recommended spectral characteristics for broadband vortex noise.

These modifications change the levels, spectra, and directivities of the predicted noise in a manner that provides good agreement for the standard three blade propeller and acceptable agreement for the acoustic three blade and standard six blade propeller.

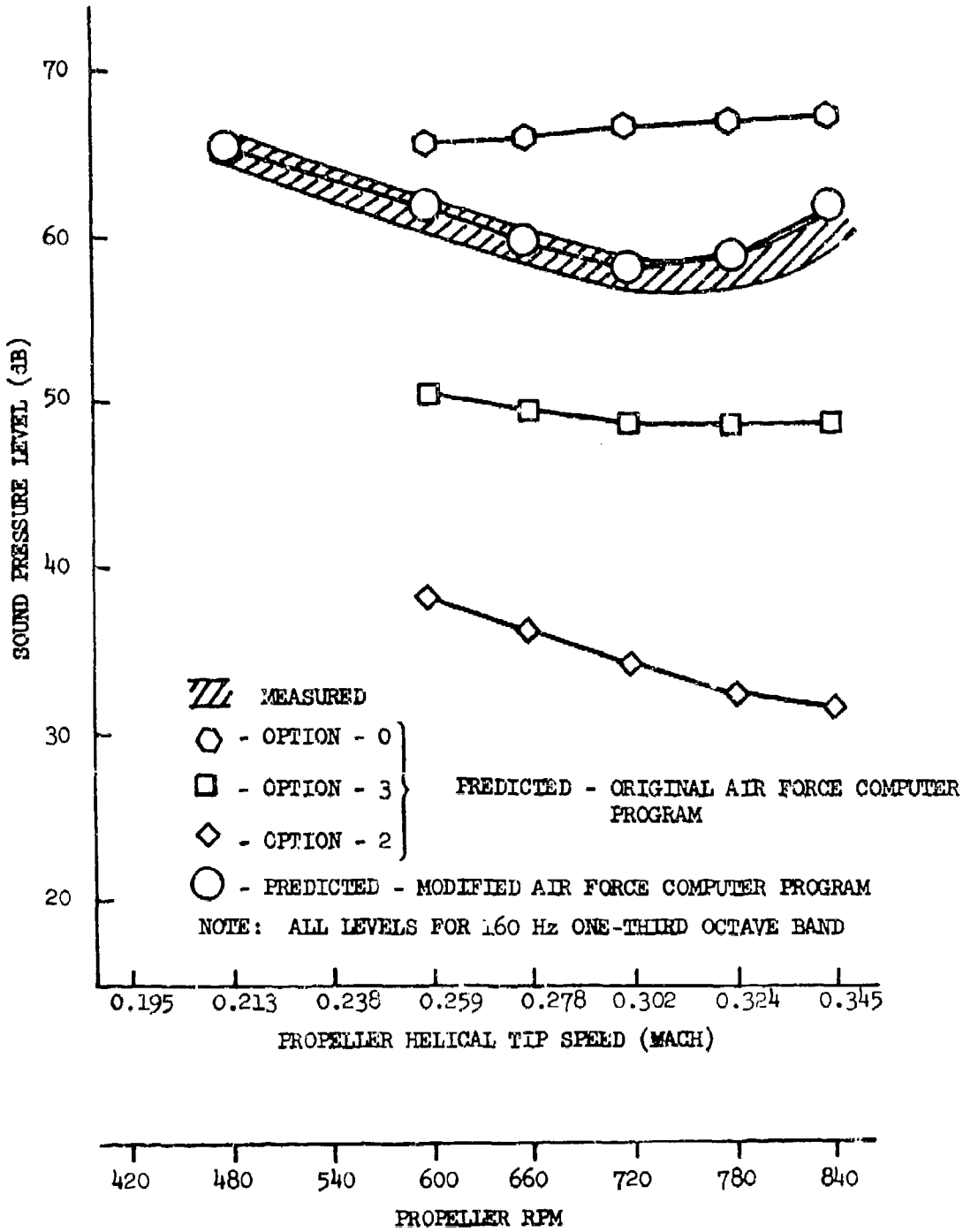


Figure 42. Comparisons of Measured Vortex Noise with Predictions of Original and Modified Air Force Computer Program (Standard 3 Blade Propeller)

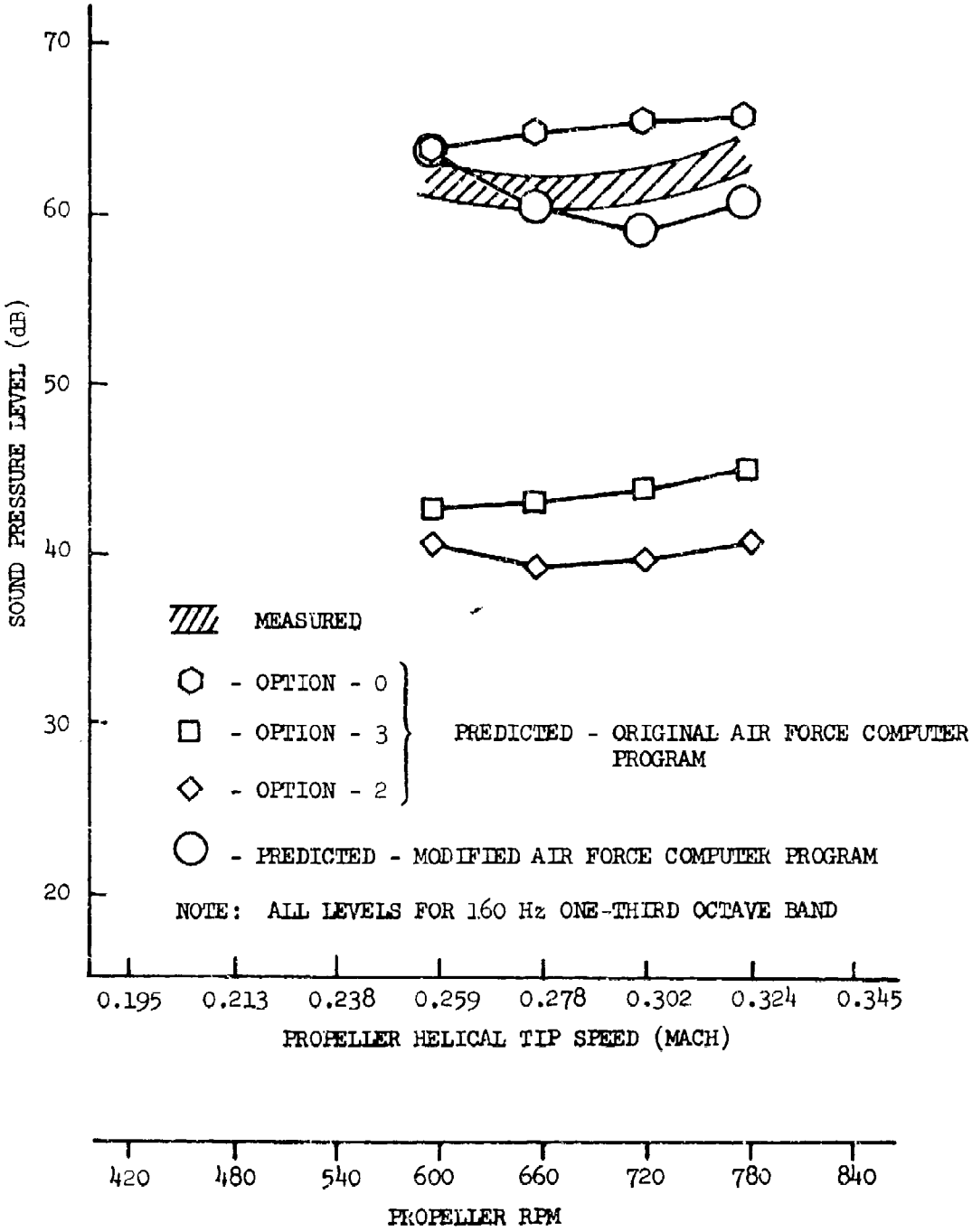


Figure 43. Comparisons of Measured Vortex Noise with Predictions of Original and Modified Air Force Computer Program (Acoustic 3 Blade Propeller)

## SECTION VII

## DESIGN CHARTS FOR LOW TIP SPEED PROPELLERS

Design charts for low tip speed propellers that can be used in the design of future propeller driven quiet aircraft are presented in this section. These charts were constructed from noise predictions made by the Air Force using the modified Air Force computer program. Input data on propeller configuration and operation were supplied by CALAC. An aircraft configuration similar to the YO-3A was assumed. Input data were as follows:

Propeller Blade Configuration: Same as standard 3 blade propeller used on YO-3A scaled to size

Diameter: 8, 10, and 12 feet  Forward Flight Speed: 125 ft/sec

Number of Blades: 2, 3, and 6

Thrust: 100, 200, 300, 400, and 500 pounds

Helical Tip Speed: 0.2 to 0.4 Mach

The modified Air Force computer program provided predictions of one third octave band levels for both rotational and vortex noise for the overhead position at an altitude of 125 feet. From these levels Overall Sound Pressure Level (OASPL) was computed. Aural Detection Ranges (ADR) were also predicted for the various propellers and operating conditions assuming the atmospheric and ambient background noise conditions stated in Reference 7 (Daytime Jungle).

In the design charts OASPL and ADR are shown as functions of the several variables. It should be noted that ADR is dependent upon spectral content and shape as well as noise level. For this reason, the trends shown in OASPL and ADR charts are usually not identical. The assumption is made in all cases, of course, that the propeller is the predominant noise source. The intended use of these design charts is discussed below and the information on the general subject of aural detection of quiet aircraft, based on several years of experience involving such aircraft, is also presented.

### 1. USE OF DESIGN CHARTS

The purpose of the low tip speed propeller design charts is to support conceptual and preliminary design of propeller driven quiet aircraft that require thrust levels from 100 to 500 pounds. Such aircraft are assumed to require propeller tip speeds in the range from Mach 0.2 to 0.4 where design information has not previously been available. While the charts presented in this section are considered adequate for these initial design studies, it must be emphasized that any final detailed design should include more extensive work involving the impact of aircraft configuration. Theoretical results show that the position of the wing relative to the propeller, for example, can influence the levels of propeller noise. Therefore, in detailed design studies

the modified Air Force computer program should be used to predict propeller noise of specific designs, and these results should be adjusted for impact of aircraft configuration as discussed above in Section V.

The design charts presented below are intended to provide the capability to involve acoustic noise criteria in the important initial trade off studies with other performance requirements in the concept and preliminary design stage. Examples of such application are given below for each of the types of charts.

a. Figure 44. - This series of charts shows the minimum OASPL and ADR that can be achieved with propeller driven aircraft. In the course of this study it has been demonstrated that minimum noise is not necessarily produced at minimum propeller tip speed. For these charts the optimum propeller tip speed to achieve minimum noise is assumed. In general, these charts show the minimum acoustic noise goals that are realistic for aircraft requiring a given thrust and are constrained by propeller diameter and number of blades.

b. Figures 45 through 47. - This series of charts show the effects of propeller helical tip speed and indicate the tip speed required to achieve the acoustic goals with given propeller diameters. A factor of prime importance in any quiet aircraft design is the amount of speed reduction required between the engine and propeller. Both size and weight penalties for the speed reduction system are involved. These charts show the tip speed, which defines speed reduction required for a given engine that is dictated by acoustic criteria. They also show the acoustic penalty in terms of OASPL and ADR if compromises must be made to satisfy other requirements. These charts are convenient to use when propeller diameter is established and cannot be changed.

c. Figures 48 through 50. - These charts are similar to those discussed above but are plotted in a format that is convenient when an aircraft of given thrust is under consideration.

These design charts for low tip speed propellers should estimate the OASPL measured in flyover tests at altitudes of 125 feet with acceptable accuracy. Likewise, the relative noise levels predicted for competing designs should provide useful quantitative information for trade off studies. However, experience has shown that realistic predictions or measurements of aural detection distances are difficult and often contradictary. In the light of this experience the following discussion is presented.

2. AURAL DETECTION RANGE

As noted at the beginning of this report, the objective of development of quiet aircraft is to operate covertly at night over enemy territory. The low acoustic noise signature of such airplanes is the means of avoiding aural detection by observers on the ground. Thus to evaluate performance of quiet aircraft designs it is important to have some realistic estimate of ADR. Experience has shown that such an estimate is difficult to obtain. Actually

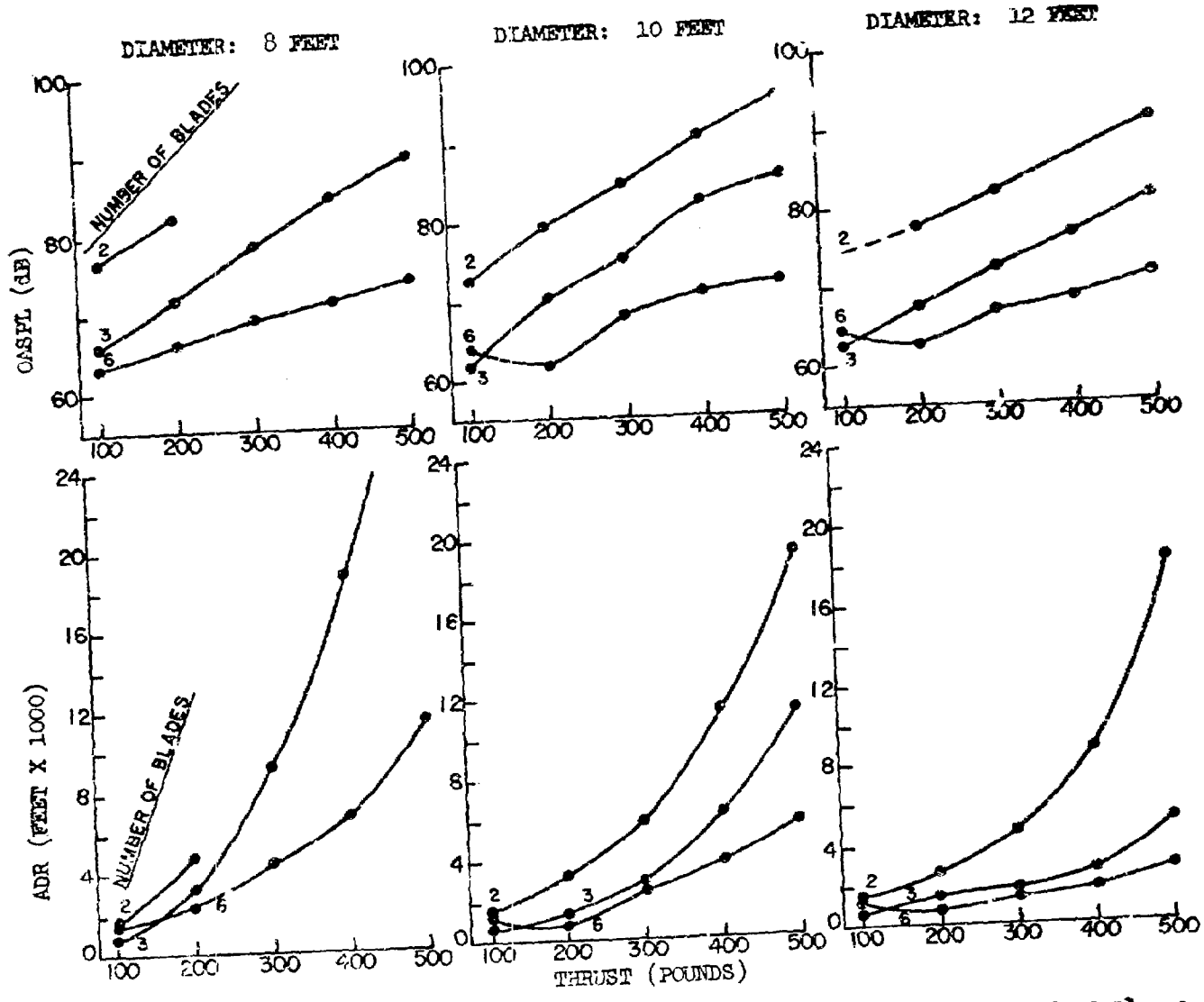


Figure 44 - Propeller Design Chart - Minimum Overall Sound Pressure Level (OASPL) and Aural Detection Range (ADR) at Optimum Tip Speed

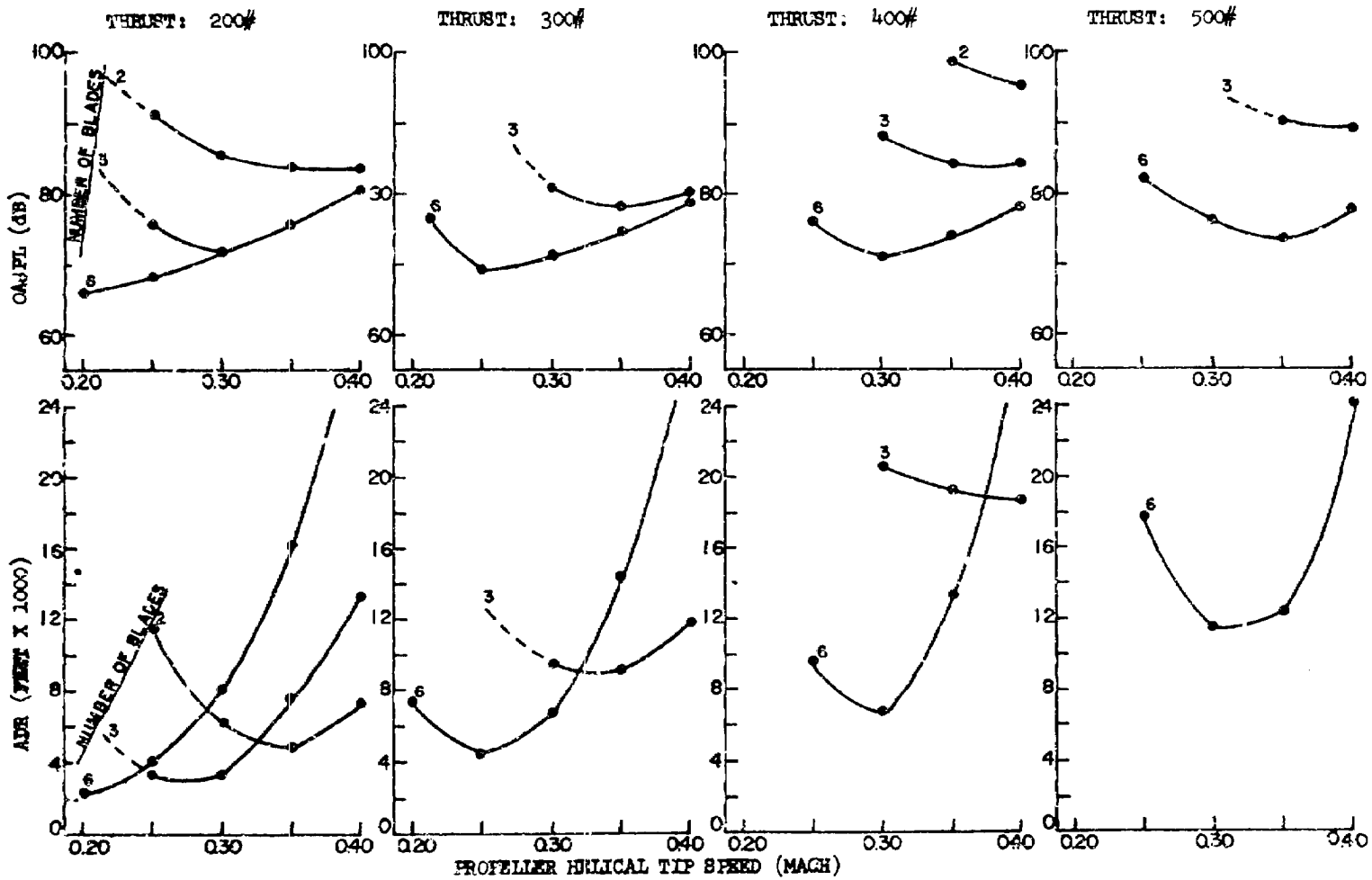


Figure 45 - Propeller Design Chart - Diameter: 8 Feet

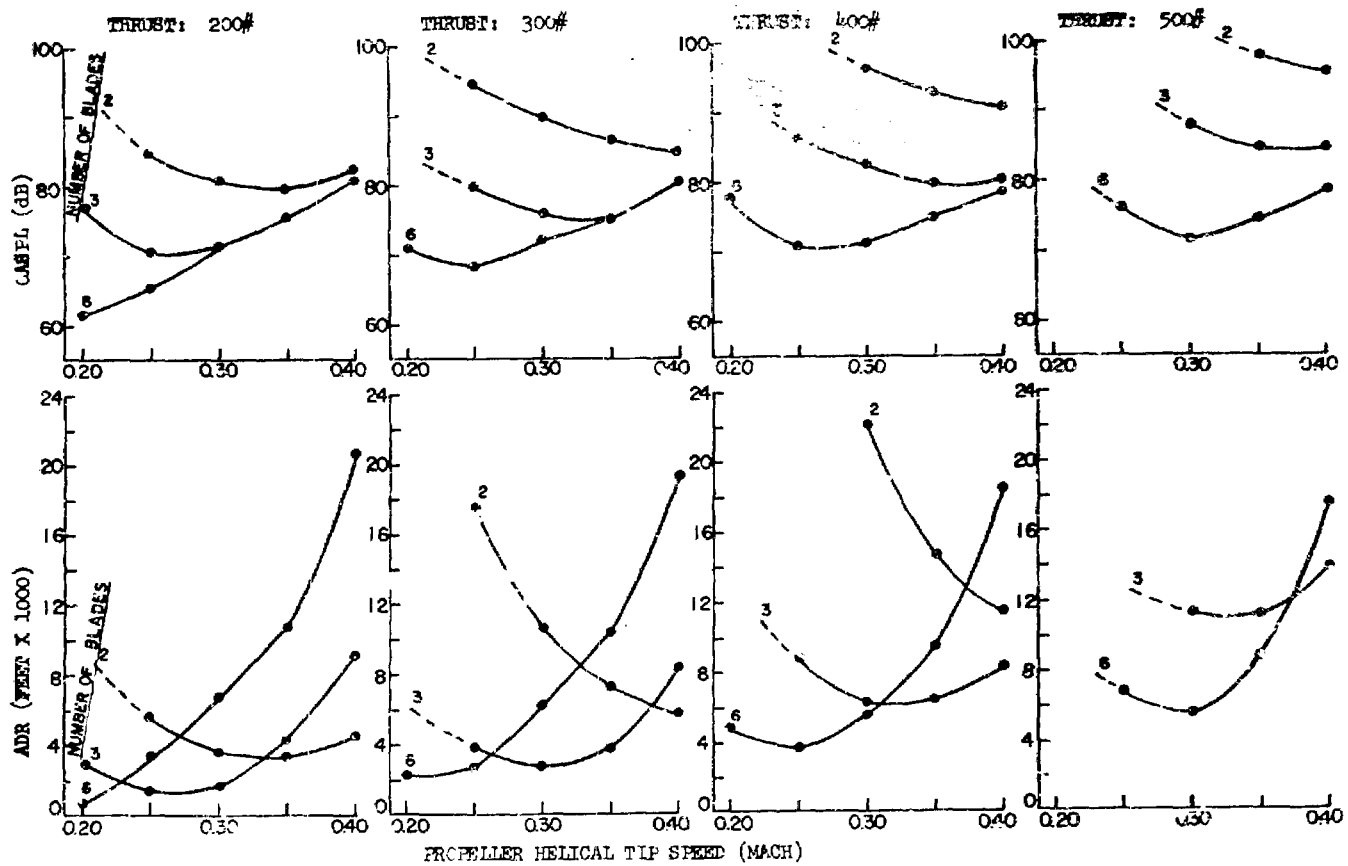


Figure 46 - Propeller Design Chart - Diameter: 10 Feet

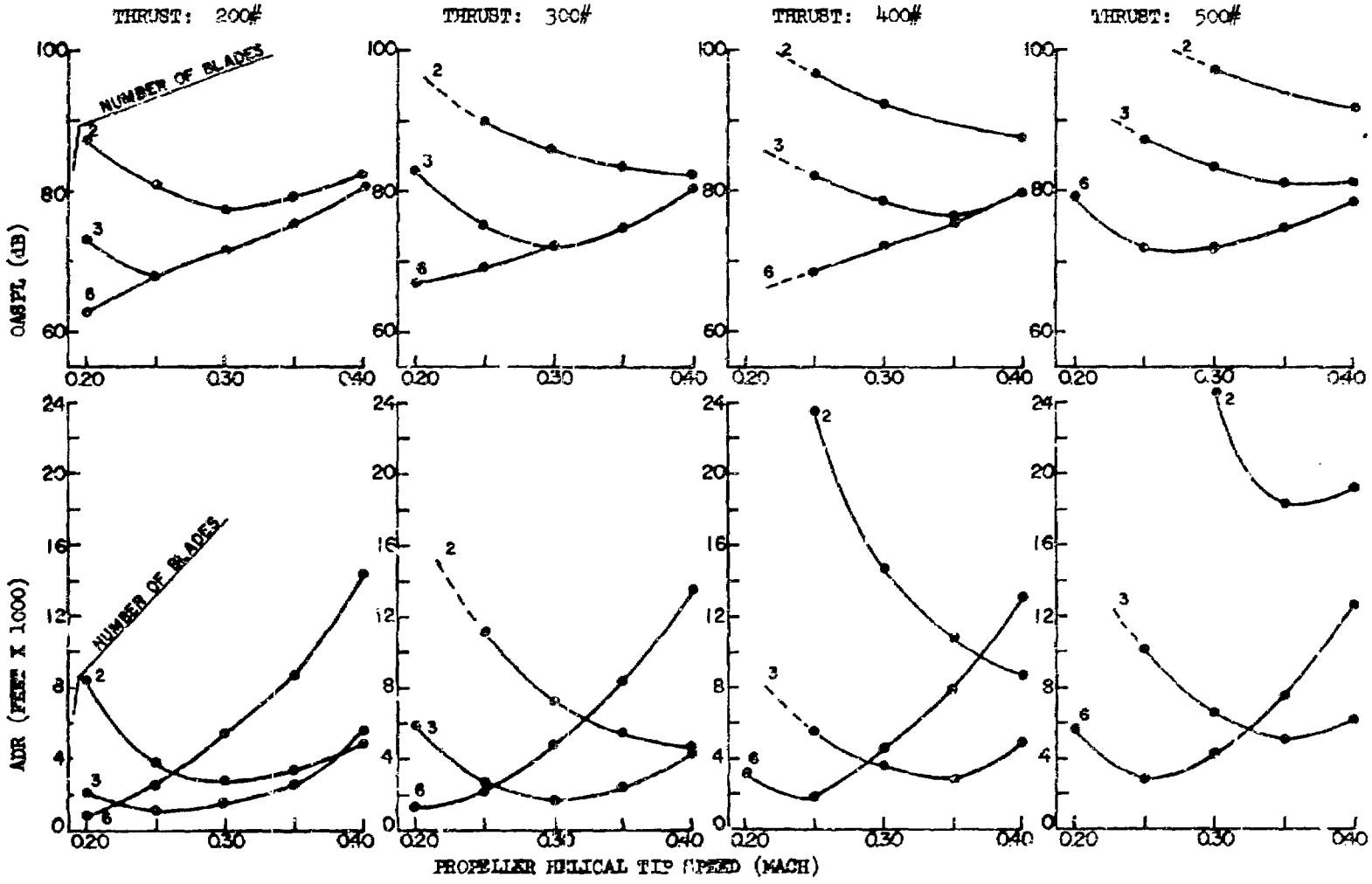


Figure 47 - Propeller Design Chart - Diameter: 12 Feet

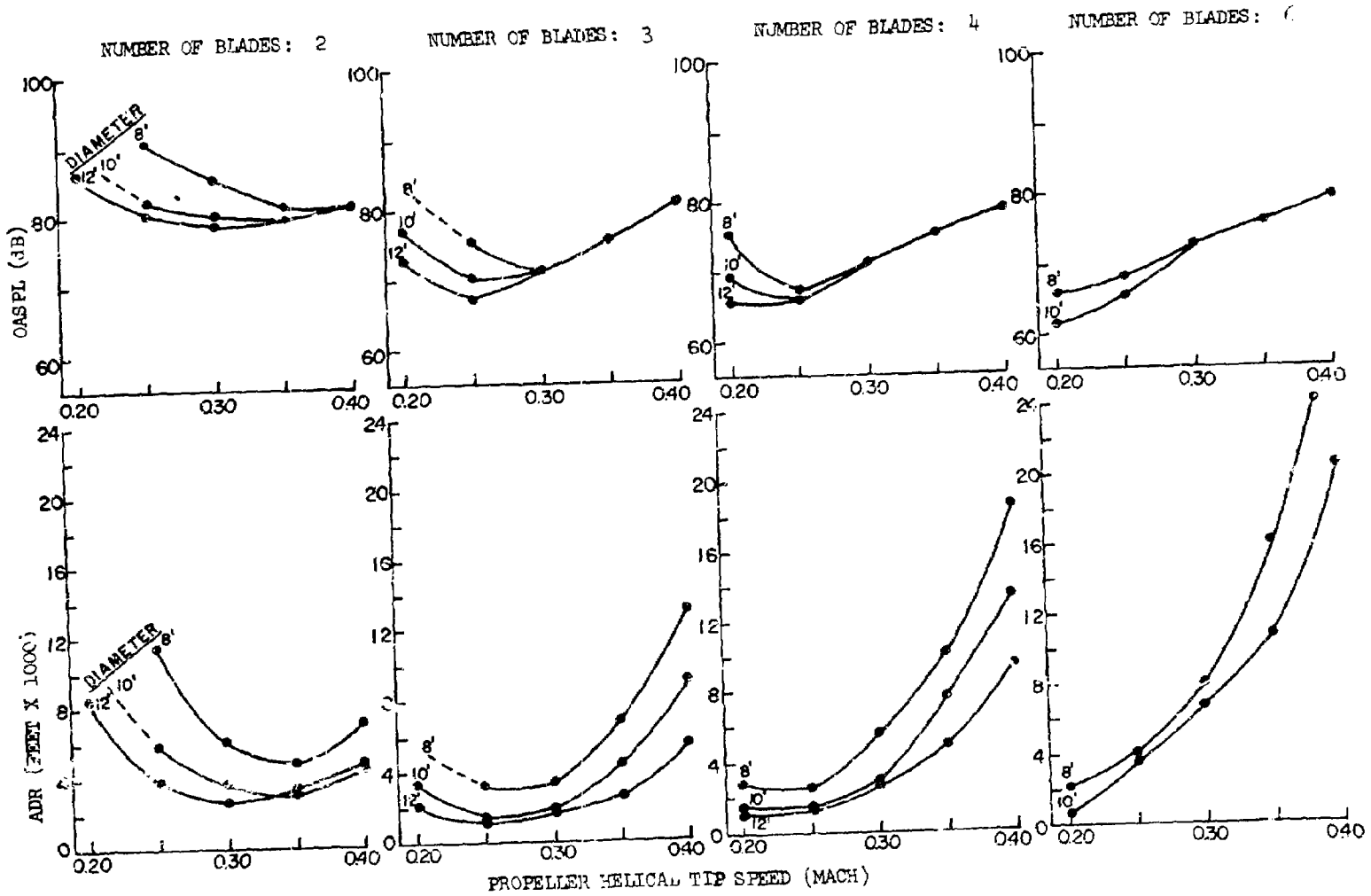


Figure 48 - Propeller Design Chart - Thrust: 200 Pounds

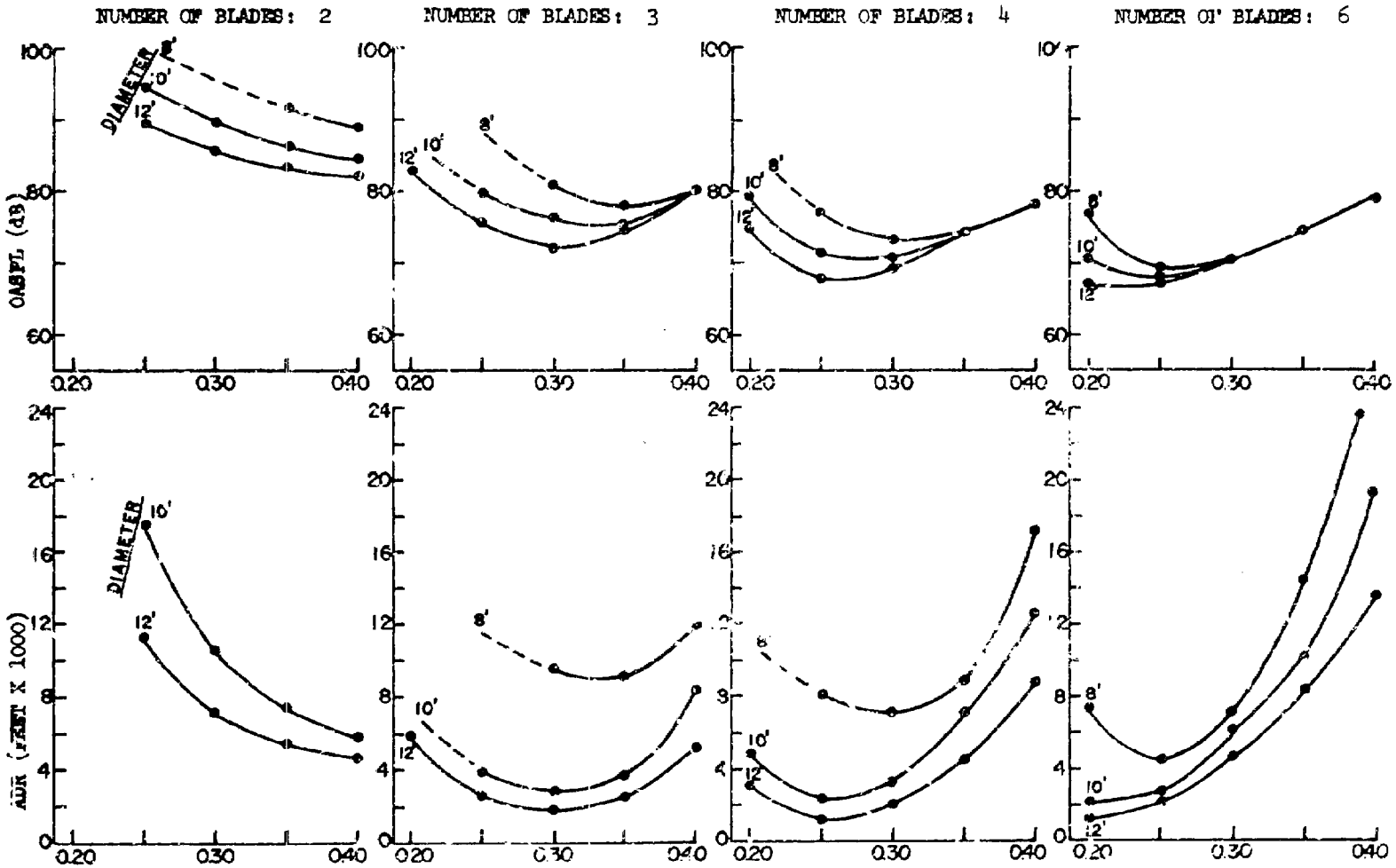


Figure 49 - Propeller Design Chart - Thrust: 300 Pounds

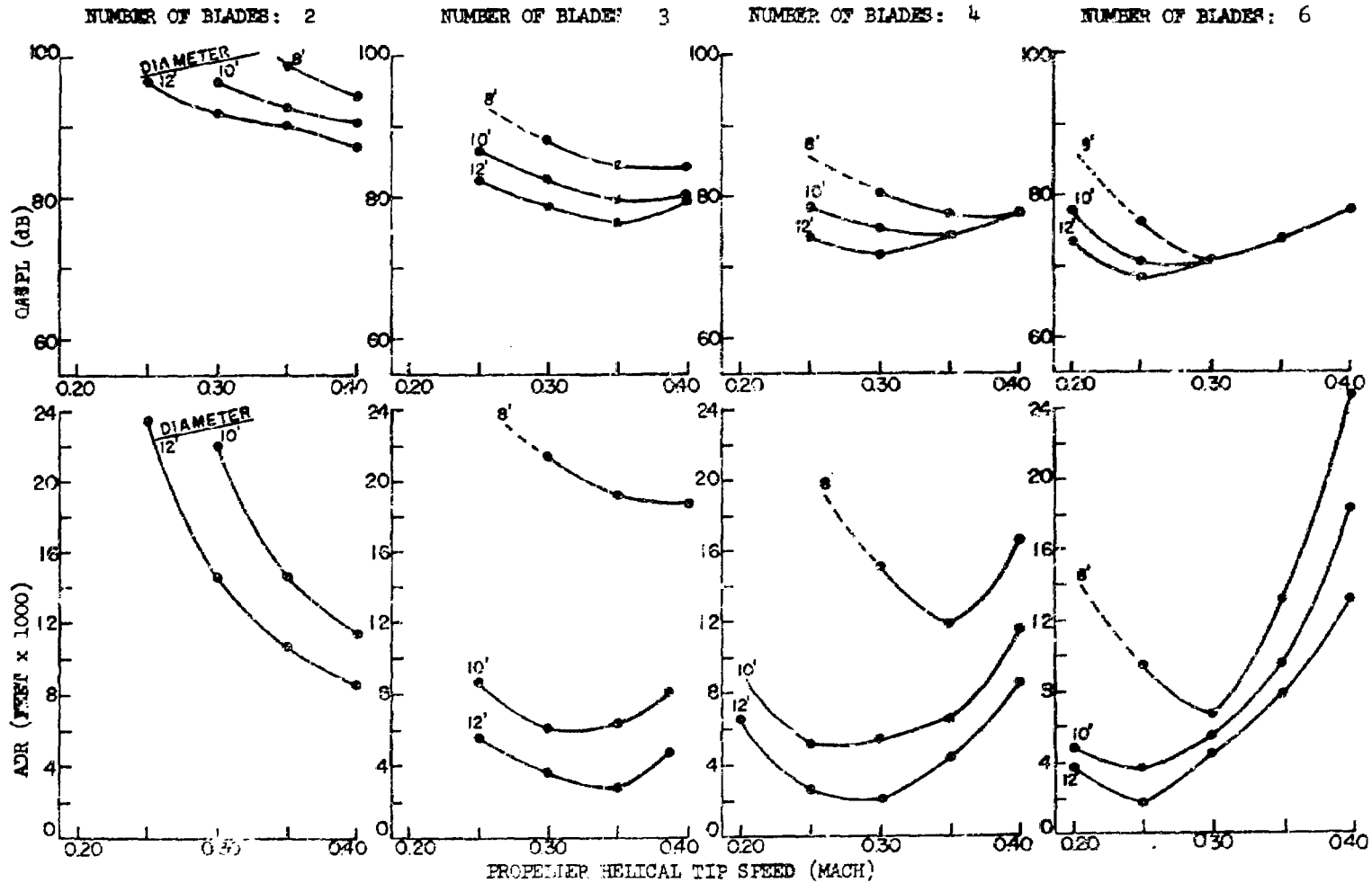


Figure 50 - Propeller Design Chart - Thrust: 400 Pounds

this range problem is fairly common and occurs in other systems such as those using radar or seismic techniques, but in the problem of determination of ADR of quiet airplanes difficulties of evaluating human response are added.

In general, the airplane emits an acoustic noise whose noise levels, spectra, and directivity can be measured. Experience with the YO-3A showed that this noise signature was fairly constant for well maintained airplanes. This noise is attentuated in the atmosphere while being radiated from the air to the ground. Experience shows that the attenuation factor varies a great deal and is most difficult to evaluate. Standard tables for atmospheric attenuation of sound is a gross assumption usually made that is not often representative of actual conditions. Finally the observer on the ground must hear and recognize the noise. Obviously the levels and spectra of ambient background noise and the masking effect of this noise is a factor, but, the observers ability to hear and recognize the airplane noise is also of importance.

In the light of these several factors, predictions of ADR must include simplifying assumptions. The method discussed in Reference 7 is typical of such calculations.

On the quiet airplane program it was possible to determine a practical ADR from thousands of operational flights in SEA. In addition, many calculations using conventional analytical methods were made for the YO-3A flying with the different propellers. Finally, in a series of field tests in California a determination of ADR of the YO-3A flying with the standard six blade propeller was made. These three different methods yield widely different determinations of ADR that seems to be yet another paradox in quiet airplane acoustics.

a. Actual Field Operations

Even though several YO-3A aircraft operated in SEA for almost a year, their use was limited to small land areas and could not be considered a typical Army night operation; therefore, ground observers probably were not alerted to expect these airplanes. This factor probably contributed to failure of many people on the ground to detect and recognize the aircraft. Because of the filtering process of the effects of atmospheric attentuation, hearing threshold, and masking, the audible noise is usually limited to a frequency range between about 200 and 700 Hz. Such noise does not "sound" like a small airplane, or if identified as originating from above may be mistaken for a high flying jet aircraft. (The low and slow quiet aircraft has an apparent sound and source trajectory similar to a high and fast commercial jet airplane.) If the observer cannot identify direction, he may also think that it is a distant truck or tank. Another possibility is that he knows there is an aircraft but doesn't care. The airborne observer is viewing the ground with a night vision device. Perhaps the man on the ground thinks he cannot be seen in the dark. On the other hand the YO-3A carried no weapons. Perhaps the people on the ground did not worry too much about being seen in their normal operation when no immediate action was taken against them.

What ever the cause, the YO-3A flying with both standard three and six blade propellers operated at night at altitudes of 1500 to 2500 feet over

SEA. Most times the actions of people observed on the ground appeared normal and they did not seem aware of the aircraft overhead. Thus, the average ADR as determined in service is considered to be about 2000 feet.

b. Typical Predictions

Using the noise signature measured in the standard 125 feet flyover tests, standard atmospheric absorption tables, and ambient background noise of typical jungle conditions (as suggested in Reference 7) or measured in the field tests in California, ADR was estimated for the YO-3A flying with all propellers. These analytical predictions produced estimates greater than those determined in SEA. Predictions of 3000 to 5000 feet were common. An average predicted ADR of 4000 feet can be assumed.

c. Simulated Field Tests

Prior to deployment of the YO-3A overseas, a series of field tests were conducted in a remote location in California. The principal author of this report was present at these tests and it is his subjective judgement that the aircraft flying with the standard six blade propeller can be heard and identified by a "cued" observer at distances of 6000 to 10,000 feet. In these tests the ambient background noise may have been somewhat below the levels attributed to night jungle conditions. However, the average ADR observed in these field tests must be assumed to be about 8000 feet.

The conclusion must be drawn that allowances must be made for a number of subjective factors when considering aural detection range. For the three methods of determination of ADR discussed above, average values of 2000, 4000, and 8000 feet were obtained, respectively. This obviously is a geometric progression that depends on method of determination.

The calculated ADR values shown in the design charts can be used to determine relative values in design studies. But it should be remembered that lower altitudes may be possible in service, and in simulated field tests greater ADR's may be measured.

3. EXAMPLE OF ANOMALOUS PROPAGATION EFFECTS

As mentioned above, it is unlikely that the air to ground propagation determined from standard atmospheric tables is realistic for field conditions. An example of this is given below.

Figure 5_ is a long time history of a flyover conducted at an altitude of approximately 3000 feet. OASPL and selected one third octave band levels are shown for a total time period of many seconds. This initial flyover with the YO-3A using the standard six blade propeller seems typical. Figure 52 [illegible] the one third octave band spectrum for near overhead position. The significant feature of this spectrum is the prominence of the fundamental rotational noise in the 63 Hz band. Apparently this discrete frequency that was attenuated by the first destructive ground reflection in lower altitude tests was not attenuated in this high altitude case. Perhaps scattering of the wave front along this greater distance accounts for this.

SEA. Most times the actions of people observed on the ground appeared normal and they did not seem aware of the aircraft overhead. Thus, the average ADR as determined in service is considered to be about 2000 feet.

b. Typical Predictions

Using the noise signature measured in the standard 125 feet flyover tests, standard atmospheric absorption tables, and ambient background noise of typical jungle conditions (as suggested in Reference 7) or measured in the field tests in California, ADR was estimated for the YO-3A flying with all propellers. These analytical predictions produced estimates greater than those determined in SEA. Predictions of 3000 to 5000 feet were common. An average predicted ADR of 4000 feet can be assumed.

c. Simulated Field Tests

Prior to deployment of the YO-3A overseas, a series of field tests were conducted in a remote location in California. The principal author of this report was present at these tests and it is his subjective judgement that this aircraft flying with the standard six blade propeller can be heard and identified by a "cued" observer at distances of 6000 to 10,000 feet. In these tests the ambient background noise may have been somewhat below the levels attributed to night jungle conditions. However, the average ADR observed in these field tests must be assumed to be about 8000 feet.

The conclusion must be drawn that allowances must be made for a number of subjective factors when considering aural detection range. For the three methods of determination of ADR discussed above, average values of 2000, 4000, and 8000 feet were obtained, respectively. This obviously is a geometric progression that depends on method of determination.

The calculated ADR values shown in the design charts can be used to determine relative values in design studies. But it should be remembered that lower altitudes may be possible in service, and in simulated field tests greater ADR's may be measured.

3. EXAMPLE OF ANOMALOUS PROPAGATION EFFECTS

As mentioned above, it is unlikely that the air to ground propagation determined from standard atmospheric tables is realistic for field conditions. An example of this is given below.

Figure 51 is a long time history of a flyover conducted at an altitude of approximately 3000 feet. OASPL and selected one third octave band levels are shown for a total time period of many seconds. This initial flyover with the YO-3A using the standard six blade propeller seems typical. Figure 52 [illegible] the one third octave band spectrum for near overhead position. The significant feature of this spectrum is the prominence of the fundamental rotational noise in the 63 Hz band. Apparently this discrete frequency that was attenuated by the first destructive ground reflection in lower altitude tests was not attenuated in this high altitude case. Perhaps scattering of the wave front along this greater distance accounts for this.

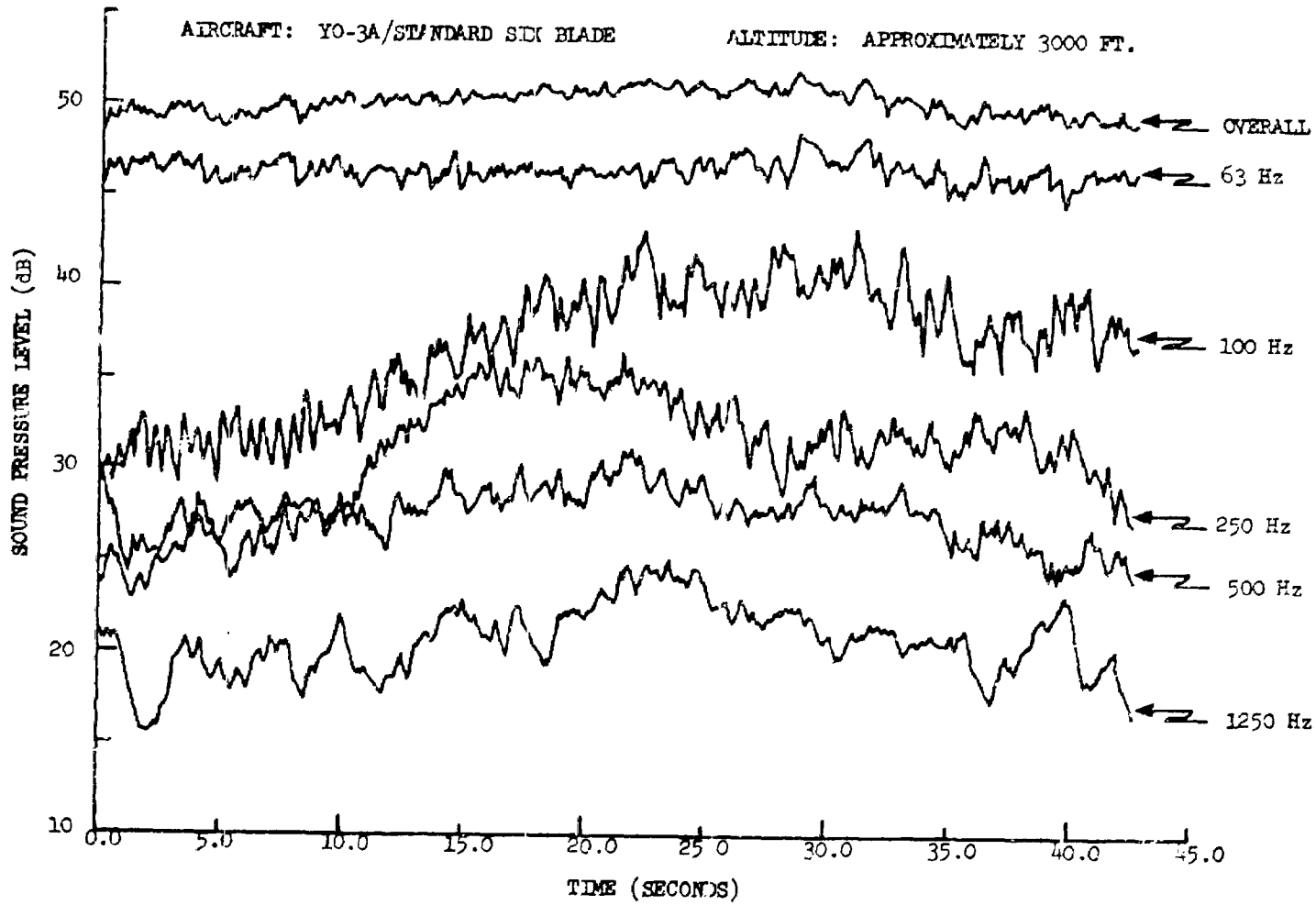


Figure 51 - Typical Long Time History of High Altitude Flyover

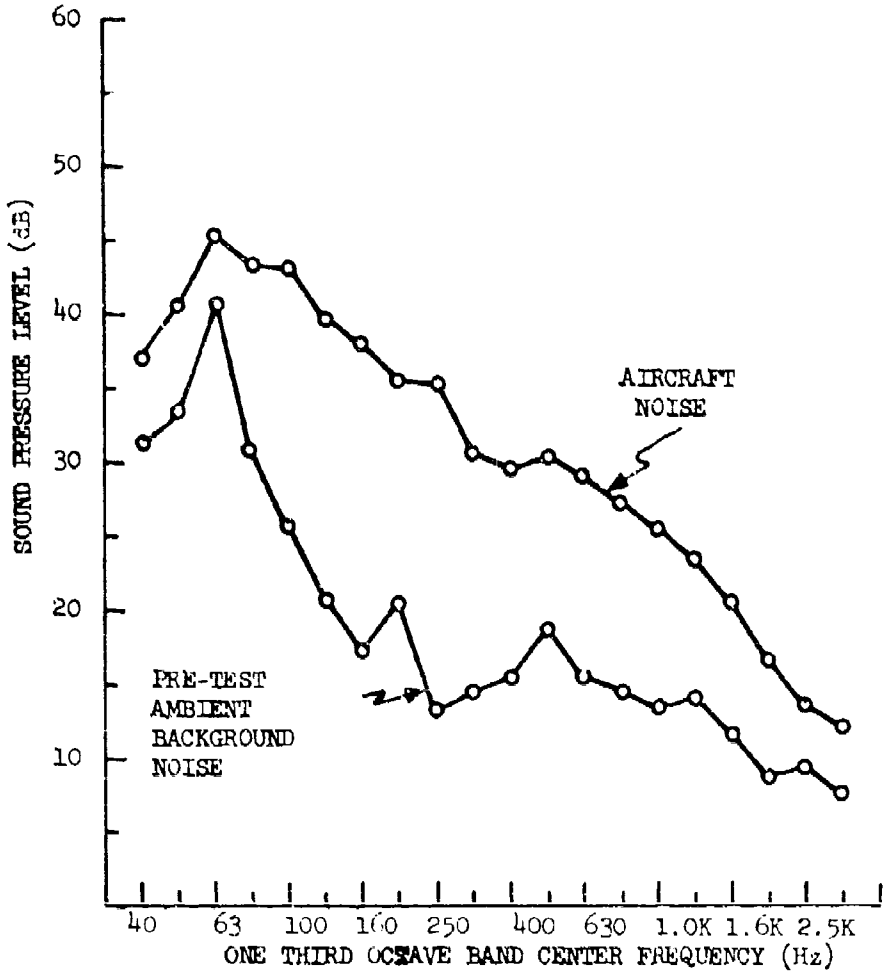


AIRCRAFT: YO-3A/STANDARD SIX BLADE
ALTITUDE: APPROXIMATELY 3000 FEET
VELOCITY: 125 FEET/SECOND (74 KTS)
PROPELLER HELICAL TIP SPEED: MACH 0.269

Figure 52 - Typical One-Third Octave Band Spectra For High Altitude Flyover

Figure 53 shows the same type of long time history taken about thirty minutes later. (Both flyovers occurred in early morning.) In this case the discrete frequency rotational noise fundamental suffers a series of depressions in levels similar to "beat" phenomena. As far as can be determined source levels did not vary. Average period of these oscillations in level is about three seconds. The reason for these observed oscillations is not known. Various assumed layered atmospheric models have not produced similar results. However, these anomalous oscillations in level are observed often in the field and should be accounted for in any new prediction technique for ADR.

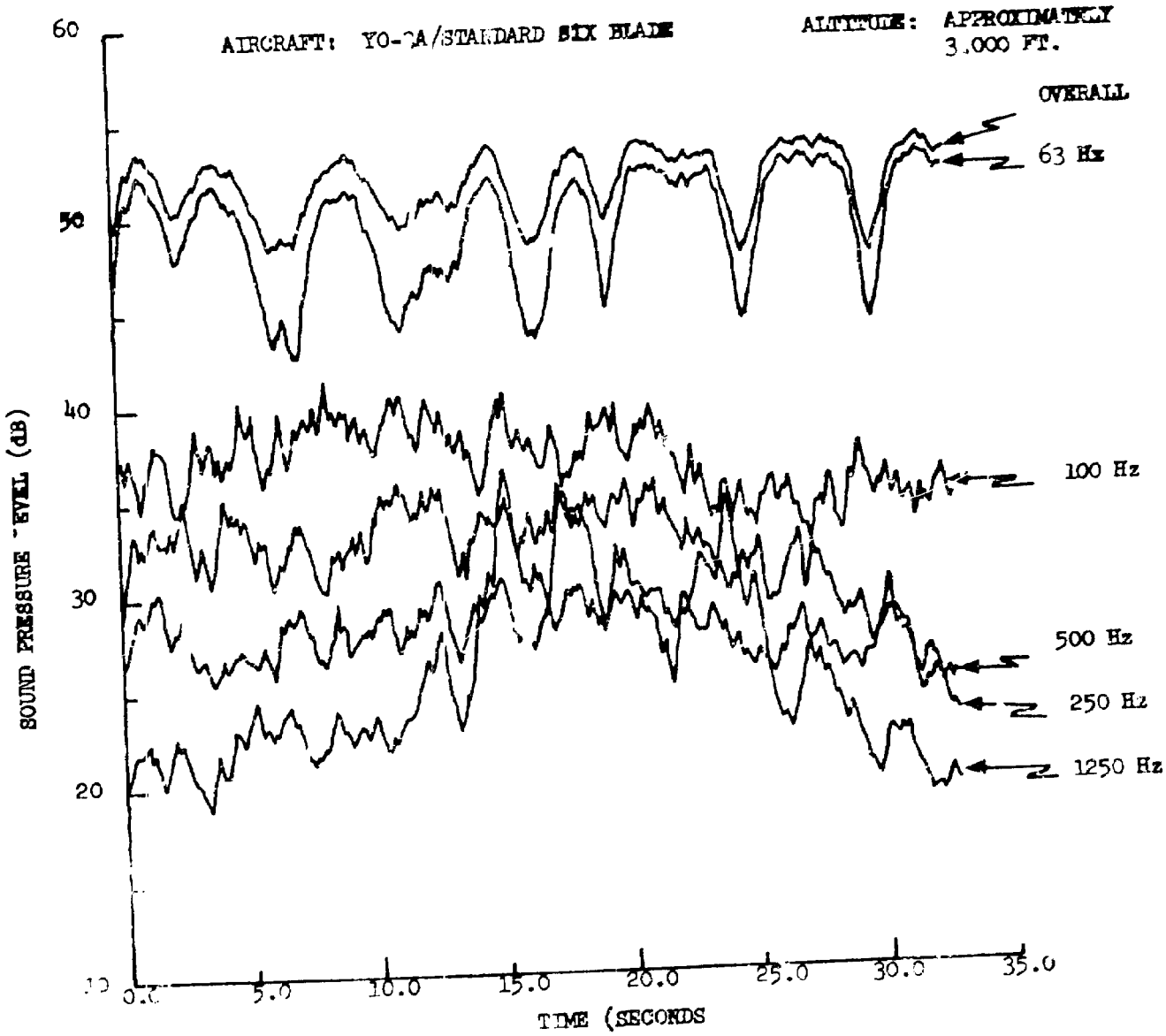


Figure [illegible] - Anomalous Long Time History of High Altitude Flyover

## SECTION VIII

## CONCLUSIONS

The following conclusions are drawn from the tasks performed in this study and described in this report.

1. Detailed analysis of noise data acquired from past flyover experiments conducted with the YO-3A aircraft provided baseline information on far field radiated noise from three different low tip speed propellers operating over a wide variety of conditions. These data, when corrected for certain factors related to test conditions, were of a suitably high quality in order to yield reliable results.

2. Evidence developed during this study verifies that the predominant noise in the YO-3A aircraft acoustic noise signature originates from the propeller.

3. Review of the measured low tip speed propeller noise from the flyover tests revealed the existence of unexpected and anomalous trends and levels that are not predicted by conventional propeller noise generation theory.

4. Discrepancies between measured flyover propeller noise and predictions of such noise made by the Air Force computer program demonstrate basic inaccuracies in this noise prediction program and suggest inadequacies in conventional theory.

5. Comparison of experimental results from static and flyover tests demonstrated that only flyover experimental data were useful in development of empirical corrections for the Air Force computer program.

6. Comparison of measured low tip speed (Mach 0.2 to 0.4) propeller flyover noise with predictions made by the modified Air Force computer program, demonstrated that the modified program will accurately predict far field rotational and vortex noise.

7. The comprehensive theoretical study made of propeller blade aerodynamic loads led to the conclusion that the "bucket" trend in the propeller rotational noise could not be explained on the basis of axisymmetric blade loading.

8. Further review of acoustic radiation theory led to the conclusion that non-uniform chordwise blade loading effects at high propeller angles of attack contributed, but are not entirely responsible for, the observed bucket trends.

9. Final review of theory led to the conclusion that the predominant cause of the bucket trends in the observed rotational noise was caused by two factors:

- Circumferentially non-uniform blade loads caused by inflow variations into the propeller disc plane

- Interaction of the propeller blade wake with the wing generating fluctuating lift forces on the wing causing a significant dipole noise assumed to be in phase with the basic propeller rotational noise

10. The theoretical and experimental efforts led to the conclusion that, in order to account for the aforementioned bucket trends, the empirical rotational noise modifications to the Air Force computer program should be related to the product of propeller blade lift coefficient and propeller chord.

11. A Review of the three propeller vortex noise prediction options in the Air Force computer program led to the conclusions that there existed:

- Minor theoretical inconsistencies

- Shortcomings in empirical constants based on static test results

12. Theoretical analysis led to the conclusion that random fluctuating torque and thrust forces, proportional to the steady state thrust and torque forces, can be expected. It was therefore concluded that empirical modifications for vortex noise levels for the Air Force computer program should be related to the levels predicted for the propeller rotational noise.

13. In general, it is concluded that the modified Air Force computer program resulting from this study will predict far field radiated noise of low tip speed propellers with sufficient accuracy to be useful in the design of propellers operating in the tip speed range from Mach 0.2 to 0.4.

## SECTION IX

## RECOMMENDATIONS

As a result of the accomplishments of this study it is recommended that:

1. The modified Air Force computer program and/or the design charts in this report be used for development of future propeller designs for quiet propeller driven aircraft.

2. Further theoretical work should be performed to exploit the gains achieved in this study toward a goal of complete understanding of propeller noise generation and development of realistic theoretical models that explain the observed far field radiated noise.

3. More experimental data should be acquired from either full scale flight tests or appropriately designed laboratory tests to support the theoretical effort recommended above.

4. Theoretical and experimental work should be performed that will explain the differences in character between the propeller noise generated in flyover and static experiments.

## REFERENCES


1. Anon., LMSC-687888 Acoustic Development Flight Test Report YO-3A Observation Aircraft, Contract DAAJ01-69-C-0059, January 1970 (Confidential) (Declassified February 1973).

2. Anon., LMSC-695189 Acoustic Qualification Flight Test Report YO-3A Observation Aircraft, Contract DAAJ01-69-C-0059, January 1970 (Confidential) (Declassified February 1973).

3. Anon., LMSC-D008877 YO-3A Constant Speed Propeller Flight Qualification and Demonstration Program Test Report, Contract DAAJ01-70-A-0326, August 1971 (Confidential) (Declassified February 1973).

4. Smith, D. L., et al., Measurements of the Radiated Noise from Sailplanes, TM-70-3-FDDA, July 1970.

5. Fidell, Sanford, Pearsons, Karl S., Bennett, Richard L., Predicting Aural Detectability of Aircraft in Noise Backgrounds, AFFDL-TR-72-16, Bolt Beranek and Neuman, July 1972.

6. Ungar, Eric E., et al., A Guide for Predicting the Aural Detectability of Aircraft, AFFDL-TR-71-22, Bolt Beranek and Neuman, March 1972.

7. Barry, Frank W., Magliozzi, Bernard, Noise Detectability Prediction Method for Low Tip Speed Propellers, AFAPL-TR-71-37, Hamilton-Standard, June 1971.

8. Barry, Frank W., User's Manual for Propeller Noise Detectability Computer Program, AFAPL-TR-71-38, Hamilton-Standard, June 1971.

9. Brown, Dale, Ollerhead, John B., Propeller Noise at Low Tip Speeds, AFAPL-TR-71-55, Wyle Laboratories, September 1971.

10. Healy, Gerald J., et al., Far Field Aerodynamic Noise Measurement Program, LR 23640, May 5, 1970.

11. Durand, Ed, Aerodynamic Theory, Vol. IV, Division L, "Airplane Propellers," by H. Glauert, Dover 1963.

12. Glauert, H., Elements of Airfoil and Airscrew Theory, Cambridge Univeristy Press, 1959.

13. Morse, P. M. and Ingard, K. U. Theoretical Acoustics, McGraw-Hill, 1968.

14. Garrick, I. E. and Watkins, C. E., "A Theoretical Study of the Effect of Forward Speed on the Free-Space Sound Pressure Field Around Propellers," NACA Report 1198, 1954.

15. Kemp, N. and Arnoldi, R. A., "Machine Calculation of Free-Space Sound Pressure Field Around Propellers in Forward Motor," Report R-22673-1, UAC Research Dept., February 1954.

16. Arnoldi, R. A., "Near Field Computations of Propeller Blade Thickness Noise," Report R-08966, UAC Research Dept., August 1956.

17. Abbott, I. H. and von Doenhoff, A. E., Theory of Wing Sections, Dover, 1959.

18. Dwinnell, J. H., Principles of Aerodynamics, McGraw-Hill, 1949.

19. Schubauer, G. M. and Tchen, C. M., Turbulent Flow, Princeton Aeronautical Paperback No. 9, Princeton University Press, 1960.

20. Schlegal, R. R., King, R., and Mull, H., "Helicopter Rotor Noise Generation and Propagation," Tech Report 66-4, AD645884, USAAVLABS; Oct. 1966.

21. Ollerhead, J. B. and Lowson, M. V., "Problems of Helicopter Noise Estimation and Reduction," AIAA Paper 69-195, Feb. 17-19, 1969.

22. Lighthill, M. J., "On Sound Generated Aerodynamically; I General Theory," Proceedings of the Royal Society, Series A, Volume 211, pp. 564-587, 1952.

23. Curle, N., "The Influence of Solid Boundaries Upon Aerodynamic Sound," Proceedings of the Royal Society, Series A, Volume 231, pp. 505-514, 1955.

24. Widnall, S. E., "A Correlation of Vortex Noise Data from Helicopter Main Rotors," Journal of Aircraft, Volume 6, Number 3, pp. 279-281, May-June, 1969.

25. Hubbard, H. H., "Propeller Noise Charts for Transport Airplanes," NACA TN-2968, June 1953.

26. Davidson, J. H., and Hargett, J. J., "Helicopter Noise," Journal of the Royal Aeronautical Society, Volume 69, pp. 325-336, May 1965.

27. Lowson, M. V., "The Sound Field for Singularities in Motion," Proceedings of the Royal Society of London, Series A, Volume 286, pp. 559-572, August, 1965.

## APPENDIX I

## AIRCRAFT DESCRIPTION

Measured acoustic noise data were taken in past quiet aircraft programs at the Lockheed Missiles and Space Company using two different aircraft and three different propellers. Figures I-1 and I-2 show, respectively, the Lockheed YO-3A Military Observation Aircraft and the Q/STAR Research Aircraft. Takeoff gross weights for these aircraft were approximately 3700 pounds for the YO-3A, and 2600 pounds for the Q/STAR.

Each aircraft was flown with each of the three different propellers. Figure I-3 shows the standard 3 blade, constant speed, propeller; Figure I-4 the standard 6 blade, fixed pitch, propeller; Figure I-5 the acoustic 3 blade, constant speed, propeller.

For static tests only the Q/STAR aircraft with wing removed was used. All three propellers were used in static testing.

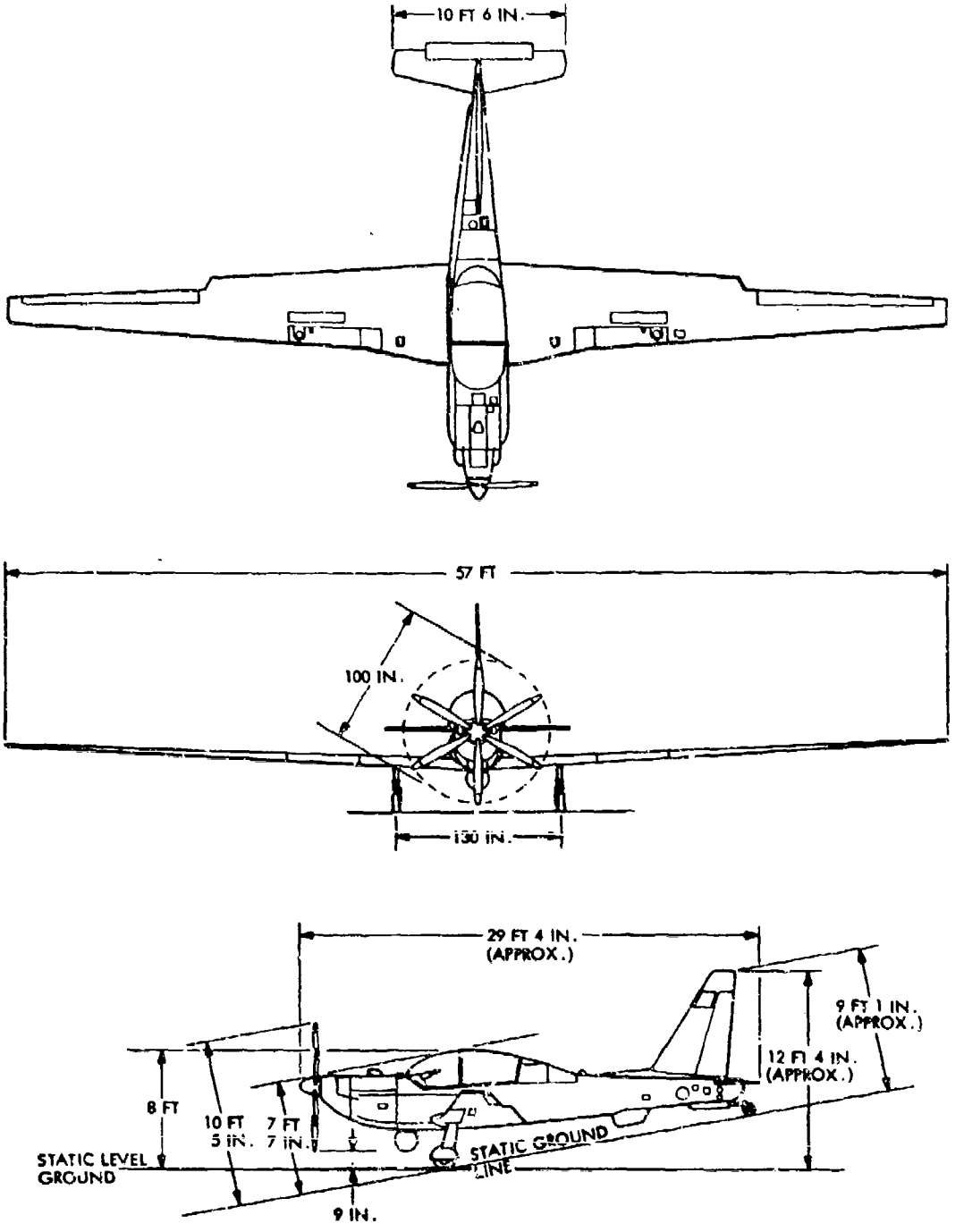


Figure I-1 YO-3A Army Observation Aircraft

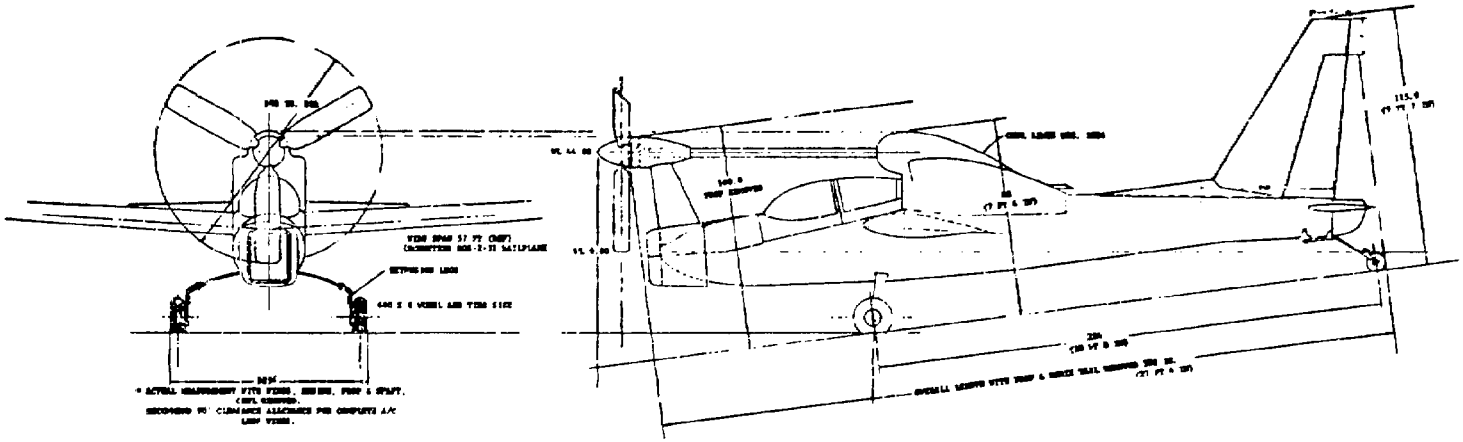

Figure I-2 Q/Star Research Aircraft

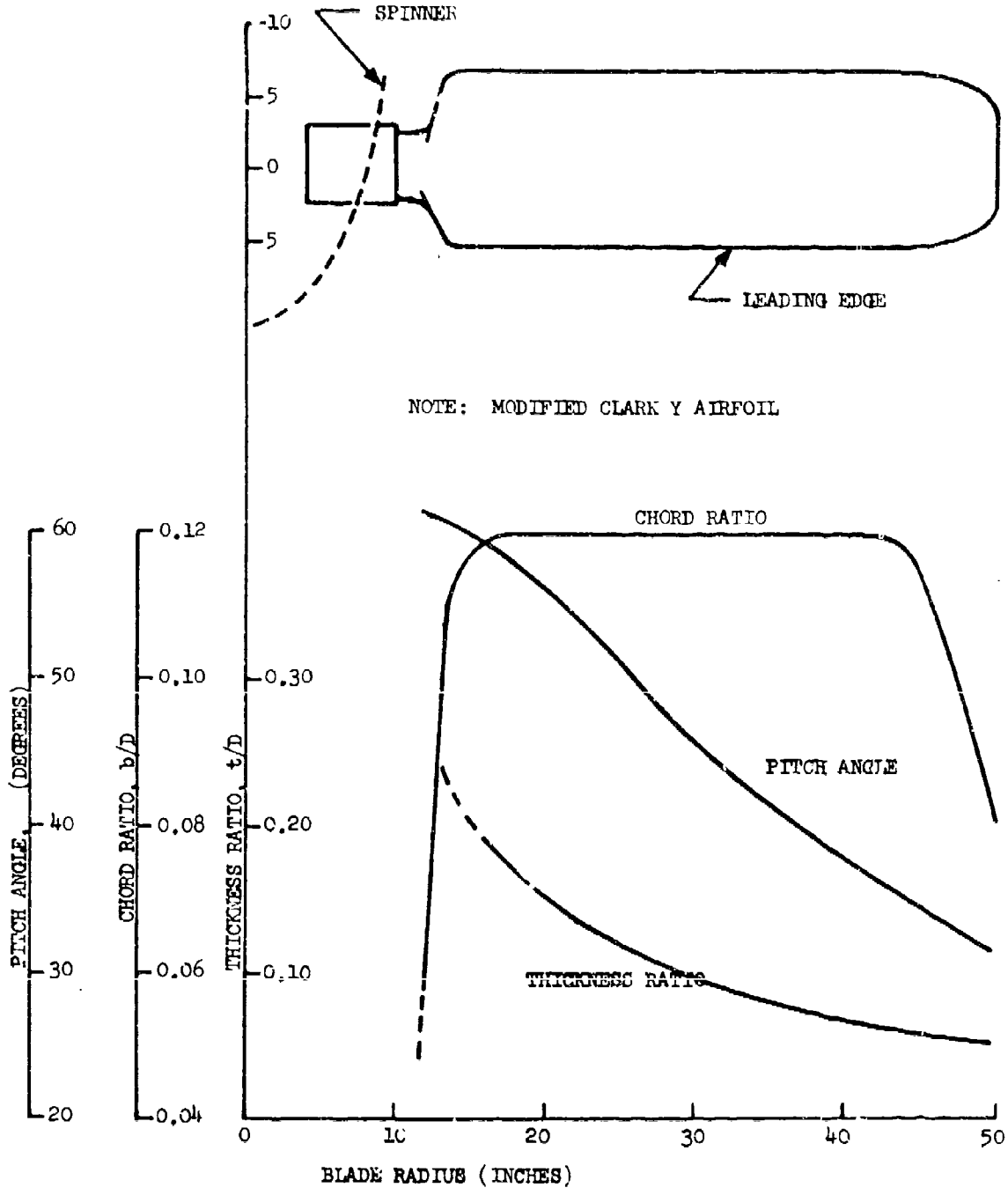


Figure I-3 Standard Three Blade Propeller

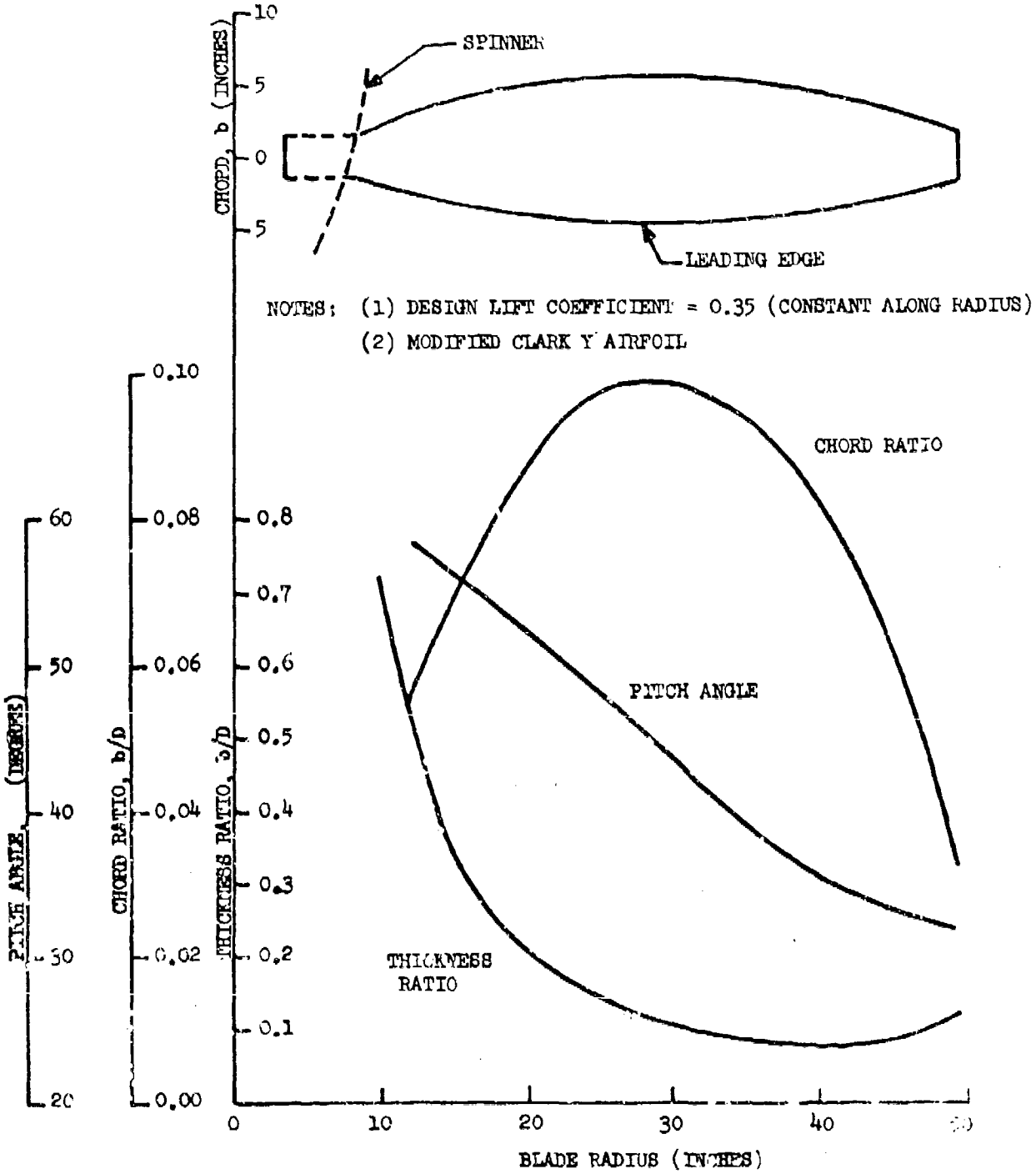


Figure I-4 Standard Six Blade Propeller

BLADE GEOMETRY

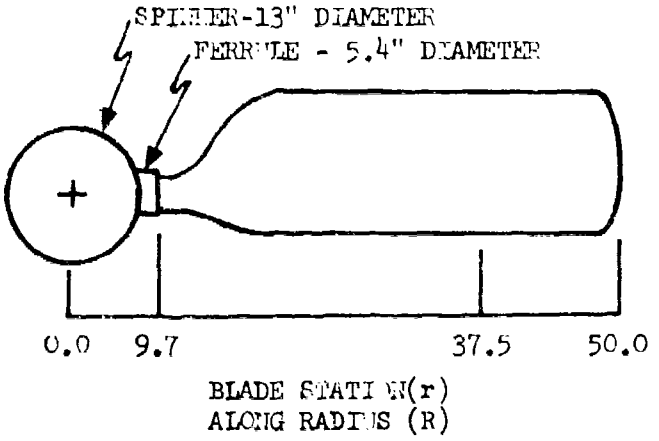


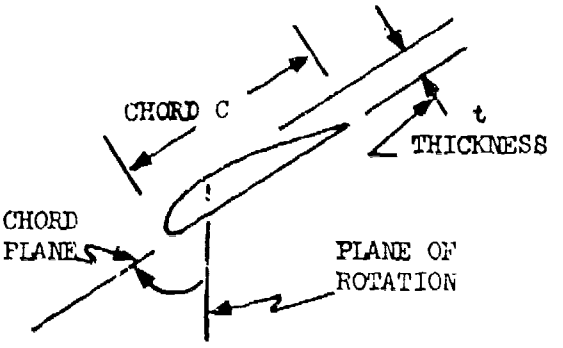


| BLADE STATION | r/R | C (") | t (") | (DEGREES) | |
|---|---|---|---|---|---|
| 12 | .24 | 5.6 | 5.0 | | |
| 18 | .36 | 14.6 | 3.7 | 70.0 | |
| 24 | .48 | 18.0 | 2.16 | 61.4 | |
| 30 | .60 | | | 54.5 | |
| 36 | .72 | | | 49.9 | |
| 37.5 | .75 | | | 47.5 | PITCH REFERENCE |
| 42 | .84 | | | 44.1 | POSITION |
| 48 | .96 | | | 40.5 | |
| 50 | 1.00 | | | 39.4 | |

NOTE: NACA 4412 AIRFOIL SECTION

Figure I-5 Acoustic 3 Blade Propeller

## APPENDIX II

## TEST AND ANALYSIS PROCEDURES

Most of the aircraft flyover runs used in this program were conducted at the Crows Landing Naval Air Station, California, at an aircraft altitude of 125 feet. The acoustic measuring station was located in a grassy area between the existing runways and taxiways on the airport proper. The LMSC mobile-acoustic test support van was the only structure in the vicinity of the test course.

The flight test course was established as shown in Figure II-1. The aircraft flyover flight path was arranged parallel and to the east of the main runway. The acoustic support van was positioned at the edge of the taxiway as far as possible from the microphone location (a separation of approximately 400 feet).

The surveyor's transit was at the altitude measuring station located 1,000 feet from the microphone station on a line perpendicular to the flight path as shown in Figure II-2. An altitude marker balloon was provided as a guide for the pilot and enabled him to fly consistently along the rather confined altitude corridor. The balloon was positioned approximately 60 feet east of the flight path, on the line-of-sight of the altitude measuring transit, and was tethered so as to be 125 feet above ground level.

The static tests were conducted in Sunnyvale, California in a cultivated area several hundred feet from any major building at the LMSC complex. Figure II-3 shows the static test course layout.

Figure II-4 shows the Lockheed Rye Canyon Research Laboratory data analysis instrumentation used on this program.

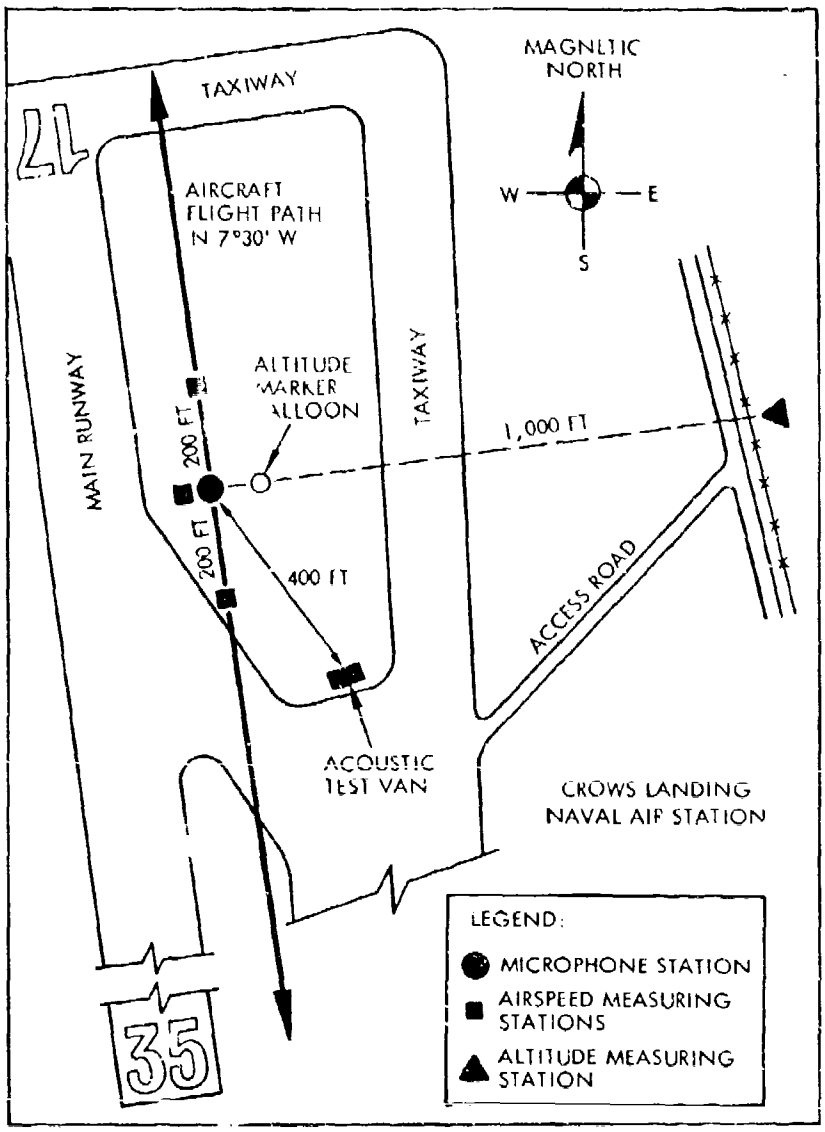


Figure II-1 Flyover Test Course Layout

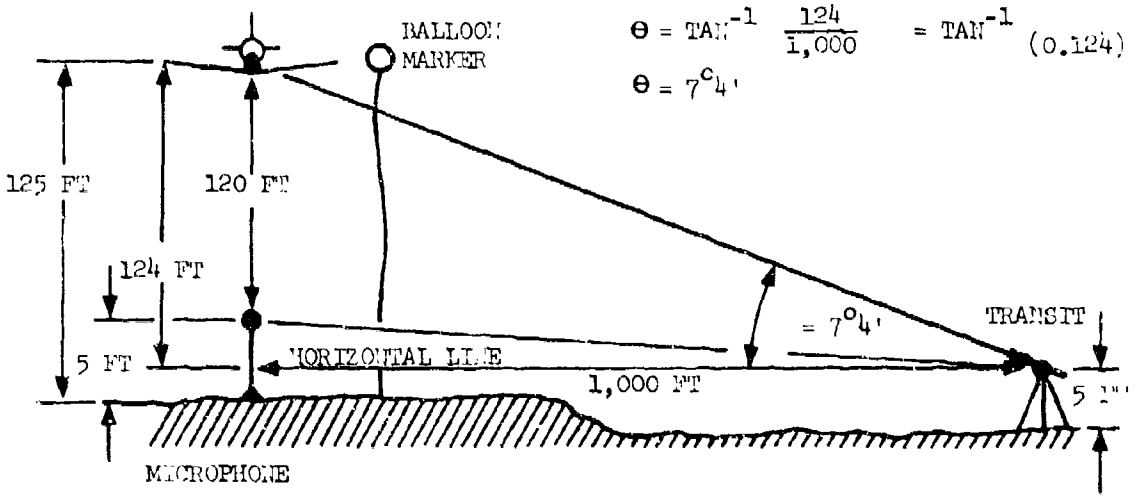


Figure II-2 Altitude Measuring Station

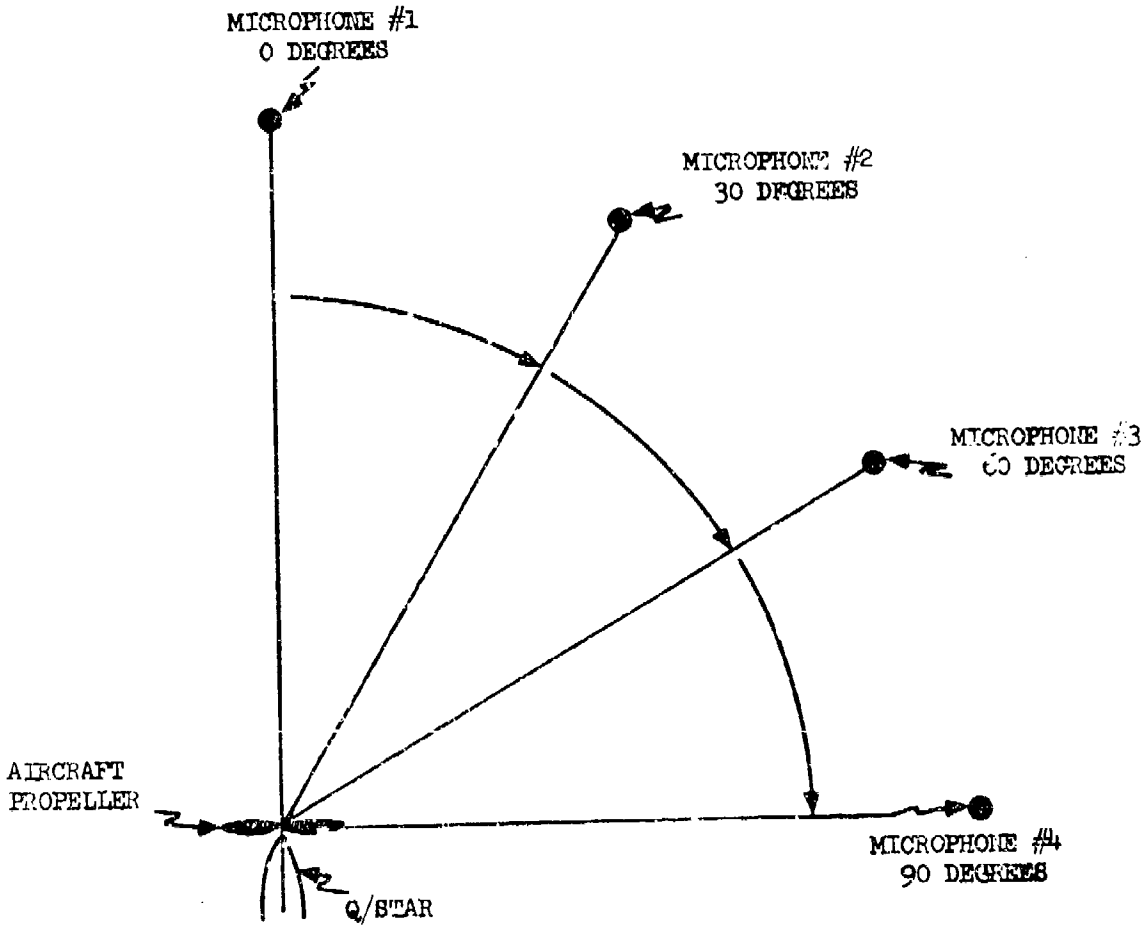


MICROPHONES LOCATED AT DISTANCES OF
50 FEET FROM THE PROPELLER HUB

Figure II-3 Static Test Course Layout

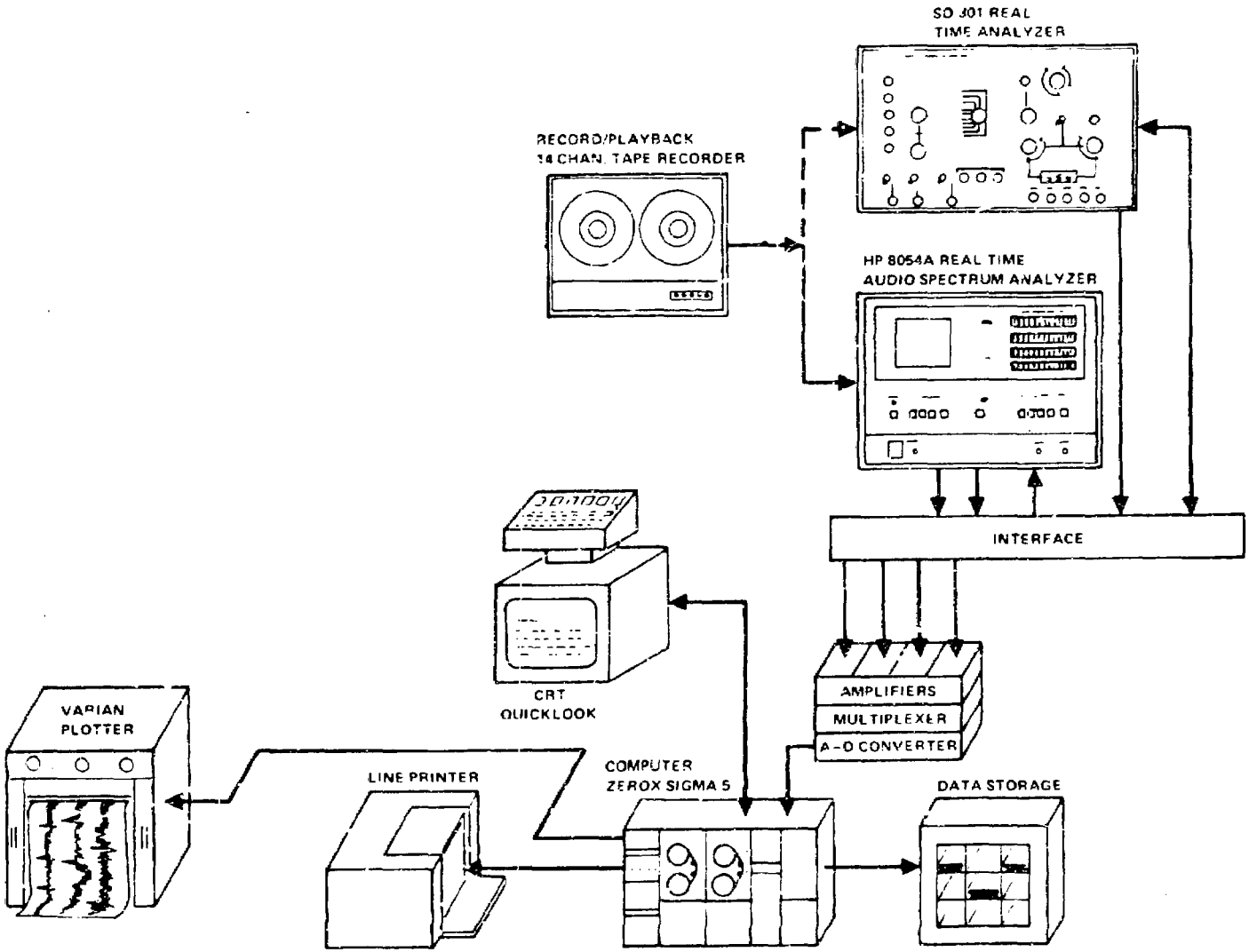


Figure II-4 Rye Canyon Research Laboratory Acoustic Data Analysis Instrumentation

## APPENDIX III

## CORRECTIONS TO ANALYZED DATA

Corrections must be made to analyze data for the effects of both ground reflection and doppler frequency shifts. These corrections are discussed below:

### 1. GROUND REFLECTION EFFECTS

Figure III-1 illustrates the routine flyover test procedure. The microphone at position (M) is always at a distance (h) of five (5) feet above the ground. The aircraft is in straight and level flight at a velocity (V). The altitude (A) above the microphone is usually 120 feet. At a given time (t) the aircraft is at position (P) at a horizontal distance (x) from the overhead position (O).

A direct acoustic noise ray travels from the aircraft the distance (D) to the microphone. In addition, a reflected acoustic noise ray travels from the aircraft and is reflected at the ground back to the microphone. The travel distance of this reflected ray is taken as the distance (Z) to the microphone image at position (M). The angles ($\alpha$) and ($\theta$) are defined as the angles of the direct and reflected rays with the horizontal flight path of the aircraft.

It should be noted that the origin of the reflected ray is at a position slightly before position (P) since Z is always greater than D and arrival times for both rays at M are the same. However, this factor is considered negligible for purposes of this discussion.

Dr. G. E. Bowie, at Rye Canyon Research Laboratory, has conducted studies on ground reflections in flyover data. He has used the following equation to predict destructive ground reflection frequencies at the overhead position.

$$f = \frac{(2n + 1)\ c}{4h}$$

where c is the velocity of sound and n is an integer (i.e., 0, 1, 2, 3 . . .).

This assumes that there is no reactive component in the reflection coefficient (i.e., there is no phase change at the point of reflection). Under most flyover conditions this equation predicts the destructive interference frequencies quite well; therefore, it will be assumed that the reflection coefficient is a real number, ($R_g$). A more general equation (for aircraft in any position P),

$$f = \frac{(2n + 1)\ c}{2\left(\frac{A + 2h}{\sin\theta} - \frac{A}{\sin\alpha}\right)}$$

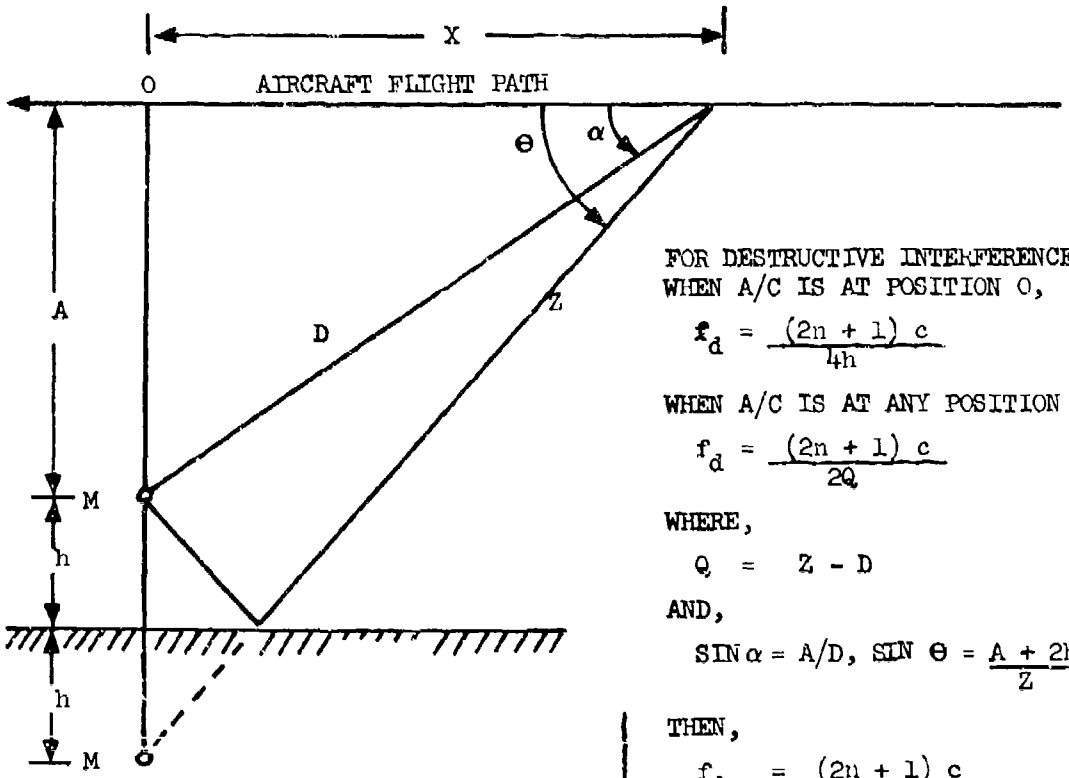


FOR DESTRUCTIVE INTERFERENCE WHEN A/C IS AT POSITION O,

$$f_d = \frac{(2n + 1)\ c}{4h}$$

WHEN A/C IS AT ANY POSITION P,

$$f_d = \frac{(2n + 1)\ c}{2Q}$$

WHERE,

$$Q = Z - D$$

AND,

$$\sin\alpha = A/D, \quad \sin\theta = \frac{A + 2h}{Z}$$

THEN,

$$f_d = \frac{(2n + 1)\ c}{2\left(\frac{A + 2h}{\sin\theta} - \frac{A}{\sin\alpha}\right)}$$

O = A/C OVERHEAD POSITION
P = A/C AT ANY POSITION ALONG FLIGHT PATH
M = MICROPHONE POSITION
M' = MICROPHONE IMAGE
A = A/C ALTITUDE
V = A/C VELOCITY
h = MICROPHONE HEIGHT ABOVE GROUND
c = VELOCITY OF SOUND
D = DIRECT RAY
Z = REFLECTED RAY

Figure III - 1 Point Source Model - Typical Flyover

is developed as shown in the figure. For estimating constructive interference frequencies the term (2n) can be used in place of (2n + 1) in either equation.

Dr. Bowie has suggested a plane wave model be used as illustrated in Figure III-2. The resulting equation for destructive interference frequencies

$$f = \frac{(2n + 1)\ c}{4h \sin \alpha}$$

is easier to use and yields approximately the same results as the equation derived from the point source model.

Using typical values for altitude and velocity of the YO-3A aircraft standard flyover test, Figure III-3 has been constructed. This figure shows destructive ground reflection frequencies as a function of aircraft position. One-third octave band center frequencies are also shown. Of course, there are also constructive interference frequencies, and degrees of reinforcement and cancellation in between. Figure III-4 shows a simple model assuming a real reflection coefficient ($R_g$) and develops equations for maximum and minimum values of SPL is also given.

Figure III-5 shows plots of these parameters as functions of $R_g$. This chart is useful in that SPL can be determined from measured data from high altitude flyovers such as shown in Figure III-6. Peaks and troughs in this narrow band spectrum are assumed to be reinforcement and cancellation maximum and minimum values. This interpretation is supported by the good agreement shown between calculated destructive ground reflection frequencies and the frequencies of the troughs.

Once SPL is determined, the chart in Figure III-5 can be used to find $R_g$. Data from four high altitude flyovers were averaged to produce the chart shown in Figure III-7 of $R_g$ as a function of frequency. No data is available at low frequencies and $R_g$ is assumed to approach unity. Values of $R_g$ thus determined can then be used in this equation

$$SPL = 10 \log (1 + R_g^2 + 2R_g \cos \pi f/f_d)$$

to produce the data correction chart shown in Figure II-5.

This chart was used to correct the analyzed data (i.e., narrow band plots) of flyover runs for production of the plots of rotational propeller noise discussed in this report.

2. DOPPLER SHIFT EFFECTS

Figure III-9 illustrates the routine flyover procedure at an altitude of 125 feet. As the aircraft flies over at this low altitude with a velocity of 74.3 kts there are obvious doppler shifts in the acoustic noise signature

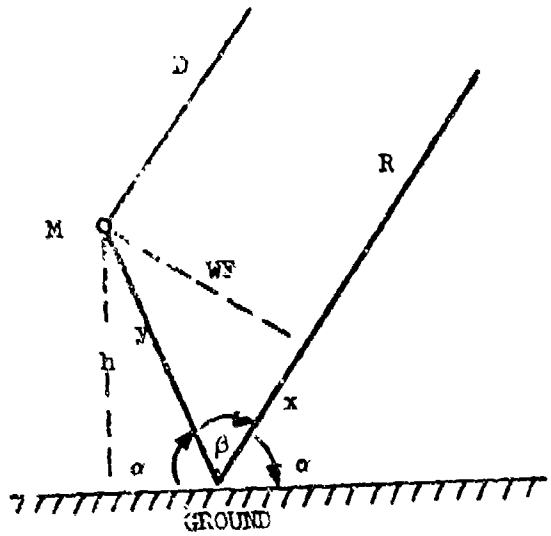


M = microphone
h = microphone height above ground
D = direct ray
R = reflected ray
y = segment of reflected ray
x = segment of reflected ray
WF = plane wave front

For destructive interference for $\alpha = 90$ degrees,

$$f_d = \frac{(2n + 1)\ c}{4h}$$

for others $\alpha$'s,

$$f_d = \frac{(2n + 1)\ c}{2Q}$$

where,

$$Q = y + x$$

and,

$$x = y \cos \beta$$

then,

$$Q = y(1 + \cos(180-2\alpha))$$

$$= y(1 - \cos 2\alpha)$$

$$= y(1 - \cos^2\alpha + \sin^2\alpha)$$

$$= 2y\sin^2\alpha$$

since,

$$y = h/\sin\alpha$$

then,

$$Q = 2h\sin\alpha$$

and,

$$f_d = \frac{(2n + 1)\ c}{4\ h\ \sin\alpha}$$

Figure III-2. Plane Wave Model - Typical Flyover

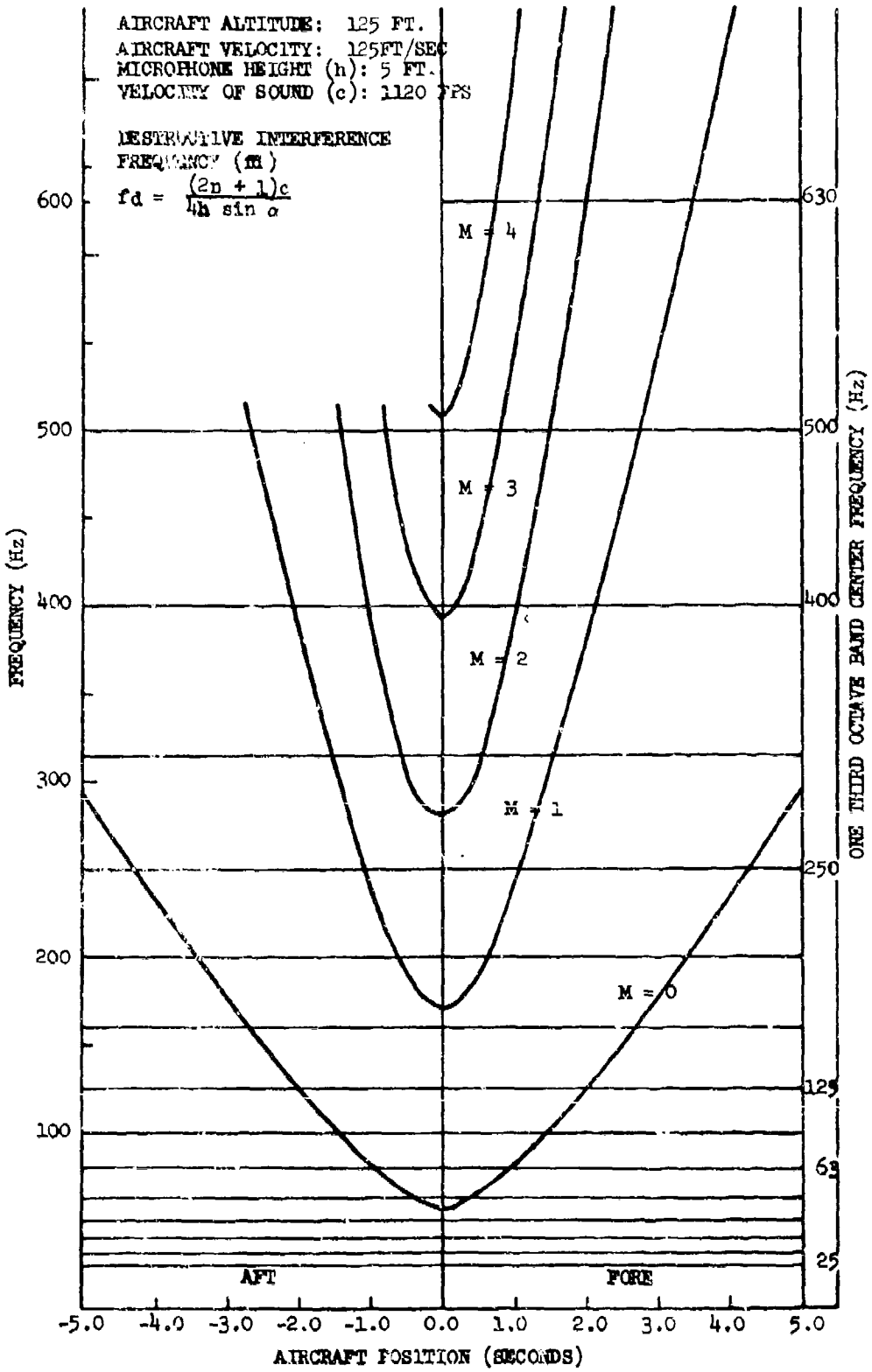


**Figure III-3** Destructive Ground Reflection Frequency As Function of Aircraft Position

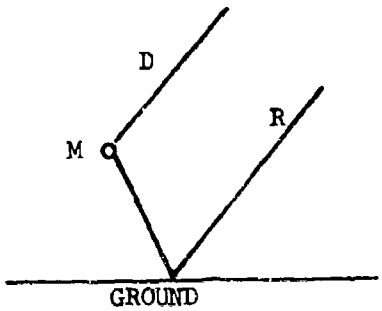


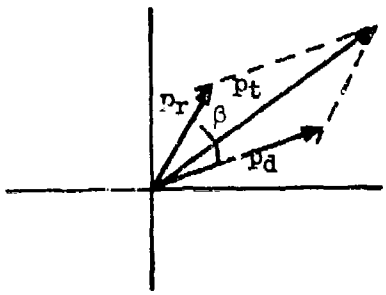


D = direct ray
R = reflected ray
M = microphone
$p_d$ = pressure at microphone due to direct ray
$p_r$ = pressure at microphone due to reflected ray
$p_t$ = total pressure at microphone due to both direct and reflected rays
SPL = Correction SPL
= SPL (re: $p_d$)

Let $R_g$ be the reflection coefficient such that,

$$R_g = p_r / p_d$$

then, by the law of cosines,

$$p_t = p_d^2 + p_r^2 + 2\, p_d p_r \cos\beta$$

where,

$\beta$ = phase angle between $p_d$ and $p_r$

$$\beta = \pi f / f_d$$

where $f_d$ is the first destructive interference frequency. The ratio of the total pressure to the pressure due to the direct ray can be found,

$$\left|\frac{p_t}{p_d}\right|^2 = 1 + R_g^2 + 2\, R_g \cos\beta$$

where $\cos\beta = 1$, the ratio squared is a maximum value,

$$\left|\frac{p_t}{p_d}\right|^2 = (1 + R_g)^2$$

and, when $\cos\beta = -1$, the ratio squared is a minimum value,

$$\left|\frac{p_t}{p_d}\right|^2 = (1 - R_g)^2$$

These squared ratios can be expressed in terms of Sound Pressure Levels,

$$SPL_{max} = 20 \log (1 + R_g) \qquad \text{and} \qquad SPL_{min} = 20 \log (1 - R_g)$$

and the difference in Sound Pressure Levels is,

$$\Delta SPL = 20 \log \left[(1 + R_g) \;/\; (1 - R_g)\right]$$

Figure III-4. Ground Reflection Equations

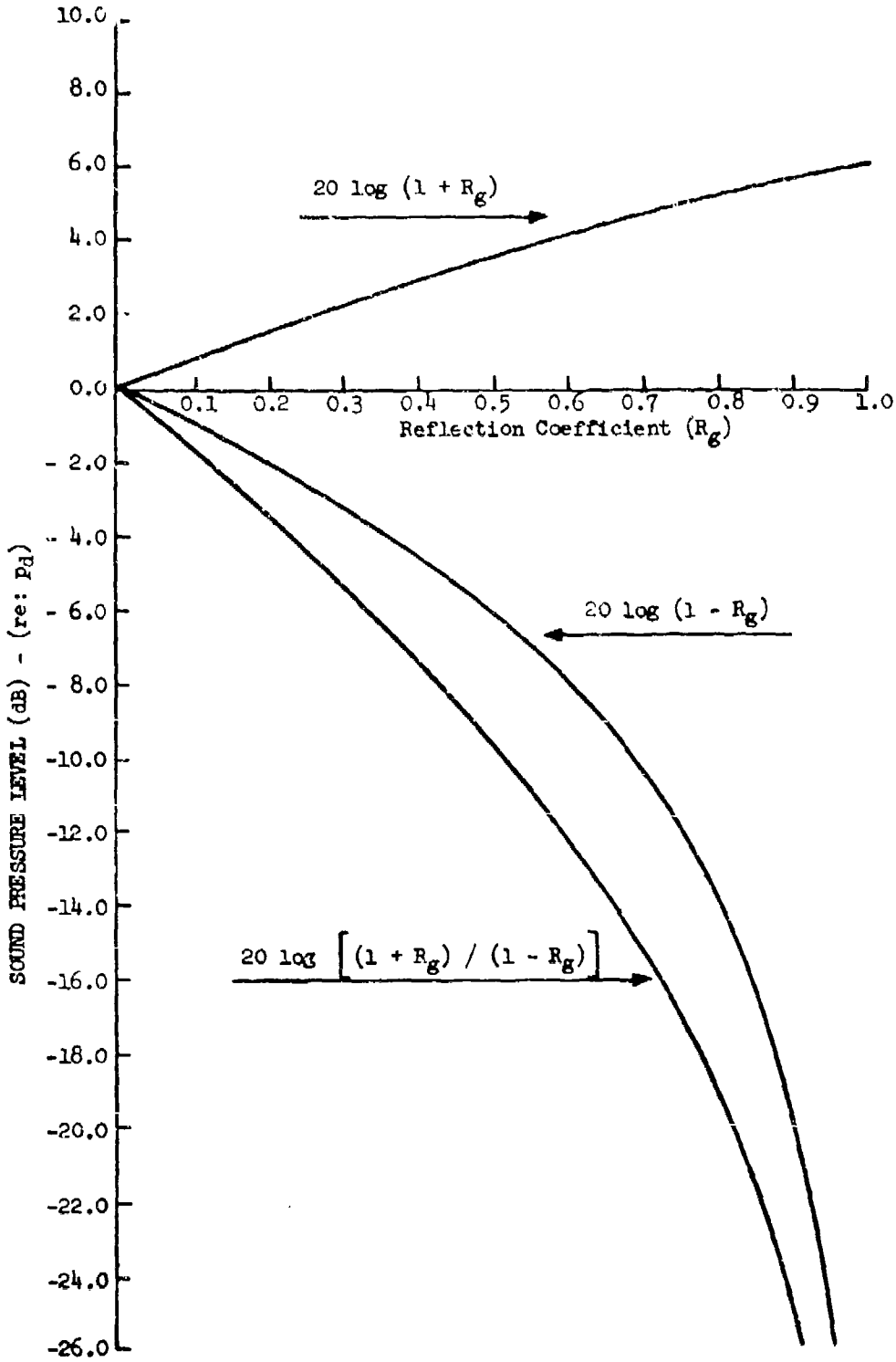


Figure III-5. SPL Values vs. $R_g$

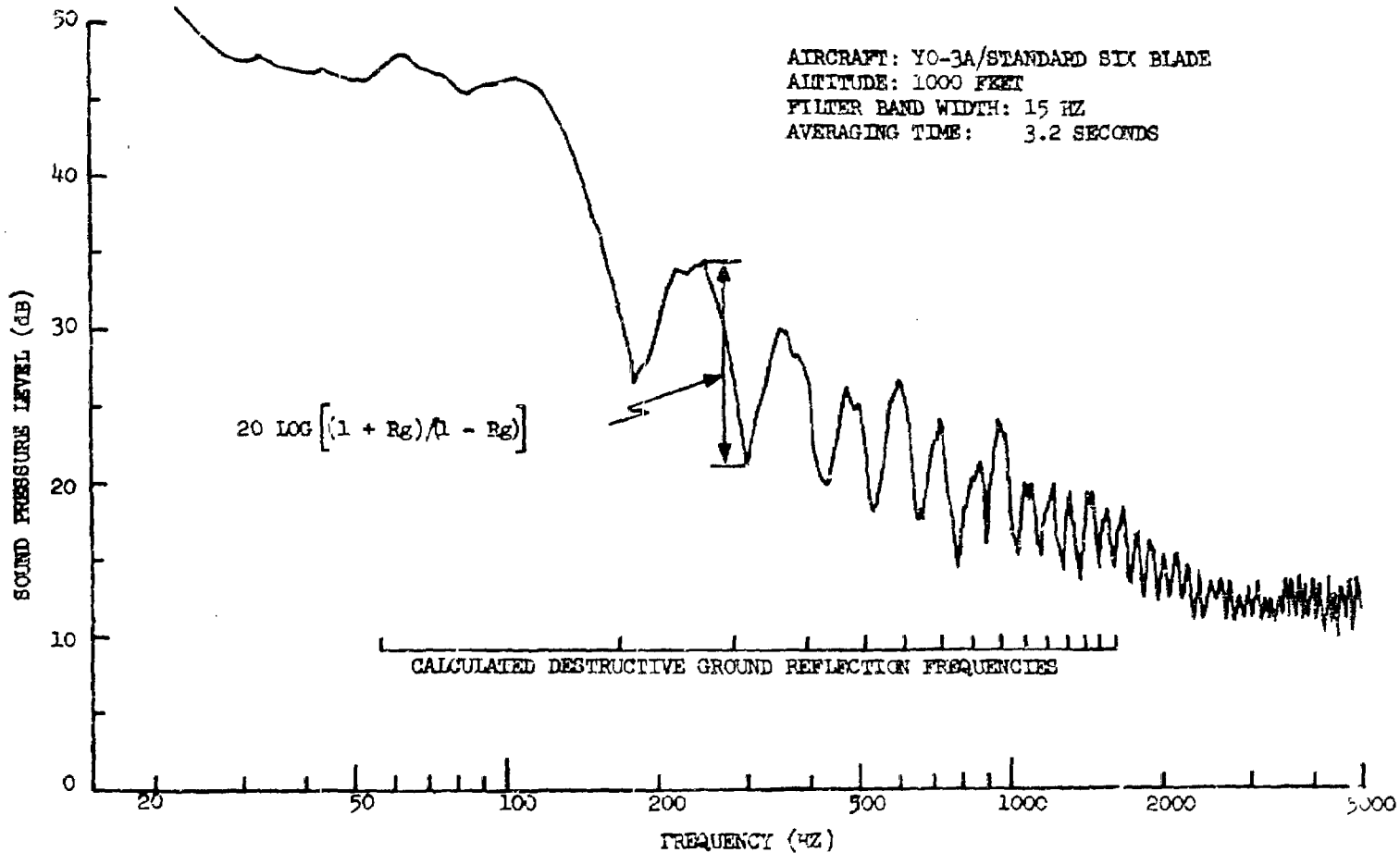


Figure III-6 Interference and Reinforcement Observed in 1000 Feet Flyover

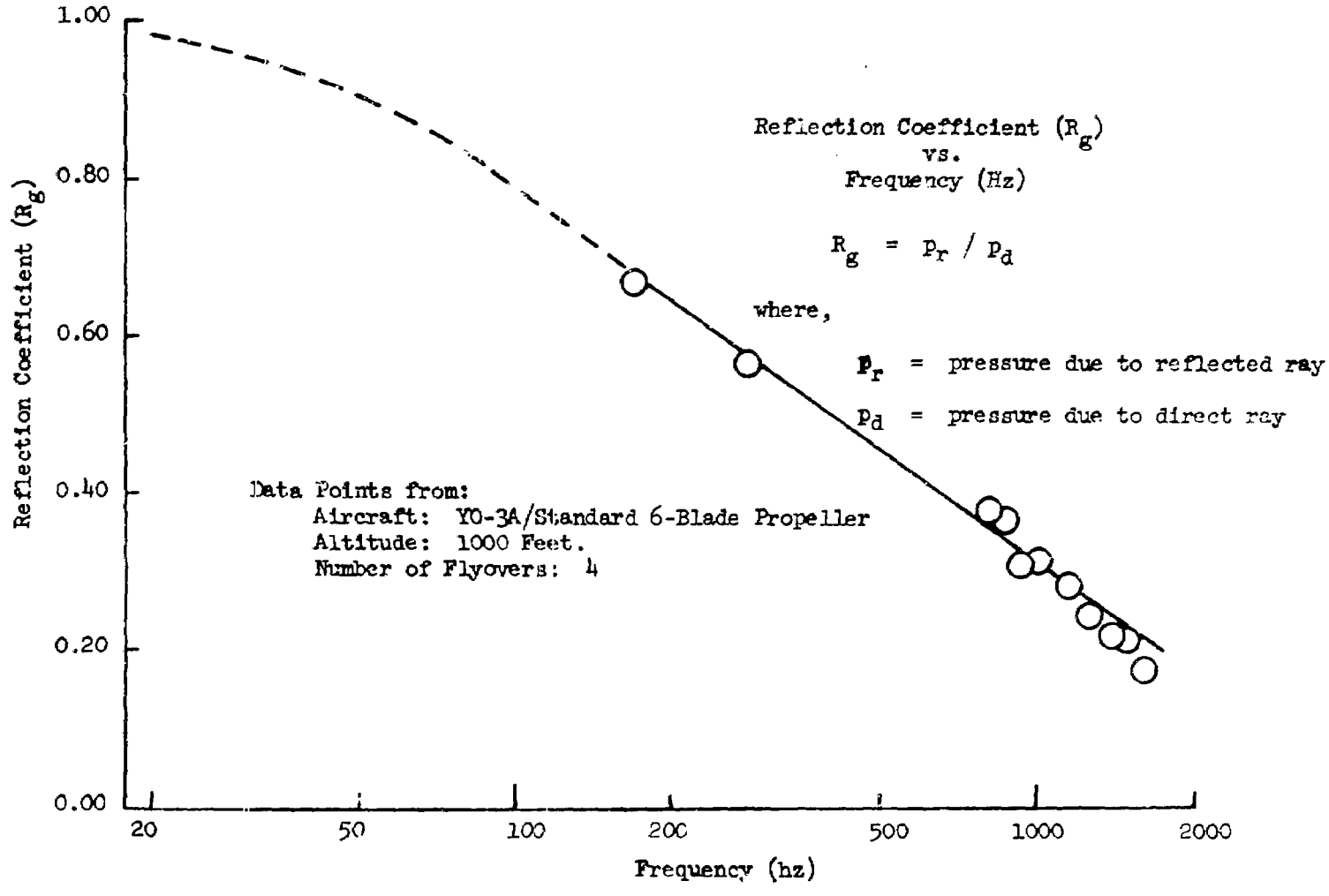


Figure III-7. Reflection Coefficient ($R_g$) vs. Frequency

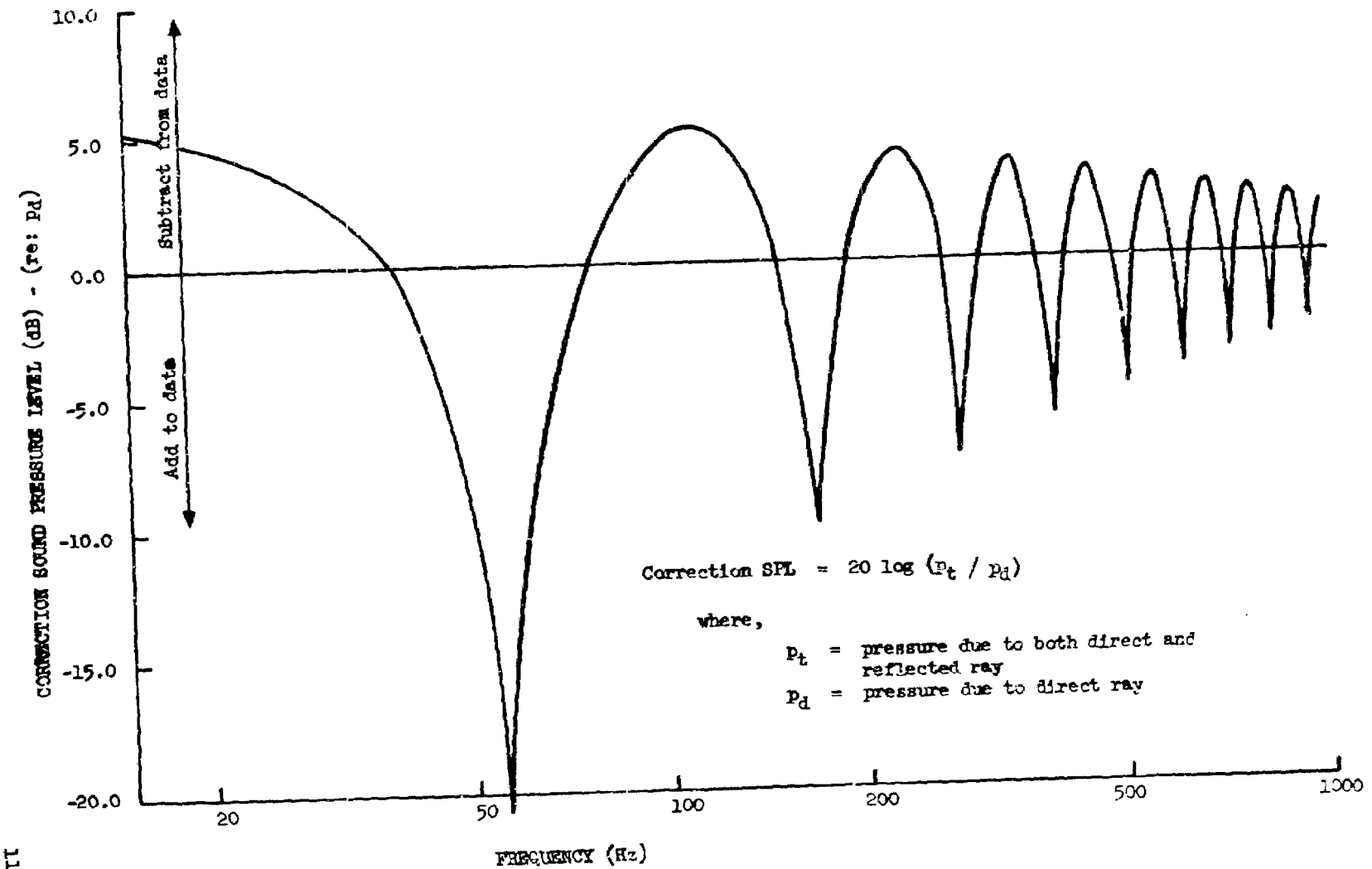


Figure III-8 Data Correction Chart

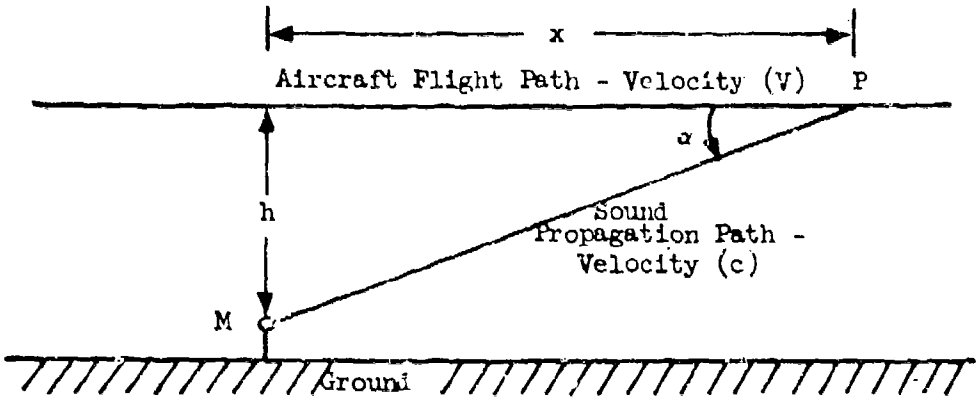


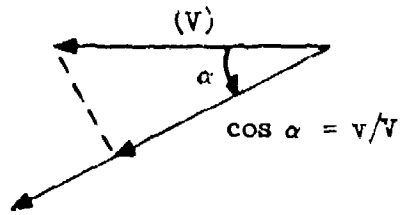


Doppler Frequency (f)

$$f = f_o \left[\frac{c \pm v}{c}\right]$$

where,

$f_o$ = emitted frequency
$v$ = component of V along sound travel path

therefore,

$$f = f_o \left[\frac{c \pm V \cos \alpha}{c}\right]$$

and,

$$\cos \alpha = \frac{x}{\sqrt{h^2 + x^2}}$$

$$x = Vt$$

where,

$h$ = height of aircraft
$x$ = horizontal distance of aircraft from overhead at time (t)

then,

(1) Find cos α as function of x and/or t,
(2) Plot f as function of x and/or t.

Figure III-9. Doppler Shift Effects

detected by the observer on the ground. These doppler shift effects can be predicted by the equations developed in the figure.

Figure III-10 shows the relationship of the fundamental rotational noise frequency, doppler shifted according to aircraft position, to the one-third octave band widths, and to the first destructive ground reflection. These predicted curves show, for example, that the 30 Hz rotational noise fundamental frequency will switch from the 31.5 Hz one-third octave band to the 25 Hz band approximately 1.0 second after the aircraft has passed overhead position. The one-third octave band time histories shown in Figure III-11 verify this interpretation.

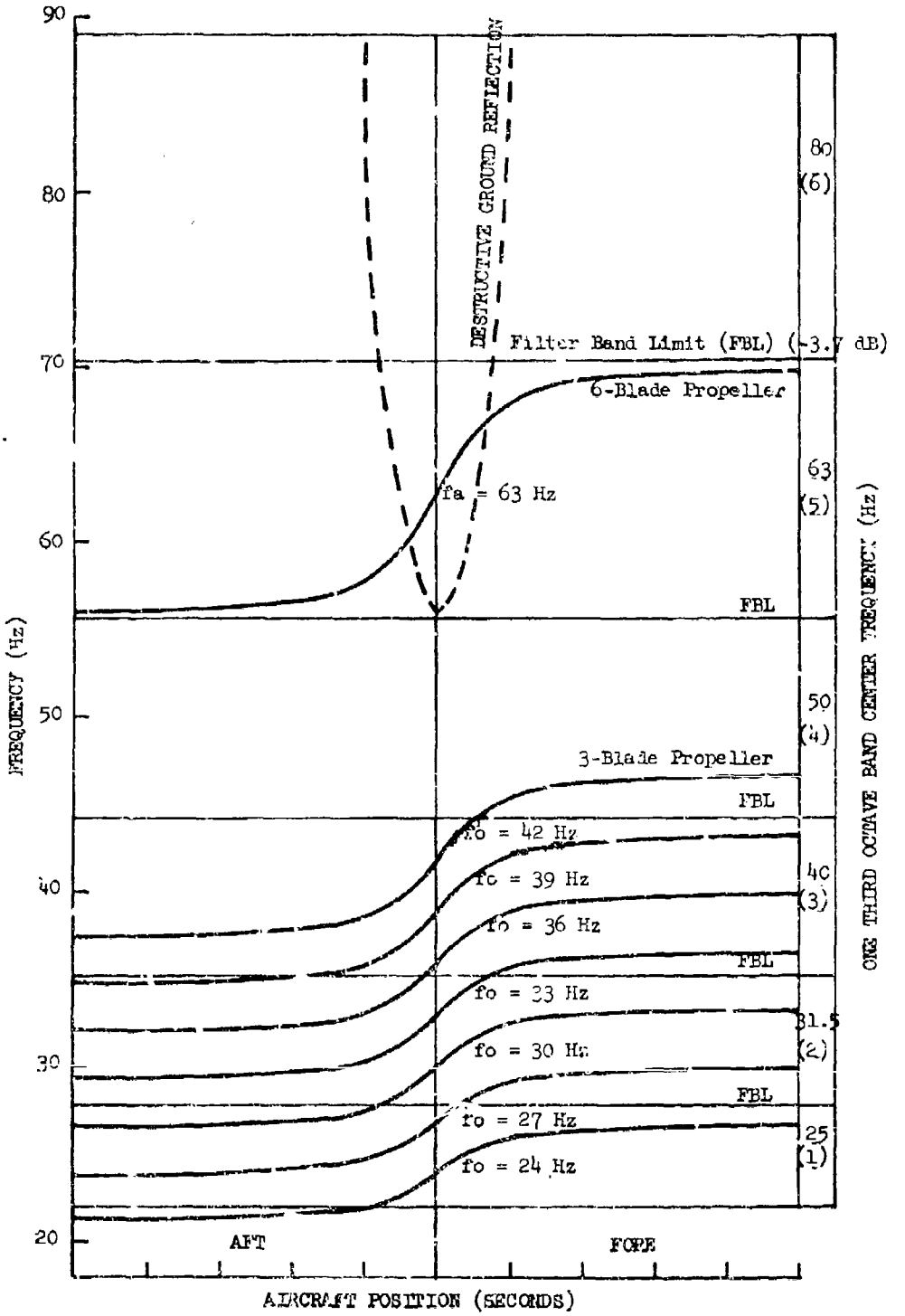


Figure III-10 Doppler Shifted Frequencies as a Function of Aircraft Position

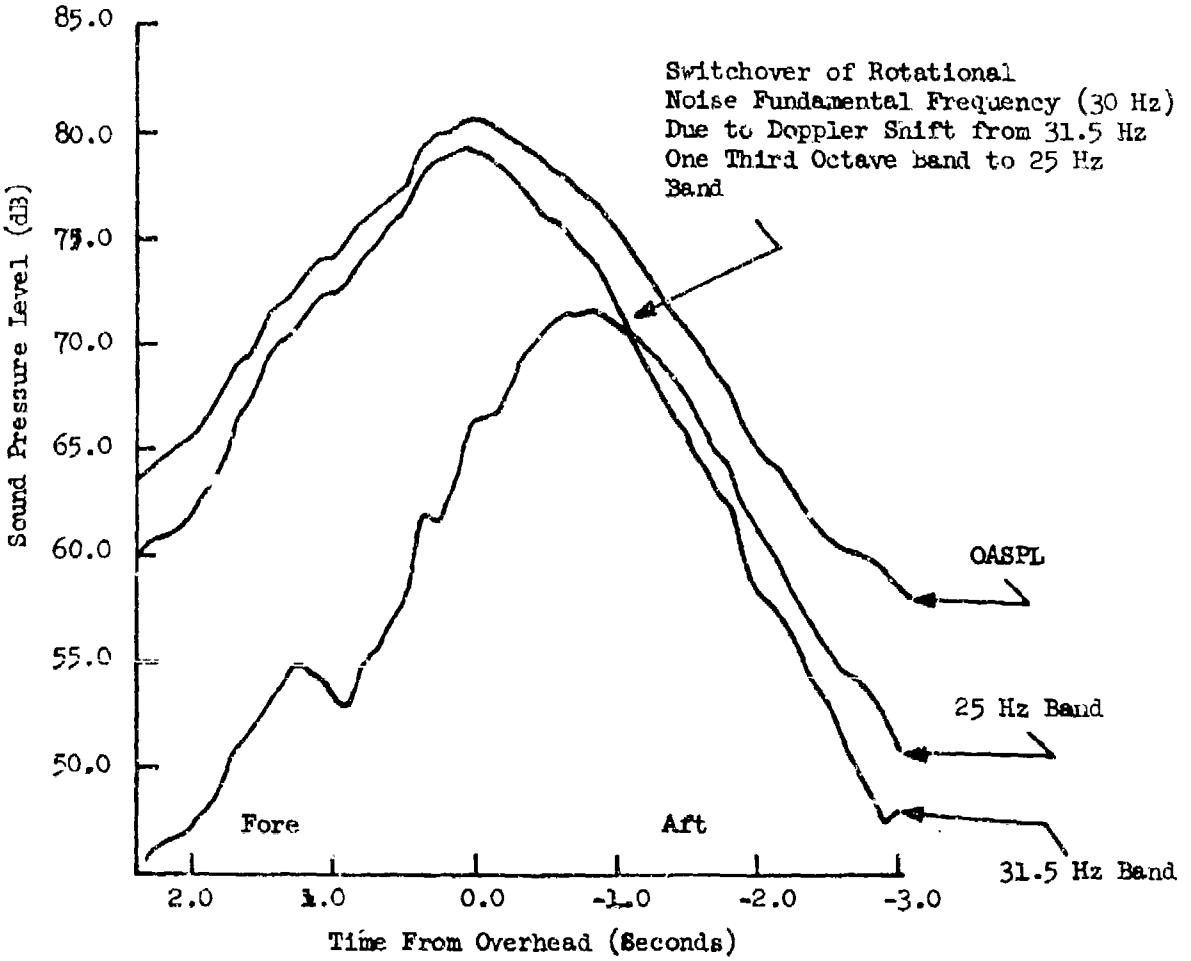


Figure III-11 Typical Flyover Time History Showing Effects of Doppler Shift

## APPENDIX IV

## SUMMARY OF PROPELLER NOISE/THEORETICAL STUDIES

### 1. HARMONIC ROTATIONAL NOISE

#### a. Purpose

The USAF Hamilton/Standard computer program (Reference 7 ) underpredicts the harmonic rotational noise of the YO-3A, and furthermore fails to detect the proper trend versus propeller rpm for the case of measured flyover noise of the Lockheed YO-3A quiet surveillance aircraft, equipped with variable propeller speed. In particular a rotational noise "bucket" is found in the YO-3A experimental data, when plotted vs. rpm, which is not predicted by the standard axisymmetric propeller noise program of References 7 and 8 . These references are based on earlier work of References 14 and 15 for loading noise and Reference 16 for thickness noise. The purpose of the present study is to explain, if possible, the sources of discrepancy between the standard theory and experiment.

#### b. Outline of Items Investigated

##### (1) Propeller Blade Loading and Aerodynamic Aspects

###### (a) Introduction

It was initially thought that exentsive blade aerodynamic stalling and flow separation effects would explain the large underprediction of rotational noise at low rpm. Therefore, two independent blade loading aerodynamic prediction methods were developed at Lockheed which are capable of matching any given experimental value of thrust, propeller efficiency, propeller torque, and horsepower at any given propeller rpm. The first method will be described below; a second method will be described later. The blade loading subroutine accepts arbitrary radial variations of blade angle, blade thickness, and chord length. Also, an aerodynamic induction efficiency is also incorporated in the input which conveniently accounts for the radial distribution of axial slipstream velocity and imparts an angular velocity to the slipstream, reducing the effective relative angular velocity between the propeller and the air. The induced velocity factors are equivalent to the induced velocity field caused by "horseshoe" vortices of classical finite span wing theory, leading to "induced drag" even in the absence of viscosity effects (see Reference 11 pages 219-222). The second method is based directly on lifting line theory for propeller blades of finite aspect ratio.

###### (b) Slipstream Effects Estimate

The first method employs an approximate momentum theory solution for the propeller slipstream axial and angular velocity (Reference 11, p. 194 Equation 4.7). Thus, if $\Omega$ is the blade angular velocity in rad/sec and $V_\infty$

the forward speed, then the propeller trailing vortices impart an interference velocity field such that the total axial velocity relative to the blade at any radial section, r, is

$$V_{xo} = V_{\infty}(1 + usb\ (r)) \qquad \text{(IV-1)}$$

The angular velocity relative to the blade is

$$\omega = \Omega\ (1 - omsb\ (r)) \qquad \text{(IV-2)}$$

From Reference 11

$$usb(r) \equiv a = x^2\ \eta_a\ (1 - \eta_a)/\left[1 + x^2\ \eta_a^{\ 2}\right] \qquad \text{(IV-3)}$$

where

$$x = \Omega\ r/a \qquad \text{(IV-4)}$$

$\eta_a$ is the propeller inductive efficiency (frictionless case). The corresponding angular velocity is

$$omsb(r) = a' = (1 - \eta_a)/\left[1 + x^2\eta_a^{\ 2}\right] \qquad \text{(IV-5)}$$

The advance angle, called $\alpha_{av}$ in this work, is defined by

$$\tan\alpha_{av} = V_{xo}/V_{\varphi o} = V_{xo}/\omega r \qquad \text{(IV-6)}$$

$$= \frac{V_{\infty}\left[1 + usb(r)\right]}{\Omega r\left[1 - omsb(r)\right]}$$

Thus, it can be seen that the advance angle, $\alpha_{av}$, is increased when usb and omsb are increased. For high efficiency propellers, $\eta_a$, the inductive efficiency, is between .7 and unity, and therefore both usb and omsb increase with decreasing propeller inductive efficiency, $\eta_a$.

(c) Adjustment of Thrust and Torque via Inductive Efficiency

An increase in the advance angle causes a decrease in thrust and an increase in required propeller torque and, therefore, a horsepower increase. This will be shown below, but the important point is that the level of thrust and power can be adjusted to match given experimental flight conditions. Figure IV-1 shows the blade element geometry.

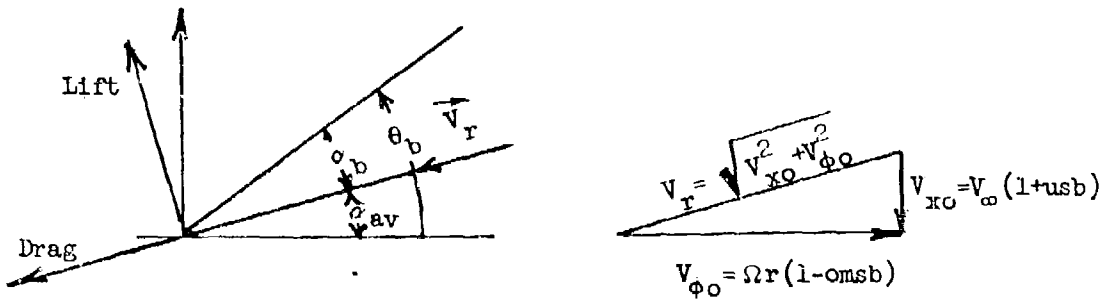


Figure IV-1 Blade Element Geometry

It is well known in aerodynamics that the lift and drag forces are defined perpendicular to and parallel to, respectively, the relative wind velocity vector

$$\vec{V}_r = \hat{1}_\varphi V_{\varphi o} + \hat{1}_x V_{xo} \qquad \text{(IV-7)}$$

Then the thrust and torque forces per unit radial distance are

$$\frac{dT}{dr} = \frac{dFx}{dr} = \frac{dL}{dr}\cos\alpha_{av} - \frac{dD}{dr}\sin\alpha_{av} \qquad \text{(IV-8)}$$

$$\frac{dF_\varphi}{dr} = \frac{dD}{dr}\cos\alpha_{av} + \frac{dL}{dr}\sin\alpha_{av} \qquad \text{(IV-9)}$$

Define thrust, torque, lift and drag coefficients in the usual manner based on blade chord length ( b following Reference 7 ) and relative velocity dynamic pressure

$$c_l = \frac{(dL/dr)}{bqr}\ ;\ c_d = \frac{(dD/dr)}{bqr} \qquad \text{(IV-10)}$$

$$c_t = \frac{(dT/dr)}{bqr}\ ;\ c_\varphi = \frac{(dF_\varphi/dr)}{bqr} \qquad \text{(IV-11)}$$

$$q_r = \tfrac{1}{2}\rho V r^2 \quad ;\ V_r^2 = V_{xo}^2 + V_{\varphi o}^2 \qquad \text{(IV-12)}$$

The torque and horsepower per unit radius are (in English units of ft., lb., sec.)

$$\frac{dQ}{dr} = r\left(\frac{dF_\varphi}{dr}\right)\ ;\ \text{ft-lb/ft} \qquad \text{(IV-13)}$$

$$\frac{dHP}{dr} = \left(\frac{\Omega}{550}\right)\frac{dQ}{dr}\ ;\ \text{HP/ft} \qquad \text{(IV-14)}$$

(d) Blade Aerodynamics

The blade lift and drag characteristics (Reference 17 pp. 125-153) were modeled after an NACA 63 series of airfoil sections with respect to the effects of variations of thickness to chord ratio, Reynolds number, laminar/turbulent boundary layer transition point, and design lift coefficient on the following characteristics:

- Maximum lift coefficient
- Lift curve slope
- Zero lift drag coefficient
- Variation of profile drag with lift coefficient

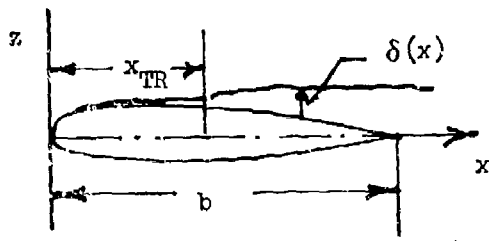


Figure IV-2 Laminar/Turbulent Boundary Layer Transition on a Propeller Blade

It can be said that the Lockheed computer program model realistically fits the airfoil section data of Appendix IV (pp. 449-541) of Reference 17 The minimum drag levels are adjustable to well known laminar/turbulent skin friction laws and with an assumed laminar/turbulent transition point as input.

The lift and drag coefficients for post-stall were modeled such that beyond $C_{l_{max}}$, the lift coefficient asymptotically approached unity, while the drag coefficient was modeled to increase with angle of attack according to a fourth degree polynomal in angle of attack. This assumption is justified by the fact that the model seems to adequately represent NACA 63 airfoil profile drag versus lift data to the highest available angles of attack. Usually, the model would slightly overestimate drag data of smooth sections of Reference 17 ; however the drag level can be adjusted by rearward movement of the assumed boundary layer transition point.

(e) Conclusions Regarding Aerodynamic Model Employed

The aerodynamic model is flexible enough to represent almost any airfoil section family, such as the Clark Y sections used in the YO-3A, including low Reynolds number effects. Since the "propeller performance subroutine" of References 7 and 8 is proprietary, the present mathematical model provided a simple and convenient means of exploring possible sensitivities of acoustic radiation to any unusual aerodynamic blade loading characteristics.

(2) Initial Aerodynamic Parametric Effects on Far Field Noise

(a) Far Field Radiation Formula Employed

Calculations have been made by the Air Force corresponding to most of the key flight test points and provided to Lockheed using the computer program of References 7 and 8 for axisymmetric loading.

The USAF/AFAPL calculations show generally that "loading noise" predominates the "thickness noise" except for a few cases on the "Acoustic" 3 Blade propeller. Accordingly, for the initial acoustic studies, the far field loading noise formula of Reference 7 (p. 27, Equation 5) was programmed. This equation reads (for axisymmetric blade loads):

$$P_m = e^{-imB\Omega t + i\Phi_m} \frac{\rho \Omega^2 D^4}{4\pi^3 S_o} \int_{hub}^{tip} \left[\frac{r}{b\cos\theta_b} \sin\left(\frac{kb\cos\theta_b}{2r}\right)\right] \left[\frac{-(M+X/S_o)}{(1-M^2)^4} \frac{\Omega}{a} \frac{dC_T}{dr} + \right.$$

$$\left. + \frac{D}{2\pi r^2} \frac{dC_P}{dr}\right] \left[J_{mB} - i\frac{(1-M^2)Yr}{2S_o^2} \left(J_{mB-1} - J_{mB+1}\right)\right] dr \qquad \text{(IV-15)}$$

$$J_{mB} = J_{mB}(arg_{mB}); \; arg_{mB} = \left(\frac{mB\Omega r}{a}\right)\frac{Y}{S_o} = \frac{kYr}{S_o} \qquad \text{(IV-16)}$$

$$\Phi_m = \frac{mB\Omega S_o}{a}(1+MX/S_o) + mB(\phi + \pi/2) \qquad \text{(IV-17)}$$

where

$$S_o^2 = X^2 + Y^2(1-M^2) \qquad \text{(IV-18)}$$

m is the harmonic number, M is the flight Mach No. $M = V_\infty/a$

B is the number of blades, $k = mB\Omega/a$,

$J_{mB}$ is a Bessel function of the first kind whose argument is $kYr/S_o$ of order mB (etc.), $dC_T/dr$, $dC_P/dr$ are the radial derivatives of the propeller thrust and horsepower coefficients defined in the usual manner (Reference 18).

$$T = (6.61 \times 10^{-7})\, \rho D^4 \left(\frac{RPM}{60}\right)^2 C_T \qquad \text{(IV-19)}$$

$$HP = (2 \times 10^{-11})\, \rho D^5 \left(\frac{RPM}{60}\right)^3 C_P \qquad \text{(IV-20)}$$

(b) Minor Theoretical Corrections to Equation

In a subsequent review of the theory, it was found that Equation IV-15 above is slightly in error. Based on a subsequent check re-derivation from

the basic Green's function for a point dipole (obtained by differentiating the Green's function for a monopole, Reference 13, p. 742 ) it was found that the "radiation factor" (the last term of Equation IV-15 with mB factored out) should read:

$$\eta_{rad} = \left[ J_{mB} + i(1-M^2)\frac{Yr}{2S_o^2} \left( J_{mB-1} - J_{mB+1} \right) \right] \qquad \text{(IV-21)}$$

The key qualitative difference is that the corrective term for radial position of the source, r, which is out of phase with respect to the $J_{mB}$ term, should have its sign changed. Since the correction term is already small because of the $Yr/So^2$ factor, the resultant numerical effect is truly negligible on a decibel scale, for $r << S_o$ in the far field, and $Y \approx S_o$ near overhead.

(c) Results of Study of Aerodynamic Blade Loading Effects on Far Field Radiation for Axisymmetric Blade Loading

To explore possible blade loading effects the following calculation procedure was conducted.

- For each assumed propeller rpm (for given blade thrust and camber) the blade pitch angle was varied along with the $\eta_a$, the propeller induction efficiency. The following was obtained from each such input:

  - Integrated propeller thrust, torque, horsepower, and net aeropropulsion efficiency.

  - Radial distribution of blade thrust and power coefficient gradient. The net aeroporpulsion efficiency, $\eta$, is defined as

$$\eta = TV_\infty / \left[ Q(RPM/60) \right] \qquad \text{(IV-22)}$$

  For typical blade airfoil section drag characteristics, the net efficiency, $\eta$, is lower than the induction efficiency $\eta_a$ (see Section (b) above) by 7 to 10 percent and further deteriorates if large blade angles of attack are required to achieve a given thrust level.

- The resulting thrust, horsepower, and efficiency were plotted against the input blade angle or efficiency parameter (whichever is being varied). All solutions giving 220 pounds of thrust ±5 pounds were considered as possible solutions.

- Of those solutions yielding 220 pounds of thrust, those generally agreeing with the YO-3A propeller efficiency values from Reference 3 were considered as further constraining the thrust solutions. Furthermore, the YO-3A project aerodynamicist has provided limits on the range of available change of the blade pitch angle, $\theta_b$, at the 75 percent of tip radius station which was said to vary between 30 degrees and 45 degrees for the standard

three blade YO-3A variable speed propeller, for which the most data were available. There were some minor discrepancies in the calculation constraints in the sense that the low propeller efficiencies at the lowest propeller rpm values (according to the LMSC estimates) would seem to require a propeller blade angle somewhat higher than 45 degrees, according to the present mathematical model.

Figures 19 and 22 summarize the initial Lockheed results. Figure 20 is the general relation between propeller horsepower and thrust for a flight speed of 125 ft/sec (74.3 knots). Figure 19 is a faired curve through many points representing fundamental rotational noise versus horsepower at constant rpm.

It was found that by whatever means a given propeller power setting was achieved, the calculated values of fundamental SPL were found to fall on a single curve. To establish the above curves, several parameters were varied systematically at constant rpm including:

- Variations of $c_{lo}$, the blade lift coefficient at zero angle of attack (e.g. the camber lift coefficient). This allows independent changes of lift coefficient at a given blade angle of attack.

- Variations of $\Delta\theta_b$, the incremental propeller blade angle relative to a fixed, built-in twist distribution (duplicating the blade twist distribution used in the USAF AFPL calculations by the method of Reference 7).

- Variations of $\eta_a$, the inductive propeller efficiency (see Section (b) ). This factor defines the slipstream effects on axial flow and angular velocity. Varying $\eta_a$ changes the advance angle, $\alpha_{av}$, which increases with decreasing $\eta_a$. This, in turn, decreases the blade angle of attack, $\alpha_b = \theta_b - \alpha_{av}$, for a given blade angle, $\theta_b = \theta_{b\ twist}(r) + \Delta\theta_b$.

- Variations of $x_{tr}$, the laminar/turbulent boundary layer transition point as a fraction of the blade chord. This affects the absolute level of drag coefficient and therefore the torque for a given $c_l$.

- It is to be noted that the Reynolds number based on blade chord and relative velocity is not an independent variable, but one which changes automatically, decreasing with decreasing rpm since

$$Re_r = \frac{\rho V r b}{\mu} = \frac{\rho b}{\mu}\sqrt{V_{xo}^2 + (\Omega r)^2 (+ \text{omsb})^2} \quad \text{(IV-23)}$$

The presently employed airfoil aerodynamic model considers Reynolds number effects on maximum lift coefficients, drag variation with lift, and zero lift drag which are typical of an NACA 63 series airfoil family which is similar to a Clark Y section, as mentioned

above. Note that the reduction or rpm lowers Reynolds numbers and raises levels, especially at the high $c_l$ values found outside of the laminar flow "drag bucket range of $c_l$."

(d) Conclusions re: Blade Aerodynamic Effect on Far Field Noise

- Despite the rather different means of achieving changes in propeller horsepower and efficiency, the calculated fundamental rotational SPL values, when plotted vs. horsepower, fall on a single curve for a given rpm (Figure 19)

- Superimposed on Figure 19 are the propeller efficiencies estimated by LMSC (Reference 3, Figure 11-10). These efficiencies indicate possibly a weak "bucket" in the SPL versus rpm at the required YO-3A value of 220 pounds thrust (possibly a 1 to 2 dB increase at 480 rpm relative to an estimated minimum at 540 rpm).

- Figures 21, 22 and 23 show crossplots of the horsepower, SPL and net propeller efficiency, $\eta$, versus rpm at the required 220 pounds thrust. These include a range of values, independently computed by Lockheed (using the loading noise formula of Reference 1 (Equation IV-15 herein) and the above described Lockheed blade load calculation method). Also included are (1) results from the Hamilton Standard method of References 7 and 8 provided by the USAF/AFPL, and (2) the propeller efficiency and h.p. estimates from LMSC (Reference 3). It is seen that the present Lockheed calculations show lower absolute SPL levels (by about 3 to 4 dB) at a given rpm but essentially the same trend of SPL versus rpm. The USAF program includes empirical corrections based on static propeller tests (Reference 7); this explains the increase of levels relative to axisymmetric theory shown in Figure 22.

- It will be recalled from the previous discussion of the empirical data that the measured fundamental SPL increased by about 7 dB at 480 rpm, relative to a minimum at 720 rpm. Therefore, it is concluded that any aerodynamic blade loading parametric variations which could reasonably be expected (which also provide adequate thrust and simultaneously match the estimated propeller efficiency and horsepower input limits for the YO-3A airplane) are insufficient to explain the deep "bucket" in the measured rotational noise and the 15 dB increase in absolute level at 480 rpm relative to USAF/AFPL predictions, or the 17 dB level increment relative to axisymmetric theory.

- Because of the failure of reasonable variations of aerodynamic parameters to fully explain the rotational noise increase, it was decided to re-examine the acoustic theory of propellers and to investigate other possible acoustic radiation mechanisms which might reasonably be related to the propeller rpm.

- Some comments on the numerical accuracy of radial integration are now offered. The preliminary calculations employed a 5 point radial integration scheme with annuli separated by unequal $\Delta r$ segments such that approximately

equal thrust is generated in each annulus. Some calculations were conducted using more integration points (up to 20 radial points). More recent calculations have employed 7, 10 and 15 point Simpson rule integration. They all tended to fall on the same curve (of SPL vs. h.p.) at constant rpm. Generally, the more accurate integrations have (a) slightly lower thrust and (b) slightly higher noise for a given input of blade angle and induction efficiency.

(3) Evaluation of Other Acoustic Radiation Aspects

(a) Propeller Disc Inflow Non-Uniformity Effects

- Description of Non-Uniformity Sources

In the above discussion of unsteady blade force effects it was mentioned that these are related to circumferential non-uniformity of the blade loads, and these are known to have a powerful effect, for example, in the case of helicopter rotor noise .

For the YO-3A aircraft there are two possible major sources of circumferential non-uniformity of the inflow to the propeller:

- The angle of attack component of the freestream velocity in the plane of the disc (directed upward for positive angle of attack of the propeller axis). The freestream velocity has the components

$$\vec{V}_\infty = \hat{1}\, V_\infty \cos \alpha_{t.v} + \hat{k}\, V_\infty \sin \alpha_{ac} \quad \text{(IV-24)}$$

These components can be resolved along the blade and tangentially as follows (see sketch):

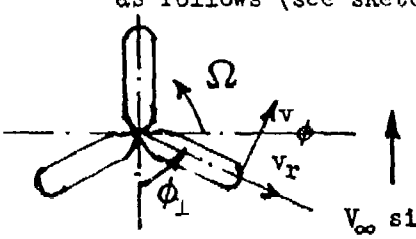


$$\hat{k}\, V_\infty \sin \alpha_{ac} = \hat{1}\, V_\infty \sin \alpha_{ac} (-\cos \varphi_1) + \hat{1}\varphi\, V_\infty \sin \alpha_{ac} \sin \varphi_1 \quad \text{(IV-25)}$$

FIG. IV-3 ANGLE OF ATTACK INFLOW GEOMETRY

- A second flow disturbance occurs because the lift-induced, circulatory flow about the wing generates "upwash" and "backwash" velocity disturbances, respectively, perpendicular to the propeller disc plane and in the disc plane, parallel to the vertical axis.

For a large aspect ratio wing, such as the YO-3A, the following simple two-dimensional "bound vortex" relation is a good approximation for describing the wing-induced velocity at the prop plane ($X_p$, $Z_p$). The backwash (perpendicular to the disc plane) is given by

$$u_{i_w}(X_p, Z_p) = \frac{-\Gamma_w (Z_p - Z_w)}{2\pi \left[(X_p - X_w)^2 + (Z_p - Z_w)^2\right]} \quad \text{(IV-26)}$$

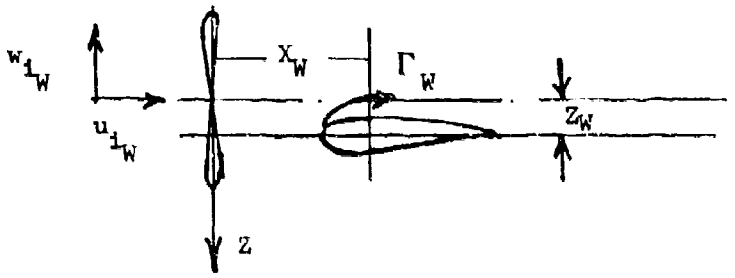


Figure IV-4 Wing Induced Inflow Disturbances

where we can set $x_p = 0$ without loss of generality. $\Gamma_W$ is the average wing bound vortex circulation per unit wing span. The wing span is denoted by $l_W$ (to avoid confusion with the blade chord notation for b):

$$\Gamma_W = \frac{L_W}{\ell_W \rho V_\infty} = C_{LW} \frac{\rho V_\infty^2}{2} S_W / (\ell_W \rho V_\infty) = C_{LW} V_\infty S_W / (2\ell_W) \qquad \text{(IV-27)}$$

For steady one g flight, the $L_W$, equals the aircraft weight, $W_{ac}$. The "upwash" (in the propeller disc plane) is:

$$w_{i_W}(X_P, Z_P) = \frac{\Gamma_W (X_P - X_W)}{2\pi \left[(X_P - X_W)^2 + (Z_P - Z_W)^2\right]} \qquad \text{(IV-28)}$$

- Preliminary Remarks and Summary of Some of the Key Results for the YO-3A as Regards Inflow Non-Uniformity

From Equation IV-24 and IV-28, it is clear that the upwash components of the angle of attack inflow and that of the wing circulation induced upwash are additive if the angle of attack, $\alpha_{ac}$, of the propeller axis is positive.

In the case of the YO-3A, it is estimated that the propeller axis angle of attack is 2.88 degrees at the wing lift coefficient corresponding to a forward speed of $V_\infty$ = 125 ft/sec (74.3 Knots). Therefore, as a principal finding of this study, the propeller angle of attack and wing upwash contributions are additive and the combined effect is estimated to be of the order of 8 to 14 dB (see Figure 25 ). The effect on absolute level of propeller angle of attack alone would be of the order of 4 dB at $\alpha_{ac}$ = +3.3 degrees for 480 rpm, decreasing to about 2 dB at 780 rpm. Thus, the angle of attack effect alone might be expected to contribute a 1 to 2 dB increment toward the measured 15 dB bucket increment at 480 rpm; however, the combined effects of in flow non-uniformity are calculated to be about 6 dB at

480 rpm relative to 600 rpm and increase of 8 to 14 dB in absolute level. As shown in Figure 25, the results agree very well with the experimental data.

- Theoretical Basis for Evaluation of Non-Uniformity Effects on Far Field Noise

Non-uniformity effects can be assessed by the following equation which is the recommended modification of Equation 11.318 of Reference 13, p. 744, and Equation 5, p. 27 of Reference 7 (Eq. IV-15 in Sec. 1b(2)(a) of this report). For the $m^{th}$ harmonic,

$$p_m = e^{-imB\Omega t + i\Phi m} \frac{\rho \Omega^2 D^4}{4\pi\, {}^3S_o} \int_{hub}^{tip} \left[SF_r + iSF_i\right] \Bigg( \Bigg[ -\cos\theta_d \frac{\Omega}{a} \frac{dC_T}{dr} \sum_{\nu=0}^{\infty} \beta_\nu$$

$$+ \frac{D}{2\pi r^2} \frac{dC_p}{dr} \sum_{\nu=0}^{\infty} \left(\frac{mB-\nu}{mB}\right) \delta_\nu^* \Bigg] \left\{ J_{mB-\nu}(arg_{mB})(-1)^\nu \exp\left(-i\nu\left(\phi + \frac{\pi}{2}\right)\right) \right\}$$

$$+ \Bigg[ -\cos\theta_d \left(\frac{\Omega}{a}\frac{dC_T}{dr}\right) \sum_{\nu=1}^{\infty} \beta_\nu + \frac{D}{2\pi r^2} \frac{dC_p}{dr} \sum_{\nu=1}^{\infty} \left(\frac{mB+\nu}{mB}\right) \delta_\nu \Bigg] \Bigg\{ J_{mB+\nu}(arg_{mB})^* *(-1)^\nu \exp\left(i\nu\left(\phi + \frac{\pi}{2}\right)\right) \Bigg\} dr \qquad \text{(IV-29)}$$

$$\delta_\nu = (a_{\nu\phi} - ib_{\nu\phi})/2; \quad \delta_{\nu\phi}^* = (a_{\nu\phi} + ib_{\nu\phi})/2 \qquad \text{(IV-30)}$$

Equation IV-29 emphasizes the $(mB+\nu)$ and $(mB-\nu)$ dependence of the radiated sound upon the loading harmonics, $\nu = \pm 1, \pm 2, \pm 3$. The mB-2 terms are predominant as a result of Bessel function properties described below.

Equation IV-29 includes a change of the solidity factor due to non-uniform chord-wise blade loads to be discussed below, but omits the minor correction for source position discussed previously. In the above equation, r is the local propeller radius, and the Bessel function argument is

$$arg_{mB} = mk_1 r \sin\theta_d = mB\Omega r \sin\theta_d \qquad \text{(IV-31)}$$

$$k_1 = B\Omega/a = \omega_1/a \qquad \text{(IV-32)}$$

In the present calculations, the directivity angle is modified for airplane

angle of attack as follows:

$$\theta_{\hat{d}} = \alpha_{ac} + \cos^{-1}\left\{\frac{(M+X/S_o)}{(1-M^2)^{\frac{1}{4}}}\right\} \qquad \text{(IV-32)}$$

where

$$S_o = \sqrt{X^2 + (1-M^2)Y^2} \qquad \text{(IV-33)}$$

In the present case the aircraft Mach number effects are negligible, as are the contributions of the $J_{mB+\nu}(\arg_{mB})$ terms. At low tip Mach numbers, the Bessel functions for $\arg_{mB} << 1$ can be approximated by

$$J_{mB-\nu}(\arg_{mB}) \simeq \left(\frac{\arg_{mB}}{2}\right)^{(mB-\nu)}/(mB-\nu)! \qquad \text{(IV-34)}$$

The factors $\beta_\nu$ and $\delta_\nu$ are the non-uniformity (complex) Fourier coefficients for thrust and torque

$$\begin{aligned} \beta_\nu &= (a_{t\nu} - ib_{t\nu})/2; \ \beta_o = 1 \\ \delta_\nu &= (a_{\phi\nu} - ib_{\phi\nu})/2; \ \delta_o = 1 \\ \delta_\nu^* &= (a_{\phi\nu} + ib_{\phi\nu})/2; \ \beta_\nu^* = (a_{t\nu} + ib_{t\nu})/2 \end{aligned} \qquad \text{(IV-35)}$$

such that the torque (tangential) force per unit disc area is described by

$$f_{\hat{\phi}}(r_1\ \phi_1) = f_{\phi_o}(r)\sum_{\nu=-\infty}^{\infty} \delta_\nu e^{i\nu\phi_1} \qquad \text{(IV-36)}$$

$$f_{\phi_o}(r) = c_{\phi_o}(r)\frac{1}{2}\rho V_r^2 \ ; \ 0 \le \phi_1 \le 2\pi$$

$$= \frac{Bb\tilde{c}_{\phi_o}}{2\pi r}$$

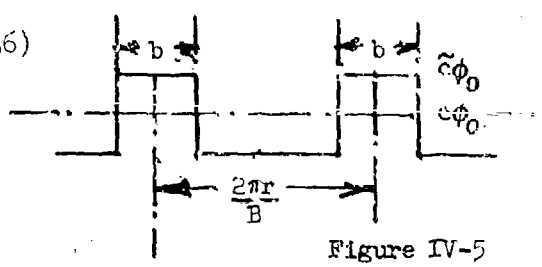


Figure IV-5
Blade Loading
Distribution
Around Disc

where on the blade itself the torque coefficient is

$$\tilde{c}_{\phi_o} = c_d \cos \alpha_{av} + c_\ell \sin \alpha_{av} \tag{IV-38}$$

$$(c_d, c_\ell) = f\ (\alpha_b = \theta_b - \alpha_{av})$$

- Derivation of Fourier Coefficients for the Circumferential Non-Uniformity of Torque Force

From Equation IV-37 it is seen that

$$\frac{\Delta f\phi}{f\phi_o} = \frac{1}{f\phi_o}\left[q_r \Delta c_\phi + c_{\phi_o} \Delta q_r\right] \tag{IV-39}$$

where at any $(r, \phi_1)$ on the propeller disc

$$q_r = \frac{1}{2}\rho V_r^2 \ ; \ V_r^2 = V_{xo}^2 + V_{\phi_o}^2 \tag{IV-40}$$

$$V_{xo} = V_\infty\ (1+usb(r))\cos \alpha_{ac} + u_{i_W}(\phi_1)$$

$$u_{i_W}(\phi_1) = \frac{-\Gamma_W (r\cos\phi_1 - Z_W)}{2\pi\left[X_W^2 + (r\cos\phi_1 - Z_W)^2\right]} \tag{IV-41}$$

$$V_\phi(\phi_1) = \Omega r(1-omsb) - (W_{i_W} + V_\infty \sin \alpha_{ac}) \sin\phi_1 \tag{IV-42}$$

$$W_{i_W}(\phi_1) = \frac{\Gamma_W X_W}{2\pi\left[X_W^2 + (r\cos\phi_1 - Z_W)^2\right]} \tag{IV-43}$$

Let $$\epsilon = \left(\frac{r\cos\phi_1 - Z_W}{X_W}\right) \tag{IV-44}$$

$$u_{i_W}(\phi_1) = \frac{-\Gamma_W X_W \epsilon}{2\pi X_W^2\left[1+\epsilon^2\right]}$$

$$\cong \frac{-\Gamma_W \epsilon}{2\pi X_W}\left[1-\epsilon^2+\epsilon^4-\epsilon^6+\ldots\right] \tag{IV-45}$$

Since $X_W \gg \left| r \cos\phi_1 - Z_W \right|$, then $\epsilon \ll 1$, and the series expansion of Equation IV-45 converges rapidly.

Expanding Equation IV-43 in a power series in epsilon, yields

$$w_{i_W}(\phi_1) = \frac{\Gamma_W}{2\pi X_W \left[1+\epsilon^2\right]} \cong \frac{\Gamma_W \left(1-\epsilon^2+\epsilon^4-\epsilon^6+\ldots\right)}{2\pi X_W} \qquad \text{(IV-46)}$$

It is clear that the power series in $\epsilon$ is related to a power series in $\cos\phi_1$, which leads to an explicit Fourier series after application of well known trigonometric identities. The required Fourier analysis of Equation IV-39 is more complicated since

$$\Delta c_\phi = \frac{\partial c_\phi}{\partial \alpha_b} \Delta\alpha_b = \frac{\partial c_\phi}{\partial \alpha_b} \Delta\left(\theta_b - \alpha_{av}\right) = -\frac{\partial c_\phi}{\partial \alpha_b} \Delta\alpha_{av} \qquad \text{(IV-47)}$$

$$\Delta q_r = \Delta\left(\tfrac{1}{2}\rho V_r^2\right) = \rho\left[V_{xo}\,\Delta V_x + V_{\phi o}\,\Delta V_\phi\right] \qquad \text{(IV-48)}$$

Furthermore

$$\begin{aligned} \frac{\partial c_\phi}{\partial \alpha_b} &= \frac{\partial}{\partial \alpha_b}\left[c_d \cos\alpha_{av} + c_\ell \sin\alpha_{av}\right] \\ &= \left[\cos\alpha_{av} \frac{\partial c_d}{\partial \alpha_b} - c_d \sin\alpha_{av} \frac{\partial \alpha_{av}}{\partial \alpha_b}\right] + \\ &\quad + \left[\sin\alpha_{av} \frac{\partial c_\ell}{\partial \alpha_b} + c_\ell \cos\alpha_{av} \frac{\partial \alpha_{av}}{\partial \alpha_b}\right] \end{aligned} \qquad \text{(IV-49)}$$

But

$$\alpha_b = \theta_b - \alpha_{av} \; ; \; \frac{\partial \alpha_{av}}{\partial \alpha_b} = -1 \qquad \text{(IV-50)}$$

Therefore,

$$\frac{\partial c_\phi}{\partial \alpha_b} = \left\{\left[\cos\alpha_{av} \frac{\partial c_d}{\partial \alpha_b} + c_d \sin\alpha_{av}\right] + \left[\sin\alpha_{av} \frac{\partial c_\ell}{\partial \alpha_b} - c_\ell \cos\alpha_{av}\right]\right\} \qquad \text{(IV-51)}$$

Now in general, for non-uniform inflow, including the wing circulation flow field effects, one can define the local advance angle as

$$\alpha_{av}(\phi_1) = \tan^{-1}\left\{\frac{V_x(\phi_1)}{V_\phi(\phi_1)}\right\} = \tan^{-1}\left\{\alpha_{avo} + \Delta\alpha_{av}\right\} \qquad \text{(IV-52)}$$

where the components of velocity relative to the blade are

$$V_x = V_{xo} + u_{i_W}(\phi_1)$$

$$V_\phi = V_{\phi o} + \Delta V_\phi(\phi_1) \qquad \text{(IV-53)}$$

Generalizing from Eq (IV-25) one obtains

$$\Delta V_\phi(\phi_1) = -\left[V_\infty \sin\alpha_{ac} + w_{i_W}(\phi_1)\right] \sin\phi_1 \qquad \text{(IV-54)}$$

where, $V_{xo}$ and $V_{\phi o}$ are given by Eqs (IV-1) and (IV-2).

From basic trigonometry relations

$$\tan\alpha_{av} = \tan(\alpha_{avo} + \Delta\alpha_{av}) = \left(\frac{\tan\alpha_{avo} + \tan\Delta\alpha_{av}}{1 - \tan\alpha_{avo}\tan\Delta\alpha_{av}}\right) \qquad \text{(IV-55)}$$

For small values of $\Delta\alpha_{av}$, Eq IV-55 may be expanded, neglecting squared terms in $\Delta\alpha_{av}$, to obtain

$$\tan\alpha_{av} = (\tan\alpha_{avo} + \Delta\alpha_{av})(1 + \tan\alpha_{avo}\,\Delta\alpha_{av})$$

$$= \tan\alpha_{avo} + \Delta\alpha_{av}(1 + \tan^2\alpha_{avo})$$

$$= \tan\alpha_{avo} + \sec^2\Delta\alpha_{avo}\,\Delta\alpha_{av} \qquad \text{(IV-56)}$$

Solving for $\Delta\alpha_{av}$, noting that $1 + \tan^2 X = \sec^2 X = 1/\cos^2 X$

$$\Delta\alpha_{av} = \cos^2\alpha_{avo}(\tan\alpha_{av} - \tan\alpha_{avo}) \qquad \text{(IV-57)}$$

Substituting for $\tan\alpha_{avo}$ and $\tan\alpha_{av}$ in terms of the velocity components yields

$$\Delta\alpha_{av} = \cos^2\alpha_{avo}\left\{\frac{V_{xo} + u_{i_W}}{V_{\phi o} + \Delta V_\phi} - \frac{V_{xo}}{V_{\phi o}}\right\}$$

$$= \cos^2\alpha_{avo}\left\{\frac{V_{xo}(1+{}^{u}i_W/V_{xo})}{V_{\phi o}(1+\Delta V_\phi(V_{\phi o})} - \frac{V_{xo}}{V_{\phi o}}\right\} \qquad \text{(IV-58)}$$

Neglecting squared terms in $\Delta V_\phi/V_{\phi o}$

$$\Delta\alpha_{av} = \cos^2\alpha_{avo}\left\{\frac{V_{xo}}{V_{\phi o}}\left(\frac{u_{i_W}}{V_{xo}} - \frac{\Delta V_\phi}{V_{\phi o}}\right)\right\} \qquad \text{(IV-59)}$$

Using Eq (IV-6) yields

$$\Delta\alpha_{av} = \cos^2\alpha_{avo}\tan\alpha_{avo}\left(\frac{u_{i_W}}{V_{xo}} - \frac{\Delta V_\phi}{V_{\phi o}}\right) \qquad \text{(IV-60)}$$

and from trigonometric identities

$$\Delta\alpha_{av} = \frac{\sin(2\alpha_{avo})}{2}\left(\frac{u_{i_W}}{V_{xo}} - \frac{\Delta V_\phi}{V_{\phi o}}\right) \qquad \text{(IV-61)}$$

One can combine the dynamic pressure and angle of attack sensitivities to obtain the desired circumferential change in tangential force in terms of circumferential changes in axial and tangential velocity. From the above expression for $\Delta\alpha_{av}$ plus Eqs IV-39 and IV-48, one obtains

$$\frac{\Delta f_\phi}{f_{\phi o}} = \left[\frac{-1}{\bar{c}_{\phi o}}\frac{\partial c_\phi}{\partial\alpha_b}\Delta\alpha_{av} + \frac{2(V_{xo}\,{}^{u}i_W + V_{\phi o}\Delta V_\phi)}{(V_{xo}^2+V_{\phi o}^2)}\right] \qquad \text{(IV-62)}$$

Let the combined upwash at the propeller disc plane be expressed as

$$w = V_\infty\sin\alpha_{ac} + w_{i_W} \qquad \text{(IV-63)}$$

Then

$$\Delta V_\phi = -\,w\sin\phi_1 \qquad \text{(IV-64)}$$

and one can write

$$\frac{\Delta f_\phi}{f_{\phi o}} = A_\phi\frac{u_{i_W}}{V_\infty} + B_\phi\frac{w\sin\phi_1}{V_\infty} \qquad \text{(IV-65)}$$

where

$$A_\phi = \left[\frac{-1}{\tilde{c}_{\phi o}} \frac{\partial c_\phi}{\partial \alpha_b} \frac{\sin}{2} (2\alpha_{avo}) \frac{V_{xo}}{V_\infty} + \frac{2V_{xo}V_\infty}{V_{ro}^2}\right] \tag{IV-66}$$

$$B_\phi = -\left[\frac{1}{\tilde{c}_{\phi o}} \frac{\partial c_\phi}{\partial \alpha_b} \frac{V_\infty}{V_{\phi o}} \frac{\sin}{2} (2\alpha_{avo}) + 2\frac{V_{\phi o}V_\infty}{V_{ro}^2}\right] \tag{IV-67}$$

and

$$V_{ro}^2 = V_{xo}^2 + V_{\phi o}^2 \tag{IV-68}$$

Because of the power series dependence on $\epsilon$ of the velocity components $u_{i_W}$ and $w_{i_W}$ as given by Eqs IV-44 to IV-46, it is seen that one can derive an explicit Fourier series for the quantities $\frac{u_{i_W}}{V_\infty}$ and $\frac{w}{V_\infty}$ above. This process will be illustrated for a few of the lower order terms.

From IV-45, 4B, one can write

$$u_{i_W}/V_\infty = \tilde{v}_W(1-\epsilon^3+\epsilon^5-\epsilon^7+\ldots) \tag{IV-69}$$

$$w_{i_W}/V_\infty = \tilde{v}_W(1-\epsilon^2+\epsilon^4-\epsilon^6+\ldots) \tag{IV-70}$$

where it is convenient to define

$$\tilde{v}_W = \Gamma_W/2\pi X_W V_\infty \tag{IV-71}$$

From the binomial expansion theorem one obtains

$$\epsilon^n = \left(\frac{r\cos\phi_1 - Z_W}{X_W}\right)^n$$

$$= \sum_{j=o}^{n} \left(\frac{r\cos\phi_1}{X_W}\right)^{n-j} \left(\frac{-Z_W}{X_W}\right)^j (nC_j) \tag{IV-72}$$

where the binomial coefficients are defined in the usual manner by

$$(nC_j) = \frac{n!}{j!(n-j)!} \tag{IV-73}$$

The term $\frac{w}{V_\infty}\sin\phi_1$, in Eq IV-65 can be written as

$$\frac{w\sin\phi_1}{V_\infty} = \left\{\left[\sin\alpha_{ac} + \tilde{v}_W\right] - \tilde{v}_W\epsilon^2 + \tilde{v}_W\epsilon^4 - \ldots\right\} \tag{IV-74}$$

Thus one could summarize Eq (IV-74) as follows

$$\frac{w\sin\phi_1}{V_\infty} = \sum_{n=o}^{\infty} b''_{n\phi}(-1)^n \epsilon^{2n}\sin\phi_1$$

$$= \sin\phi_1 \left\{ \left[ \sin\alpha_{ac} + \tilde{v}_W \right] - \tilde{v}_W \epsilon^2 + \tilde{v}_W \epsilon^4 - \cdots \right\} \qquad \text{(IV-75)}$$

From Eq IV-72 above, one can expand the epsilon squared term, for example, as follows

$$\epsilon^2 = (r^2 \sin\phi_1 \cos^2\phi_1 - 2rZ_W \cos\phi_1 + Z_W^2)/X_W^2 \qquad \text{(IV-76)}$$

The contribution to Eq (IV-75) is given by the product

$$\epsilon^2 \sin\phi_1 = (r^2 \sin\phi_1 \cos^2\phi_1 - 2rZ_W \sin\phi_1 \cos\phi_1 + Z_W^2 \sin\phi_1)/X_W^2 \qquad \text{(IV-77)}$$

From well-known trigonometric identities

$$2\sin\phi_1 \cos\phi_1 = \sin 2\phi_1 \qquad \text{(IV-78)}$$

$$\sin\phi_1 \cos^2\phi_1 = \sin\phi_1 - \sin^3\phi_1$$

$$= \sin\phi_1 - \frac{1}{4}(-\sin 3\phi_1 + 3\sin\phi_1)$$

$$= \frac{1}{4}(\sin\phi_1 + \sin 3\phi_1) \qquad \text{(IV-79)}$$

Hence, one can see that the leading terms of Eq (IV-75) are

$$\frac{w\sin\phi_1}{V_\infty} = \left\{ \left[ \sin\alpha_{ac} + \tilde{v}_W \right] \sin\phi_1 - \tilde{v}_W \left[ \frac{1}{4}(\sin\phi_1 + \sin 3\phi_1) r^2/X_W^2 \right.\right.$$

$$\left.\left. - \frac{rZ_W}{X_W^2} \sin 2\phi_1 + \frac{Z_W^2}{X_W^2} \sin\phi_1 \right] + \cdots \right\} \qquad \text{(IV-80)}$$

Collecting coefficients of $\sin(n\phi_1)$ yields

$$\frac{w\sin\phi_1}{V_\infty} = \sum_{n=1}^{\infty} w_{Wn} \sin(n\phi_1) \qquad \text{(IV-81)}$$

which is a Fourier sine series in the classical sense. Similarly, one can manipulate Eq IV-69 for $u_{i_W}/V_\infty$ to obtain a power series of the form

$$\frac{u_{i_W}}{V_\infty} = \sum_{n=0}^{\infty} u_n^1 \cos^n \phi_1 \qquad \text{(IV-82)}$$

Substituting trigonometric identities for $\cos^n \phi_1$ yields a Fourier cosine series of the form

$$\frac{u_{i_W}}{V_\infty} = \sum_{n=0}^{\infty} u_{Wn} \cos\,(n\phi_1) \qquad \text{(IV-83)}$$

When the Eqs (IV-81 and IV-83) are substituted into Equation IV-65 one obtains using as the index

$$\frac{\Delta\Gamma_\phi}{\Gamma_{\phi o}} = \sum_{\nu=0}^{\infty} \left[a_{\nu\phi}\cos(\nu\phi_1)+b_{\nu\phi}\sin(\nu\phi_1)\right] \qquad \text{(IV-84)}$$

The above series can be put in terms of a complex Fourier series represented by Eq IV-36 where from IV-65, IV-81 and IV-83 one obtains

$$a_{\nu\phi} = A_\phi\, u_{W\nu} \qquad \text{(IV-85)}$$

$$b_{\nu\phi} = B_\phi\, w_{W\nu} \qquad \text{(IV-86)}$$

One sees that the Fourier coefficients representing circumferential non-uniformity of the blade loading are aircraft configuration dependent. Numerical results for the YO-3A configuration are discussed later in this Appendix, and are regarded as representative for a single engine aircraft.

o Estimation of Propeller Axis Angle of Attack

Because of the possible importance of inflow non-uniformities, it was felt necessary to document the estimation of the propeller axis angle of attack. The accompanying sketch shows that the propeller axis lies on the airplane center-line parallel to the water plane and that the wing possesses a $+2.5^\circ$ incidence relative to the water plane or aircraft center-line. Therefore, the so-called airplane angle of attack, $\alpha_{ac}$, is the same as the propeller angle of attack. The airplane angle of attack is estimated as follows: (Reference 3) The reference wing area $S_W$ is 180 ft.$^2$ and for one g flight the reference lift coefficient based on this area and for $L_W = W_{ac} =$ 3750 lb is computed as follows

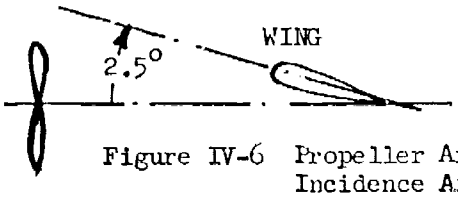


$$C_{LW_{Ref.}} = \frac{W_{ac}}{q_\infty S_{W_{Ref.}}} = \frac{3750 \text{ lb}}{18.6 \text{ psf} \times 180 \text{ ft}^2} = 1.12$$

Figure IV-6 Propeller Axis/Wing Incidence Angle

The lift curve slope for the YO-3A is estimated to be .16 per degree, considering prop wash effects and that the true wing area is 204 ft.$^2$ (higher by 13.5% than the reference area $S_{W_{ref}}$ = 180 ft.$^2$). The YO-3A wing is characterized by the absence of flaps, and the airfoil sections consists of NACA 63-418 inboard of the ailerons and an NACA 23012 airfoil outboard. The estimated average lift coefficient for the wing at zero angle of attack is $C_{L\alpha = 0} = .331$. From this, it is estimated that the angle of attack is $5.38^\circ$ at $C_{L_{W_{ref}}} = 1.12$. The corresponding propeller angle of attack at $C_{L_W}$ is calculated to be $\alpha_{ac} = 5.38^\circ - 2.5 = 2.88$ degrees.

The details of the inflow non-uniformity analysis assessment will be further explained after discussion of propeller blade wake/wing interaction loads which is found contribute significantly to the bucket in the curve of rotational noise vs. rpm.

(b) Propeller Blade Wake/Wing Interaction

The following discussion outlines the problem.

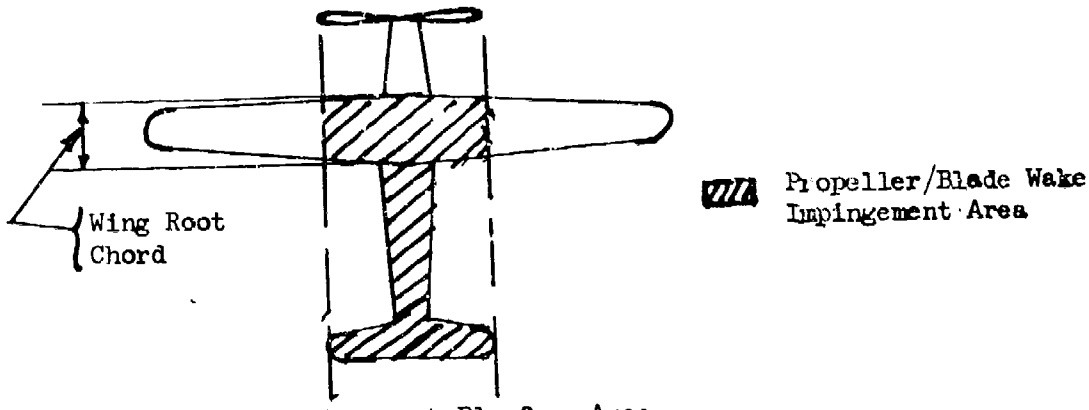


Figure IV-7 Wake Impingement Planform Area

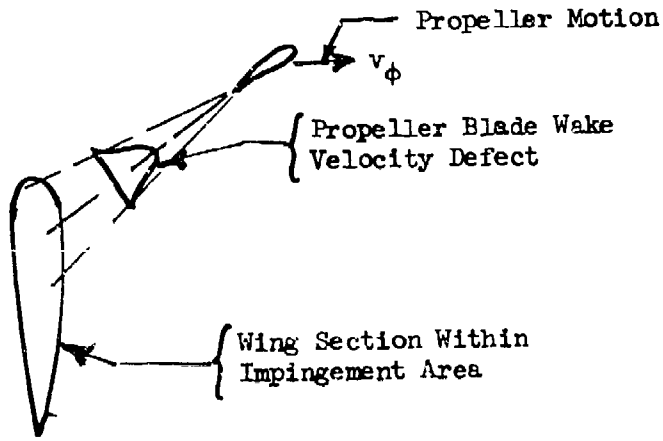


Figure IV-8 Blade Wake Velocity Defect Profile Approaching Wing

As shown in Sketch IV-8 , the propeller blade wake velocity defect profile impinges on the wing. The impingement planform is the shaded area of Sketch IV-7 . The effect is to produce a fluctuating lift force on the wing, as if the wing were flying through a sinusoidal gust whose wave length equals the width of the wake of the propeller blade as it crosses the wing. The strength of the unsteady lift force on the wing is

$$\Delta\tilde{L}_W = \frac{\rho V_\infty^2}{2} C_{L_{\alpha w}} \times [\text{Sears Function}] \times (D_{prop} x c_{wr}) \left(\frac{W_{GW}}{V_\infty}\right) \quad \text{(IV-87)}$$

The fluctuating lift force on the wing acts as a dipole acoustic source whose axis is perpendicular to the wing and is estimated to be approximately in phase with the propeller/torque dipole producing maximum intensity at the overhead position. The magnitude of the far field sound pressure is

$$PFF_{WI} = \frac{\left(\frac{\omega}{a}\Delta\tilde{L}_W\right)}{4\pi R} \quad \text{(IV-88)}$$

Using wake velocity defect data from Reference 19, p. 100, the estimated propeller blade wake and wing interaction noise is 66 to 70 dB at 480 rpm (adding about 2 dB) and lesser amounts above 600 rpm. (See Figure 25).

Conclusion - The combined effects of inflow non-uniformity and blade wake interaction with the wing as estimated in Figure 25 seem to account for the major part of the measured bucket in rotational noise vs. rpm and for the discrepancies in level at all rpms between measured data and predictions, either of classical axisymmetric propeller noise theory or of the USAF computer program (Reference 7 ) which employs empirical corrections from static test data.

(c) Angle of Attack Effect on Chordwise Blade Loading

Reference 7, 8, and 13 employ the standard assumption that the blade loading is uniformly distributed in the chordwise direction, so that the time history of loading at a point in the disc plane is a square wave, repeating B times per revolution of the propeller (see sketch).

Based on the above assumption, the "blade solidity factor" of Reference 7 (Equation IV-15 of Section (2)(a) above) becomes (after multiplying and dividing by $\frac{mB}{2}$):

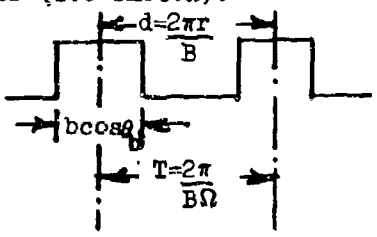


Figure IV-9 Blade Loading Time History Idealized

$$SF_o = \frac{r}{b\cos\theta_b} \sin\left(\frac{mBb\cos\theta_b}{2r}\right) \qquad \text{(IV-89)}$$

A factor 2 was absorbed in the multiplying constant leading to Equation IV-15 (Equation 5 of Reference 7 ) along with the introduction of the dimensionless thrust and power coefficient gradients (defined by Equations IV-19, IV-20). See also 1b(2)(a) above.

The tangential force coefficient $\tilde{c}_\phi$ was given by Equation IV-38.

$$\tilde{c}_\phi = c_d \cos\alpha_{av} + c_\ell \sin\alpha_{av}$$

At low blade lift coefficients, it is reasonable to assume that is uniformly distributed chordwise; however, it is well know from airfoil theory that the additional lift distribution at an angle of attack for a thin wing has a distribution of the following form (Reference 17 , p. 66 ).

$$\frac{dc_\ell}{d\bar{x}} = \frac{\Delta c_p}{2} \; ; \quad \begin{cases} -1 \le \bar{x} \le 1 \\ \bar{x} = 2x/b \end{cases}$$

$$= 2\sin\alpha_b \sqrt{\frac{1-\bar{x}}{1+\bar{x}}} \left(\frac{c_{\ell\alpha}}{2\pi}\right) \qquad \text{(IV-55)}$$

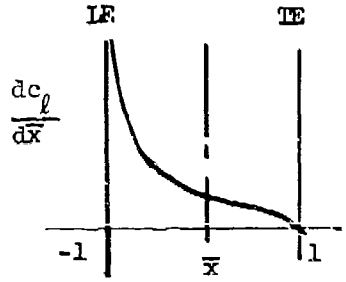


Figure IV-10 Realistic Chordwise Blade Loading due to Angle of Attack

The angle of attack loading described in Equation IV-55 is characterized by a sharp suction peak near the leading edge (inversely proportional to square foot of the distance from the leading edge). The factor $(c_{\ell\alpha}/2\pi)$ is a correction factor for the slope of the lift curve, which depends on airfoil shape, thickness, Reynolds number, and Mach number effects.

If it is assumed that the lift coefficient, $c_{\ell o}$ , at zero angle of attack (due to camber) is uniformly distributed, then one has

$$\frac{dc_\ell}{d\bar{x}} \cong \frac{c_{\ell o}}{2} + 2\left(\frac{c_{\ell\alpha}}{2\pi}\right) \sin\alpha_b \sqrt{\frac{1-\bar{x}}{1+\bar{x}}} \; ; \; -1 \le \bar{x} \le 1 \qquad \text{(IV-91)}$$

Making the substitution

$$\bar{x} = -\cos\theta \qquad \text{(IV-92)}$$

and using a well known Bessel function identity (Reference 13, p. 743)

$$e^{iz\cos\theta} = \sum_{n=-\infty}^{\infty} (i)^n e^{in\theta} J_n(z) \qquad \text{(IV-93)}$$

$$e^{-iz\cos\theta} = \sum_{n=-\infty}^{\infty} (i)^n e^{in\theta} J_n(z)(-1)^n$$

it can be shown that the solidity factor for tangential (torque) force becomes (after dividing and multiplying by mB/2) the following complex number function of radial position

$$SF = SF_r + iSF_i \qquad \text{(IV-94)}$$

where the real and imaginary parts are given by

$$SF_r = \frac{1}{\tilde{c}_{\phi_o}} \left\{ SF_o \left(c_d \cos\alpha_{av} + c_{\ell o} \sin\alpha_{av}\right) + \frac{mB}{2} \left(\frac{c_{\ell\alpha}}{2\pi}\right) 2\pi \sin\alpha_b \sin\alpha_{av} J_o(z) \right\} \qquad \text{(IV-95)}$$

$$SF_i = \frac{1}{\tilde{c}_{\phi_o}} \left\{ \frac{mB}{2} \left(\frac{c_{\ell\alpha}}{2\pi}\right) \left(-2\pi \sin\alpha_b \sin\alpha_{av}\right) J_1(z) \right\} \qquad \text{(IV-96)}$$

and where $J_o(z)$ and $J_1(z)$ are Bessel functions of the first kind of order zero and one whose argument is

$$z = mBb\cos\theta_b/2r \qquad \text{(IV-97)}$$

From Equation IV-95 it is readily apparent that if $\alpha_b = 0$, then all of the lift is attributable to camber $(c_{lo})$, which is assumed uniformly distributed as before. In this special case

$$SF_r = SF_o$$
$$SF_i = 0 \qquad \text{(IV-93)}$$

z is generally less than unity so that $J_0(z) = 1$ and $J_1(z) = z/2$.

It is important to note that $SF_r$ is larger than $SF_0$ when $\alpha_b$ and $\alpha_{av}$ are large; this condition is typical of low rpm/high blade lift conditions. Therefore, the above defined blade loading solidity factor used in the present

noise calculations tends to increase at low rpm giving rise to a slight "bucket tendency." Typical results at 480 rpm yield blade angles of attack (at $r = .75\ r_t$) ranging from 6 to 11 degrees with corresponding advance angles $\alpha_{av}$ ranging from 50 to 55 degrees. At 480 rpm typical values of $SF_o$ are 1.48 and $SF_r$ = 1.6 to 1.8. The present correction to axisymmetric rotational noise as predicted by Reference 7 would be

$$\Delta SPL_m = 20 \log_{10} \left( \frac{\sqrt{SF_r^2 + SF_i^2}}{SF_o} \right) \qquad \text{(IV-99)}$$

At 480 rpm (maximum) value would be

$$\Delta SPL_m = 20 \log_{10} \left( \frac{1.8}{1.5} \right) = 1.6\text{dB}$$

At high rpm the correction rapidly approaches zero.

(4) Effects of Propeller Aerodynamic Performance and Configuration On The Non-Uniform Loading (NUL) Environment

(a) Preliminary Remarks

As noted in the previous discussion of this Appendix, the principal source of discrepancy between the USAF computer program results and the experimental results for rotational noise is attributed to non-uniform loading (NUL) effects. The Fourier series coefficients for the NUL will be called loading harmonics (LH). The NUL effect is caused by the non-uniform inflow velocity field generated primarily from two sources, (1) the aircraft propeller shaft angle of attack, and (2), the upwash and backwash velocity field generated by the lifting flow field of the wing at specified longitudinal and vertical separation distances from the center of the propeller disc.

It has been noted that the USAF computer program propeller efficiencies at low rpm are predicted to be higher than the efficiency data obtained from the YO-3A flight test report (Reference 3 ). These results are shown in Figure 23 where at 480 rpm the USAF computer program estimates an efficiency of about 76%, while the YO-3A flight test data indicates an efficiency of the order of 50%. The corresponding horsepower values at 220 lb. thrust and 125 ft./sec. true airspeed are 66 and 100 respectively which would cause a 4 dB difference on the basis of purely axisymmetric theory (see Figure 19). It is found that the loading harmonics increase in magnitude as the blade efficiency decreases, further augmenting the rotational noise. Therefore, it is of interest to independently resolve the discrepancies in propeller efficiency data. In the calculations by the first method, discussed earlier in this Appendix, an ideal induction efficiency was assumed, which was adjusted to match the YO-3A propeller efficiency data.

The induction efficiency defines slipstream factors for linear and angular velocity which are physically related to the trailing vortices shed from the propeller tip. Therefore, assuming a value for induction efficiency amounts to specifying the induced drag and downwash velocity at each radial station. The components of the downwash velocity vector add to the axial flow velocity and subtract from the relative tangential velocity, as shown in the figure below.

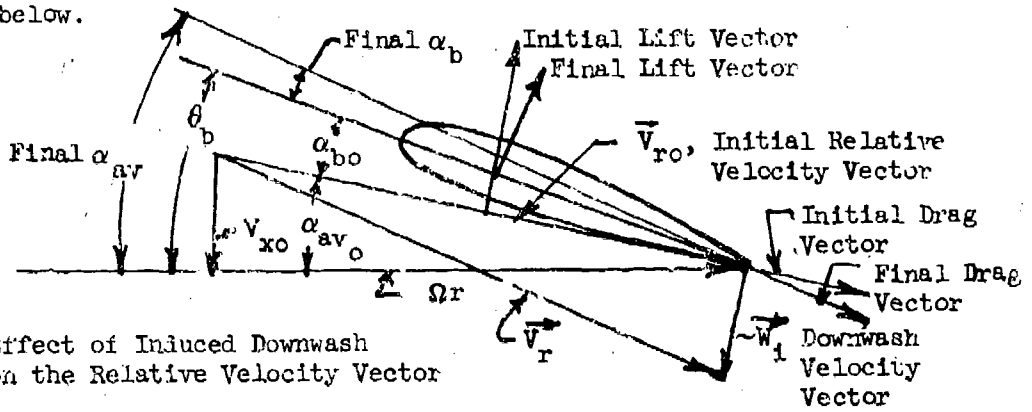


Fig IV-11 Effect of Induced Downwash on the Relative Velocity Vector

Also, as shown in the above figure, the downwash angle causes the resultant angle of attack to decrease. Since the downwash is perpendicular to the relative velocity vector it is seen that as rpm decreases, the downwash velocity tends increasingly to negate the tangential velocity component. The factors called usb and omsb in the first method are equivalent to the axial and tangential components of the induced downwash velocity vector, which are directly calculated in the method described below.

To provide an independent assessment of the propeller efficiency, and at the same time generate a self consistent set of propeller blade loads and loading harmonics (JR), a second method, using an approximate lifting line theory calculation was developed (see Reference [12]) with a modification to allow for spanwise variation of the relative velocity vector. The relative velocity is the equivalent freestream velocity for a propeller blade. The results of this second blade load prediction method will be described below.

As part of the evaluation of non-uniform loading effects, additional studies have been conducted to refine the calculation of radiated rotational noise by accounting for the exact radial distribution of loading harmonics vs. simplified but more convenient calculations wherein the loading harmonics are calculated only at a single reference radius. Some useful conclusions will be presented concerning this aspect.

For aircraft design studies, it is of interest also to evaluate the sensitivity of the LH values to wing separation distance and angle of attack, so that possible deviations from the current YO-3A configuration might be assessed. A simplified approach is presented below. It will be seen that the first loading harmonic is the dominant one and therefore, a correlation

of the excess rotational noise due to NUL effects can be made in terms of the first loading harmonic only. This simple correlation permits estimates of the effects on rotational noise of wing separation, angle of attack and angle of side slip, merely by examining the change of the first loading harmonic, evaluated at a reference radius, as a function of the aircraft configuration variable.

(b) Propeller Performance Estimate from 3 Dimensional Lifting Line Theory

This second blade load analysis method employed is one of successive approximation in which (1) an "effective aspect ratio" is assumed for the propeller blade, yielding, as a first approximation, a value of downwash angle per unit $c_l = 1/(\pi AR_e)$. This yields a blade lift curve slope per unit geometric angle of attack which accounts for finite span effects. (2) The loading is multiplied by $\sqrt{1-\eta^2}$ where $\eta$ is the semi-span fraction (equal to -1 at the hub and plus 1 at the tip). (3) For each assumed blade angle and effective aspect ratio the lift, thrust and torque are integrated radially. When the total thrust equals 220 lb., one has a possible solution for each assumed effective aspect ratio. (4) The criterion for selecting the effective aspect ratio is as follows: (a) The first approximate span loading is expressed as a Fourier series, from which the induced downwash angle is calculated by a slight modification of the classical Glauert theory (Reference 12 , page 138 to account for spanwise variation of the relative velocity. (b) Next, a comparison is made between the approximate downwash angle, $c_l/\pi AR_e$, and those of the lifting line calculation. If the lifting line downwash values are larger, then the calculation is repeated using a smaller value of effective aspect ratio and the process is continued iteratively. Usually the method converges in about two iterations. The results at 480 rpm indicate that the effective aspect ratio of the Standard 3 Bladed YO-3A is about 1.7. Since the geometric aspect ratio is 3, then the "spanloading (Oswald) efficiency factor" (Reference 17 ) would be about 0.57. On the basis of such a calculation the propeller efficiency at 480 rpm is about .58. Figure 24 shows the calculated propeller efficiencies vs. effective aspect ratio. The results of Figure 24 and Table IV-I below indicate that the calculated propeller efficiencies upon which the USAF propeller noise computer program is based are too high. Note that even if one assumes the maximum possible span loading efficiency of 100% ($AR_e = 3$) the resultant propeller efficiency is still much lower than Reference 8.

Table IV-I Comparison of Propeller Efficiency at 480 rpm

| Source | Thrust lb | Efficiency | HP | Axisymmetric Fundamental SPL |
|---|---|---|---|---|
| USAF/Ref 1 | 220 | .76 | 66 | 57 |
| LMSC/Ref 2 | 220 | .50 | 100 | 62 |
| Present CALAC ($AR_e = 1.7$) | 220 | .58 | 86 | 60 |
| $AR_e = 3$ | 220 | .69 | 76.6 | 58 |

As will be seen below, the lower propeller blade efficiencies are accompanied by an enhancement of blade loading harmonics which have already been shown (Figures 29 and 30) to increase with increasing blade lift coefficient which increases with decreasing rpm. The increased loading harmonics improve the acoustic radiation efficiency as has already been mentioned.

(c) Factors Affecting Propeller Blade Loading Harmonics LH Dependence on Harmonic Number

The method for calculating the complex Fourier coefficients

$$\delta_\nu = (a_{\nu\phi} - ib_{\nu\phi})/2 \; ; \; \nu = 0, \pm 1, \pm 2$$

has already been described (Section (3) (a) above). The basic equations suggest that the loading harmonics increase with both lift coefficient and advance angle. Figures 26 and 27 below show typical values of the first six loading harmonics ($a_\nu$, and $b_\nu$ )vs. loading harmonic number $\nu$. The results are shown at 480 rpm at 125 ft./sec. flight speed for various propeller efficiency conditions. It can be seen that the loading harmonics under forward flight conditions decay very rapidly with increasing load harmonic number. Note also that the first loading harmonic increases with decreasing propeller efficiency. This curve pertains to the YO-3A configuration but similar results are found at other values of wing separation distance and is shown below. It is seen in Equation IV-29 that the third loading harmonic ($\nu$ = mB) gives a zero contribution to the torque dipole radiation which dominates the overhead noise. Since the fourth loading harmonic is typically very small, it is concluded that, for all practical purposes, two loading harmonics (or more generally mB - 1) suffice for a three (B) bladed propeller for calculating far field noise in the propeller disc plane (or near overhead position). This is in contrast to (the NUL effect on) rotational noise along the thrust axis which is strongly re-enforced by the $\nu$ = mB harmonic. This latter case is of paramount importance to helicopter rotor noise.

To further simplify matters it is seen in Figures 26 and 27 that the first tangential force LH (the $b_{1\phi}$ term) is much larger than the others; therefore, it is natural to seek a correlation between the rotational noise increment, $\Delta SPL_{NUL}$ due to non-uniform loading(NUL)as a function of the coefficient $b_{1\phi}$ Such a correlation would then provide a method for rapid estimation of NUL effects upon rotational noise, merely by calculating the variation of $b_{1\phi}$ as a function of various configuration variables.

(d) Radial Variation of Loading Harmonics

First consider the radial variation of $b_{1\phi}$ at 480 rpm. Typical results are shown in Figure 28 at two loading conditions, representing different propeller efficiencies; (1) the L2 loading is very similar to Reference 7 results; (2) the L4 loading is compatible with the lower propeller efficiencies provided by YO-3A project data (Reference 3 ) and the L3 data estimated independently in this study. As can be seen the loading harmonics increase rapidly

near the hub where the blade lift coefficient and advance angle increase towards the hub. The higher $c_l$ values associated with the L3 or L4 loads yield $b_{1\phi}$ values at any given r/rt, compared with the more efficient (L2) load condition.

The noise increments, due to non-uniform loading $\Delta SPL_{NUL}$ for the YO-3A configurations are plotted against rpm in Figure 31, in which the radial variation of the harmonics has been considered. These results show an increase in the non-uniform load (NUL) effect at decreasing rpm which is considered to provide the major contribution to the explanation for under prediction by the USAF computer program of absolute levels of rotational noise and the bucket in the rotational noise vs. rpm curve. These data are included in the previously discussed theoretical vs. experimental comparison (Figure 25) which is one of the most important contributions of the theoretical part of the present study.

As a calculation convenience, it is of interest to determine if the NUL effect can be accurately computed by using input of loading harmonic (LH) values calculated only at a single effective radius position. Figure 32 shows the calculated NUL effect as a function of the radius location for which the LH were evaluated. In this case a set of two LH values, including both sine and cosine terms were evaluated at the radial location noted. Also shown are the values of SPL obtained by input of the radial variation of the LH. It is concluded that evaluation of loading harmonic Fourier coefficient values at r/rt = .55 gives nearly the same result as is obtained by considering the radial variations of the LH. This conclusion is of special value when considering configuration parametric effects on the NUL effect such as changing the wing separation distance, or airplane angle of attack.

(e) Correlation of NUL Effect as a Function of the First LH

A further computational simplicity is afforded by establishing a correlation between the NUL/SPL increment and the strongest loading harmonic, $b_{1\phi}$. This is accomplished by plotting the exact $\Delta SPL$ due to NUL, including radial variation of the first two LH vs. $b_{1\phi}$ as calculated for various r/rt and rpm values. The results are shown in Figure 33. Also tabulated are corrections for evaluation of $b_{1\phi}$ at (r/rt) = .62 and .75. One would expect a dependence on rpm which will be demonstrated analytically below. According to theory

$$\Delta SPL_{NUL} = 20 \log_{10}\left\{\sum_{\nu=-\infty}^{\infty} \left(\frac{mB+\nu}{mB}\right) (-1)^{\nu} e^{i\nu(\phi+\pi/2)} \frac{J_{mB+}(argmB)}{J_{mB}(argmB)} \frac{(a_{\nu\phi}-ib_{\nu\phi})}{2} \frac{(SF_r+iSF_i)}{\sqrt{SF_r^2+SF_i^2}}\right\} \quad \text{(IV-100)}$$

where $Y = S_o$, and $\phi = 0$ for a far field observer under the flight path in the propeller disc plane, and it will be recalled (Equation IV-31).

$$argmB = mB\, k_1 r = \left(\frac{mB\,\Omega Y}{a\, S_o}\right) r$$

The negative values of $\nu$ are predominant so that the following approximation is valid for the overhead far field observer position ($\phi = 0$).

$$\Delta SPL_{NUL} = 20 \log_{10} \left\{ \sum_{\nu=0}^{\infty} \left(\frac{mB-\nu}{mB}\right) (-1)^{\nu} e^{-i\nu\pi/2} \left(\frac{a_{\nu\phi}+ib_{\nu\phi}}{2}\right) \right.$$

$$\left. \times \frac{J_{mB-\nu}(argmB)}{J_{mB}(argmB)} \frac{(SF_r+iSF_i)}{\sqrt{SF_r^2+SF_i^2}} \right\} \qquad \text{(IV-101)}$$

If the above expression is truncated at $\nu = 1$, based on the already established dominance of the first load harmonic, one has

$$\Delta SPL_{NUL} = 20 \log_{10} \left\{ 1 - \left(\frac{mB-1}{mB}\right) \frac{J_{mB-1}(argmB)}{J_{mB}(argmB)} \frac{(b_{1\phi}SF_r - a_{1\phi}SF_i)}{\sqrt{SF_r^2+SF_i^2}} \right\} \qquad \text{(IV-102)}$$

It is noted that $b_{1\phi}$ is negative by its definition, leading to a positive $\Delta SPL_{NUL}$. At low rpm the Bessel function argument is small and the Bessel functions are approximated by

$$J_{mB-\nu}(argmB) \cong \frac{1}{(mB-\nu)!} \left(\frac{argmB}{2}\right)^{mB-\nu} \qquad \text{(IV-103)}$$

Using the above approximation and neglecting the small product $a_{1\phi}$ times $SF_i$ one finds

$$\Delta SPL_{NUL} \cong 20 \log_{10} \left\{ 1 - \left(\frac{mB-1}{mB}\right) \frac{(mB)!}{(mB-1)!} \frac{(b_{1\phi}/2)}{(argmB/2)} \right\} \qquad \text{(IV-104)}$$

Introducing the absolute value of $b_{1\phi}$ which is by definition positive

$$\Delta SPL_{NUL} \cong 20 \log_{10} \left\{ 1 + \left|b_{1\phi}\right| \left(\frac{mB-1}{mB}\right) \frac{1}{(\Omega rY/aS_o)} \right\} \qquad \text{(IV-105)}$$

This result demonstrates that the NUL effect should increase with decreasing rpm both through the direct effect of the dominator ( a radiation efficiency enhancement factor) and indirectly because of the increase of ($b_{1\phi}$ ) at low rpm which is related to the increase of lift coefficient and advance angle, as shown earlier.

(f) Effects of Wing Separation and Propeller Angle of Attack on the Non-Uniform Loading Environment

It has been established above that the NUL increment to rotational noise depends primarily on the first tangential force loading harmonic, $b_{1\phi}$ , evaluated approximately at r/rt = .55. Therefore, the effects of changing wing separation distance or propeller shaft angle of attack can by examining the variation of $b_{1\phi}$ at convenient (r/rt) values as a function of Xw/D, Zw/D or $\alpha_{ac}$ where Xw and Zw represent, respectively, the longitudinal and vertical wing separation distances and, $\alpha_{ac}$ is the aircraft or propeller shaft angle of attack.

Figure 34 shows the calculated effect of changing the wing separation distance for the YO-3A whose basic parameters are Xw/D = 1, Zw/D = 0.214 and $\alpha_{ac} = 2.88^{\circ}$. The convergence criteria for the series expansion method for calculating the loading harmonics restricts Xw/D to values greater than 0.5. The Δ SPL due to NUL effects are shown in Figure 35 . It is seen that small increases of wing separation are not likely to be very beneficial. Therefore, careful examination of the design impact of weight and balance changes would be required if it were desired, for example, to double the present YO-3A wing separation distance. Figures 36 and 37 show the effects of propeller shaft (aircraft) angle of attack variation for the present YO-3A configuration. The airplane angle of attack could be decreased significantly by use of trailing edge flaps, or generally decreased by increasing the flight speed.

(g) Possibilities for Aircraft Design Changes to Reduce Rotational Noise

It is estimated that the YO-3A gliding airframe vortex noise is sufficiently lower than the propeller blade vortex noise that the forward speed could be increased possibly by 25 percent (reducing the wing lift coefficient for the same wing loading). This would reduce both the wing angle of attack, and the wing lift circulation-induced upwash at the propeller disc plane by 36 percent. The airframe vortex noise penalty would be 6 dB according to a $V^6$ law.

Decreasing the wing loading by increasing the wing area would decrease the angle of attack without the benefits of reducing the upwash; also this would cause frame noise increment. Depending on the aircraft mission, it would appear that an optimum combination (of partial deflection of full span trailing edge flaps, increased wing area, and increased forward speed) could be found which might reduce the rotational plus vortex noise. Also, it is thought that the discontinuity caused by the extension of the

trailing edge of the inboard part of the YO-3A wing is responsible for its rather low span loading efficiency ($e \cong .7$) (Reference 3 ). This was the result of a need for a low cost method to increase the area of an existing glider wing, simply by extending the chord of the inboard sections.

It is believed that trailing edge flaps to allow angle of attack reduction at any forward speed would be a desirable feature of a "quiet" airplane.

## 2. VORTEX NOISE

### a. Summary

The measured vortex noise for the YO-3A has been compared with predictions of the USAFPL computer program based on References 7 and 8. The predictions were based on three different options which will be reviewed below. Unfortunately, it has been found that large discrepancies exist between the experimental data and predictions from any of the three options.

Lockheed has herein developed a simple empirical method for estimating the vortex noise which offers excellent agreement with measured data for the standard three-bladed propeller and good agreement with experimental data for the three-bladed "Acoustic Propeller". This method can be regarded as another "option" which can be described as an empirical correction to the level of the fundamental rotational noise, previously discussed in this Appendix. A simple empirical correction to the theoretical rotational noise as predicted by References 7 and 8 has already been recommended in the present study, as discussed earlier in this report; therefore, the vortex noise is easily predictable by the sum of these two empirical corrections. A rationale for this method is discussed below, after discussing the vortex noise options of Reference 7.

### b. Discussion of Existing Options

#### (1) Introduction

Reference 7 contains a review of a number of previous techniques for prediction of vortex noise, and then outlines three options which are coded in the computer program documented in References 7 and 8. These three options will be discussed in order of their simplicity.

#### (2) Option 2 of References 7 and 8 : Consistency Analysis

This method employs (1) an overall SPL formula, (2) a spectral peak frequency determination, and (3) a frequency spectrum for determining 1/3 octave band levels relative to overall SPL as a function of the ratio band center frequency/ peak frequency. This spectrum is labelled HS correlation of 3/69 and is shown in Figure IV-21 below (Fig. 7 of Ref. 7). Figure IV-21 also displays the 1/3 octave band level spectral shapes employed in the other options to be discussed below.

The overall SPL relation is attributed to Schlegal, King and Mull (Ref. 20) in modified form and a directivity function obtained from Ollerhead and Lowson (Ref. 21).

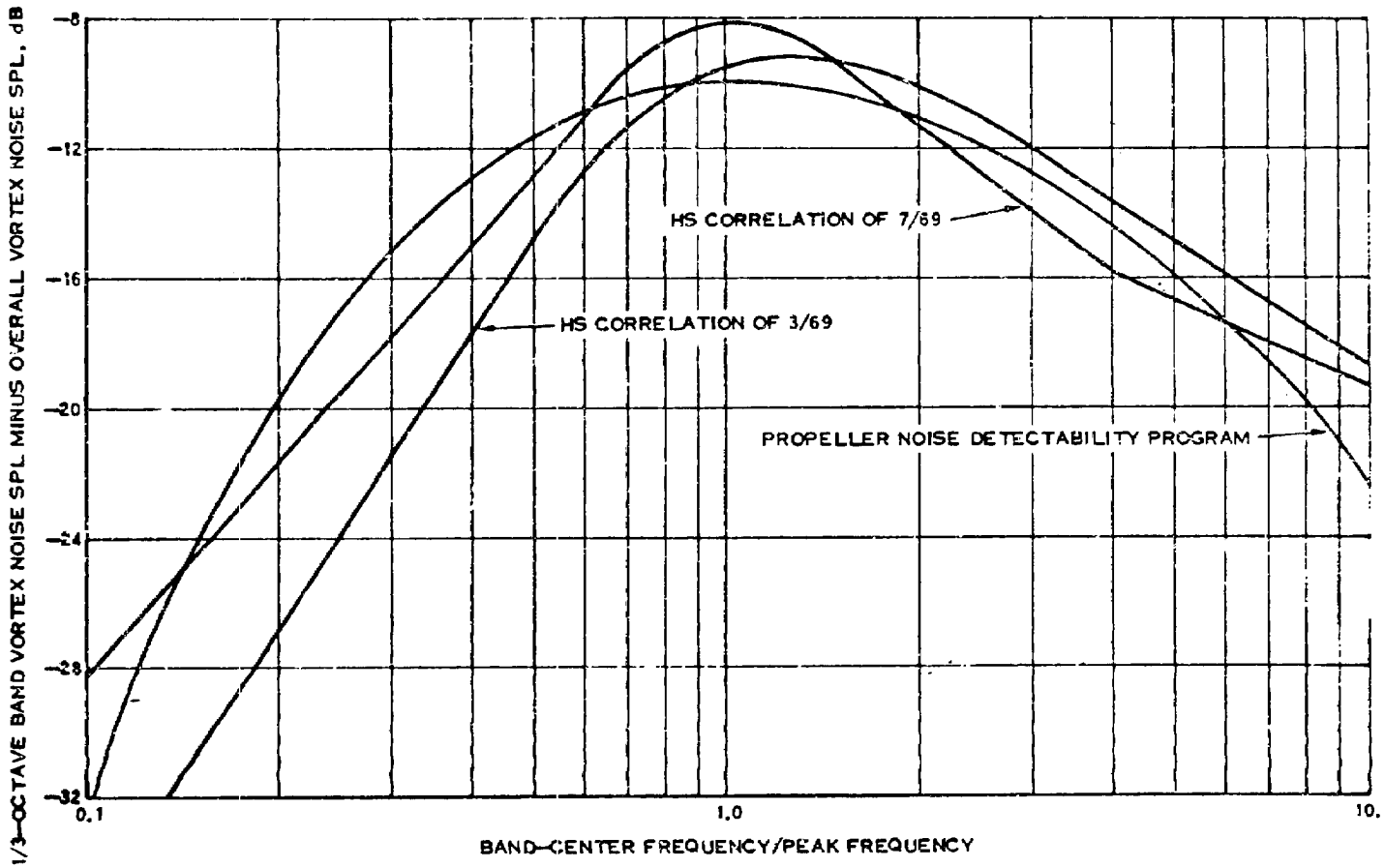


Figure IV-12 Frequency Spectra Employed in Vortex Noise Prediction (From Ref. 7)

The peak frequency is determined by

$$f_{peak} = \frac{0.28V_{0.7}}{(h_{0.7}\cos\alpha + b_{0.7}\,|\sin\alpha|)} \qquad \text{(IV- 106)}$$

The denominator of Eq. IV-106 is the projected blade frontal thickness.

The overall SPL relation is

$$SPL_{OA}^{OPT2} = 10\log_{10}\left(\frac{V_t^2 C_L^2 S_b(\cos^2\psi + 0.1)(0.217)}{d^2}\right) - 44.645 \qquad \text{(IV-107)}$$

where $\psi$ is the directivity angle (0 on thrust axis) and d is the far field slant distance.

The original form of the Schlegal, King and Mull formula is (Ref. 7 p. 32)

$$SPL_{OA}^{SKM} = 10\log_{10}\left(V_{0.7}^2\, T^2/S_b d^2\right) + 13.8 \qquad \text{(IV- 108)}$$

Some fundamental comments are in order here. Lighthill (Ref. 22 ) and Curle (Ref. 23 ) have discussed the hierarchy of multipole point sources which model various aerodynamic sound generating mechanisms. These sources emphasize several key points:

- Monopole sources are associated with pulsations of fluid volume flow (such as bubbles collapsing and "breathing mode" vibrations of adjacent solid bodies). The monopole is the most efficient acoustic radiator at low frequencies (compared to higher order multipole sources).

- Dipole sources are next strongest in acoustic radiation efficiency. The strength of a dipole is associated with fluctuating fources acting on the fluid (reacting upon an adjacent solid) in such a way that the rms value of the total net force is finite. This is the predominant aerodynamic noise generating mechanism which, for airfoils, propellers, and turbomachinery, is often called "broad band vortex noise". The radiated acoustic power is proportional to the $M^3$ times mechanical power, where M is the Mach number.

- Quadrupole sources produce the third strongest mechanism, one which predominates in the absence of monopole and dipole sources. The principal examples are free shear layer turbulent mixing noise radiated from jets and wakes. This mechanism is also present in the wakes of airfoils, rotors, and propellers, but the acoustic power

radiated is proportional to $M^5$ and therefore weaker (by a factor of M2) than the dipole noise associated with force fluctuations on airfoils propellers, etc. at low Mach numbers. Thus, at low Mach numbers, the far field noise is predominently dipole noise, and can be written as (Refs. 22 , 23).

$$SPL_{dipole} = K+10\log_{10}\left(M^3\rho V^3 S_b/d^2\right) \qquad \text{(IV-109)}$$

where K can be a function of various aerodynamic dimensionless similarity, shape parameters and dimensionless force coefficients.

The thrust of a propeller can be written in terms of the classicial propeller thrust coefficient (see this Appendix, Sec. 2b(2)(a) Eq. IV-19); also see Ref. 18 , p. 276.

$$\begin{aligned} T &= K_2\,\rho D^4 (RPM/60)^2 C_T \\ &= K_2\,(D^2/S_b)\rho S_b\,(V_t/2\pi r_t)^2 D^2 C_T \end{aligned} \qquad \text{(IV-110)}$$

$$\begin{aligned} \therefore T/S_b &= K_2\,(D^2/S_b)(D/2\pi r_t)^2\,\rho V_t^2 S_b \\ &= K_2\,(D^2/\pi^2 S_b)\,\rho V_t^2 C_T \;;\; K_2 = 6.61\times10^{-7} \end{aligned} \qquad \text{(IV-111)}$$

Substitution of (IV-111) for $T/S_b$ in Eq. IV-111 produces the result

$$\begin{aligned} SPL_{OA}^{SKM} &= 10\log_{10}\left(V_{0.7}^2\left[K_2(D^2/\pi^2 S_b)\rho V_t^2 C_T\right]^2 S_b/d^2\right) + 13.8 \\ &= 10\log_{10}\left(V_{0.7}^2\,\rho^2 V_t^4 S_b/d^2\left[K_2 C_T\,(D^2/\pi^2 S_b)\right]^2\right) + 13.8 \\ &= 10\log_{10}\left(\rho V_t^6 S_b/d^2\,\rho\left[K_2 C_T\left(\frac{V_{0.7}}{V_t}\right)D^2/\pi^2 S_b\right]^2\right) + 13.8 \end{aligned} \qquad \text{(IV-112)}$$

Introduction of the tip Mach number, $M_t = V_t/a$, $M_t = V_t/a$ yields

$$\begin{aligned} SPL_{OA}^{SKM} &= 10\log_{10}\left\{M_t^3\,\rho V_t^3 S_b/d^2\left[K_2 C_T\left(\frac{V_{0.7}}{V_t}\right)D^2/\pi^2 S_b\right]^2\rho a^3\right\} + 13.8 \\ &= 10\log_{10}\left(\rho V_t^3 M_t^3 S_b/d^2\right) + 20\log_{10}\left[K_2 G\left(\frac{V_{0.7}}{V_t}\right)D^2/\pi^2 S_b\right] + K_3 \end{aligned} \qquad \text{(IV-113)}$$

Thus, Equation IV-113, which was derived from Equation IV-108 is fundamentally the same as Equation IV-109 except that a dimensionless thrust coefficient and blade area factor have been expressed separately. Next, consider the overall SPL expression used in Option 2 as defined by Equation IV-107.

It is often convenient to define an average blade lift coefficient in terms of blade area and tip speed; for example:

$$C_L = T/(\rho V_t^2 S_b/2) \qquad \text{(IV-114)}$$

Alternatively, this can be written in terms of $V_{0.7} = V$ at $r/r_t = 0.7$

$$C_{L0.7} = T/(\rho V_{0.7}^2 S_b/2) \qquad \text{(IV-115)}$$

Note that such expressions under estimate the required blade lift coefficient at finite forward speed conditions where the lift vector is rotated through the advance angle.

Then, for example, substitution of VI-114 in IV-107 would yield

$$SPL_{OA}^{OPT2} = 10\log_{10}\left[\frac{V_t^2 S_b}{d^2}\left(\frac{T}{\rho V_t^2 S_b/2}\right)^2(\cos^2\psi + 0.1)(0.217)\right] - 44.645$$

$$= 10\log_{10}\left[\frac{T^2 V_t^2}{S_b d^2}\left(\frac{2}{\rho V_t^2}\right)^2(\cos^2\psi + 0.1)(0.217)\right] - 44.645 \qquad \text{(IV-116)}$$

If Equation IV-111 is introduced into IV-115 for T/S the result is

$$SPL_{OA}^{OPT2} = 10\log_{10}\left\{\left[\frac{K_2 D^2 \rho V_t^2 C_T}{\pi^2 S_b}\right]^2\left(\frac{4S_b}{\rho^2 V_t^2 d^2}\right)(\cos^2\psi + 0.1)(0.217)\right\} - 44.645$$

$$= 10\log_{10}\left(\frac{S_b V_t^2}{d^2}\left[\frac{K_2 D^2 C_T}{\pi^2 S_b}\right]^2 4(\cos^2\psi + 0.1)(0.217)\right) - 44.645 \qquad \text{(IV-117)}$$

Therefore, it would appear that Equation IV-107, which is in the form used in Option 2 (and is attributed to Schlegal, King and Mull) implies a $V_t^2$ law, whereas the original form given by Eq. IV-108 implies a $V_t^6$ law (as can be seen by Eqs. IV-112 or IV-113). Thus, it appears that Eq. IV-107, which is employed in Option 2, is not strictly consistent with either the basic dipole law Eq. IV-749 or the original Schlegal, King and Mull version (Eqs. IV-108, IV-112, or IV-113). The motivation for choosing Eq. IV-107 is unclear in view of this inconsistency. Presumably, it is based upon further empirical data (not presented in Ref. 7 which is implied by "HS Correlation of 3/69" (Ref. 7, p. 35). One can make a stronger argument, however, for equations such as IV-107 when the blade lift coefficient is large, as in the case of a low rpm high thrust condition.

(3) Option 3 of References 7 and 8 : Consistency Analysis

This method is attributed to Widnall (Ref. 24 ) and takes the form:

$$SPL = -71.02 + 57{,}000\left(\frac{T}{S_b V_t^2}\right) + 10\log_{10}\left(\frac{V_t^6 S_b}{d^2}\right) - 3.3\sin^2(\psi+10^\circ) \qquad \text{(IV-118)}$$

and the peak frequency defined by

$$f_{peak} = \frac{0.06\, V_{0.7}}{h_{0.7}(1-.265\, X_{stall})} \qquad \text{(IV-119)}$$

where $X_{stall} = (r/r_t)_{stall}$, defined as the propeller radius ratio where blade stall occurs and is defined in Ref. 24 as the outer limit radius where the blade angle of attach first exceeds 11 degrees.

If Eq. IV-111 is substitued for $T/S_b$ in Eq. IV-116 the result is

$$SPL_{OA}^{OPT3} = -71.02 + 57{,}000\left(K_2 \frac{\rho C_T D^2}{\pi^2 S_b}\right) + 10\log_{10}\left(\frac{V_t^6 S_b}{d^2}\right)$$

$$-3.3\sin^2(\psi+10^\circ) \qquad \text{(IV-120)}$$

Apart from the directivity function, Option 3 defined by Equation IV-120 is theoretically consistent with the basic dipole radiation law, Equation IV- 109 with the original Schlegel, King and Mull relation, Equations IV-108, IV-112 to IV-113, and other dipole versions such as Hubbards' (Reference 25 ) and Davidson and Hargett (Reference 26 ) See Reference 7, p. 32 ). These simple methods (Options 2 and 3) have the advantage, for preliminary prediction purposes, of depending only on gross propeller parameters (tip speed, diameter, thrust or thrust coefficient, and blade area).

It is clear, at least in principle, that some kind of radial distribution analysis (such as is done for rotational noise) is also desirable for vortex noise estimation of rotating blades, in view of the significant radial change of relative velocity which affects both spectral center frequency and the level of radiated far field vortex noise from a given radial segment of the propeller blade. These and other theoretical refinements motivated the development of Option 1 (or Option 0) of Reference 8.

(4) Option 0 or 1: Description and Consistency Analysis

This theory is based on work by Lowson (Reference 27 ) which considers the effects of the source motion due to propeller rotation and forward speed. The basic equation for far field noise radiation is, in Cartesian Coordinates

$x_i$: $i = 1,2,3$ of the field point; $y_i$: $i = 1$ to 3 of the source point (Reference 7 , Equation 30, page 37 )

$$p = \sum_{i=1}^{3} \left[ \frac{(x_i - y_i)}{4\pi(1-M_r^2)ad^2} \left\{ \frac{\partial F_i}{\partial t} + \frac{\partial F_i}{(1-M_r)} \frac{\partial M_r}{\partial t} \right\} \right] \qquad \text{(IV-121)}$$

where $M_r$ is the component of convention Mach number in the direction of the observer and $\{F_i\}$ are the unsteady blade load components.

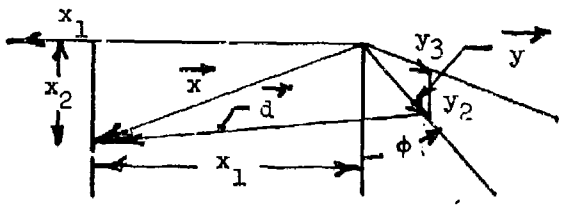


Figure IV-13 Cartesian Components of Field Point and Source Point Position Vectors

The components of the point source position on the blade are (per Reference 7 )

$$y_1 = 0 \qquad y_2 = r\cos\phi \qquad y_3 = +r\sin\phi \qquad \text{(IV-122)}$$

where $\phi$ is a circumferential angle for the blade position. The field point locations are

$$x_1 = x_p, \qquad x_2 = Y, \qquad x_3 = 0 \qquad \text{(IV-123)}$$

Note that in this notation, Y would be the altitude and $x_3$ would be lateral distance from the flight path. The distance between the source point vector, $\vec{y}$ and the field point vector, $\vec{x}$ , is

$$|\vec{d}| = \sqrt{|\vec{x} - \vec{y}|^2}$$

$$= \sqrt{X_p^2 + (Y - r\cos\phi)^2 + r^2\sin^2\phi} \qquad \text{(IV-124)}$$

The component of convection Mach number, $M_r$, is

$$\vec{M}_r = M \cdot (\vec{x} - \vec{y})/d = \sum_{i=1}^{3} (x_i - y_i) M_i / d$$

$$= M x_p/d - (\Omega r/ad) \sin\phi \, (y - 2r\cos\phi) \qquad \text{(IV-125)}$$

where a is the speed of sound, $\Omega$ , is the propeller angular velocity in radians/sec.

The unsteady blade force components are

$$F_1 = F \cos \theta_b \; e^{-i\omega t}$$

$$F_2 = F \sin \theta_b \sin \phi \, e^{-i\omega t} \qquad \text{(IV-126)}$$

$$F_3 = -F \sin \theta_b \cos \phi \, e^{-i\omega t}$$

and the Mach number components are

$$M_1 = M; \; M_2 = -(\Omega r/a) \sin \phi; \quad M_3 = (\Omega r/a) \cos \phi \qquad \text{(IV-127)}$$

The pressure field becomes (Reference 7, Page 39)

$$p = (F/4\pi d^2 a) \left[ -i\omega \left\{ X_p \cos\theta_b + (Y - 2r\cos\phi) \sin\theta_b \sin\phi \right\} + \Omega \sin\theta_b \left\{ r\sin^2\phi + (Y - r\cos\phi)\cos\phi \right\} \right] e^{-i\omega t}/(1 - M_r^2) \qquad \text{(IV-128)}$$

The fluctuating force, F, is assumed to be random (out of phase radially) so that mean square values are summed anti-logarithmically in the ten point, Simpson Rule integration technique of References 7 and 8, after circumferential integration with respect to $\phi$.

The magnitude of the fluctuating force is expressed as:

$$F = C_F \, \rho h \sqrt{b \Delta r} \; V^2 (R_e/10^6)^{exp} \qquad \text{(IV-129)}$$

where $R_e$ is the Reynolds number

$$R_e = (\rho V b/\mu) \qquad \text{(IV-130)}$$

V is the section relative velocity

$$V = \sqrt{V_x^2 + V\phi^2} \qquad \text{(IV- 131)}$$

In Section VI of reference 7 (p. 119) it is suggested, based on experimental data for propeller noise on the static test stand, that

$$C_F = 8.0$$

and the Reynolds number exponent is recommended to be

$$\exp = -1.0$$

The frequency at the center of the spectral peak is defined as

$$f_{peak} = \frac{\omega\,peak}{2\pi} = C_f\, V/h \quad Hz \qquad \text{(IV- 132)}$$

where (Reference 7 , page 119) the recommended value is

$$C_f = 0.06$$

The choice, exp = -1, yields a $V^4$ variation for mean squared sound pressure according to Equations IV-128 and IV-129. Option 1 employs circumferential and radial integration of Equation IV-128 using 36 intervals of $\phi$, separated by $10^\circ$, and using the same 10 radial integration stations employed in the performance analysis.

Clearly, this method appears potentially as more logical than either Options 2 or 3, and it is obvious that at least two possible roads to refinement would be (1) to relate values of ($C_F$, $C_f$ and exp) to aerodynamic parameters associated with the blade loading analysis, and (2) to empirically alter these three empirical constants to match the YO-3A flyover data (as opposed to the selection based on the static test stand data cited in Section VI of Reference 7).

It turns out that another very simple alternative empirical technique has been devised which is very successful in fitting the YO-3A data. This method, and its rationale, will be described below.

(5) Empirical Corrections to Vortex Noise: Rationale

(a) Comparison of Reference 7 Predictions with Experimental Data for the YO-3A

Figures 16 to 18 show the predictions of References 7 and 8 compared with experimental data on a basis of 1/3 octave band data. The experimental

data curves were faired through data for those bands not containing the rotational noise harmonics, and the experimental data was corrected for ground reflections. It is clear that the levels and spectral shapes for all three of the options described above are in error. Option 1 or 0, based on radial integration of Lowson's theory (Reference 27 ), is closest with respect to peak 1/3 octave band level, but it is high by 2.5 dB in peak level at the 600 rpm and by 9 dB at 720 rpm. Option tends to be too flat with respect to the spectral shape and predicts a peak frequency which is somewhat too high.

Option 2, based on a modified form of Schlegal, King and Mull (Reference 20 ) and the Ollerhead-Lowson directivity (Reference 21 ) appears to be low in peak level by 15 dB at 600 rpm and by 11 dB at 840 rpm. The spectral shape of Option 2 at frequencies above the predicted spectral peak frequency is fairly good, though the decrease of predicted level beyond the spectral peak is somewhat too rapid.

Option 3 also under-predicts the peak 1/3 octave band levels by 11.5 dB at 600 rpm, and by 8 dB at 780 rpm. The spectral peak frequencies predicted by Option 3 are surprisingly good, and the spectral shape is also fairly good.

With respect to spectral shape below the peak frequency, it must be said that the available YO-3A experimental points are limited, and all of the methods are reasonable, though Options 2 and 3 appear to fall off somewhat too steeply below the spectral peak frequency and Option 1 or 0 falls off somewhat too slowly.

(b) Comments on Peak Frequencies and Spectral Shapes

The failure of Option 1 or 0 to improve the spectral shapes is disappointing since it considers more of the propeller blade design details, especially the radial variation of blade aerodynamic parameters and the relative velocity. It must be concluded that the choice of empirical parameters ($C_F$, $C_f$, and exp) (See Reference 7 ) must be the principal source of error.

With respect to all of the above described methods, Lockheed feels that the choice of a single length dimension for Strouhal number scaling is an oversimplification (such as was defined in Equations IV-100, IV-119, and IV-132) for Option 2, 3, and 1 or 0, respectively. In Option 3, there is a factor in the denominator ($1 - .265\ X_{stall}$) which would increase with rpm, since $X_{stall}$ approaches $r_{hub}/r_{tip}$ as the blade angles of attack decrease, which they do at higher rpm. This factor would tend to offset the increase of tip speed with rpm, and would explain why the predicted center frequency for the spectral peak does not change with rpm. Because of the limited rpm range of the YO-3A data and the slow variation of one-third octave band levels adjacent to the spectral peak, the reader should not conclude that there is no dependence of peak frequency on tip speed.

(c) Comments on Peak Levels of One-Third Octave Bands and Directivity Functions

It is believed that inadequacy of the directivity functions for any

of the options of Reference 7 is at least partly responsible for failure to predict the vortex noise at near overhead conditions. This fact also leads directly to a rationale for the method adopted by Lockheed in this study for correcting the data by referencing the peak 1/3 octave band vortex noise level to the level of the fundamental rotational noise.

(d) An Empirical Correction to Vortex Noise Related to Rotational Noise

- Fluctuating Blade Force Strength Trends versus rpm

It will be recalled from Equation IV-9 of this Appendix (Section 1b(1)(c) that the tangential force, or torque force, per unit radial distance is given by

$$\frac{dF_\phi}{dr} = \frac{dD}{dr} \cos \alpha_{av} + \frac{dL}{dr} \sin \alpha_{av} \qquad \text{(IV-133)}$$

where, dL/dr, is the lift gradient: dD/dr, is the drag gradient; and $\alpha_{av}$ is the advance angle (between the propeller disc plane and the direction of the relative wind vector, $V_r$). The parameters $V_r$ and $\alpha_{av}$ are defined as follows

$$V_r = \sqrt{V_{xo}^{\ 2} + V_{\varphi\ o}^{\ 2}}$$

$$\alpha_{av} = \tan^{-1} (V_{xo}/V_{\phi\ o})$$

where, for axisymmetric inflow,

$$V_{xo} = V_\infty \ (1 + usb\ (r))$$

$$V_{\phi\ o} = \Omega r \ (1 - omsb\ (r))$$

In the case of forward flight (as opposed to static conditions) at low rpm the advance angle becomes large so that the blade lift force contributes significantly to the torque force, via the second term of Equation IV-133. Also, at low rpm, the blade angles of attack and lift coefficients must increase to generate a given thrust, with a corresponding increase in drag.

In the case of vortex noise at the overhead position, the dipole strength for vortex noise is porportional to the fluctuation in the tangential force; therefore, one could write as an "ac" analogy

$$\frac{d\tilde{F}_\phi}{dr} = \frac{d\tilde{D}}{dr} \cos \alpha_{av} + \frac{d\tilde{L}}{dr} \sin \alpha_{av}$$

$$+ \frac{dD}{dr} \widetilde{\cos \alpha}_{av} + \frac{dL}{dr} \widetilde{\sin \alpha}_{av} \qquad \text{(IV-134)}$$

where the ( $\widetilde{\ }$ ) implies a transient fluctuation. The advance angle, itself, is subject to a fluctuation at rotational frequency, owing to its own circumferential non-uniformity.
where

$$\frac{\partial \alpha_{av}}{\partial t} = \frac{\partial \alpha_{av}}{\partial \phi_1} \frac{\partial \phi_1}{\partial t} = \frac{\Omega \partial \alpha_{av}}{\partial \phi_1} \qquad \text{(IV- 135)}$$

In the higher frequency range, governed by vortex noise, the last two terms of Equation IV-134 become negligible since $\omega >> \Omega$ and Equation IV-102 reduces to

$$\frac{d\tilde{F}_\phi}{dr} = \frac{d\tilde{D}}{dr} \cos\alpha_{av} + \frac{d\tilde{L}}{dr} \sin\alpha_{av} \qquad \text{(IV-136)}$$

- Hypothesis for Vortex Noise Prediction

In the present study the empirical correction is based on the premise that there exists a fluctuation in the tangential force which is proportional to the steady state tangential force.

The above hypothesis immediately leads to several conclusions:

- The vortex noise should be directly related to the fundamental rotational noise because the rotational noise is proportional to the torque force.

- The directivity maximum for the fluctuating torque force dipole is in the plane of rotation. By contrast, the directivity functions of Options 2 and 3 are maximum in the thrust direction, appropriate only for a fluctuating thrust dipole.

- The strength of the fluctuating torque force dipole can be expected to increase with decreasing rpm because of (a) increased advance angle and (b) increased blade angle of attack of lift coefficient.

- Since the random dipole radiation efficiency increases according to wave number squared ($k^2 \sim \omega^2/a^2$) which increases with rpm, the combined (opposing) trends of radiation efficiency and source strength vs. rpm can lead to a "bucket" in the curve of peak vortex noise level versus rpm, such as has been found in the YO-3A flyover data. (See Figures 14 and 15 ).

The conclusions above provide a logical impetus to seeking a correlation between the fundamental rotational noise and the vortex noise at the

overhead condition, since it has been shown that the rotational noise has a "bucket" which is to be expected from the fundamental considerations discussed previously in this Appendix.

It is also to be expected that there exists a fluctuating thrust force (see Equation IV-8, Section 2b(1)(c) of the form

$$\frac{d\tilde{T}}{dr} = \frac{d\tilde{L}}{dr} \cos \alpha_{av} + \frac{d\tilde{D}}{dr} \sin \alpha_{av} \qquad \text{(IV-137)}$$

This would give rise to a fluctuating thrust dipole radiation having its maximum directivity along the thrust axis, which would not contribute to vortex noise at the overhead condition. At the lowest rpm (480 rpm) the YC-3A propeller has advance angles in the range of 50 to 60 degrees; therefore, the fluctuating lift dipole contributes more to the torque force fluctuation than to the thrust force fluctuation (since $\sin \alpha_{av} > \cos \alpha_{av}$ for $\alpha_{av} > 45^{\circ}$). Note also that one should expect a finite cross correlation between fluctuating thrust and torque forces which would have a directivity maximum at $45^{\circ}$ from the thrust axis.

- Comments on the Acoustic Radiation Efficiency for Vortex Noise versus Rotational Noise

It will be recalled from the first part of this Appendix that a major part of the explanation for the underprediction of rotational noise levels by the standard axisymmetric rotational noise theory of Reference 7 is caused by non-uniformity of the inflow to the propeller disc. These effects are displayed in Equation IV-29, Section 1b(3)(a)ofthis Appendix. A simpler version showing the effects of the non-uniformity harmonics can be written as

$$p_{m\phi} \cong F_m \Big\{ \delta_o J_{mB}(\arg) + \left(\frac{mB-1}{mB}\right) \delta_1 e^{i\Phi_1} J_{mB-1}(\arg)$$

$$+ \left(\frac{mB-2}{mB}\right) \delta_2 e^{i\Phi_2} J_{mB-2}(\arg) + \left(\frac{mB-3}{mB}\right) \delta_3 e^{i\Phi_3} J_{mB-3}(\arg) + \ldots \Big\} \qquad \text{(IV-138)}$$

where if $\theta$ is the directivity angle (= 0 on thrust axis)

$$\arg = kr \sin \theta$$

$$k = (m\omega_1/a) = (mB\,\Omega/a) \qquad \text{(IV-139)}$$

The $\{\delta_n \quad n = 0,1,2\ldots\}$ are the complex Fourier coefficients which describe the circumferential non-uniformity of tangential force. For a 3-bladed propeller, the fundamental rotational noise becomes (noting $\delta_o = 1$, by definition, and $mB = 3$):

$$p_{1\phi}^{B-3} \cong F_1 \left\{ J_3(\arg) + \delta_1 \left(\frac{3-1}{3}\right) J_2(\arg) e^{i\Phi_1} + \delta_2 \left(\frac{3-2}{3}\right) e^{i\Phi_2} J_1(\arg) + \right.$$

$$\left. + \delta_3 \left(\frac{3-3}{3}\right) J_o(\arg) e^{i\Phi_3} + \delta_4 \left(\frac{3-4}{3}\right) J_{-1}(\arg) e^{i\Phi_4} + \ldots \right\} \quad \text{(IV-140)}$$

We note that the $J_o$ term is cancelled identically. For slow rotation speeds and small radii, the quantity arg = kr $\sin\theta \ll 1$, and from well known Bessel function relations

$$\begin{aligned} J_3(\arg) &\cong (kr/2)^3 \sin^3\theta \\ J_2(\arg) &\cong (kr/2 \sin\theta)^2 \\ J_1(\arg) &\cong (kr \sin\theta/2) \\ J_o(\arg) &\cong 1 \end{aligned} \quad \text{(IV-141)}$$

Thus, for rotational noise the radiation efficiency is proportional to

$$\eta_{rad} \cong \left\{ \left(\frac{kr\sin\theta}{2}\right)^3 + \frac{2\delta_1}{3} \left(\frac{kr\sin\theta}{2}\right)^2 + \frac{\delta_2}{3} \left(\frac{kr\sin\theta}{2}\right) \right.$$

$$\left. - \frac{1}{3} \delta_4(-1) \left(\frac{kr\sin\theta}{2}\right) + \ldots \right\} \quad \text{(IV-142)}$$

where

$$J_{-1}(\arg) = -J_1(\arg) \cong -(kr\sin\theta/2) \quad \text{(IV-143)}$$

$$\therefore \eta_{rad} \cong \left\{ \left(\frac{kr\sin\theta}{2}\right)^3 + \frac{2\delta_1}{3} \left(\frac{kr\sin\theta}{2}\right)^2 + \frac{1}{3}\left(\delta_2 + \delta_4\right)\left(\frac{kr\sin\theta}{2}\right) + \ldots \right\} \quad \text{(IV-144)}$$

By contrast, the radiation efficiency for a point dipole is proportional to

$$\eta_{rad} \cong (kr \sin\theta) \quad \text{(IV-145)}$$

The difference between the weak radiation efficiency of axisymmetric rotational noise of propellers and the relatively greater efficiency of point dipoles is explained by destructive interference. In the case of axisymmetric

rotational noise, $\delta_n = 0$, for $n > 0$. Therefore for a 3-bladed propeller

$$\eta_{rad,\ axisymm} \cong \frac{1}{mB!}\left(\frac{kr\sin\theta}{2}\right)^{mB} = \frac{1}{3!}\left(\frac{kr\sin\theta}{2}\right)^{3} \qquad \text{(IV-146)}$$

Thus, the mean squared sound pressure level for rotational noise varies according to

$$\Delta SPL_{axisymm} \cong 20\ mB\log_{10}\left(\frac{kr\sin\theta}{2}\right) \qquad \text{(IV- 147)}$$

$$= 60\log_{10}\left(\frac{kr\sin\theta}{2}\right) \qquad \text{(IV-148)}$$

for a three-bladed propeller with axisymmetric inflow.

For the case of a point dipole the correction for radiation efficiency is

$$\Delta SPL_{\substack{point\\dipole}} = 20\log_{10}(kr\sin\theta) \qquad \text{(IV-149)}$$

In the case of propeller blade vortex noise, the fluctuating forces on the blade are correlated for only a small distance (of the order of one trailing edge boundary layer thickness, and possibly a few percent of the blade tip radius near the blade tip). Therefore, the radial distribution of vortex noise radiators are summed as random loads, rather than being considered to have definite phase relations as displayed by Equation IV-29, Section of this Appendix describing rotational noise.

Of even greater significance is the randomness of phase of the loads on different blades. Consequently, when intergrating the circumferential contributions to the far field vortex noise at a given radial station, each blade, whose force fluctuations are random in phase in relation to the other blades, always adds energy to the far field random noise, and does so with a radiation efficiency proportional to $(kr)^2$ which is the efficiency associated with a sum of randomly phased point sources. By contrast, the circumferential integration of the properly phased blade load contributions for rotational noise gives rise mathematically to the Bessel functions whose small magnitudes at low wave numbers can be thought of, physically, as the result of destructive interference.

When the circumferential loading of the blades is non-uniform, as described by the Fourier loading harmonic (LH) amplitudes, additional, more efficient rotational noise radiation modes are brought into play which radiate in proportion to lower order Bessel functions. In the case of rotational noise, one can regard the non-uniformity effects as a tendency to randomize the phase relations, and hence a process that breaks up the destructive interference which characterizes purely axisymmetric rotational noise.

In the case of propeller vortex noise, the blade-to-blade phase relations are clearly random; therefore, one would never expect to find the kind of destructive interference phenomenal such as is associated with propeller rotational noise. Because these random point sources have a weaker wave number dependence (by a factor of 40 log (kr sin $\theta$)) for a 3 bladed propeller, it may be expected that the variation of fluctuating blade force with rpm should have a more direct affect on far field noise radiation, since the radiation efficiency does not decrease so rapidly with reduced rpm as is the case with axisymmetric propeller noise.

It will be recalled in this Appendix (Section 1b(2)(a), Figures 19 and 22) that (in the case of purely axisymmetric propeller noise radiation) the predicted fundamental SPL at a fixed airplane flyover speed and thrust shows only a slight bucket in the curve vs. rpm, with decreasing rpm for all reasonable estimates of propeller efficiency and horsepower. It was concluded that the decreased radiation efficiency ($\eta_{rad}$ 20mB log (kr) ) at low rpm largely offsets any increases in steady state propeller power input associated with low efficiency propeller operation at low rpm. As mentioned above, the radiation efficiency for random point dipole sources does not decrease so rapidly at low rpm. Consequently, there is a greater expectation for finding a "bucket" in the vortex noise versus rpm curve than for the rotational noise.

## APPENDIX V

## TABULATED PREDICTIONS OF PROPELLER NOISE AND AURAL DETECTION RANGE

The design charts presented in Section VII were constructed from propeller noise and aural detection range predictions made with the modified Air Force computer program by Mr. Jerry Martin (ASD/XRHD) and Mr. Walter Lichtenburg (ASD/XRHP ). These noise and range data are tabulated in this appendix.

Parametric data on which these predictions were made were as follows:

Propeller Diameter: 8, 10 and 12 feet

Number of Blades, 2, 3, 4, 5, and 6

Thrust: 100, 200, 300, 400, and 500 pounds

Helical Tip Speed: 0.20, 0.25, 0.30, 0.35, and 0.40 Mach

Thus the tabulated data reflects variation in four independent variables. Held constant were the following:

Propeller Blade Configuration: Same as the standard 3 blade propeller used on the YO-3A aircraft described in Appendix I and scaled to size

Aircraft Velocity: 125 feet per second (74 kts).

Aircraft Altitude: 125 feet.

Each table of tabulations represent a given propeller blade diameter (D) and given number of blades (B). For each value of thrust (T), the calculated values of helical tip speed ($M_t$), propeller efficiency ($\eta$), and blade angle of attack at 3/4 radius ($\theta_{3/4}$) are tabulated. The predicted values of overall sound pressure level (OASPL) on the ground radiated from the aircraft in overhead position at an altitude of 125 feet and the minimum aural detection range (ADR) implied by these noise levels assuming daytime jungle background noise are also tabulated.

TABLE I

Propeller Diameter: 8 feet Number of Blades: 2

| T (Pounds) | $M_t$ (MACH) | | $\theta_{3/4}$ (Degrees) | OASPL (dB) | ADR (feet) |
|---|---|---|---|---|---|
| 100 | 0.20 | 0.810 | 52.53 | 80.6 | 3,397 |
| | 0.25 | 0.858 | 38.69 | 79.1 | 1,628 |
| | 0.30 | 0.862 | 30.69 | 76.9 | 2,243 |
| | 0.35 | 0.842 | 25.27 | 80.6 | 3,820 |
| | 0.40 | 0.799 | 21.25 | 83.6 | 8,052 |
| 200 | 0.20 | | 66.03 | | |
| | 0.25 | 0.728 | 49.58 | 91.3 | 11,434 |
| | 0.30 | 0.816 | 36.52 | 85.6 | 6,018 |
| | 0.35 | 0.833 | 29.43 | 82.5 | 4,815 |
| | 0.40 | 0.830 | 24.43 | 82.2 | 7,027 |
| 300 | 0.20 | | | | |
| | 0.25 | | | | |
| | 0.30 | 0.659 | 46.24 | | |
| | 0.35 | 0.788 | 33.92 | 91.5 | 14,122 |
| | 0.40 | 0.805 | 27.67 | 88.9 | 15,990 |
| 400 | 0.20 | | | | |
| | 0.25 | | | | |
| | 0.30 | | | | |
| | 0.35 | 0.705 | 39.91 | 98.9 | 35,808 |
| | 0.40 | 0.767 | 31.19 | 95.4 | 36.185 |
| 500 | 0.20 | | | | |
| | 0.25 | | | | |
| | 0.30 | | | | |
| | 0.40 | 0.716 | 35.26 | 100.7 | 78,760 |

TABLE II

Propeller Diameter: 10 feet Number of Blades: 2

| T (Pounds) | $M_t$ (MACH) | | $\theta_{3/4}$ (Degrees) | OASPL (dB) | ADR (Feet) |
|---|---|---|---|---|---|
| 100 | 0.20 | 0.858 | 47.31 | 75.4 | 2,052 |
| | 0.25 | 0.872 | 35.44 | 72.9 | 1,545 |
| | 0.30 | 0.852 | 28.77 | 77.3 | 2,552 |
| | 0.35 | 0.800 | 23.56 | 80.9 | 3,837 |
| | 0.40 | 0.730 | 19.98 | 83.6 | 5,241 |
| 200 | 0.20 | | | | |
| | 0.25 | 0.838 | 40.70 | 84.6 | 5,865 |
| | 0.30 | 0.855 | 32.39 | 80.7 | 3,771 |
| | 0.35 | 0.847 | 26.16 | 79.5 | 3,274 |
| | 0.40 | 0.819 | 22.00 | 82.5 | 4,625 |
| 300 | 0.20 | | | | |
| | 0.25 | 0.771 | 47.20 | 94.4 | 17,545 |
| | 0.30 | 0.821 | 36.18 | 89.8 | 10,578 |
| | 0.35 | 0.836 | 28.78 | 86.5 | 7,307 |
| | 0.40 | 0.830 | 24.02 | 84.8 | 5,972 |
| 400 | 0.20 | | | | |
| | 0.25 | | | | |
| | 0.30 | 0.776 | 40.55 | 96.6 | 22,087 |
| | 0.35 | 0.810 | 31.52 | 92.9 | 14,745 |
| | 0.40 | 0.819 | 26.06 | 90.6 | 11,473 |
| 500 | 0.20 | | | | |
| | 0.25 | | | | |
| | 0.30 | | | | |
| | 0.35 | 0.779 | 34.48 | 97.9 | 25,431 |
| | 0.40 | 0.799 | 28.14 | 95.3 | 19,232 |

TABLE III

Propeller Diameter: 12 feet Number of Blades: 2

| T (Pounds) | $M_t$ (MACH) | | $\theta_{3/4}$ (Degrees) | OASPL (dB) | ADR (Feet) |
|---|---|---|---|---|---|
| 100 | 0.20 | 0.873 | 44.88 | 71.7 | 1,463 |
| | 0.25 | 0.862 | 33.88 | 73.3 | 1,750 |
| | 0.30 | 0.821 | 27.77 | 77.4 | 2,764 |
| | 0.35 | 0.754 | 23.26 | 80.4 | 3,900 |
| | 0.40 | 0.664 | 19.41 | 83.3 | 5,434 |
| 200 | 0.20 | 0.825 | 51.26 | 87.2 | 8,439 |
| | 0.25 | 0.865 | 37.45 | 80.6 | 3,968 |
| | 0.30 | 0.863 | 30.29 | 77.4 | 2,772 |
| | 0.35 | 0.838 | 25.13 | 79.3 | 3,443 |
| | 0.40 | 0.785 | 20.90 | 82.5 | 4,936 |
| 300 | 0.20 | 0.682 | 59.76 | | |
| | 0.25 | 0.834 | 41.16 | 89.7 | 11,115 |
| | 0.30 | 0.853 | 32.81 | 85.8 | 7,183 |
| | 0.35 | 0.849 | 27.01 | 83.5 | 5,527 |
| | 0.40 | 0.823 | 22.32 | 82.1 | 4,744 |
| 400 | 0.20 | | | | |
| | 0.25 | 0.792 | 45.51 | 96.5 | 23,508 |
| | 0.30 | 0.829 | 35.46 | 92.3 | 14,768 |
| | 0.35 | 0.840 | 28.89 | 80.4 | 10,796 |
| | 0.40 | 0.831 | 23.72 | 87.4 | 8,666 |
| 500 | 0.20 | | | | |
| | 0.25 | | | | |
| | 0.30 | 0.801 | 38.27 | 97.4 | 25,572 |
| | 0.35 | 0.824 | 30.81 | 94.2 | 18,145 |
| | 0.40 | 0.827 | 25.14 | 91.9 | 14,175 |

TABLE IV

Propeller Diameter: 8 feet Number of Blades: 3

| T (Pounds) | $M_t$ (MACH) | | $\theta_{3/4}$ (Degrees) | OASPL (dB) | ADR (Feet) |
|---|---|---|---|---|---|
| 100 | 0.20 | 0.842 | 47.96 | 66.2 | 793 |
| | 0.25 | 0.862 | 36.26 | 68.2 | 1,344 |
| | 0.30 | 0.845 | 29.09 | 73.0 | 3,954 |
| | 0.35 | 0.801 | 24.13 | 76.6 | 8,089 |
| | 0.40 | 0.735 | 20.40 | 81.5 | 14,732 |
| 200 | 0.20 | | | | |
| | 0.25 | 0.814 | 42.20 | 75.7 | 3,161 |
| | 0.30 | 0.837 | 33.09 | 71.7 | 3,312 |
| | 0.35 | 0.834 | 27.08 | 75.5 | 6,830 |
| | 0.40 | 0.810 | 22.70 | 80.8 | 13,136 |
| 300 | 0.20 | | | | |
| | 0.25 | | 52.98 | | |
| | 0.30 | 0.795 | 37.27 | 81.0 | 9,511 |
| | 0.35 | 0.813 | 30.05 | 78.1 | 9,069 |
| | 0.40 | 0.811 | 24.98 | 80.1 | 11,939 |
| 400 | 0.20 | | 80.93 | | |
| | 0.25 | | 73.25 | | |
| | 0.30 | 0.740 | 42.29 | 88.1 | 21,450 |
| | 0.35 | 0.779 | 33.18 | 84.8 | 19,139 |
| | 0.40 | 0.792 | 27.29 | 84.3 | 18,852 |
| 500 | 0.20 | | 96.62 | | |
| | 0.25 | | 62.40 | | |
| | 0.30 | | 65.19 | | |
| | 0.35 | 0.742 | 36.60 | 90.1 | 34,819 |
| | 0.40 | 0.765 | 29.69 | 89.4 | 35,020 |

TABLE V

Propeller Diameter: 10 feet Number of Blades: 3

| T (Pounds) | $M_t$ (MACH) | | $\theta_{3/4}$ (Degrees) | OASPL (dB) | ADR (Feet) |
|---|---|---|---|---|---|
| 100 | 0.20 | 0.864 | 44.75 | 62.1 | 532 |
| | 0.25 | 0.853 | 33.94 | 69.0 | 1,173 |
| | 0.30 | 0.809 | 27.76 | 73.0 | 2,111 |
| | 0.35 | 0.732 | 22.86 | 76.4 | 4,826 |
| | 0.40 | 0.643 | 19.45 | 81.1 | 9,694 |
| 200 | 0.20 | 0.812 | 51.15 | 77.3 | 3,045 |
| | 0.25 | 0.855 | 37.56 | 70.5 | 1,406 |
| | 0.30 | 0.851 | 30.29 | 71.7 | 1,764 |
| | 0.35 | 0.820 | 24.72 | 75.8 | 4,307 |
| | 0.40 | 0.770 | 20.93 | 80.8 | 9,003 |
| 300 | 0.20 | | 54.33 | | |
| | 0.25 | 0.821 | 41.32 | 79.7 | 3,990 |
| | 0.30 | 0.840 | 32.89 | 76.0 | 2,840 |
| | 0.35 | 0.833 | 26.58 | 75.1 | 3,879 |
| | 0.40 | 0.807 | 22.39 | 80.3 | 8,346 |
| 400 | 0.20 | | 89.69 | | |
| | 0.25 | 0.777 | 45.67 | 86.7 | 8,826 |
| | 0.30 | 0.815 | 35.52 | 82.5 | 6,082 |
| | 0.35 | 0.824 | 28.95 | 79.7 | 6,487 |
| | 0.40 | 0.814 | 2[illegible].83 | 80.1 | 8,028 |
| 500 | 0.20 | | 70.39 | | |
| | 0.25 | | 47.92 | | |
| | 0.30 | 0.785 | 38.33 | 87.7 | 11,193 |
| | 0.35 | 0.807 | 30.33 | 84.6 | 11,280 |
| | 0.40 | 0.808 | 25.28 | 84.6 | 13,973 |

TABLE VI

Propeller Diameter: 12 feet Number of Blades: 3

| T (Pounds) | $M_t$ (MACH) | | $\phi_{3/4}$ (Degrees) | OASPL (dB) | ADR (Feet) |
|---|---|---|---|---|---|
| 100 | 0.20 | 0.861 | 43.14 | 62.7 | 605 |
| | 0.25 | 0.824 | 32.86 | 69.3 | 1,288 |
| | 0.30 | 0.759 | 27.08 | 72.8 | 1,934 |
| | 0.35 | 0.670 | 22.77 | 75.5 | 2,646 |
| | 0.40 | | | | |
| 200 | 0.20 | 0.849 | 47.35 | 73.2 | 2,021 |
| | 0.25 | 0.863 | 35.34 | 67.6 | 1,059 |
| | 0.30 | 0.839 | 28.85 | 71.9 | 1,748 |
| | 0.35 | 0.791 | 24.10 | 75.3 | 2,591 |
| | 0.40 | 0.714 | 20.15 | 80.4 | 5,531 |
| 300 | 0.20 | 0.805 | 52.05 | 82.7 | 5,948 |
| | 0.25 | 0.853 | 37.87 | 75.7 | 2,67[illegible] |
| | 0.30 | 0.852 | 30.61 | 72.4 | 1,843 |
| | 0.35 | 0.827 | 25.44 | 74.8 | 2,452 |
| | 0.40 | 0.776 | 21.16 | 80.1 | 5,239 |
| 400 | 0.20 | | 65.34 | | |
| | 0.25 | 0.829 | 40.46 | 83.2 | 5,618 |
| | 0.30 | 0.844 | 32.45 | 78.6 | 3,729 |
| | 0.35 | 0.836 | 26.77 | 76.5 | 2,970 |
| | 0.40 | 0.804 | 22.19 | 79.8 | 4,959 |
| 500 | 0.20 | | | | |
| | 0.25 | 0.802 | 43.22 | 87.4 | 10,150 |
| | 0.30 | 0.829 | 34.22 | 83.5 | 6,552 |
| | 0.35 | 0.832 | 28.12 | 81.2 | 5,042 |
| | 0.40 | 0.814 | 23.21 | 81.5 | 6,036 |

TABLE VII

Propeller Diameter: 8 feet Number of Blades: 4

| T (Pounds) | $M_t$ (MACH) | | $\theta_{3/4}$ (Degrees) | OASPL (dB) | ADR (Feet) |
|---|---|---|---|---|---|
| 100 | 0.20 | 0.847 | 46.74 | 62.5 | 692 |
| | 0.25 | 0.853 | 35.80 | 69.5 | 1,098 |
| | 0.30 | 0.824 | 28.97 | 76.2 | 9,748 |
| | 0.35 | 0.771 | 24.21 | 80.2 | 16,724 |
| | 0.40 | 0.699 | 20.60 | 83.3 | 33,776 |
| 200 | 0.20 | 0.763 | 54.55 | 75.1 | 2,951 |
| | 0.25 | 0.827 | 39.77 | 67.3 | 2,687 |
| | 0.30 | 0.836 | 31.54 | 71.2 | 5,570 |
| | 0.35 | 0.818 | 25.99 | 75.2 | 10,004 |
| | 0.40 | 0.780 | 21.88 | 78.5 | 18,401 |
| 300 | 0.20 | | | | |
| | 0.25 | 0.773 | 44.87 | 77.0 | 8,147 |
| | 0.30 | 0.808 | 34.78 | 73.5 | 7,147 |
| | 0.35 | 0.813 | 28.38 | 74.3 | 8,940 |
| | 0.40 | 0.798 | 23.76 | 78.0 | 17,240 |
| 400 | 0.20 | | | | |
| | 0.25 | | | | |
| | 0.30 | 0.770 | 38.19 | 80.2 | 15,024 |
| | 0.35 | 0.791 | 30.78 | 77.1 | 11,936 |
| | 0.40 | 0.791 | 25.61 | 77.5 | 16,289 |
| 500 | 0.20 | | | | |
| | 0.25 | | | | |
| | 0.30 | 0.727 | 42.16 | 85.8 | 27,279 |
| | 0.35 | 0.762 | 33.29 | 82.3 | 20,008 |
| | 0.40 | 0.773 | 27.47 | 80.3 | 23,100 |

TABLE IX

Propeller Diameter: 10 feet Number of Blades: 4

| T (Pounds) | $M_t$ (MACH) | | $\theta_{3/4}$ (Degrees) | OASPL (dB) | ADR (Feet) |
|---|---|---|---|---|---|
| 100 | 0.20 | 0.854 | 43.55 | 62.0 | 642 |
| | 0.25 | 0.826 | 33.26 | 68.1 | 1,611 |
| | 0.30 | 0.766 | 27.29 | 73.1 | 4,389 |
| | 0.35 | 0.672 | 22.54 | 76.1 | 8,626 |
| | 0.40 | 0.576 | 19.24 | | |
| 200 | 0.20 | 0.828 | 48.39 | 69.6 | 1,552 |
| | 0.25 | 0.851 | 36.12 | 66.2 | 1,279 |
| | 0.30 | 0.834 | 29.33 | 71.8 | 3,278 |
| | 0.35 | 0.786 | 24.04 | 75.6 | 7,817 |
| | 0.40 | 0.721 | 20.42 | 78.4 | 13,531 |
| 300 | 0.20 | 0.769 | 54.05 | 79.5 | 4,792 |
| | 0.25 | 0.831 | 39.05 | 71.5 | 2,354 |
| | 0.30 | 0.837 | 31.39 | 70.8 | 3,278 |
| | 0.35 | 0.815 | 25.56 | 74.9 | 7,123 |
| | 0.40 | 0.775 | 21.61 | 78.1 | 12,656 |
| 400 | 0.20 | 0.637 | 61.04 | | |
| | 0.25 | 0.800 | 42.10 | 78.2 | 5,169 |
| | 0.30 | 0.822 | 33.47 | 75.3 | 5,486 |
| | 0.35 | 0.818 | 27.06 | 74.3 | 6,642 |
| | 0.40 | 0.794 | 22.81 | 77.8 | 11,907 |
| 500 | 0.20 | | | | |
| | 0.25 | 0.763 | 45.55 | 83.7 | 9,876 |
| | 0.30 | 0.800 | 35.59 | 80.4 | 9,814 |
| | 0.35 | 0.809 | 28.56 | 77.4 | 9,191 |
| | 0.40 | 0.797 | 23.98 | 77.5 | 11,285 |

TABLE X

Propeller Diameter: 12 feet Number of Blades: 4

| T (Pounds) | M (MAH) | | $\theta_{3/4}$ (Degrees) | OASPL (dB) | ADR (Feet) |
|---|---|---|---|---|---|
| 100 | 0.20 | 0.838 | 42.32 | 62.6 | 726 |
| | 0.25 | 0.783 | 32.40 | 68.4 | 1,427 |
| | 0.30 | 0.703 | 26.77 | 73.0 | 2,565 |
| | 0.35 | 0.602 | 22.55 | 75.6 | 5,338 |
| | 0.40 | 0.517 | 19.01 | | |
| 200 | 0.20 | 0.851 | 45.61 | 66.0 | 1,070 |
| | 0.25 | 0.847 | 34.36 | 66.9 | 1,189 |
| | 0.30 | 0.809 | 28.18 | 72.1 | 2,271 |
| | 0.35 | 0.745 | 23.62 | 75.2 | 4,970 |
| | 0.40 | 0.652 | 19.82 | 78.1 | 9,544 |
| 300 | 0.20 | 0.822 | 49.06 | 75.0 | 3,019 |
| | 0.25 | 0.850 | 36.46 | 67.8 | 1,324 |
| | 0.30 | 0.836 | 2[illegible].60 | 71.3 | 2,041 |
| | 0.35 | 0.797 | 24.71 | 74.7 | 4,620 |
| | 0.40 | 0.730 | 20.64 | 77.9 | 9,087 |
| 400 | 0.20 | 0.782 | 52.97 | 82.0 | 6,683 |
| | 0.25 | 0.837 | 38.39 | 74.1 | 2,712 |
| | 0.30 | 0.839 | 31.03 | 71.7 | 2,141 |
| | 0.35 | 0.817 | 25.80 | 74.3 | 4,313 |
| | 0.40 | 0.769 | 21.47 | 77.7 | 8,653 |
| 500 | 0.20 | 0.704 | 58.67 | 88.7 | 13,956 |
| | 0.25 | 0.617 | 40.47 | 79.2 | 4,851 |
| | 0.30 | 0.831 | 32.49 | 76.6 | 3,769 |
| | 0.35 | 0.821 | 26.87 | 74.3 | 4,304 |
| | 0.40 | 0.788 | 22.30 | 77.5 | 8,270 |

TABLE XI

Propeller Diameter: 8 feet Number of Blades: 5

| T (Pounds) | $M_t$ (MACH) | | $\theta_{3/4}$ (Degrees) | OASPL (dB) | ADR (Feet) |
|---|---|---|---|---|---|
| 100 | 0.20 | 0.844 | 44.85 | 61.7 | 1,060 |
| | 0.25 | 0.835 | 34.46 | 69.0 | 4,147 |
| | 0.30 | 0.790 | 27.92 | 73.1 | 8,540 |
| | 0.35 | 0.717 | 23.31 | 76.0 | 13,597 |
| | 0.40 | 0.628 | 19.81 | 78.3 | 24,433 |
| 200 | 0.20 | 0.782 | 51.54 | 69.6 | 2,616 |
| | 0.25 | 0.830 | 38.35 | 66.7 | 3,215 |
| | 0.30 | 0.827 | 30.61 | 71.4 | 7,044 |
| | 0.35 | 0.799 | 25.35 | 74.9 | 11,819 |
| | 0.40 | 0.749 | 21.42 | 77.7 | 22,837 |
| 300 | 0.20 | | | | |
| | 0.25 | 0.788 | 42.39 | 72.6 | 6,326 |
| | 0.30 | 0.811 | 33.35 | 70.1 | 6,126 |
| | 0.35 | 0.806 | 27.39 | 74.0 | 10,643 |
| | 0.40 | 0.781 | 23.02 | 77.1 | 21.424 |
| 400 | 0.20 | 0.734 | 47.06 | 79.8 | 14,101 |
| | 0.25 | 0.781 | 36.14 | 74.5 | 9,793 |
| | 0.30 | 0.792 | 29.43 | 73.2 | 9,768 |
| | 0.35 | 0.783 | 24.63 | 76.6 | 20,225 |
| | 0.40 | | | | |
| 500 | 0.20 | | | | |
| | 0.25 | | | | |
| | 0.30 | 0.748 | 39.07 | 79.8 | 16,872 |
| | 0.35 | 0.770 | 31.48 | 76.2 | 13,798 |
| | 0.40 | 0.772 | 26.21 | 76.2 | 19,286 |

TABLE XII

Propeller Diameter: 10 feet Number of Blades: 5

| T (Pounds) | $M_t$ (MACH) | | $\theta_{3/4}$ (Degrees) | OASPL (dB) | ADR (Feet) |
|---|---|---|---|---|---|
| 100 | 0.20 | 0.839 | 42.84 | 62.7 | 797 |
| | 0.25 | 0.797 | 32.86 | 65.8 | 2,998 |
| | 0.30 | 0.725 | 27.04 | 73.3 | 6,297 |
| | 0.35 | 0.620 | 22.37 | 76.1 | 10,976 |
| | 0.40 | 0.527 | 19.15 | | |
| 200 | 0.20 | 0.832 | 46.85 | 64.6 | 990 |
| | 0.25 | 0.842 | 35.26 | 68.0 | 2,341 |
| | 0.30 | 0.813 | 28.77 | 72.1 | 5,438 |
| | 0.35 | 0.752 | 23.67 | 75.1 | 10,084 |
| | 0.40 | 0.676 | 20.15 | 77.8 | 15,073 |
| 300 | 0.20 | 0.787 | 51.24 | 74.1 | 2,949 |
| | 0.25 | 0.833 | 37.71 | 67.2 | 2,231 |
| | 0.30 | 0.828 | 30.50 | 71.7 | 4,823 |
| | 0.35 | 0.797 | 24.95 | 74.7 | 9,30[illegible] |
| | 0.40 | 0.742 | 21.17 | 77.5 | 1[illegible],235 |
| 400 | 0.20 | 0.742 | 56.67 | 81.7 | 6,929 |
| | 0.25 | 0.805 | 40.23 | 74.1 | 9,731 |
| | 0.30 | 0.821 | 32.26 | 70.2 | 4,320 |
| | 0.35 | 0.806 | 26.25 | 74.1 | 8,564 |
| | 0.40 | 0.771 | 22.19 | 77.1 | 13,513 |
| 500 | 0.20 | | | | |
| | 0.25 | 0.780 | 42.94 | 79.4 | 8,684 |
| | 0.30 | 0.806 | 34.04 | 74.9 | 7,423 |
| | 0.35 | 0.803 | 27.53 | 73.6 | 8,202 |
| | 0.40 | 0.782 | 23.20 | 76.8 | 12,896 |

TABLE XIII

Propeller Diameter: 12 feet Number of Blades: 5

| T (Pounds) | $M_t$ (MACH) | | $\theta_{3/4}$ (Degrees) | OASPL (dB) | ADR (Feet) |
|---|---|---|---|---|---|
| 100 | 0.20 | 0.814 | 41.85 | 63.3 | 881 |
| | 0.25 | 0.745 | 32.14 | 70.2 | 1,962 |
| | 0.30 | 0.654 | 26.60 | 73.4 | 4,288 |
| | 0.35 | 0.547 | 22.45 | 75.8 | 7,943 |
| | 0.40 | | | | |
| 200 | 0.20 | 0.845 | 44.53 | 61.3 | 700 |
| | 0.25 | 0.828 | 33.79 | 68.8 | 1,657 |
| | 0.30 | 0.777 | 27.81 | 72.5 | 3,844 |
| | 0.35 | 0.708 | 23.37 | 75.3 | 7,520 |
| | 0.40 | 0.602 | 19.63 | 77.7 | 11,787 |
| 300 | 0.20 | 0.828 | 47.42 | 70.1 | 1,927 |
| | 0.25 | 0.842 | 35.46 | 67.6 | 1,458 |
| | 0.30 | 0.816 | 29.02 | 71.6 | 3,481 |
| | 0.35 | 0.766 | 24.29 | 74.7 | 6,967 |
| | 0.40 | 0.68[illegible] | 20.35 | 77.4 | 11,306 |
| 400 | 0.20 | 0.797 | 50.48 | 76.9 | 4,137 |
| | 0.25 | 0.837 | 37.17 | 70.4 | 1,988 |
| | 0.30 | 0.828 | 30.23 | 70.9 | 3,192 |
| | 0.35 | 0.794 | 25.22 | 74.2 | 6,593 |
| | 0.40 | 0.734 | 21.07 | 77.2 | 10,844 |
| 500 | 0.20 | 0.759 | 53.91 | 82.5 | 7,840 |
| | 0.25 | 0.823 | 38.89 | 75.3 | 3,499 |
| | 0.30 | 0.826 | 31.43 | 71.4 | 3,373 |
| | 0.35 | 0.806 | 26.14 | 73.8 | 6,188 |
| | 0.40 | 0.761 | 21.77 | 76.9 | 10,431 |

TABLE XIV

Propeller Diameter: 8 feet Number of Blades: 6

| T (Pounds) | $M_t$ (MACH) | | $\theta_{3/4}$ (Degrees) | OASPL (dB) | ADR (Feet) |
|---|---|---|---|---|---|
| 100 | 0.20 | 0.790 | 49.85 | 66.0 | 2,174 |
| | 0.25 | 0.827 | 37.45 | 68.1 | 4,012 |
| | 0.30 | 0.816 | 30.06 | 72.6 | 8,014 |
| | 0.35 | 0.778 | 24.97 | 75.8 | 16,090 |
| | 0.40 | 0.720 | 21.15 | 79.4 | 28,819 |
| 200 | 0.20 | 0.837 | 44.13 | 63.0 | 1,546 |
| | 0.25 | 0.818 | 34.07 | 70.3 | 5,137 |
| | 0.30 | 0.761 | 27.86 | 74.2 | 9,457 |
| | 0.35 | 0.681 | 23.35 | 77.0 | 18,331 |
| | 0.40 | 0.586 | 19.70 | 80.3 | 31,382 |
| 300 | 0.20 | 0.708 | 57.03 | 76.6 | 7,370 |
| | 0.25 | 0.794 | 40.96 | 69.2 | 4,592 |
| | 0.30 | 0.808 | 32.43 | 71.4 | 7,080 |
| | 0.35 | 0.795 | 26.78 | 74.9 | 14,443 |
| | 0.40 | 0.761 | 22.59 | 73.8 | 26,847 |
| 400 | 0.20 | | | | |
| | 0.25 | 0.751 | 44.68 | 76.1 | 9,642 |
| | 0.30 | 0.784 | 34.90 | 71.0 | 6,786 |
| | 0.35 | 0.787 | 28.60 | 74.1 | 13,231 |
| | 0.40 | 0.770 | 24.01 | 78.2 | 25,293 |
| 500 | 0.20 | | | | |
| | 0.25 | 0.701 | 42.23 | 82.1 | 17,823 |
| | 0.30 | 0.755 | 37.40 | 76.2 | 11,513 |
| | 0.35 | 0.770 | 30.40 | 73.5 | 12,327 |
| | 0.40 | 0.765 | 25.46 | 77.7 | 24.014 |

TABLE XV

Propeller Diameter: 10 feet Number of Blades: 6

| T (Pounds) | $M_t$ (MACH) | | $\theta_{3/4}$ (Degrees) | OASPL (dB) | ADR (Feet) |
|---|---|---|---|---|---|
| 100 | 0.20 | 0.823 | 42.41 | 64.0 | 1,022 |
| | 0.25 | 0.769 | 32.62 | 71.2 | 3,949 |
| | 0.30 | 0.688 | 26.90 | 74.6 | 7,831 |
| | 0.35 | 0.577 | 22.29 | 77.3 | 11,749 |
| | 0.40 | 0.485 | 19.11 | | |
| 200 | 0.20 | 0.830 | 45.88 | 61.8 | 788 |
| | 0.25 | 0.830 | 34.73 | 69.5 | 3,251 |
| | 0.30 | 0.791 | 28.43 | 73.4 | 6,843 |
| | 0.35 | 0.720 | 23.45 | 76.5 | 10,876 |
| | 0.40 | 0.637 | 20.00 | 79.9 | 20,524 |
| 300 | 0.20 | 0.795 | 49.58 | 70.6 | 2,168 |
| | 0.25 | 0.829 | 36.88 | 68.1 | 2,796 |
| | 0.30 | 0.815 | 29.58 | 72.4 | 6,124 |
| | 0.35 | 0.772 | 24.59 | 75.8 | 10,130 |
| | 0.40 | 0.711 | 20.92 | 79.3 | 19,310 |
| 400 | 0.20 | 0.746 | 53.84 | 77.9 | 4,995 |
| | 0.25 | 0.811 | 39.06 | 70.8 | 3,793 |
| | 0.30 | 0.815 | 31.50 | 71.5 | 5,591 |
| | 0.35 | 0.790 | 25.74 | 75.2 | 9,493 |
| | 0.40 | 0.747 | 21.82 | 78.9 | 18,335 |
| 500 | 0.20 | | | | |
| | 0.25 | 0.787 | 41.31 | 76.0 | 6,852 |
| | 0.30 | 0.804 | 33.07 | 71.6 | 5,610 |
| | 0.35 | 0.793 | 26.88 | 74.6 | 8,975 |
| | 0.40 | 0.763 | 22.74 | 78.5 | 17,499 |

TABLE XVI

Propeller Diameter: 12 feet Number of Blades: 6

| T (Pounds) | $M_t$ (MACH) | | $\theta_{3/4}$ (Degrees) | OASPL (dB) | ADR (Feet) |
|---|---|---|---|---|---|
| 100 | 0.20 | 0.789 | 41.57 | 64.7 | 1,124 |
| | 0.25 | 0.709 | 31.99 | 71.7 | 2,761 |
| | 0.30 | 0.611 | 26.51 | 74.8 | 5,943 |
| | 0.35 | 0.501 | 22.40 | 77.0 | 9,447 |
| | 0.40 | 0.424 | 18.97 | | |
| 200 | 0.20 | 0.836 | 43.93 | 62.7 | 858 |
| | 0.25 | 0.807 | 33.44 | 70.3 | 2,355 |
| | 0.30 | 0.747 | 27.58 | 73.9 | 5,368 |
| | 0.35 | 0.664 | 23.23 | 76.5 | 8,896 |
| | 0.40 | 0.558 | 19.54 | 79.9 | 14,221 |
| 300 | 0.20 | 0.827 | 46.40 | 67.0 | 1,475 |
| | 0.25 | 0.831 | 34.91 | 69.2 | 2,067 |
| | 0.30 | 0.796 | 28.66 | 73.1 | 4,886 |
| | 0.35 | 0.736 | 24.05 | 75.9 | 8,448 |
| | 0.40 | 0.649 | 20.19 | 79.6 | 13,653 |
| 400 | 0.20 | 0.803 | 48.98 | 73.5 | 3,083 |
| | 0.25 | 0.831 | 36.40 | 68.2 | 1,855 |
| | 0.30 | 0.814 | 29.73 | 72.3 | 4,513 |
| | 0.35 | 0.771 | 24.87 | 75.4 | 7,956 |
| | 0.40 | 0.702 | 20.83 | 79.2 | 13,111 |
| 500 | 0.20 | 0.771 | 51.81 | 79.0 | 5,767 |
| | 0.25 | 0.822 | 37.90 | 72.2 | 2,941 |
| | 0.30 | 0.817 | 30.80 | 71.7 | 4,167 |
| | 0.35 | 0.788 | 25.60 | 74.9 | 7,524 |
| | 0.40 | 0.734 | 21.97 | 78.8 | 12,612 |